CLINICAL AND MOLECULAR ASPECTS OF ORBITAL INFLAMMATION AND LYMPHOMA

2020

KAMIL LABAN

Clinical and molecular aspects of orbital inflammation and lymphoma

Kamil Laban

Cover and lay-out: K. Laban, inspired by *art nouveau* and *art deco* styles, including the *Palau de la Música Catalana* stained glass ceiling in Barcelona, Spain.

Printed by: Ridderprint | ridderprint.nl

ISBN: 978-94-6375-905-2

Printing of this thesis was kindly financially suported by Stichting Blindenhulp, Landelijke Stichting voor Blinden en Slechtzienden (LSBS), Théa Pharma, Bayer, Tramedico, Chipsoft and Infection & Immunity Utrecht.

Clinical and molecular aspects of orbital inflammation and lymphoma

Klinische en moleculaire aspecten van orbitale inflammatie en lymfoom
(met een samenvatting in het Nederlands)

Proefschrift

ter verkrijging van de graad van doctor aan de Universiteit Utrecht op gezag van de rector magnificus, prof. dr. H.R.B.M. Kummeling, ingevolge het besluit van het college voor promoties in het openbaar te verdedigen op
donderdag 18 juni 2020 des middags te 2.30 uur

door

Kamil Gabriël Laban

geboren op 18 januari 1989
te Utrecht

Promotoren: Prof. dr. T.R.D.J. Radstake
Prof. dr. J.H. de Boer

Copromotoren: Dr. R. Kalmann
Dr. J.J.W. Kuiper

Commissie:	Prof. dr. R. Goldschmeding
	Prof. dr. S.M. Imhof
	Prof. dr. M.C. Minnema
	Prof. dr. I. Mombaerts
	Prof. dr. M.P. Mourits
Paranimfen:	Ivo Soliman
	Vincent Laban

CONTENTS

CHAPTER 1	General introduction and thesis outline.	9
CHAPTER 2	Orbital lymphomas missed by first biopsies of orbital masses.	27
CHAPTER 3	A clinical 5-parameter-model for differentiation between non-Hodgkin orbital lymphoma and idiopathic orbital inflammation	33
CHAPTER 4	Severe outcome of idiopathic inflammatory mass lesions primarily located in the posterior orbit and orbital apex.	51
CHAPTER 5	Reflections in the mirror - Idiopathic intracranial hypertension and non-specific orbital inflammation in identical twins.	61
CHAPTER 6.1	Zirconium-89-labelled rituximab PET-CT in orbital inflammatory disease.	67
CHAPTER 6.2	Zirconium-89-labelled rituximab PET-CT imaging of Graves' orbitopathy.	81
CHAPTER 7	A pan-inflammatory microRNA-cluster is associated with orbital non-Hodgkin lymphoma and idiopathic orbital inflammation.	85
CHAPTER 8	cDC2 and plasmacytoid dendritic cells diminish from tissues of patients with non-Hodgkin orbital lymphoma and idiopathic orbital inflammation.	117
CHAPTER 9	Mass-spectrometry imaging of orbital biopsies identifies disease-specific peptide profiles.	145
CHAPTER 10	Summary, general discussion and future perspectives.	157
Appendices	Nederlandse samenvatting (summary in Dutch) Acknowledgements List of publications PhD curriculum vitae About the author	173


Chapter 1

General introduction and thesis outline

Clinical problem and aim

Idiopathic orbital inflammation (IOI) and non-Hodgkin orbital lymphoma (NHOL) are two important orbital diseases, that both can have a difficult and time-consuming diagnostic process.[1–4] Within the diagnostic process, the distinction between the two conditions can especially be complex due to the large variety – as well as similarities – in clinical and radiological features.[2–5] Therefore, the diagnostic process is strongly based on the need for invasive incisional biopsies for histopathology.[1,6,7] However, biopsies in deep orbital localizations can be difficult, with potential non-representative tissue sampling and risk of complications, causing a delay in a final diagnosis and treatment.[1,2,8] Because accurate and timely diagnosis and treatment are critical for both IOI and NHOL,[9,10] there is a need for minimally invasive tools in the diagnostic armamentarium. Additionally, the pathophysiology underlying IOI and NHOL remains largely unknown.[9,11] More knowledge of pathophysiological mechanisms could benefit the development of new diagnostic techniques and management strategies.

In this thesis, we investigate several aspects within the diagnostic process of IOI and NHOL. We aim to improve current diagnostic strategies and explore the potential of new possibilities for minimally invasive diagnostic tools. Additionally, by using state-of-the-art techniques, including untargeted profiling of blood and tissue, we hope to unveil underlying mechanisms that can lead to new insights for future diagnostic strategies.

Orbital mass lesions

The orbits are bony cavities in the scull that contain the eyes and supporting structures for visual function (**Figure 1**). The complex anatomy of the orbit protects the eye from trauma and exposure, but also allows for eye-movement.[12] Additionally, a direct route from the eye to the central nervous system, by the optic nerve, finds its way through the optic canal.[12] Important structures to support the eye and optic nerve are the extraocular muscles, the orbital septum, the eyelids, conjunctiva and the lacrimal apparatus.[12] Eye movement in three axes is facilitated by action of six extraocular muscles, of which five originate from the back of the orbit (orbital apex).[12] Around the extraocular muscles, adipose and connective tissue fill the orbit.[12] Anteriorly, the orbit is enclosed by the orbital septum, extending from the bony orbital rim into the fibrous portion of the eyelids.[12] The extra-ocular muscles, adipose and connective tissue within the orbit, the lacrimal apparatus, conjunctivae and eyelids form the *ocular adnexal structures*. In this thesis we will use the word '*orbit*' to describe the bony cavity including the ocular adnexal structures.

A wide spectrum of disorders can involve the orbit, of which an important subgroup are mass lesions.[6,13] Orbital mass lesions are often slow-growing and patients may not be aware of their presence until orbital or visual changes occur.[14] Due to the bony confinement of the orbit, mass lesions can displace the globe or cause an increased pressure in the orbital apex (orbital apex syndrome). However, there is a variety of symptoms in the presentation of orbital mass lesions due to the abundance of causes. Large patient series indicate that the most frequent causes of orbital mass lesions are orbital lymphoma and inflammatory orbital diseases.[13,15] Consequently, orbital lymphoma is the most common orbital malignancy in adults and nearly all cases are non-Hodgkin orbital lymphoma (NHOL).[9] Inflammatory orbital diseases, however, occur more often than orbital lymphoma. Several inflammatory disorders can present in the orbit, such as thyroid associated eye disease (Graves' orbitopathy), granulomatosis with polyangiitis (former Wegener's disease), sarcoidosis, Sjögren's disease and Immunoglobulin –G type 4 related orbital disease (IgG4-ROD). The most common non-thyroid associated inflammatory condition that presents as orbital mass lesion is IOI.[7]

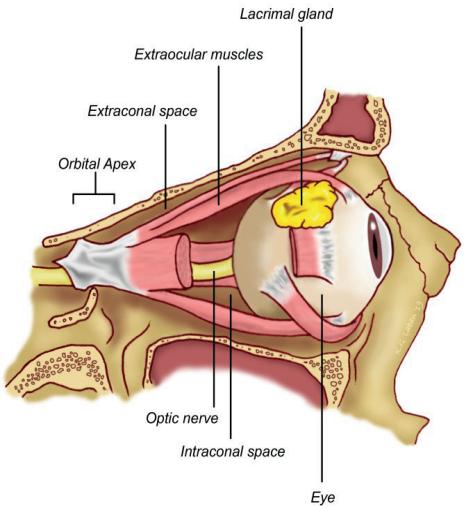

Figure 1. The human orbit holding the eye.

What are IOI and NHOL?

Definition and epidemiology

Patients with an orbital mass lesion of a mixed inflammatory nature were first described as an orbital *pseudotumor* by Birch-Hirschfield in 1905 because of the clinical resemblance to orbital malignancy.[16] The term *pseudotumor* led to confusion on the nature of the disease and more descriptive terms were later introduced including '*orbital inflammatory pseudotumor*', '*non-specific orbital*

inflammation' in contrast to the specific orbital inflammatory disorders. The term '*idiopathic orbital inflammation'* (IOI) has been used commonly in recent literature. To date, IOI refers to family of orbital conditions, and is often used to describe cases with orbital inflammatory masses after excluding all other differential diagnostic considerations.[1,17] Although IOI is reported to be the most prevalent non-thyroid orbital inflammatory disorder and the most common cause of an orbital mass lesion, the exact incidence of IOI is difficult to assess because of varying definitions used across studies.[1] Also, IgG4-ROD was considered as IOI until recently.[18] However, new consensus diagnostic criteria have been proposed that can give rise to more comprehensive epidemiological studies.[1] In several cohort studies, IOI has been observed equally distributed in men and women and occurs predominantly in adults with an average onset at 47 years of age.[10,19]

Nearly all orbital and ocular adnexal lymphomas are considered non-Hodgkin lymphoma (NHL).[20] NHL can arise from clonal expansion of B, T or natural killer (NK) cells, although 97% of cases are B-cell lymphoma.[9] Non-Hodgkin lymphoma is the most common malignancy in the adult orbit, where it comprises 5–10% of all extranodal lymphoma localizations.[9] Most cases of non-Hodgkin orbital lymphoma (NHOL) primarily occur within the orbit, although metastases from systemic disease is also seen.[21] The incidence of NHOL is found to be increasing over time in a rapid rate, with the most recent observations reporting an incidence of 2:100.000 new cases per year for people above 80 years of age.[22] Similar to IOI, NHOL occurrence is equal for men and women,[21] although some subtypes are more common in one of the sexes.[9,21] In contrast with IOI, NHOL presents more often in the elderly with a median age of presentation at 64 years.[21] Occurrence under 40 years of age is rare.[9] Several subtypes can be identified within B-cell NHOL, based on histological properties and cell developmental stage. The most common orbital B-cell lymphoma subtypes are extranodal marginal zone lymphoma (EMZL) in 57–59% of cases, diffuse large B-cell lymphoma (DLBCL) in 15–23% of cases, follicular lymphoma in 9–11% of cases and mantle cell lymphoma (MCL) in 5–8% of cases.[9,21]

IOI and NHOL can be classified on the basis of the localization within the orbit.[23] In this thesis, we used the following localizations: an isolated mass within the orbit in the intraconal or extraconal space; the posterior orbit and orbital apex; the lacrimal gland; the extra-ocular muscles; and diffuse within the orbit affecting multiple localizations.

Staging of NHOL

The Ann Arbor and the *tumour-lymph node-metastasis* (TNM) staging systems are both used for NHOL, although in literature the Ann Arbor staging system is used almost exclusively.[9] The Ann Arbor staging system includes four stages

based on the extend of the disease and metastatic spread (**Table 1**). [24,25] The TNM staging system was developed because the Ann Arbor staging system lacks site-specific information that is needed for prognostic predictions.[9] The TNM staging system is used to support the Ann Arbor system in clinics.

Table 1. Ann Arbor staging system (adapted from Carbone et al.)[25]

Stage	Location of disease
I	A single lymph node (I) or single extralymphatic organ or site (I-E) Without (a) of with (b) the presence of B-symptoms
II	Involvement of two or more lymph nodes on the same side of the diaphragm (II) or extralymphatic organ or site *and* one or more lymph nodes on the same side of the diaphragm (II-E) Without (a) of with (b) the presence of B-symptoms
III	Involvement of lymph nodes on both sides of the diaphragm (III), and extralymphatic organ or site (III-E), or spleen involvement (III-S), or both (III-ES) Without (a) of with (b) the presence of B-symptoms
IV	Diffuse or disseminated involvement of extralymphatic organs or tissue with or without lymph node involvement. Without (a) of with (b) the presence of B-symptoms

Clinical presentation of IOI and NHOL

The clinical presentation of both diseases is dependent on the orbital structure involved and the degree of inflammation or malignancy. Clinical indicators are currently not part of the diagnostic criteria, as they are thought to be largely nonspecific.[1,9]

Several characteristic features of IOI are associated with the classical signs of acute or subacute inflammation.[7] Periorbital or orbital pain is described in up to 70% of IOI patients, and can exacerbate with ocular movement.[10] Eyelid swelling and erythema are common and can be found along other symptoms and signs including the presence of diplopia, a palpable mass, ptosis, visual loss and proptosis.[10,11] Signs of optic nerve compression or involvement might be visible as papilledema in funduscopic examination and can be accompanied by a relative afferent pupillary defect, loss of colour vision and visual field defects. Eye muscle restriction with a paretic or restrictive pattern can be objectified in many patients by orthoptic assessments. Although no dedicated severity score is established for IOI, the modified Werner classification for grading of orbital inflammation is often used, based on clinical assessment.[26,27]

In NHOL, a palpable mass, proptosis and a conjunctival salmon patch are

the most common symptoms based on localization of the tumour.[21] Additionally, they can be accompanied by symptoms that overlap with IOI including pain, diplopia, eyelid swelling, ptosis, redness, chemosis and a decreased visual acuity.[21] B-symptoms are present in a small subgroup of patients.[9] Usually, NHOL has an acute to subacute onset with varying degrees of severity.[11] All subtypes can have features indicating low or high grade disease. Low grade lymphomas are often slow growing and have a long duration of symptoms before diagnosis is acquired (median between 6.5 to 24 months depending on subtype).[9] High grade lymphomas have a more subacute to acute symptom development due to more aggressive growth.

Both IOI and NHOL mostly occur unilaterally, although bilateral occurrence has been described for both diseases.[9,11,21] Bilateral involvement occurs in the NHOL – MCL subtype in up to 45% of the cases.[21]

The role of radiology and laboratory findings in the diagnostic process

Computed tomography (CT) and magnetic resonance imaging (MRI) are commonly used to evaluate the location, extent and nature of IOI and NHOL.[1,6] Lesion enhancement with contrast for CT and MRI are present in both diseases. For IOI, iso- or hypointensity on T2 weighted MRI are typical, while iso- or hyperintensity is more common in NHOL.[28,29] T1 weighted imaging shows a similar intensity for IOI and NHOL (**Figure 2**). Lesion margins can be ill-defined for both diseases, and bony involvement is uncommon. A technique that has shown advancement for the differentiation of malignant and benign lymphoproliferative disease is the diffusion weighted imaging on MRI (DW-MRI), in which the Brownian movement of water molecules is measured.[28,30] Highly cellular tissue and tissue with cellular swelling show more diffusion restriction. Relative to benign lymphoid proliferation, NHOL has been found to show more diffusion restriction,[30,31] showing that the technique can be a valuable addition in the diagnostic process.[31,32] Other imaging techniques include fluorodeoxyglucose (FDG) positron emission tomography–computed tomography (PET-CT), often used in the staging of NHOL, although visibility is not optimal within the orbit.[32]

Blood work-up in IOI and NHOL is generally performed to indicate systemic associations or specific causes of orbital inflammation. Investigations include routine biochemistry (white blood cell count with differential, platelet count, calcium and liver function tests), inflammatory markers (erythrocyte sedimentation rate and C-reactive protein) and an autoimmune panel (antineutrophil cytoplasmic antibody subtype, immunoglobulin type 4, angiotensin converting enzyme, lysozyme).[1] When the lacrimal gland is involved, additional investigation for primary Sjögren's disease and rheumatoid arthritis (anti-Ro and anti-La antibodies, antinuclear antibody, rheumatoid factor, anti-cyclic citrullinated peptide antibody and anticitrullinated

protein antibody) are performed. For localization in the extraocular muscles, thyroid associated hormones and antibodies are investigated to exclude thyroid associated disease.[1] In IOI and NHOL, laboratory findings are usually normal, unless systemic disease or comorbidity occur. The laboratory workup also has an important role in NHOL staging and follow-up.

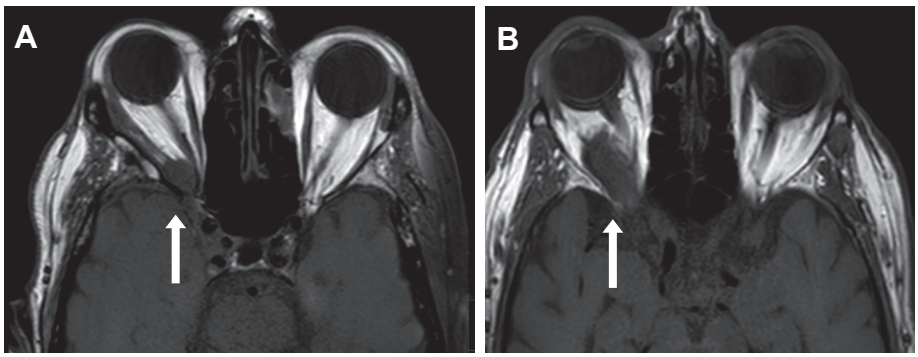

Figure 2. T1 – spin echo magnetic resonance imaging of a patients with an idiopathic orbital inflammation (A) and non-Hodgkin orbital lymphoma of the diffuse large B-cell lymphoma subtype (B). In both cases the mass was located in the right orbit intraconal and included the orbital apex (arrow).

Histopathological evaluation

The diagnostic value of orbital mass lesion biopsies is dependent on the site, size and biopsy technique, sample processing and type of tissue analysis.[6] For the differentiation and diagnosis confirmation, incisional biopsies are preferred over cytological techniques, for the latter loses the architectural features essential in morphological assessment.[6] Techniques used for biopsy analysis include routine histopathological investigation, including histochemistry for the morphological distribution, microorganism detection, and immunohistochemistry for further identification.[6] Clonal rearrangement assessment and molecular testing is being performed more commonly in recent years.[6]

Typically, IOI shows non-specific polymorphous lymphocytic infiltrates with or without the presence of additional immune-cells, such as plasma cells, neutrophils, eosinophils, histiocytes and macrophages.[6,17] Fibrosis of the connective tissue is often seen, and a disproportional amount of fibrosis is termed a "sclerosing" IOI.[1] B cell clonal rearrangement supports a malignant diagnosis.[1] For IOI involving the extra-ocular muscles, a biopsy assessment is uncommon.[1]

Although some lymphoma subtypes have characteristic histopathological profiles, histopathological examination of orbital lymphomas can be challenging.[33] Subtype classification is based on morphological examination, haematoxylin-eosin staining and immunohistochemistry testing for the differentiation of B- and T-cell lymphomas (CD3,CD5, CD20, CD79a) and B-cell lymphoma subtyping (BCL2,

BCL6, CD10, CD23, CD30, Cyclin D-1, MUM-1 and Kappa and Lambda light chains distributions).[9] Additionally, clonal expansion of immunoglobulin heavy chains, amplified with polymerase chain reaction, can confirm B-cell lymphoma when associated morphological and histopathological features are present.[6] Furthermore, translocations can be found with the fluorescence in situ hybridization (FISH) technique. In practice, FISH can be used to assess a prognosis prediction in patients with DLBCL through specific translocations.[9]

Pathophysiology of IOI

The aetiology of IOI remains largely unknown. Generally, there are several signs of immune-related pathology, including the histopathological inflammatory infiltrates and a favourable response to immunosuppressive therapy such as steroid treatment. Molecular analyses of IOI tissue have shown an upregulation of cytokines including interleukin-12, interferon-γ and tumour-necrosis-factor-α, suggesting a pro-inflammatory environment.[34] The involvement of innate pathways is evidenced by increased expression of toll-like-receptor proteins in IOI tissues.[35] Additionally, circulating antibodies against eye muscle membrane proteins have been identified in IOI.[36] Although a history of subclinical infection has been postulated to increase the susceptibility to IOI, these studies remain controversial and inconclusive.[37] Interestingly, transcriptome studies of orbital biopsies identified similarities in gene expression profiles of an IOI subgroup with granulomatosis with polyangiitis.[38]

Pathophysiology of NHOL

In order to support an effective immune system, B cells repeatedly rearrange their genome by VDJ recombination, somatic hypermutation, and class switch recombination, to be able to generate unique antigen receptors.[39] However, this process is error-prone and can result in mutations and translocations of genes promoting clonal proliferation. In B-cell NHOL, several genes have been identified in which translocations or mutations cause a clonal proliferation including *NF-KB1*, *BCL2*, *BCL6*, *MYC*, *EZH2* or *MEF2B* genes.[9] These genetic abnormalities have been found in varying frequency in NHOL subtypes.[40] Additionally, some studies have indicated a chronic inflammatory process preceding the lymphoma development.[9,41] Chronic inflammation in conditions with B cell hyperactivity, such as primary Sjögren's disease, also have an increase in the risk for lymphoma development.[9] Infections are also associated with orbital lymphoma (e.g. *C. psittaci* infection) similar to gastric lymphoma development in patients with *H. pylori* infections.[41] However, the association with infection is less robust in other studies,[9] that are supported by the lack of response to antibiotic treatment compared to gastric lymphoma.[9]

Management and prognosis

The primary treatment goal in IOI treatment is a swift inflammatory suppression to avoid permanent loss of function and to reduce pain and (permanent) dysmorphic appearance alteration.[10] Systemic corticosteroids are the most widely accepted first-line therapy for IOI.[10] Usually, a remarkably rapid response is noticed in an extent that a corticosteroid trial was previously used as diagnostic confirmation for IOI.[1] However, not all cases benefit from corticosteroid treatment and relapses occur often and can be frequent in some patients.[27] To avoid relapses steroid tapering over the course of months has been standard practice, although relapses remain common.[42] Initially, 37% are cured by steroid treatment, while 52% experience recurrences and 12% is steroid dependent.[34] In refractory cases or when steroid sparing treatment is preferred, other systemic immunosuppressive or immunomodulatory treatments including methotrexate, leflunomide, azathioprine, rituximab, infliximab mycophenolate, chlorambucil, cyclophosphamide and radiotherapy have been described.[11,14,27,42] However, there are no clear guidelines to direct management for these cases, and the pathophysiological basis for decision making is scarce.[34] Surgical resection is generally not indicated for IOI.[14]

Management strategies in NHOL are dependent on lymphoma subtype, extension and metastases, prognostic factors, impact on the eye and visual function.[9] The decision for the treatment approach needs to be taken multidisciplinary, and is advised to include an ophthalmologist, radiotherapist and haemato-oncologist.[9] Radiotherapy is the standard treatment of choice for curative treatment, bulk reduction and palliative management. Generally, radiotherapy has a good effect on local control, with commonly used small dose radiation in multiple fractions.[9] Radiotherapy can be supplemented with chemotherapy in case of systemic disease or high-grade aggressive lymphoma subtype.[9] R-CHOP regimen are considered effective in lymphoma patients. Rituxumab monotherapy has been used in several cases,[9] but evidence of clinical trial is limited. Surgery is performed infrequently. The histological subtype, disease extent and disease grade are the most important predictors for disease outcome. Orbital EMZL has a relatively good prognosis, while DLBCL is regarded high-grade and presents more aggressive. Disease specific survival of EMZL has been found to be 88-96% after 5 years, compared to 52-54% in patients with DLBCL subtype.[21] Other common NHOL subtypes include follicular lymphoma (5-year disease specific survival of 78-88%) and MCL (5-year disease specific survival of 47-62%).[9,21] If NHOL is left untreated, there is a high chance of disease progression.[9]

Differential diagnostic considerations

Although IOI and NHOL are the most common non-thyroid associated orbital

mass-lesions,[13] there is a large differential diagnosis that is considered in the diagnostic process.[7,13] Diseases other than IOI and NHOL usually have indicative clinical, radiological or blood-based laboratory characteristics that can aid the diagnostic process. For example, infectious causes presenting as cellulitis or orbital abscess, often have more distinct clinical signs with an acute presentation, including fever, swelling and pain. In these cases, radiological and serology are crucial to confirm diagnosis and biopsies are rarely needed.[7,43] Vascular causes, retained foreign bodies, neurogenic lesions and cystic lesions can also be visualized with conventional imaging techniques.[7,44] Neoplasms have a varying presentation, but can have characteristic features, for example in the medical history.[32,44] For neoplasms, histopathological assessment is needed for confirmation, subtyping and prognostic assessment. Infamously, orbital mass lesions can have atypical presentations and mimic other conditions.[45]

Opportunities in the diagnostic process of IOI and NHOL

The diagnostic process of orbital mass lesions covers clinical aspects, radiological aspects, blood-based laboratory findings and in most cases histopathological examination.

Although the patient characteristics and disease signs and symptoms are critical for suspecting orbital mass lesions, the diagnostic value for disease entities is limited.[1] However, clinical comparisons between IOI and NHOL have not been studied extensively. Some individual factors have been found to differ between IOI and NHOL, although a multivariable analysis or prediction method to assess the discriminative power is currently lacking. Such analysis could provide a more comprehensive clinical distinction that can aid the diagnostic process before biopsy confirmation is acquired.

Imaging can be used to assess radiological characteristics of orbital mass lesions. The differentiation of IOI and NHOL is limited for CT and conventional MRI techniques, due to the heterogeneity of radiological characteristics within both diseases, with the exception of DW-MRI.[32] Alternatively, positron emission tomography–computed tomography (PET-CT) is used for staging in NHOL, but does not have an advantage over CT and MRI for lesions confined to the orbit.[32] However, with new available radiotracers specific proteins involved in disease mechanisms can be visualized.[46] These techniques have not been investigated in the orbital mass lesions and their role in IOI and NHOL is therefore unknown.

Standardized blood work-up is important to exclude other conditions in the differential diagnosis, but is usually normal in IOI and NHOL. With the rise of new techniques for blood-based biomarkers, especially in the immune-system, new research options are possible to investigate the potential of blood-based differentiation, described in more detail below. In our aim for minimally invasive

diagnostic tools, we have a great interest in this diagnostic opportunity.

Histopathological assessment through an incisional biopsy is currently used for diagnosis confirmation in orbital mass lesions.[6,7] Several techniques are used to assess biopsy tissues, and more molecular-based techniques are getting available.[6] Yet these molecular techniques are not able to consider morphological distribution, which is important in the histopathological assessment for IOI and NHOL. The potential of molecular techniques that are able to incorporate the morphology within biopsy tissue is currently unknown.

The UMC Utrecht is a tertiary referral center for orbital diseases and is specialized in orbital mass lesions both in clinics and research.[47] In a collaboration with the laboratory of translational immunology and many others, the ophthalmology department in the UMC Utrecht has the means to perform immune-related research that can address opportunities above in the diagnostic process of orbital disease.

Investigating the immune systems of orbital disease

With the complex immunology underlying both NHOL and IOI, advanced immune-profiling techniques can unveil more accurate pathophysiological differences that could have potential for future diagnostics.[48] Phenotyping of various distinct layers of biological information (including DNA, mRNA, microRNA, proteome and the metabolome) can be compared between tissue compartments of serum, circulating cells and tissue material. Measurements with these techniques can be analysed by powerful computational modelling to identify general and disease specific pathways, leading to new diagnostic insights. Additionally, clinical endpoints can be combined with molecular characteristics to provide subgroups, based on molecular classification. In this thesis we will investigate several biological layers for NHOL and IOI using the following techniques:

Techniques used in this thesis:

MicroRNA profiling of blood serum

Micro-ribonucleic acids or microRNAs, abbreviated as *miRNAs*, are small non-coding RNAs that are present in almost all biological materials. Since the first discovery of miRNAs in humans nearly twenty years ago, over 2500 human miRNAs have been identified and annotated in publicly available databases.[49] MiRNAs can be measured using sequencing techniques, microarrays and polymerase chain reaction (PCR) platforms.[50] Functionally, miRNAs interfere with RNA translation to proteins, and have been found to regulate more than half of the protein-coded genome.[51] With this interference, miRNAs orchestrate complex biological circuits, including immune signalling.[51] Functional studies have also revealed the important

role of miRNAs in many biological functions such as developmental timings, cell differentiation, embryogenesis, metabolism, organogenesis, and apoptosis.[49] Changes in the composition of miRNAs are therefore abundantly investigated in profiling studies, and have been linked to many human pathologies including cancer and inflammation.[52–54] MiRNAs can be considered candidate biomarkers that have potential to aid in diagnostics and prognostic prediction.[55,56]

Flow cytometry of circulating immune-cells

Using flow cytometry, immune cells in blood can be characterized and quantified based on surface and intracellular protein expression.[57] Moreover, a detailed phenotype can be obtained by labelling the cells with fluorescent antibodies. The fluorescent intensity of antibodies on the surface or inside a cell can be measured using the absorption and emitting characteristics on laser light of specific wave lengths.[57] With a panel of specific fluorescent antibodies – usually cluster of differentiation markers – discreet cell populations can be gated on the relative intensity for each marker. Gating is most commonly a manual process of selecting populations within populations from a two-dimensional plane, on the presence or absence of the labelled markers. Manual gating has several limitations, including sample related population shifts and biased positioning of gates.[58,59] In contrast, automatic gating of populations with computational algorithms[58–60] uses self-organizing maps and hierarchical clustering to identify clusters of cells based on marker expression levels. Automatic gating is therefore more robust and consistent compared to manual gating.[58–60] Flow cytometry can be performed on several types of tissue and is used in the diagnostic process of several diseases. Phenotyping of peripheral blood mononuclear cells (PBMC) can give a detailed view on the circulatory immune-cell composition.[61]

^{89}Zr-rituximab PET-CT imaging

Positron emission tomography–computed tomography (PET-CT) can be used to locate and visualize a specific administered tracer within the body.[62] Tracers can be selected to target cell types or processes based on uptake of the tracer by a cell or binding to proteins. A tracer is created by labelling a compound with a radioactive isotope that will emit positrons for a certain amount of time, and can be detected by the PET-CT machine.[62] The tracer localization can be annotated to CT images that are simultaneously generated. The most commonly used PET-CT is fluorodeoxyglucose (FDG), labelled with fluor-18 isotopes. High-glucose-using cells incorporate FDG reflecting structures with an increased metabolism, often seen in pathological processes (e.g. cancer and inflammation).[63] However, FDG has limited use in orbital disease because of physiological uptake of the extraocular muscles and strong uptake in the brain.[64] In contrast, antibody based

tracers, such as the 89-Zirconium labelled monoclonal antibody rituximab(^{89}Zr-rituximab), can visualize specific cell-types by binding to CD markers.[65] The ^{89}Zr-rituximab PET-CT binds to CD20, mainly visualizing B-cells and has not been studied extensively. Previous studies showed, however, an excellent uptake in patients with lymphoma.[65,66] Uptake of disorders in the orbit has not been investigated previously.

Mass spectrometry imaging for tissue analysis

Analysis of tissue material with mass spectrometry imaging (MSI), gives rise to a combination of identification and quantification of molecular masses with spatial orientation within the tissue. This combination allows for comprehensive molecular imaging that can separate tissue types by molecular spectra.[68] As the investigation of morphology in the assessment of orbital biopsy tissue is important,[6] MSI may have a potential in identifying molecular profiles for specific areas within biopsy material. Investigated molecules are dependent on the material and MSI technique used, and range in size from metabolites, lipids, peptides, to even full proteins.[69] An example of a technique used for high-throughput MSI is the matrix-assisted laser desorption/ionization (MALDI) system. With this technique, a matrix is applied on tissue cross-sections that assists the ionization of tissue molecules when hit by a laser-beam. The molecules are then accelerated and measured using a time-of-flight (TOF) method in abundance of mass-to-charge ratio (*m/z*).[69] The molecule measurements form a spectrum for each laser-beam shot on the tissue, creating pixels of the whole tissue section. The MSI measurements are co-registered to scans of the tissue stained with haematoxylin and eosin after MSI, to allow histopathological annotations.[70] Area distributions can be compared for specific *m/z* values and computational modelling can further be deployed for discriminant analysis.[71] Importantly, most diagnostic biopsy tissues are stored formalin-fixed and paraffin-embedded (FFPE) for purpose of histopathological examination. This FFPE storing creates a limit for detection in MSI, as the paraffin needs to be removed for analysis, causing a removal of small molecules (metabolites) and lipids.[70] However, untargeted protein and peptide analysis remain possible for FFPE tissue using the MALDI-TOF MSI technique.[70]

Thesis outline

In this thesis, we aimed to improve the diagnostic process of orbital diseases by investigating clinical and immunological aspects of NHOL and IOI. We focused on several aspects within the diagnostic process of NHOL and IOI, and deployed untargeted approaches to unveil pathophysiological mechanisms the could lead to new targets for further investigations.

- To better understand the diagnostic problem, we describe cases of patients where a second biopsy revealed an orbital lymphoma in **chapter 2**.
- The use of clinical parameters to differentiate NHOL from IOI is investigated in **chapter 3**.
- To illustrate that the clinical course can be more severe in specific localizations, the implications of IOI in the posterior orbit and orbital apex are discussed in **chapter 4**.
- The complex pathology underlying IOI is illustrated by identical twins with IOI and idiopathic intracranial hypertension in **chapter 5**.
- As imaging is an important factor to identify the presence of orbital pathology, the potential of the ^{89}Zr-rituximab PET-CT in orbital inflammatory disease is investigated in **chapter 6.1 & 6.2**.
- To elucidate immune-phenotypes underlying patients with NHOL and IOI, we investigate the miRNA profile of blood serum of patients with NHOL and IOI and healthy controls in **chapter 7**, and the immune-cell composition of PBMCs for these groups in **chapter 8**.
- Next, we used the untargeted MSI approach to assess the peptide profiles of NHOL and IOI in biopsy material while retaining the architectural structure in **chapter 9**.

The results of these investigations and the implications for clinics and future research are summarized and discussed in **chapter 10**.

References

1. Mombaerts I, Bilyk JR, Rose GE, et al. Consensus on Diagnostic Criteria of Idiopathic Orbital Inflammation Using a Modified Delphi Approach. JAMA Ophthalmol. 2017;135(7):769-776
2. Eenhorst CAE, Laban KG, Leguit RJ, Radstake TRDJ, Kalmann R. Orbital lymphomas missed by first biopsies of orbital masses. Acta Ophthalmol. 2017;95(8):858-859
3. Yan J, Wu Z, Li Y. The differentiation of idiopathic inflammatory pseudotumor from lymphoid tumors of orbit: analysis of 319 cases. Orbit. 2004;23(4):245-254
4. Gordon LK. Orbital inflammatory disease: a diagnostic and therapeutic challenge. Eye. 2006;20(10):1196-1206
5. Sullivan TJ, Whitehead K, Williamson R, et al. Lymphoproliferative disease of the ocular adnexa: a clinical and pathologic study with statistical analysis of 69 patients. Ophthal Plast Reconstr Surg. 2005;21(3):177-188
6. Mombaerts I, Ramberg I, Coupland SE, Heegaard S. Diagnosis of orbital mass lesions: clinical, radiological, and pathological recommendations. Surv Ophthalmol. 2019;64:741-756
7. Mombaerts I, Rose GE, Garrity JA. Orbital inflammation: Biopsy first. Surv Ophthalmol. 2016;61(5):664-669
8. Dagi Glass LR, Freitag SK. Orbital inflammation: Corticosteroids first. Surv Ophthalmol. 2016;61(5):670-673
9. Olsen TG, Heegaard S. Orbital lymphoma. Surv Ophthalmol. 2019;64(1):45-66
10. Yuen SJA, Rubin PAD. Idiopathic orbital inflammation: distribution, clinical features, and treatment outcome. Arch Ophthalmol (Chicago, Ill 1960). 2003;121(4):491-499
11. Mulay K, Honavar SG. Idiopathic (non-specific) orbital inflammation. Diagnostic Histopathol. 2015;21(1):34-47. doi:10.1016/j.mpdhp.2014.11.005
12. Gospe SM, Bhatti MT. Orbital Anatomy. Int Ophthalmol Clin. 2018;58(2):5-23
13. Shields JA, Shields CL, Scartozzi R. Survey of 1264 patients with orbital tumors and simulating lesions: The 2002 Montgomery Lecture, part 1. Ophthalmology. 2004;111(5):997-1008
14. Neems L, Echalier EL, Subramanian PS. Orbital Tumors and Inflammatory Disorders. Int Ophthalmol Clin. 2018;58(2):181-195
15. Tang W, Hei Y, Xiao L. Recurrent orbital space-occupying lesions: a clinicopathologic study of 253 cases. Chin J Cancer Res. 2013;25(4):423-429
16. Birch-Hirschfeld A. Zur diagnostic and pathologic der orbital tumoren. Ber Dtsch Opthalmol Ges. 1905;32:127-135.
17. Mombaerts I, Goldschmeding R, Schlingemann RO, Koornneef L. What is orbital pseudotumor? Surv Ophthalmol. 41(1):66-78
18. Andrew N, Kearney D, Selva D. IgG4-related orbital disease: a meta-analysis and review. Acta Ophthalmol. 2013;91(8):694-700
19. Günalp I, Gündüz K, Yazar Z. Idiopathic orbital inflammatory disease. Acta Ophthalmol Scand. 2009;74(2):191-193
20. Swerdlow SH, Campo E, Pileri SA, et al. The 2016 revision of the World Health Organization classification of lymphoid neoplasms. Blood. 2016;127(20):2375-2390
21. Olsen TG, Holm F, Mikkelsen LH, et al. Orbital Lymphoma—An International Multicenter Retrospective Study. Am J Ophthalmol. 2019;199:44-57
22. Sjö LD, Ralfkiaer E, Prause JU, et al. Increasing incidence of ophthalmic lymphoma in Denmark from 1980 to 2005. Invest Ophthalmol Vis Sci. 2008;49(8):3283-3288
23. Bijlsma WR, Van 't Hullenaar FC, Mourits MP, Kalmann R. Evaluation of classification systems for nonspecific idiopathic orbital inflammation. Orbit. 2012;31(4):238-245
24. Coupland SE, White VA, Rootman J, Damato B, Finger PT. A TNM-based clinical staging system of ocular adnexal lymphomas. Arch Pathol Lab Med. 2009;133(8):1262-1267
25. Carbone PP, Kaplan HS, Musshoff K, Smithers DW, Tubiana M. Report of the Committee on Hodgkin's Disease Staging Classification. Cancer Res. 1971;31(11):1860-1861
26. Werner SC. Modification of the classification of the eye changes of Graves' disease: recommendations of the Ad Hoc Committee of the American Thyroid Association. J Clin Endocrinol Metab. 1977;44(1):203-204
27. Suhler EB, Lim LL, Beardsley RM, et al. Rituximab therapy for refractory orbital inflammation: results of a phase 1/2, dose-ranging, randomized clinical trial. JAMA Ophthalmol. 2014;132(5):572-578
28. Ferreira TA, Saraiva P, Genders SW, Buchem M V, Luyten GPM, Beenakker J-W. CT and MR imaging of orbital inflammation. Neuroradiology. 2018;60(12):1253-1266

29. Akansel G, Hendrix L, Erickson BA, et al. MRI patterns in orbital malignant lymphoma and atypical lymphocytic infiltrates. Eur J Radiol. 2005;53(2):175–181
30. Haradome K, Haradome H, Usui Y, et al. Orbital lymphoproliferative disorders (OLPDs): value of MR imaging for differentiating orbital lymphoma from benign OPLDs. AJNR Am J Neuroradiol. 2014;35(10):1976–1982
31. Sepahdari AR, Politi LS, Aakalu VK, Kim HJ, Razek AAKA. Diffusion-Weighted Imaging of Orbital Masses: Multi-Institutional Data Support a 2-ADC Threshold Model to Categorize Lesions as Benign, Malignant, or Indeterminate. Am J Neuroradiol. 2014;35(1):170–175
32. Purohit BS, Vargas MI, Ailianou A, et al. Orbital tumours and tumour-like lesions: exploring the armamentarium of multiparametric imaging. Insights Imaging. 2016;7(1):43–68
33. Amin S, Ramsay A, Marafioti T. Diagnostic Pitfalls in "Low-Grade Lymphoma" of the Orbit and Lacrimal Gland. Orbit. 2015;34(4):206–211
34. Wladis EJ, Iglesias B V., Gosselin EJ. Characterization of the Molecular Biologic Milieu of Idiopathic Orbital Inflammation. Ophthalmic Plast Reconstr Surg. 2011;27(4):251–254
35. Wladis EJ, Iglesias B V, Adam AP, Nazeer T, Gosselin EJ. Toll-like receptors in idiopathic orbital inflammation. Ophthal Plast Reconstr Surg. 2012;28(4):273–276
36. Atabay C, Tyutyunikov A, Scalise D, et al. Serum antibodies reactive with eye muscle membrane antigens are detected in patients with nonspecific orbital inflammation. Ophthalmology. 1995;102(1):145–153
37. Bijlsma WR, Kalmann R, Dekkers J, et al. Identification of infectious entities in idiopathic orbital inflammation biopsies. Br J Ophthalmol. 2013;97(5):664–665
38. Rosenbaum JT, Choi D, Harrington CA, et al. Gene Expression Profiling and Heterogeneity of Nonspecific Orbital Inflammation Affecting the Lacrimal Gland. JAMA Ophthalmol. 2017;135(11):1156
39. Dunn-Walters D, Townsend C, Sinclair E, Stewart A. Immunoglobulin gene analysis as a tool for investigating human immune responses. Immunol Rev. 2018;284(1):132–147
40. Takahashi H, Usui Y, Ueda S, et al. Genome-Wide Analysis of Ocular Adnexal Lymphoproliferative Disorders Using High-Resolution Single Nucleotide Polymorphism Array. Invest Ophthalmol Vis Sci. 2015;56(6):4156–4165
41. Ferreri AJM, Guidoboni M, Ponzoni M, et al. Evidence for an Association Between Chlamydia psittaci and Ocular Adnexal Lymphomas. JNCI J Natl Cancer Inst. 2004;96(8):586–594
42. Lutt JR, Lim LL, Phal PM, Rosenbaum JT. Orbital inflammatory disease. Semin Arthritis Rheum. 2008;37(4):207–222
43. Danishyar A, Sergent SR. Orbital Cellulitis. 2019 Jun 18. StatPearls [Internet]. Treasure Island (FL): StatPearls Publishing; 2020
44. Cunnane MB, Curtin HD. Imaging of orbital disorders. In: Handbook of Clinical Neurology. Vol 135; 2016:659–672
45. Selva D, Rootman J, Crompton J. Orbital lymphoma mimicking optic nerve meningioma. Orbit. 2004;23(2):115–120
46. Jauw YWS, Menke-van der Houven van Oordt CW, Hoekstra OS, et al. Immuno-Positron Emission Tomography with Zirconium-89-Labeled Monoclonal Antibodies in Oncology: What Can We Learn from Initial Clinical Trials? Front Pharmacol. 2016;7:131
47. Bijlsma WR. Progress in etiology, diagnosis, and therapy of idiopathic orbital inflammatory disease. Thesis; November 2011.
48. Fong LE, Muñoz-Rojas AR, Miller-Jensen K. Advancing systems immunology through data-driven statistical analysis. Curr Opin Biotechnol. 2018;52:109–115
49. Saliminejad K, Khorram Khorshid HR, Soleymani Fard S, Ghaffari SH. An overview of microRNAs: Biology, functions, therapeutics, and analysis methods. J Cell Physiol. 2019;234(5):5451–5465
50. Pritchard CC, Cheng HH, Tewari M. MicroRNA profiling: approaches and considerations. Nat Rev Genet. 2012;13(5):358–369
51. Baek D, Villén J, Shin C, Camargo FD, Gygi SP, Bartel DP. The impact of microRNAs on protein output. Nature. 2008;455(7209):64–71
52. Solé C, Arnaiz E, Lawrie CH. MicroRNAs as Biomarkers of B-cell Lymphoma. Biomark Insights. 2018;13:117727191880684
53. Marques-Rocha JL, Samblas M, Milagro FI, Bressan J, Martínez JA, Marti A. Noncoding RNAs, cytokines, and inflammation-related diseases. FASEB J. 2015;29(9):3595–3611
54. Mi S, Zhang J, Zhang W, Huang RS. Circulating microRNAs as biomarkers for inflammatory diseases. MicroRNA (Shariqah, United Arab Emirates). 2013;2(1):63–71

55. Larrabeiti-Etxebarria A, Lopez-Santillan M, Santos-Zorrozua B, Lopez-Lopez E, Garcia-Orad A. Systematic Review of the Potential of MicroRNAs in Diffuse Large B Cell Lymphoma. Cancers (Basel). 2019;11(2):144
56. Tuo J, Shen D, Yang HH, Chan C-C. Distinct microRNA-155 expression in the vitreous of patients with primary vitreoretinal lymphoma and uveitis. Am J Ophthalmol. 2014;157(3):728-734
57. Bendall SC, Nolan GP, Roederer M, Chattopadhyay PK. A deep profiler's guide to cytometry. Trends Immunol. 2012;33(7):323-332
58. Saeys Y, Van Gassen S, Lambrecht BN. Computational flow cytometry: helping to make sense of high-dimensional immunology data. Nat Rev Immunol. 2016;16(7):449-462
59. Weber LM, Robinson MD. Comparison of clustering methods for high-dimensional single-cell flow and mass cytometry data. Cytom Part A. 2016;89(12):1084-1096
60. Van Gassen S, Callebaut B, Van Helden MJ, et al. FlowSOM: Using self-organizing maps for visualization and interpretation of cytometry data. Cytometry A. 2015;87(7):636-645
61. Baumgart DC, Metzke D, Schmitz J, et al. Patients with active inflammatory bowel disease lack immature peripheral blood plasmacytoid and myeloid dendritic cells. Gut. 2005;54(2):228-236
62. Berg E, Cherry SR. Innovations in Instrumentation for Positron Emission Tomography. Semin Nucl Med. 2018;48(4):311-331
63. Rahman WT, Wale DJ, Viglianti BL, et al. The impact of infection and inflammation in oncologic 18F-FDG PET/CT imaging. Biomed Pharmacother. 2019;117:109168
64. Valenzuela AA, Allen C, Grimes D, Wong D, Sullivan TJ. Positron Emission Tomography in the Detection and Staging of Ocular Adnexal Lymphoproliferative Disease. Ophthalmology. 2006;113(12):2331-2337
65. Jauw YWS, Zijlstra JM, de Jong D, et al. Performance of 89Zr-Labeled-Rituximab-PET as an Imaging Biomarker to Assess CD20 Targeting: A Pilot Study in Patients with Relapsed/Refractory Diffuse Large B Cell Lymphoma. Glod JW, ed. PLoS One. 2017;12(1):e0169828
66. Muylle K, Flamen P, Vugts DJ, et al. Tumour targeting and radiation dose of radioimmunotherapy with 90Y-rituximab in CD20+ B-cell lymphoma as predicted by 89Zr-rituximab immuno-PET: impact of preloading with unlabelled rituximab. Eur J Nucl Med Mol Imaging. 2015;42(8):1304-1314
67. Bruijnen S, Tsang-A-Sjoe M, Raterman H, et al. B-cell imaging with zirconium-89 labelled rituximab PET-CT at baseline is associated with therapeutic response 24 weeks after initiation of rituximab treatment in rheumatoid arthritis patients. Arthritis Res Ther. 2016;18(1):266
68. Jungmann JH, Heeren RMA. Emerging technologies in mass spectrometry imaging. J Proteomics. 2012;75(16):5077-5092
69. Vaysse P-M, Heeren RMA, Porta T, Balluff B. Mass spectrometry imaging for clinical research – latest developments, applications, and current limitations. Analyst. 2017;142(15):2690-2712
70. Buck A, Heijs B, Beine B, et al. Round robin study of formalin-fixed paraffin-embedded tissues in mass spectrometry imaging. Anal Bioanal Chem. 2018;410(23):5969-5980
71. Ščupáková K, Soons Z, Ertaylan G, et al. Spatial Systems Lipidomics Reveals Nonalcoholic Fatty Liver Disease Heterogeneity. Anal Chem. 2018;90(8):5130-5138


Chapter 2

Orbital lymphomas missed by first biopsies of orbital masses

Christine A.E. Eenhorst
Kamil G. Laban
Roos J. Leguit
Timothy R.D.J. Radstake
Rachel Kalmann

Acta Ophthalmol. 2017 Dec;95(8):858-859.
doi: 10.1111/aos.13350.

A 68-year-old man presented with an 18-month history of painful eye movements, diplopia and proptosis of the right eye, and no past medical history. On examination, a relative proptosis of 5 mm was measured and a computed tomography scan (CT) showed a right inferior muscle swelling (**Figure 1A**). Full systemic work-up and positron emission tomography-CT (PET-CT) showed no abnormalities. A biopsy was performed, showing striated muscle with some fibrosis and a small lymphocytic infiltrate in histopathology (**Figure 1B**). Additional staining showed a cluster of differentiation (CD) 20+ B-cells and CD3+ T-cells consistent with a reactive infiltrate. The patient was treated for idiopathic orbital inflammation (IOI) with steroids.

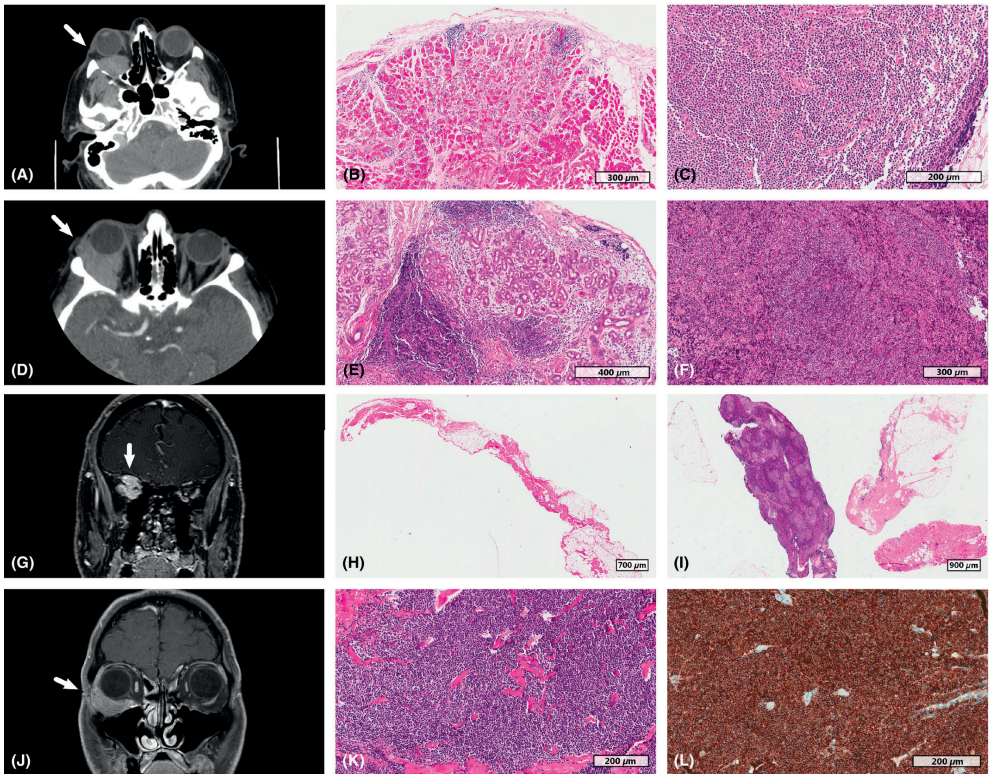

Figure 1. Case I through IV imaging and histopathology. *Case I:* computed tomography (CT) showing a mass (arrow) in the right inferior muscle (A). Initial biopsy (B; haematoxylin and eosin stain (H&E)) showing striated muscle with some fibrosis and a small lymphocytic infiltrate. Secondary biopsy (C; H&E) demonstrates a dense and diffuse infiltrate of small lymphocytes. *Case II:* CT (D) showing a contrast-enhanced supero-lateral orbital swelling (arrow). Initial biopsy (E; H&E) showing atrophic lacrimal glands with several foci of small lymphocytes. Secondary biopsy (F; H&E) demonstrates tissue almost completely infiltrated by small lymphocytes. *Case III:* T1 magnetic resonance imaging (MRI) with gadolinium contrast (G) showing a right apical mass (arrow). Initial biopsy (H; H&E) showing connective and adipose tissue but no lymphocyte infiltrates. A secondary biopsy (I; H&E) demonstrates a diffuse lymphocytic infiltrate. *Case IV:* T1 MRI with gadolinium contrast (J) demonstrated a right anterior-inferior orbital mass (arrow). Secondary biopsy (K; H&E) showed connective tissue diffusely infiltrated by a small cell lymphoid cell population, CD20+ (L).

Five months later however, symptoms recurred with progression of the mass on CT. A secondary biopsy showed a diffuse infiltrate of small CD20+ lymphocytes (Figure 1C), admixed with plasma cells with lambda clonality. Monoclonality was confirmed by polymerase chain reaction (PCR) for B-cell receptor gene rearrangement. A low-grade stage I-E non-Hodgkin orbital lymphoma (NHOL) was diagnosed, with a differential diagnosis of extranodal marginal zone lymphoma (EMZL) or lymphoplasmacytic lymphoma, and treated with curative radiotherapy (30 Gray). One year after treatment, an associated stage IIIa extranodal marginal zone non-Hodgkin lymphoma was found in the soft tissue adjacent to the vertebrae thoracic 6–10, for which chemotherapy (6x R-chlorambucil) is currently given.

A 76-year-old man with a history of a centrocytic lymphoma in the neck region 24 years earlier was referred with diplopia and proptosis of the right eye. Full systemic work-up yielded no abnormalities, but a CT demonstrated a supero-lateral orbital mass (Figure 1D). A biopsy showed atrophic lacrimal glands with several foci of small lymphocytes composed of B-cells as well as T-cells in histopathology (Figure 1E). No B-cell clonality was present. The patient was diagnosed with IOI and treated with steroids. One year after treatment, the proptosis recurred with progression of the mass on CT. A secondary biopsy revealed tissue fragments almost completely infiltrated by small B-lymphocytes (Figure 1F). B-cell monoclonality was confirmed with PCR. After systemic investigation, an EMZL NHOL stage I-E was diagnosed and curative radiotherapy (30 Gray) resulted in full regression.

A 50-year-old man presented with diplopia and no past medical history. Examination revealed a restriction of ocular muscles, and magnetic resonance imaging (MRI) showed an apical mass (Figure 1G). The patient was treated for IOI with steroids, but a slight radiological progression was found on a follow-up MRI 2 months later. A biopsy revealed connective and adipose tissue without lymphocyte infiltrates (Figure 1H). Four months later, the disease progressed and a secondary biopsy showed striated muscle, diffusely infiltrated by small B-lymphocytes (Figure 1I), and monoclonality was proven by PCR. Without systemic abnormalities, an EMZL NHOL stage I-E was diagnosed and curative radiotherapy (30 Gray) was given.

A 55-year-old man was referred for a second opinion of a painless swelling under his right eye, noticed after a fistula treatment of the right upper jaw. Magnetic resonance imaging (MRI) showed a mass in the right orbit (Figure 1J), of which a biopsy revealed adipose tissue, diagnosed as lipoma. Due to incoherence of the biopsy diagnosis with the clinical course, a second biopsy was taken revealing

connective tissue diffusely infiltrated by a small cell lymphoid cell population (Figure 1K &1L), and monoclonality was proven by PCR. Without systemic abnormalities, an EMZL NHOL stage I-E was diagnosed and curative radiotherapy (30 Gray) was given. Currently, the patient is suspected of a systemic recurrence.

Orbital lymphoma can mimic inflammatory orbital disease and other diseases in clinical presentation and imaging.[1-4] In present report, a secondary biopsy was necessary in each case because of either recurring symptoms during treatment, or clinical presentation that did not match with pathology diagnosis. In retrospect, all initial biopsies were not representative, and larger or deeper biopsies were required.

Although orbital biopsies are considered the golden standard for orbital lymphoma diagnosis, in some cases, biopsies are inconclusive or unjustifiably reported as normal.[1,3,5] Also, some localizations of orbital masses can be difficult to approach. Sometimes, a biopsy is not taken deep enough and the diagnosis lOl is only the inflammatory infiltrate surrounding the actual tumour. Ambiguous biopsies can lead to a delay in appropriate treatment, potentially leading to a worse prognosis.
When the clinical course shows signs of malignancy, treatment effect is deferred or symptoms/signs return under treatment, a secondary biopsy should not be delayed. Orbital biopsies should match clinical presentation, and a secondary biopsy must be considered otherwise.

References

1. Gordon LK (2006): Orbital inflammatory disease: a diagnostic and ther apeutic challenge. Eye 20: 1196– 1206.
2. Hwang CS, Diaz-Marchan P & Marx DP (2014): Mucosa-associated lymphoid tissue lymphoma masquerading as herniated orbital fat. Ophthal Plast Reconstr Surg 30: e45– e47.
3. Igarashi T, Shimizu A, Yamaguchi H, Fukushima Y, Igarashi T & Takahashi H (2013): A definitive diagnosis of mucosa-associated lymphoid tissue lymphoma made at a second biopsy. J Nippon Med Sch 80: 475– 480.
4. Polito E, Galieni P & Leccisotti A (1996): Clinical and radiological presentation of 95 orbital lymphoid tumors. Graefes Arch Clin Exp Ophthalmol 234: 504– 509.
5. Ting DS, Perez-Lopez M, Chew NJ, Clarke L, Dickinson AJ & Neoh C (2015): A 10-year review of orbital biopsy: the Newcastle Eye Centre Study. Eye 29: 1162– 1166.


Chapter 3

A Clinical 5-parameter-model for Differentiation between Non-Hodgkin Orbital Lymphoma and Idiopathic Orbital Inflammation

Kamil G. Laban
Ilse Mombaerts
Peerooz Saeed
Stijn W. Genders
Dyonne T. Hartong
Ozlem Köse
Dion Paridaens
Julia Drylewicz
Roos Leguit
Richard M.H.M. van Aarle
Timothy R.D.J. Radstake
Joke H. de Boer
Rachel Kalmann

Submitted

Abstract

Purpose: The diagnosis of non-Hodgkin orbital lymphoma (NHOL) can be challenging, in particular due to clinical overlapping symptoms with idiopathic orbital inflammation (IOI). We therefore investigated the potential of a support model to distinguish NHOL from IOI at initial presentation of disease based on clinical parameters only.

Design: A two phase retrospective cohort study, incorporating a discovery analysis and independent replication.

Subjects: Patients with pathologically proven NHOL or IOI seen between 2000 and 2019 at a single orbital center (discovery phase) and four independent orbital centers (replication phase).

Main outcome measures: Clinical parameters that have discriminatory power between the diagnosis NHOL and IOI.

Methods: Clinical symptoms and signs were recorded and a multivariable regression analysis was deployed. The area under the receiver operator curve (AUC) and positive (PPV) and negative (NPV) predictive values were calculated.

Results: The discovery phase (NHOL=85; IOI=73) revealed that the combination of age, (peri)orbital pain, eyelid swelling, ptosis and proptosis at presentation accurately discriminates between NHOL and IOI (AUC 0.93, PPV 87%, NPV 82% and Nagelkerke R^2 of 68%). Compared to IOI, NHOL was characterized by age ≥60 years and proptosis, without pain, eyelid swelling or ptosis. The model was replicated (AUC 0.92, PPV 87%, NPV 81%) in the independent multi-center cohort (NHOL=130; IOI=90). The model was similarly accurate in sub-analysis for lesions affecting the lacrimal gland or other orbital structures.

Conclusion: A combination of five clinical parameters at initial presentation can make a highly accurate differentiation between NHOL and IOI, regardless of localization. This clinical tool can be useful to support the diagnostic process before acquiring a tissue biopsy. We advise prospective studies to use standardized assessments to confirm these results.

Introduction

Non-Hodgkin orbital lymphoma (NHOL), the most common orbital malignancy in adults, requires early diagnosis and treatment due to the possibility of systemic disease (encountered in 30% of cases).[1] In general, NHOL presents as a slow-onset non-specific mass lesion affecting the orbit or ocular adnexal structures, but can be accompanied by symptoms including (peri-)orbital pain, chemosis and eyelid swelling.[2–4] Distinction from orbital inflammatory disorders, such as the most common 'idiopathic orbital inflammation' (IOI), is therefore necessary.[5,6] The current diagnostic process for orbital masses consists of clinical assessment followed by radiological and laboratory investigations, and an open tissue biopsy for diagnostic confirmation and disease subtyping.[1,6,7]

Importantly, prolonged symptom duration is often present before a final diagnosis is made.[2] For example, in extra-nodal marginal zone lymphoma (EMZL), the most frequent NHOL subtype, symptom duration entails a median of 5 months.[2] Although more diagnostic tools become available,[8] clinical assessment is the corner stone for early stratification in the diagnostic process.[7,9] Assessments at first presentation include medical history taking and a thorough ophthalmological examination. Characteristic features for NHOL and IOI are used as clinical indicators in the diagnostic workup, but are considered non-specific as individual symptoms or signs.[8] However, a combination of parameters may improve the accuracy of the clinical assessment and may aid in the early differentiation of NHOL and IOI. The objectives of our study are: a) to define a set of clinical indicators of NHOL and IOI and b) to validate a comprehensive multivariable model for clinical differentiation between NHOL and IOI.

Methods

Study design

In this retrospective cohort study, we used a discovery and replication approach as outlined in **Figure 1**. Available data were collected and analysed from the medical records of consecutive patients diagnosed with pathologically proven IOI or NHOL between 2000 and 2019 from the University Medical Center Utrecht (UMCU), The Netherlands (discovery phase), and an independent cohort (replication phase) of patients from the orbital clinics of the Amsterdam University Medical Center (AUMC), The Netherlands; University Hospitals Leuven (UHL), Belgium; Rotterdam Eye Hospital (REH), The Netherlands; and Leiden University Medical Center (LUMC), The Netherlands. The study was conducted in conformity with the declaration of Helsinki and its further amendments. The study design was approved by the

Medical Research Ethical Committee of UMCU (Protocol no. 17-166). Institutional Review Board approval for data-collection and transfer were obtained from each participating center (AUMC, UHL, REH, and LUMC).

Study population

All cases of NHOL were classified following the World Health Organization criteria at time of diagnosis with histopathological assessment of incisional biopsies.[10,11] Ancillary histopathological diagnostics were performed on indication and included polymerase chain reaction (PCR) based clonality assessment, translocation analysis with fluorescence in situ hybridization, and specific mutations (including MYD88 mutation).

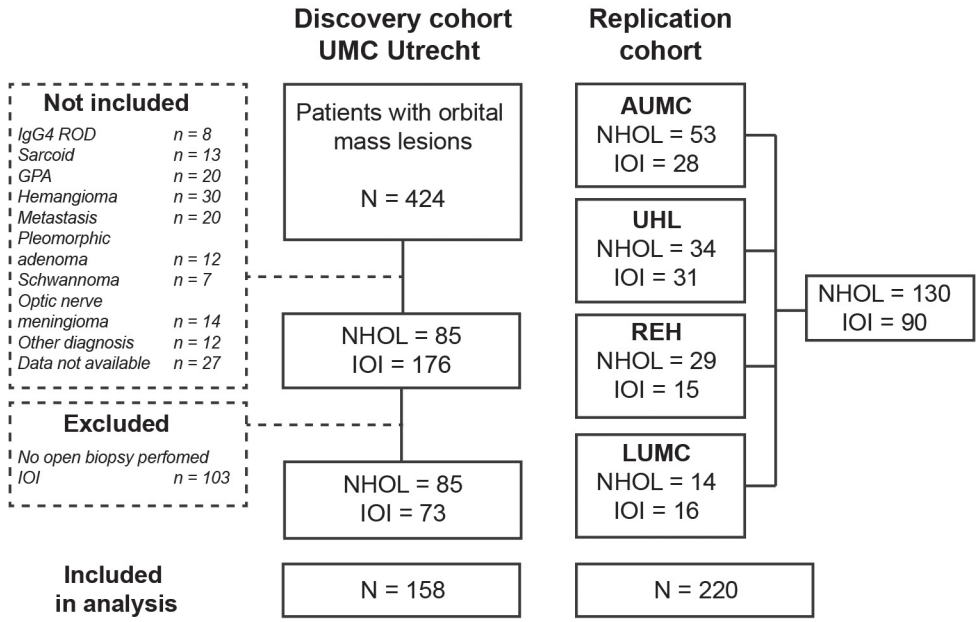

Figure 1. Flowchart of study patients included in this study. The study is divided in a discovery phase (n = 158) and replication phase (n = 220). The reasons for not including subjects and reasons for exclusion are shown for the discovery cohort. Abbreviations: IgG4 ROD = immunoglobulin G-4 related orbital disease; GPA = granulomatosis with polyangiitis; IOI = idiopathic orbital inflammation; NHOL = non-Hodgkin orbital lymphoma; UMC Utrecht = University Medical Center Utrecht, Utrecht, The Netherlands; AUMC = Amsterdam University Medical Center, Amsterdam, The Netherlands; UZL = University Hospitals Leuven, Leuven, Belgium; REH = Rotterdam Eye Hospital, Rotterdam, The Netherlands; LUMC = Leiden University Medical Center, Leiden, The Netherlands.

Patients were diagnosed as IOI based on clinical, serological, radiological imaging and histopathological exclusion of infection, benign or malignant neoplasia, systemic disease, histiocytic disease, thyroid eye disease, granulomatosis with

polyangiitis, sarcoidosis, primary Sjögren's syndrome, benign lymphoid hyperplasia, or IgG4-related pathology.[6,7] We included patients with histopathological tissue confirmation of IOI, ie., non-specific (plasma-) lymphocytic infiltrate, [6,7] with varying amounts of fibrosis between lacrimal, adipose, connective or muscle tissue, with two specimens showing additional non-specific granulomatous infiltration. All specimens were immunostained for IgG4 to exclude IgG4-related orbital disease.[6]

Clinical data

Collected data included patient (age, sex, body mass index, history of inflammatory diseases, immuno-suppressive medication, diabetes mellitus, allergic or atopic constitution, and smoking) and disease characteristics at presentation (symptoms: the(peri)orbital pain, double vision, eye dryness; and signs: vision (decimal) <0.7, restricted eye movement, palpable swelling, proptosis, eyelid oedema, eyelid erythema, upper eyelid ptosis, conjunctival chemosis and injection, papilledema and pupillary defect and presence of B-symptoms). The definitions of the parameters are listed in Supplementary Table 1. Where possible, the recorded clinical data were confirmed with the facial photographs taken at time of initial presentation. We were unable to extract sufficient data on racial background to include in the data analysis.

Statistical analysis.

Percentages were calculated for nominal values, and group means and standard deviations (SD) were calculated for continuous variables with a normal distribution. Univariable group comparisons between NHOL and IOI were performed with the Pearson's Chi-square test or independent samples t-test. Clinically meaningful variables with $P < 0.1$ between the investigated groups were selected for multivariable analysis. No more than one variable per ten cases of the smallest investigated group was allowed. We tested for multicollinearity between the selected variables using the '*collinearity diagnostic*' function from linear regression in SPSS. The discovery phase consisted of 6.8% missing data without pattern (Little's MCAR test P=0.219).[11] We therefore performed a regression-based multiple imputation strategy of 7 imputed datasets with subsequent data analysis of pooled data with SPSS for Windows, version 25.0 (IBM Corp, Armonk, N.Y., USA). We used the R-package "*mice*"[12] to pool and analyse the Pearson's Chi-square statistics using the *micombine.Chi-square* function, and the area under the receiver operator curve (AUC) with 95% confidence interval (95% CI) with the *pool.scalar* function after a logit transformation.

We built the clinical model using a logistic regression with a forward selection of variables in SPSS. The goodness of fit was assessed with the Hosmer-Lemeshow method,[13] and the percentage of variance explained by the model was expressed

with the Nagelkerke R^2.[14] The discriminatory value of the model was tested in a receiver operator curve and resulted in a corresponding AUC with 95% CI and sensitivity, specificity, positive predictive value (PPV) and negative predictive value (NPV) for both the discovery and replication phase. Additionally, a simplified scoring system was calculated and tested, providing a probability for each score. Because our aim was to develop a clinical tool that can be used at presentation, we did not include anatomical localization (often assessed using imaging modalities) in the model. However, to investigate the validity of the clinical model regardless of localization, we performed a sub-analysis for lacrimal gland and other orbital lesions.

Results

Patients and baseline characteristics

From 424 patients with an orbital mass lesion seen at the UMCU, 158 (37%) patients with biopsy proven NHOL (n = 85) and IOI (n = 73) were included for the discovery phase (**Figure 1**). Although we were unable to extract data on the onset of symptoms (acute, subacute or chronic), the median duration (interquartile range) between start of symptoms and first presentation was 67 days (34–158 days) for NHOL and 28 days (14–66 days) for IOI. Baseline characteristics at presentation are presented in **Table 1**. When comparing between NHOL and IOI, we observed differences in age, (peri) orbital pain, eyelid swelling, eyelid erythema, upper eyelid ptosis, and proptosis. The most common location of IOI was the lacrimal gland, while most NHOL were located in extraconal structured other than the lacrimal gland. Orbital lymphoma consisted of several subtypes, of which EMZL was the most common with 53 cases (62%), followed by diffuse large B-cell lymphoma with 16 cases (19%), follicular lymphoma with 12 cases (14%) mantle-cell lymphoma (2 cases, 2%) and small lymphocytic lymphoma (2 cases, 2%).

A set of five discriminatory clinical parameters

To test the combined discriminatory value of the variables between NHOL and IOI, we deployed a multiple logistic regression model on the imputed datasets. Six variables were selected: age, presence of (peri) orbital pain, eyelid swelling, eyelid erythema, ptosis and proptosis. To improve usability of the model, we dichotomized age based on the most optimal cut-off value following the Youden's index[15] (**Supplementary Figure 1**). We did not find signs of multicollinearity between the six variables (variance inflation factor <2.0 and condition index <6.0). However, within the original data and all imputed datasets, the parameter eyelid erythema did not improve the model and was hence excluded. The model of the remaining five

Table 1. Baseline characteristics of the discovery cohort.

Variable	IOI N = 73	NHOL N = 85	MI analysis p-value
Age (years)[a]	49.8 (17)	66.5 (14)	**<0.001**
Age ≥60 years[b]	21 (28.8)	59 (69.4)	**<0.001**
Age range (years)	19–86	33–95	
Female[b]	44 (60.3)	43 (50.6)	0.222
Body mass index[a]	27.3 (5.4)	26.0 (4.9)	0.163
Diabetic[b]	8 (11.0)	13 (15.5)	0.397
Atopic constitution[b]	18 (25.4)	18 (23.4)	0.862
Smoking[b]	17 (29.3)	10 (15.6)	0.162
Bilateral[b]	12 (16.4)	13 (15.3)	0.843
B-symptoms[b]	3 (4.7)	8 (10.8)	0.244
(peri) orbital pain[b]	49 (67.1)	15 (17.6)	**<0.001**
Diplopia[b]	29 (45.3)	27 (33.3)	0.176
Motility reduction[b]	30 (41.1)	28 (33.7)	0.349
Palpable swelling[b]	34 (65.4)	63 (75.9)	0.365
Eyelid swelling[b]	58 (85.3)	25 (31.3)	**<0.001**
Eyelid erythema[b]	35 (59.3)	11 (14.7)	**<0.001**
Chemosis[b]	22 (33.8)	20 (25.6)	0.214
Conjunctival Injection[b]	28 (40.0)	23 (29.9)	0.302
Sicca[b]	12 (19.0)	19 (24.1)	0.575
IOP[a]	17.7 (4.4)	17.7 (4.5)	0.459
Ptosis[b]	39 (55.7)	25 (29.4)	**0.001**
Proptosis[b]	27 (37.0)	44 (52.4)	**0.047**
Vision <0.7 (decimal)[b]	25 (34.2)	20 (23.5)	0.137
Papilledema[b]	2 (2.7)	1 (1.2)	0.726
RAPD[b]	1 (1.4)	2 (2.7)	0.326
Location			
Lacrimal gland[b]	45 (61.6)	23 (27.1)	
Intraconal[b]	2 (2.7)	6 (7.1)	
Extraconal[b]	3 (4.1)	40 (47.1)	
Extraocular muscle[b]	9 (12.3)	2 (2.4)	
Apex[b]	7 (9.6)	2 (2.4)	
Diffuse[b]	7 (9.6)	12 (14.1)	

a = mean (standard deviation), independent samples t-test; b = number (percentage), Pearson's Chi-square test. **Abbreviations:** IOI = Idiopathic orbital inflammation; NHOL = non-Hodgkin orbital lymphoma; MI = multiple imputations; SD = standard deviation; IOP = intraocular pressure; RAPD = relative afferent pupillary defect.

variables (Table 2) showed a good model fitness (Hosmer–Lemeshow P>0.80 in all imputed datasets), and a high variance explanation (Nagelkerke R^2 between 67–68%). The pooled AUC (95% CI) for NHOL was 0.93 (0.87–0.94), corresponding with a high sensitivity (range 82–85%), specificity (range 84–88%), PPV (range 86–89%) and NPV (range 81–83%) within the imputed datasets.

A simplified scoring system was created, including a calculated probability for NHOL diagnosis for individual scores (Table 3). This score was created by converting the smallest beta to a workable number (2) and adjusted all other numbers accordingly to a rounded number. We re-scored all patients and performed a univariable logistic regression to calculate the probabilities.

Table 2. Pooled analysis of the final step (5) of forward conditional stepwise regression

					95% CI	
Variable	B	SE	p-value	OR	Low	High
Age ≥60 years	2.258	0.542	**<0.001**	9.563	3.305	27.671
Pain	-2.908	0.610	**<0.001**	0.055	0.016	0.181
Eyelid swelling	-2,257	0.531	**<0.001**	0.105	0.037	0.296
Upper eyelid ptosis	-2.025	0.562	**<0.001**	0.132	0.044	0.397
Proptosis	1.338	0.562	**0.017**	3.810	1.266	11.463
Constant	*1.874*	*0.567*	*0.001*	*6.516*	*2.144*	*19.801*

Abbreviations: B = beta; SE = standard error; OR = odds ratio (e^B); CI = confidence interval.

Replication cohort

The independent multi-center cohort consisted of 220 patients (81 from AUMC; 65 from UHL; 44 from REH; and 30 from LUMC). Age, (peri) orbital pain and eyelid swelling were significantly different between the two groups (Table 4). Although not significantly different, upper eyelid ptosis and proptosis followed the same trend as in the discovery cohort. Multivariable logistic regression analysis of the 5-parameter-model showed a good model fit (Hosmer Lemeshow P = 0.62) with high explanation of variance (Nagelkerke R^2 of 65%). The AUC (95% CI) for NHOL was 0.92 (0.88–0.96) with a sensitivity of 86%, specificity of 83%, PPV of 87% and NPV of 81%. The model showed a high discriminative power for differentiating NHOL and IOI, corroborating the initial results from the discovery cohort. The ROC curves for both cohorts are depicted in Supplementary Figure 2A.

Subset analysis for lacrimal gland or non-lacrimal gland involvement

For a better clinical appliance of the model, we performed a sub-analysis based on affected orbital structures in the discovery and the independent replication cohorts.

For lacrimal gland lesions, the 5-parameter-model yielded a high discriminatory accuracy with a pooled AUC (95%CI) of 0.94 (0.89–0.97) for

the discovery cohort, with a mean sensitivity of 71%, specificity of 95%, PPV of 88% and NPV of 86% in the imputed datasets. These results were similar for the replication cohort (AUC (95% CI): 0.98 (0.94–0.99), sensitivity: 95%, specificity: 87%, PPV: 83% and NPV 96%).

For non-lacrimal gland lesions of the orbit, the pooled AUC (95% CI) for the model in the discovery cohort was 0.93 (0.86–0.96), with a mean sensitivity of 92%, specificity of 70%, PPV of 88% and NPV of 83% in the imputed datasets. The replication cohort confirmed these results (AUC (95% CI): 0.90 (0.85–0.96), sensitivity: 87%, specificity: 73%, PPV: 85% and NPV 77%. The ROC curves from the two localization for both cohorts are depicted in Supplementary Figure 2B.

Table 3. Simplified clinical score & approximate prediction values

Variable	Score
Age ≥60 years	3
Periorbital pain	-4
Eyelid swelling	-3
Upper eyelid ptosis	-3
Proptosis	2
Total score	...

Total score	P-NHOL (%)
≥2	>95
1	93
0	87
-1	76
-2	61
-3	43
-4	26
-5	15
≤-6	<10

Abbreviations: P-NHOL: prediction value for the diagnosis non-Hodgkin orbital lymphoma for each total score

Discussion

In this study, we identified a set of five clinical parameters to accurately discriminate between NHOL and IOI. Additionally, we were able to replicate and hence validate the 5-parameter-set in an independent multi-center cohort. The model also allowed for accurate discrimination of the two diseases in lacrimal gland and non-lacrimal gland orbital lesions.

A thorough history and physical examination are important initial assessments that can guide tailored ancillary testing in the diagnostic process of orbital mass lesions.[9] However, individual clinical indicators are currently considered non-specific in the diagnostic work-up, as described in the recent consensus on diagnostic criteria for IOI using the Delphi approach.[6] Although we confirm that individual parameters can be considered non-specific, we now show that a combination of signs and symptoms can make a highly accurate differentiation between NHOL and IOI.

These results can therefore be used for early stratification to aid the diagnostic process, before tissue confirmation is available.

Table 4. Characteristics of the replication cohort.

Variable	IOI n = 90	NHOL n = 130	p-value	Adjusted p-value*
Age (Years)[a]	52.4 (13.9)	69.6 (14.4)	**<0.001**[c]	-
Age ≥60 years[b]	30 (33.3)	104 (80.0)	**<0.001**[d]	**<0.001**
(peri) orbital pain[b]	59 (66.3)	12 (9.4)	**<0.001**[d]	**<0.001**
Eyelid swelling[b]	59 (68.6)	50 (39.7)	**<0.001**[d]	**<0.001**
Upper eyelid ptosis[b]	37 (41.1)	40 (34.8)	0.209[d]	0.949
Proptosis[b]	35 (38.9)	79 (63.2)	**<0.001**[d]	0.566

a = mean (standard deviation); b = number (percentage); c = independent samples t-test; d = Pearson's Chi-square test; * = multivariable logistic regression analysis. **Abbreviations:** IOI = Idiopathic orbital inflammation; NHOL = non-Hodgkin orbital lymphoma

In this clinical-model study, radiological imaging and serological results were not included to create the differentiating model. As there is a growing potential in distinguishing benign from highly malignant lymphoproliferative lesions with diffusion weighted imaging as magnetic resonance imaging technique, the combination of radiological and clinical assessments could further improve an algorithm to aid the diagnostic work-up.[16] This could be especially useful for deep orbital mass lesions where morbidity of a tissue biopsy is high.

Clinical differentiation between IOI and lymphoid tumors have been described by Yan *et al* using signs as pain, eyelid swelling, palpable mass, eyelid or conjunctival congestion, retinal folds and hemorrhages.[3] The more frequent presence of pain and eyelid swelling in IOI in their study is in line with our findings. In contrast to Yan's study, however, we did not observe a difference in palpable mass as a clinical indicator. We believe that this is dependent on the anterior localization within the orbit, as lacrimal gland NHOL and IOI more often present as a palpable mass. Likewise, we did not demonstrate a statistical difference for the clinical signs of congestion. Although they can represent inflammation, congestive signs can also occur from a build-up of orbital pressure towards the eye.[17]

Age of onset

Inherent to the nature of both diseases, an age difference is evident between NHOL and IOI. NHOL is more common in elderly, and the incidence is increasing.[18] NHOL, however, can occur in all ages, including in children.[19] In our study, the

mean age was >65 years in both cohorts and the youngest NHOL patient was 33 years of age (Supplementary Figure 1). A presentation at early-adult or adult age is common for inflammatory disorders of the orbit, and an occurrence at any age can be seen.[3]

Pain

Orbital or periorbital pain is considered characteristic of IOI. The pain is often experienced as severe and worse at night-time or with eye-movement, and strongly varies in degree and nature. Besides being part of the classic inflammatory symptoms, it remains unknown why IOI patients often experience more severe pain, compared to other inflammatory conditions within the orbit. Usually, pain is the major complaint in patients with IOI, and the reason for an urgent consultation to an orbital specialist. Objective assessment of the location and pattern of (peri) orbital pain can be difficult, although the time-course during follow-up can be well assessed using the visual analog scale.[20]

Pain in NHOL can be caused by tissue-expansion or bony invasion, which is often encountered in high-grade lymphomas, and is considered unfavourable for the prognosis.[2,4,21] Alternatively, NHOL may be accompanied by a local inflammatory response that causes pain.[4] For proper assessment of (peri) orbital pain, other causes of orbital pain or (unilateral) headaches need to be excluded.

Eyelid swelling

Swelling is, similar to pain, a classic inflammatory symptom. Eyelid swelling occurs in most IOI patients and only a portion of patients with NHOL (up to 40%). The swelling can occur directly as part of the inflammatory process or anterior NHOL, but also indirectly through orbital venous congestion. Consequently, eyelid swelling can contribute to a mechanical upper eyelid ptosis. In cases with extensive swelling a palpable mass can be difficult to assess. Note that eyelid swelling can coexist with eyelid erythema, but this is not exclusive.

Upper eyelid ptosis

Mechanical ptosis can be seen in lacrimal gland lesions for both NHOL and IOI, especially for more anterior localizations. However, IOI that present with a paretic ptosis often have involvement of the levator palpebrae superioris muscle. Note that upper eyelid ptosis can also occur in lesions of the orbital apex when the third cranial nerve is involved.

Proptosis

We found proptosis more frequent in patients with NHOL compared to IOI. This difference could be caused by a more easily volume expansion posteriorly during

tumour growth of NHOL, while, due to the fibrotic component, IOI more often remain confined to anatomical structures. Proptosis was more common in patients with a non-lacrimal gland orbital localization.

Several limitations of this study need to be addressed, that pose considerations for the clinical use of the described model. First, this study is limited by the retrospective nature: non-standardized clinical assessments led to missing data and the lack of parameter metadata. Although we were able to statistically impute missing data with a multiple imputation strategy, we had to limit parameters to a dichotomous value (usually the presence or absence of a variable). Consequently, we were not able to assess important data, including the severity of disease flowing the modified Werner classification.[22,23] Second, as we demonstrate in the sub-analysis, the location of the lesion in the orbit influences the clinical presentation. We were unfortunately unable to assess the model for all sub-localizations due to low case numbers (e.g. intraconal, extraocular muscle, orbital apex). Additionally, we only included patients with a biopsy confirmed IOI. As histological confirmation is not standard in myositis (IOI of the extraocular muscles),[6] the results might deviate for this patient group. Third, clinical assessment can be difficult due to the varying nature in orbital mass-lesions and limitations of measurement techniques. For example, pain can be scored with the visual analogue scale, although intensity throughout the day, nature and exacerbating factors influence this score. Similarly, upper eyelid ptosis can have varying degrees and shapes (e.g. S-shaped). Eyelid swelling is assessed subjectively, and should therefore be photographed for good documentation. In case of changing signs and symptoms, or clinical doubt, the assessed score should be re-evaluated. Fourth, atypical presentation of NHOL can occur and frustrate the diagnostic process, facilitating a severe prognosis in high grade lymphomas.[4] We advise caution with interpretation of the 5-parameter model if there are indications of a high-grade malignant lesion, such as a history of a high-grade lymphoma. However, evaluation of the 5-parameter model shows a comparable accuracy for EMZL and DLBCL patients (**Supplementary Table 2**), indicating a broad usability for the model within NHOL and IOI. Finally, we focussed this study on orbital disorders that reflect the important distinction between benign and malignant and inflammation. However, there are a plethora of other conditions that cause orbital mass lesions.[7] Although other disorders may present with characteristic clinical, radiological imaging and laboratory findings, future studies should include multiple conditions to determine the diagnostic value of current results in relation to other conditions.

Regarding the limitations in this study, we would recommend future prognostic studies to use standardized clinical assessments that rely on objective measurements. For

example, diagnostic facial photographs could play a role in objective assessment of several variables using machine learning algorithms.[24] We also advice to combine clinical, radiological imaging and laboratory findings to further improve the usability of the diagnostic 5-parameter-model. Additionally, multiple orbital conditions could be included to broaden the clinical use. It is important to note that the clinical assessment should be performed before (systemic) corticosteroids are given. Corticosteroids can alter clinical, radiological and pathological findings, and a diagnostic trial has limited value in the diagnostic process.[8]

In conclusion, we found that, independent of the location in the orbit, a combination of the five parameters (age ≥60 years, (peri-)orbital pain, eyelid swelling, ptosis and proptosis) at presentation can highly accurate distinguish NHOL from IOI. We would recommend future studies to use a prospective design with standardized clinical assessments to confirm these results.

Acknowledgements:
We thank Pascale Cooijmans for her valuable help during this study.

References

1. Olsen TG & Heegaard S. Orbital lymphoma. Surv. Ophthalmol. 64, 45–66 (2019).
2. Olsen TG, et al. Orbital Lymphoma—An International Multicenter Retrospective Study. Am. J. Ophthalmol. 199, 44–57 (2019).
3. Yan J, Wu Z & Li Y. The differentiation of idiopathic inflammatory pseudotumor from lymphoid tumors of orbit: analysis of 319 cases. Orbit 23, 245–54 (2004).
4. Sullivan TJ, et al. Lymphoproliferative disease of the ocular adnexa: a clinical and pathologic study with statistical analysis of 69 patients. Ophthal. Plast. Reconstr. Surg. 21, 177–88 (2005).
5. Mombaerts I, Goldschmeding R, Schlingemann RO & Koornneef L. What is orbital pseudotumor? Surv. Ophthalmol. 41, 66–78.
6. Mombaerts I, et al. Consensus on Diagnostic Criteria of Idiopathic Orbital Inflammation Using a Modified Delphi Approach. JAMA Ophthalmol. 135, 769–776 (2017).
7. Mombaerts I, Rose GE & Garrity JA. Orbital inflammation: Biopsy first. Surv. Ophthalmol. 61, 664–669 (2016).
8. Mombaerts I, Ramberg I, Coupland SE & Heegaard S. Diagnosis of orbital mass lesions: clinical, radiological, and pathological recommendations. Surv. Ophthalmol. 64:741-756, (2019).
9. Dagi Glass LR & Freitag SK. Orbital inflammation: Corticosteroids first. Surv. Ophthalmol. 61, 670–673 (2016).
10. Swerdlow SH, World Health Organization & International Agency for Research on Cancer. WHO classification of tumours of haematopoietic and lymphoid tissues.
11. Swerdlow SH, et al. The 2016 revision of the World Health Organization classification of lymphoid neoplasms. Blood 127, 2375–2390 (2016).
12. van Buuren S, Groothuis-Oudshoorn K. mice: Multivariate Imputation by Chained Equations in R. J. Stat. Softw. 45, 1–67 (2011).
13. Hosmer DW. & Lemeshow S. Goodness of fit tests for the multiple logistic regression model. Commun. Stat. - Theory Methods 9, 1043–1069 (1980).
14. Nagelkerke NJD. A note on a general definition of the coefficient of determination. Biometrika 78, 691–692 (1991).
15. Youden WJ. Index for rating diagnostic tests. Cancer 3, 32–5 (1950).
16. Ferreira TA, et al. CT and MR imaging of orbital inflammation. Neuroradiology 60, 1253–1266 (2018).
17. Bahn RS. Graves' ophthalmopathy. N. Engl. J. Med. 362, 726–38 (2010).
18. Sjö LD, et al. Increasing incidence of ophthalmic lymphoma in Denmark from 1980 to 2005. Invest. Ophthalmol. Vis. Sci. 49, 3283–8 (2008).
19. Bakhshi S & Sidhu T. Pediatric orbital and ocular lymphomas. Pediatr. Blood Cancer 50, 940–941 (2008).
20. Seymour RA, Simpson JM, Charlton EJ & Phillips ME. An evaluation of length and end-phrase of visual analogue scales in dental pain. Pain 21, 177–185 (1985).
21. Demirci H, Shields CL, Karatza EC & Shields JA. Orbital lymphoproliferative tumors: analysis of clinical features and systemic involvement in 160 cases. Ophthalmology 115, 1626–31, 1631.e1–3 (2008).
22. Suhler EB, et al. Rituximab therapy for refractory orbital inflammation: results of a phase 1/2, dose-ranging, randomized clinical trial. JAMA Ophthalmol. 132, 572–8 (2014).
23. Werner SC. Modification of the classification of the eye changes of Graves' disease: recommendations of the Ad Hoc Committee of the American Thyroid Association. J. Clin. Endocrinol. Metab. 44, 203–4 (1977).
24. Dawes TR, et al. Objectively measuring pain using facial expression: is the technology finally ready? Pain Manag. 8, 105–113 (2018).

Supplementary Table 1. Definitions of parameters used.

Parameter	Definition
Age	Age in years
Female	Female sex
Body mass index	Weight in kilogram divided by (height in meter)2
Diabetic	Diagnosed with diabetes mellitus type 1 or 2
Atopic constitution	Patients with known allergies, eczema or asthma.
Smoking	Current smoking habit or cessation within three months of presentation
Bilateral	Disease in the contralateral orbit synchronously at presentation, or metachronously two years before or after presentation
B-symptoms	Unexplained fever, extensive sweating during the night or unexplained weight loss (>10%)
(peri-) orbital pain	The subjective notation of pain in or around the orbit, including pain triggered by ocular movement
Diplopia	Binocular double vision in any direction
Motility reduction	Limitation of eye movement, from paretic, mechanic or restrictive origin
Palpable swelling	Presence of a peri-ocular palpable mass, not considering oedematous eyelid swelling
Eyelid swelling	Puffy or oedematous swelling of one or both eyelids of the affected eye, not within normal limits of the non-affected or reference eye
Eyelid erythema	Redness or moderate or severe injection of one or both eyelids of the affected eye, not within normal limits of the non-affected or reference eye
Chemosis	Swelling or oedema of the conjunctiva
Conjunctival Injection	Enlargement of conjunctival vessels
Sicca	Objective signs of corneal dryness (e.g. corneal staining)
IOP	Intra-ocular pressure measured by non-contact or applanation tonometry
Ptosis	Drooping or falling upper eyelid, including of mechanical origin. Ptosis was considered as a margin to reflex (1) measurement of 2 millimetre or less
Proptosis	Anterior globe displacement with a difference of 3 mm or more compared to the non-affected eye or normal reference
Vision <0.7 (decimal)	Vision less than 0.7 decimal
Papilledema	Papilledema found on fundus exam or imaging
RAPD	Relative afferent pupillary defect

Supplementary Table 2. Characteristics of the model for NHOL subtypes.

Variable	IOI *n = 73*	EMZL *n = 53*	DLBCL *n = 16*	IOI vs EMZL	IOI vs DLBCL
Age (Years)[a]	49.8 (16.7)	64.2 (13.3)	76.4 (12.3)	<0.001[c]	<0.001[c]
Age ≥60 years[b]	21 (28.8)	35 (66.0)	14 (87.5)	<0.001[d]	<0.001[d]
(peri) orbital pain[b]	49 (67.1)	7 (13.2)	5 (31.3)	<0.001[d]	0.008[d]
Eyelid swelling[b]	58 (85.3)	14 (26.4)	4 (25.0)	<0.001[d]	<0.001[d]
Upper eyelid ptosis[b]	39 (55.7)	14 (26.4)	6 (37.5)	0.001[d]	0.188[d]
Proptosis[b]	27 (37.0)	26 (49.1)	8 (50.0)	0.147[d]	0.334[d]
5-parameter model	**AUC**	**Sensitivity**	**Specificity**	**PPV**	**NPV**
IOI vs EMZL	0.94	81	90	86	87
IOI vs DLBCL	0.94	65	94	72	93

a = mean (standard deviation); b = number (percentage); c = independent samples t-test; d = Pearson's Chi-square test; * = multivariable logistic regression analysis. **Abbreviations**: IOI = Idiopathic orbital inflammation; EMZL = extranodal marginal zone lymphoma; DLBCL = diffuse large B-cell lymphoma; AUC = area under the receiver operator curve; PPV = positive predictive value; NPV = negative predictive value.

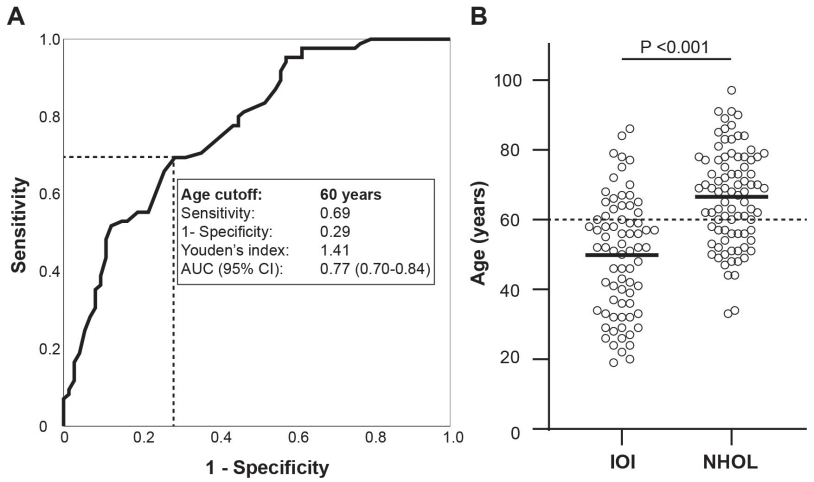

Supplementary Figure 1. Optimal cut-off assessment for age. A. Receiver operator analysis and curve, showing the most optimal age cut-off based on the Youden's index in the discovery cohort (N = 158) B. Scatterplot showing the age distribution for each patient in the two disease groups and the relation to the optimal cut-off (age 60 years; dotted line). The mean age is highlighted with the black bar for the IOI group (N = 85) and the NHOL group (N = 73). Abbreviations: AUC (95% CI) = area under the curve with 95% confidence interval; IOI = idiopathic orbital inflammation; NHOL = non-Hodgkin orbital lymphoma.

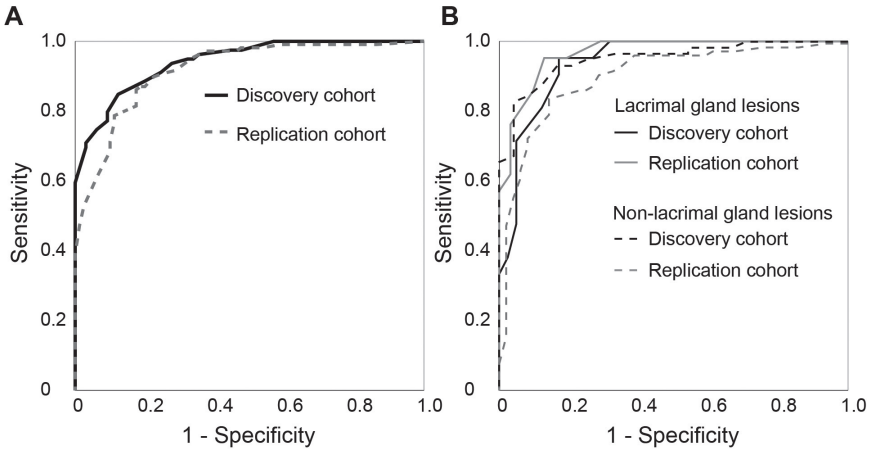

Supplementary Figure 2. Receiver operator curves for the 5-parameter-model. A. The curves represent all the patients in the discovery cohort (solid line, N = 158) and the replication cohort (dashed line, N = 220). B. Receiver operator curves for lacrimal gland lesions in the discovery cohort (solid black line, N = 68) and replication cohort (solid grey line, N = 66), and non-lacrimal gland lesions in the discovery cohort (dashed black line, N = 90) and replication cohort (dashed grey line, N = 154).


Chapter 4

Severe outcome of idiopathic inflammatory mass lesions primarily located in the posterior orbit and orbital apex

Kamil G. Laban
Rachel Kalmann
Roos, J. Leguit
Peter H. Uijttewaal
Timothy R.D.J. Radstake
Joke H. de Boer
Rob L.P. van der Veen

Submitted

Abstract

Purpose: Orbital inflammation can sporadically be located in the posterior orbit and orbital apex, and is often diagnosed as idiopathic orbital inflammation (IOI). Here, we aim to give more insight in the presentation, disease course and treatment outcome of posterior IOI.

Methods: Patients with a suspected IOI of the posterior 1/3rd of the orbit, diagnosed in a tertiary orbital referral center between 2000 and 2018 were investigated. Retrospectively, medical data from patient charts were collected and described. Patients with a favourable and unfavourable outcome were compared.

Results: Eight patients (five males, three females) were included with a suspected IOI of the posterior orbit, of which seven were histologically proven IOI. Treatment regimen consisted primarily of high dose intravenous or oral corticosteroids, reducing clinical activity in six out of eight patients. However, the clinical and visual outcome was poor in five out of eight patients, having no light perception of the affected eye. Of these, two patients deceased related to IOI complications. Patients with a poor outcome were older, had a history of diabetes and had more severe symptoms on presentation.

Conclusion: Posterior IOI can have a serious clinical presentation with a poor outcome, resulting in blindness, severe morbidity and a potentially lethal outcome. Ophthalmologists should be aware of the difficulties in management of posterior IOI.

Introduction

Orbital inflammation is an inflammatory process that causes a mass or enlargement of the structures within the orbit.[1,2] Specific orbital inflammatory disorders include thyroid associated orbitopathy (Graves' disease), sarcoidosis, vasculitis such as granulomatosis with polyangiitis, immunoglobulin G type-4 related orbital disease (IgG4-ROD), giant cell myositis, connective tissue disorders such as primary Sjögren's syndrome, and inflammation associated with conditions like systemic lupus erythematosus and rheumatoid arthritis.[2,3] However, the majority of non-thyroid associated lesions are considered idiopathic orbital inflammation (IOI).[4] IOI is part of the orbital and retro-orbital inflammatory disorders of unknown cause and can present as orbital apex syndrome or Tolosa-Hunt syndrome.[1,5–9] Most IOI's occur within the lacrimal gland or extra-ocular muscles (myositis), while intra- or extraconal or diffuse localization within the orbit is less common.[10] A location in the posterior orbit - including the orbital apex – occurs in sporadic cases.[10]

Diagnosing posterior IOI can be difficult and requires a specific combination of clinical features, radiological imaging, laboratory findings and a surgical biopsy.[2,3] Histological assessment is needed to demonstrate idiopathic or specific orbital inflammatory diseases and rule out malignant pathologies (e.g. lymphoma or metastasis).[3] However, patient morbidity can be high in tissue biopsies of deep orbital mass lesions, outweighing a clinical benefit in some cases.[11] As suggested in previous work[12] and in our experience, posterior IOI's tend to have a severe clinical presentation with poor outcome. We therefore describe patients with suspected posterior IOI and compare characteristics between cases with a favourable or unfavourable outcome.

Methods

This study was conducted in compliance with the Helsinki principles and federal laws in the Netherlands and the study protocol was reviewed and approved by the Utrecht Medical Ethical Research Committee.

Records of patients with suspected IOI, referred to the department of ophthalmology at the University Medical Center Utrecht between 2000 and 2018, were investigated. Primary location of the mass in the posterior orbit was defined as a mass lesion visible with contrast enhanced imaging at presentation, confined within the most posterior 1/3rd of the orbit. Lesions extending in the optic canal or the superior orbital fissure were included. Patients with diffuse orbital inflammation or a mass lesion localized more anteriorly were not included.

The diagnosis posterior IOI was considered in patients with a mass lesion without evidence of infection, malignancy, or a specific orbital inflammatory disorder (e.g. thyroid eye disease, sarcoidosis, vasculitis, IgG4-ROD and connective tissue disorders). Patients were diagnosed based on a combination of clinical indicators, imaging, negative serology and confirmed with histopathology. In one patient, a biopsy was deemed not possible. This patient was diagnosed as suspected IOI, based on a combination of clinical indicators with imaging characteristics of an orbital inflammatory lesion,[1] without clinical, laboratory or imaging characteristics of another diagnosis. The diagnosis was even more probable when clinical disease activity reduced upon therapeutic intervention.

Medical data were collectively described. Dichotomous variables were represented in a number with percentage (%), while continuous variables were represented in mean ± standard deviation (SD) or median with interquartile range (IQR). Due to the rare occurrence, statistical comparison was not possible.

Results

Disease presentation and diagnostic process

Out of 176 patients with suspected IOI, eight (4.5%) patients (five males, three females) had posterior orbital localization. All patients had unilateral disease without a history of eye-disease of the affected eye. The patients all described the start of the symptoms to be subacute with increasing moderate to severe pain, accompanied by a varying degree of visual loss, upper eyelid ptosis and diplopia. At presentation (**Table 1**), median (IQR) Modified Werner score[13] was 23 (20-26) out of 40 (most severe), with (paretic or mechanic) eye-movement limitations. The median duration between symptom onset and presentation was 22 days (IQR 6-75).

Imaging findings

All lesions showed contrast enhancement and were iso- or hypointense compared with extra-ocular muscles. There was extension of the lesion into the cavernous sinus through the superior orbital fissure and a minor extension through the optic canal in two cases (**Figure 1A & B**). In the other six cases, a minor extension within the superior orbital fissure was present, but not in the optic canal (**Figure 1C & D**). All lesions showed mass effect in respect to the optic nerve (**Figure 1**).

Biopsy analysis

Histopathological analysis was performed in seven patients, with one patient that could not be biopsied due to several cardiovascular and musculo-skeletal

Table 1. Patient and disease characteristics based on visual outcome.

Variable	All	Visual outcome <0.5	Visual Outcome ≥0.5
Total patients[a]	8	5	3
Age (year)[b]	66.3 (14.2)	74.2 (12.1)	53.0 (3.3)
Sex (female)[a]	3 (38%)	1 (20%)	2 (67%)
Diabetes[a]	3 (38%)	3 (60%)	-
BCVA at presentation[a]			
NLP	3 (38%)	3 (60%)	-
LP-0.05	2 (25%)	1 (20%)	1 (33%)
0.05-0.5	1 (13%)	-	1 (33%)
0.5-0.7	2 (25%)	1 (20%)	1 (33%)
Total ophthalmoplegia[a]	3 (38%)	1 (20%)	2 (67%)
IOP ipsilateral[b]	18.2 (6.6)	13.8 (1.5)	24.3 (6.0)
IOP contralateral[b]	17.3 (3.9)	14.8 (1.6)	20.6 (3.4)
Motility reduction[a]			
moderate	3 (38%)	2 (40%)	1 (33%)
severe	5 (63%)	3 (60%)	2 (67%)
Modified Werner criteria[c]	23 (20-26)	24 (21-26)	23 (20-25)
Onset to ophthalmologist (days)[c]	22 (6-75)	15 (6-62)	22 (14-64)
Treatment[a]			
Oral prednisone only	2 (25%)	1 (20%)	1 (33%)
IV MP + oral prednisone	6 (75%)	4 (80%)	2 (67%)
Additional treatment[a]	2 (25%)	1 (20%)	1 (33%)
Initial response[a]			
Visual improvement	3 (38%)	-	3 (100%)
Pain improvement	7 (88%)	5 (100%)	2 (67%)
Motility improvement			
Follow-up (months)[c]	18 (7-30)	8 (3-45)	22 (18-24)
Visual and clinical outcome[a]			
NLP	5 (63%)	5 (100%)	-
LP-0.05	-	-	-
0.05-0.5	-	-	-
0.5-1.0	3 (38%)	-	3 (100%)
Residual Pain (mild)	2 (25%)	1 (20%)	1 (33%)
Residual Pain (moderate/ severe)	3 (38%)	2 (40%)	-
Deceased during follow-up	3 (38%)	3 (60%)*	-

*in two patients related to the IOI. a = number (%), b = mean (standard deviation), c = median (inter quartile range) Abbreviations: BCVA = best corrected visual acuity, NLP = no light perception, LP = light perception, IOP = intraocular pressure, IQR = interquartile range, MP = methylprednisolone

comorbidities, and high age (87 years). In six cases, an open biopsy was performed through lidcrease approach or endoscopic procedure including decompressive surgery. Material from the remaining case, however, was obtained at post-mortem autopsy. Histopathology yielded non-granulomatous polymorphous lymphocytic infiltrates, three with severe sclerosis. Alongside lymphocytes, eosinophils, histiocytes, neutrophils and polytypic plasma cells were present within the IOI infiltrates. Immunostaining for IgG4 was negative. No pathogenic microbes were found in any of the specimen, and no granulomatous infiltration was found.

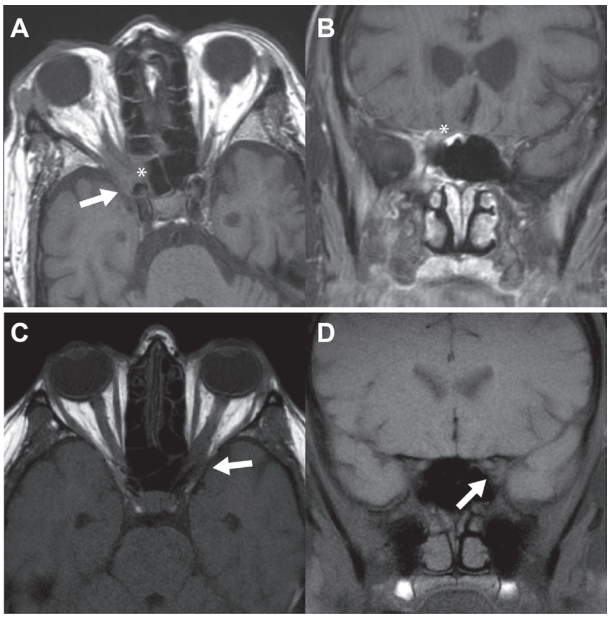

Figure 1. Examples inflammation of the posterior orbit. A & B. T1 weighted MR imaging in axial (A) and coronal (B) planes of a patient with an IOI of the posterior orbit. There is extension of the lesion through the orbital fissure (arrow) and the optic canal (asterisk). C & D. A second patient with an IOI of the posterior orbit with extension of the lesion in the orbital fissure (arrow) on a T1 weighted MR imaging in axial (C) and coronal (D) planes.

Treatment

All patients were treated with corticosteroids (**Table 1**), either oral prednisone (60mg/ day with a three-month tapering schedule) and/or at least one intravenous (i.v.) methylprednisolone course (500 or 1000 mg/ day for three consecutive days) followed by tapering of oral corticosteroids (20 mg prednisone/day). Methylprednisolone dosage depended on disease severity and additional courses were given if the response was not satisfactory. In two cases, additional treatments were administered: in one patient radiation therapy (10x2 Gy) and azathioprine (150 mg/day) without improvement; and another receiving rituximab (2x1000mg i.v.) leading to a full recovery.

Outcome

The median follow-up time was 18 months (IQR 7-30 months), and was shorter for three patients that deceased. Improvement of pain during steroid treatment was substantial in seven patients, leaving one patient with a confirmed IOI not responding to corticosteroids and additional treatments. At the end of the follow-up time, one patient with initial improvement had IOI recurrences, resulting in severe pain when prednisone was tapered until a non-related death. Visual acuity improved in three patients to >0.5 decimal, but deteriorated in five patients to no light perception. A comparison of patients with a favourable and unfavourable visual acuity is presented in Table 1. Although the outcome groups are too small to perform statistic testing, patients with a more severe outcome were generally older (74±12 years versus 53±3.3), presented with a low visual acuity of 0.1 decimal (80% versus 67%) and were diabetic in the majority of cases (60% versus 0%).

Two patients had complications of their (biopsy confirmed) IOI that resulted in premature decease. The first patient did not respond to treatment and developed a severely painful blind eye, with persisting pain after eventual enucleation. In combination with a concurrent mental health condition, the patient later committed suicide. The second patient suffered from a subarachnoid haemorrhage because of IOI ingrowth into the cavernous sinus and internal carotid artery as shown by autopsy.

Discussion

In this study, we describe seven cases of posterior IOI and one suspected posterior IOI. An overview of the clinical findings shows that all patients had a sub-acute presentation with severe (peri) orbital pain and varying amounts of vision loss. After treatment with either oral or i.v. corticosteroids, five patients (63%) had an unfavourable outcome with no light perception of the affected eye, severe pain in two patients and IOI related mortality in two patients.

Yuen et al. described a subset of six patients with apical IOI from a large IOI cohort, reported a lack of response to treatment.[14] Additionally, IOI with retro-orbital extension were found to have a poor outcome with partial or no relief of symptoms after treatment in 7 out of 8 patients,[12] corroborating our findings of a difficult management and a severe prognosis of posterior IOI. In comparison to IOI in other localizations, we found a higher age (mean age 67 years versus 45 years) and more male-to-female ratio (5:3 versus 1:5).[14] This leads to believe that patients with posterior orbit or apical IOI are generally older and male. We found that these factors (age and sex), in combination with a history of diabetes and low visual acuity (<0.1 decimal) during presentation, were more frequent in patients with a poor outcome.

In contrast to the typical Tolosa-Hunt syndrome, in which visual acuity is usually not affected, the majority of patients in our study presented with or resulted in a poor visual acuity. Tolosa-Hunt syndrome is most commonly described as a granulomatous inflammatory condition that affects the orbital apex, superior orbital fissure and cavernous sinus.[9,15] The distinction between an isolated posterior IOI and Tolosa-Hunt, however, can be unclear.[6,15]

Once IOI of the posterior orbit is diagnosed, treatment should be ensued rapidly in our opinion. In almost all our cases there was initial relief of pain on high-dose steroid treatment. However, visual acuity did not improve, and deteriorated further in some patients. We believe that this is due to lasting mass effect on the tissues surrounding the optic nerve and cranial nerves within the tight space of the orbital apex, even after decongestion by steroids. Therefore, steroid treatment alone is not always sufficient for treating IOI of the posterior orbit. Additionally, sclerosing-type idiopathic orbital inflammation is known to be treatment resistant and additional secondary treatment is often necessary.[16] [12] Although corticosteroids remain the mainstay treatment, other treatments such as radiation therapy[17] and immunomodulation therapy with rituximab[18] could add to mass reduction and contribute to further and long-lasting decongestion of the inflamed tissue. This is corroborated by one patient successfully treated with rituximab in this study, having a favourable outcome. Further research for additional management strategies regarding early and more aggressive treatments in posterior orbital inflammation, is warranted and could lead to better outcomes in the future.

This study has limitations due to the retrospective nature and few numbers, not allowing for group comparisons. We hope that this study can help the clinician to be aware of the diagnosis of IOI in the posterior orbit when confronted with a patient with severe (peri) orbital pain, headaches and/or diplopia and severe vision loss, hence preventing a poor clinical outcome by initiating an early and extensive treatment regime.

Conclusion

Posterior IOI tends to have a serious clinical presentation with severe orbital pain, loss of visual acuity and poor outcome after treatment. Although initial treatment can be effective to reduce pain, visual acuity improvement is often absent. Adequate diagnosis, including a biopsy if possible, and early treatment with high dose (i.v.) corticosteroids are pivotal to prevent further loss of visual acuity after initial presentation. Corticosteroids remain the mainstay of treatment, but additional immunosuppressive treatments such as rituximab may be effective.

References

1. Lutt JR, Lim LL, Phal PM, Rosenbaum JT. Orbital inflammatory disease. Semin Arthritis Rheum. 2008;37(4):207–222.
2. Mombaerts I, Rose GE, Garrity JA. Orbital inflammation: Biopsy first. Surv Ophthalmol. 2016;61(5):664–669.
3. Mombaerts I, Bilyk JR, Rose GE, et al. Consensus on Diagnostic Criteria of Idiopathic Orbital Inflammation Using a Modified Delphi Approach. JAMA Ophthalmol. 2017;135(7):769–776.
4. Shields JA, Shields CL, Scartozzi R. Survey of 1264 patients with orbital tumors and simulating lesions: The 2002 Montgomery Lecture, part 1. Ophthalmology. 2004;111(5):997–1008.
5. Borchard NA, Nayak J V. Orbital Apex Syndrome. N Engl J Med. 2018;378(17):e23.
6. Goyal P, Lee S, Gupta N, et al. Orbital apex disorders: Imaging findings and management. Neuroradiol J. 2018;31(2):104–125.
7. Gordon LK. Orbital inflammatory disease: a diagnostic and therapeutic challenge. Eye. 2006;20(10):1196–1206.
8. Weber AL, Romo L V, Sabates NR. Pseudotumor of the orbit. Clinical, pathologic, and radiologic evaluation. Radiol Clin North Am. 1999;37(1):151–168, xi.
9. Zurawski J, Akhondi H. Tolosa-Hunt syndrome--a rare cause of headache and ophthalmoplegia. Lancet (London, England). 2013;382(9895):912.
10. Bijlsma WR, Van 't Hullenaar FC, Mourits MP, Kalmann R. Evaluation of classification systems for nonspecific idiopathic orbital inflammation. Orbit. 2012;31(4):238–245.
11. Dagi Glass LR, Freitag SK. Orbital inflammation: Corticosteroids first. Surv Ophthalmol. 2016;61(5):670–673.
12. Li Y, Lip G, Chong V, Yuan J, Ding Z. Idiopathic Orbital Inflammation Syndrome with Retro-Orbital Involvement: A Retrospective Study of Eight Patients. Rosenbaum JT, ed. PLoS One. 2013;8(2):e57126.
13. Werner SC. Modification of the classification of the eye changes of Graves' disease: recommendations of the Ad Hoc Committee of the American Thyroid Association. J Clin Endocrinol Metab. 1977;44(1):203–204.
14. Yuen SJA, Rubin PAD. Idiopathic orbital inflammation: distribution, clinical features, and treatment outcome. Arch Ophthalmol (Chicago, Ill 1960). 2003;121(4):491–499.
15. Lueck CJ. Time to retire the Tolosa-Hunt syndrome? Pract Neurol. 2018;18(5):350–351.
16. Hsuan JD, Selva D, McNab AA, Sullivan TJ, Saeed P, O'Donnell BA. Idiopathic sclerosing orbital inflammation. Arch Ophthalmol (Chicago, Ill 1960). 2006;124(9):1244–1250.
17. Prabhu RS, Kandula S, Liebman L, et al. Association of Clinical Response and Long-term Outcome Among Patients With Biopsied Orbital Pseudotumor Receiving Modern Radiation Therapy. Int J Radiat Oncol. 2013;85(3):643–649.
18. Suhler EB, Lim LL, Beardsley RM, et al. Rituximab therapy for refractory orbital inflammation: results of a phase 1/2, dose-ranging, randomized clinical trial. JAMA Ophthalmol. 2014;132(5):572–578.


Chapter 5

Reflections in the mirror – Idiopathic intracranial hypertension and non-specific orbital inflammation in identical twins

Kamil G. Laban
Jonas J. W. Kuiper
Rachel Kalmann
Joke. H. de Boer
Timothy R. D. J. Radstake

Acta Ophthalmol. 2017 Jun;95(4):e339-e340.
doi: 10.1111/aos.13286

Editor,

In August 2013, a 17-year-old girl presented with progression of severe headaches accompanied with double vision for 2 weeks. Ophthalmologic examination showed bilateral papilledema and right-sided abducens paresis. Whilst extensive neurological screening (CT and MRI) showed no abnormalities, lumbar puncture revealed an increased intracranial pressure (>50 cm H2O, with normal CSF constituency) supporting the diagnosis of idiopathic intracranial hypertension (IIH). A successful ventriculo-peritoneal shunt was placed. Two years later however, the patient returned with a painful and red left eye. Ophthalmologic examination revealed impaired abduction caused by a diffuse swelling of the left medial rectus muscle (Figure 1A & 1B). After exclusion of systemic involvement, the patient was diagnosed with non-specific orbital inflammation (NSOI) and successfully treated with oral prednisolone.

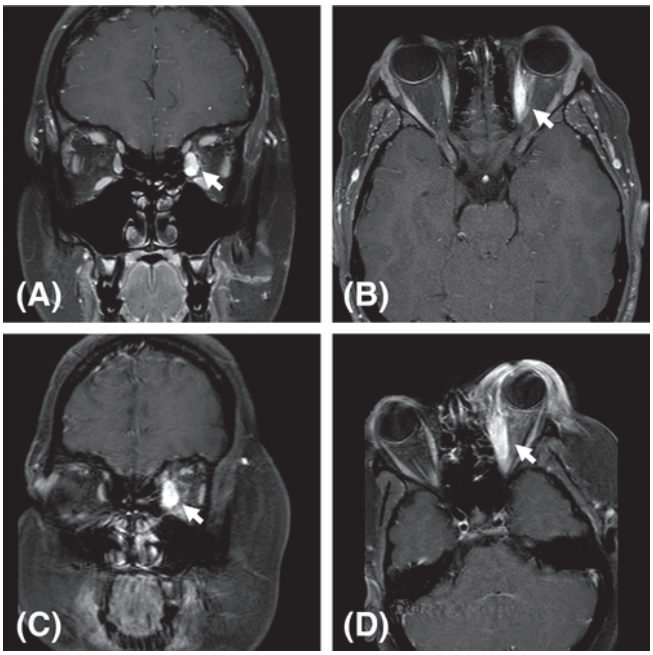

Figure 1. Gadolinium-enhanced T1 magnetic resonance imaging revealing a swelling of the medial rectus muscle of the left eye (arrows) of the first patient in coronal plane (A) and transversal plane (B), and the second patient in the coronal plane (C) and transversal plane (D).

In November 2013, the identical twin presented with severe pain on eye movement of the left eye. Examination showed a significant proptosis and MRI revealed an enlargement of the left medial rectus muscle, exactly at the same location as her

sister (Figure 1C & 1D). Without abnormalities in systemic workup, the diagnosis of NSOI was established. Treatment was initiated with 3-day IV methylprednisolone (500 mg) followed by oral prednisolone, with a good response. In contrast to her sister, multiple relapses occurred for which additional therapies were given, including methotrexate, biologics, radiotherapy and IV immunoglobulins with minimal results. Eighteen months after diagnosis, the patient returned with a diffuse headache, decreased visual acuity and papilledema bilaterally. CT and MRI of the cranium showed no abnormalities, but lumbar puncture revealed an increased intracranial pressure (>50 cm H2O, with normal CSF constituency). Similar to her sister, a ventriculo-peritoneal shunt was placed. Until today, oral prednisone is needed for treatment of her NSOI. No other family members were affected by any of the symptoms or diagnoses.

NSOI is a benign, non-infectious, inflammatory disease of which the diagnosis is based on exclusion of specific local or systemic causes.[1] A biopsy should be performed when malignancy is suspected or no effect of treatment is noticed.[2] Relapses after treatment occur frequently and NSOI can remain refractory.[1]

IIH is a disorder with signs and symptoms of raised intracranial pressure, with no established pathogenesis.[3] The predominant clinical feature of IIH is headache, although diagnosis is made through a combination of increased intracranial pressure with either papilledema or a 6th nerve palsy.[3] Treatment consists of lifestyle, pharmaceutical and/or surgical interventions. Early and adequate treatment is needed to prevent permanent visual loss.

IIH and NSOI can have overlapping clinical features complicating individual diagnosis. A clinical tool for differentiation is the distinction between paresis and mechanical limitation of eye movement.

Within literature, no cases of coexisting IIH and NSOI have previously been reported, and the conditions were previously considered unrelated. Several reports in families suggest possible (epi)genetic factors that confer risk for developing these conditions.[1,3,4] However, no genetic loci have yet been linked to either conditions. The co-occurrence of IIH and NSOI reported here in twins, with presentation in reversed order within a time period of 2 years, suggests possible shared disease mechanisms. An association between IIH and NSOI can be used in future research for both conditions.

References

1. Yuen SJ & Rubin PA. (2003): Idiopathic orbital inflammation: distribution, clinical features, and treatment outcome. Arch Ophthalmol 121: 491– 499.
2. Bijlsma WR, Elbert NJ & Kalmann R. (2012): The role of biopsy in diagnosing patients suspected of idiopathic orbital inflammation. Curr Eye Res 37: 251– 253.
3. Markey KA, Mollan SP, Jensen RH & Sinclair AJ. (2016): Understanding idiopathic intracranial hypertension: mechanisms, management, and future directions. Lancet Neurol 15: 78– 91.
4. Jacob M, Ollagnon Roman E & Vighetto A. (2007): Familial orbital myositis. J Neurol 254: 666– 667.


Chapter 61

Zirconium-89-labelled rituximab PET-CT in orbital inflammatory disease

Kamil G. Laban
Rachel Kalmann
Roos J. Leguit
Bart de Keizer

EJNMMI Res. 2019 Jul 30;9(1):69.
doi: 10.1186/s13550-019-0530-9.

Abstract

Background: Orbital inflammatory diseases are a heterogenic group of conditions that often entail a difficult diagnostic process and many patients are treatment resistant. Inflammatory diseases can be visualized by Zirconium-89-labelled rituximab PET-CT (^{89}Zr-rituximab PET/CT). In this study, we describe our experience and possible potential of the ^{89}Zr-rituximab PET/CT for diagnostic and therapeutic management of refractory orbital inflammation.

Results: Retrospectively, ^{89}Zr-rituximab uptake was assessed and related to clinical data. The main outcome measures were the characteristics of the scan and the clinical relation of uptake with the diagnostic process and treatment effectivity. Twelve patients with thyroid eye disease (TED) and suspected idiopathic orbital inflammation (IOI) were scanned. Six patients had a strong ^{89}Zr-rituximab uptake and showed a focal distribution within the lesion. Four patients (one TED, three IOI) responded well to rituximab treatment after a positive scan. ^{89}Zr-rituximab PET/CT was essential to the diagnosis of optic nerve meningioma in one patient.

Conclusion: ^{89}Zr-rituximab PET/CT has the potential to be a powerful tool for the detection of B cell-mediated disease within the orbit and ocular adnexa. This technique can be a valuable addition for diagnosing diseases around the eye and can potentially predict rituximab treatment response in patients with refractory inflammation.

Background

Orbital inflammatory disease comprises of several inflammatory conditions around the eye with different underlying causes.[1] The most common and well-studied cause is thyroid-associated eye disease (TED), while non-thyroid associated orbital inflammation can be a diagnostic challenge and most are considered idiopathic orbital inflammation (IOI).[2,3] The most important challenge is the differentiation from malignant entities, especially lymphoid malignancies, because of the grave therapeutic consequences. Currently, the best diagnostic tool available is to perform a biopsy of the orbital process with immunohistochemistry.[3] A biopsy is, unfortunately, not always deemed possible because of deep localization behind the eye and the related risk of complications.[4] From a pathological point of view, biopsies of orbital inflammation often reveal a lymphoplasmacytic infiltrate consisting of (cluster of differentiation (CD) 20+) B cells, CD5+ T cells and polytypical plasma cells. Imaging modalities that can directly detect elements of the pathophysiology of the disease, such as CD20+ B cells, may therefore have potential as an aid in the diagnostic process and management strategies. CD20+ B cell infiltrates have previously been visualized in patients with immune diseases and lymphoma with Zirconium-89-labelled (^{89}Zr) rituximab positron emission tomography-computed tomography (PET-CT).[5,6,7] The use of ^{89}Zr-rituximab PET/CT in orbital disease has not yet been investigated. Here, we describe our experience and the potential of this technique in aiding in the diagnosis of refractive orbital inflammation.

Methods

In this retrospective study, we included 12 patients with an ^{89}Zr-rituximab PET/CT in the University Medical Center Utrecht for ophthalmologic pathology. The scans were performed because of suspected orbital inflammatory disease refractory to standard treatment. In five patients, the use of rituximab was considered as alternative treatment and it was given in four patients. At the time of the scan, all patients were rituximab naïve. The standard therapy for IOI and TED consisted of oral prednisone regimen (60 mg) tapered over 3 months or intravenous (IV) methylprednisolone (500–1000 mg/day for 3 days depending on the severity of disease), with the continuation of oral prednisone or IV methylprednisolone regimen in case of insufficient response. Refractory to standard therapy was defined as intolerance, failure to respond to, or inability to taper oral prednisone treatment, the use of multiple IV methylprednisolone regimens or systemic immunosuppressive treatment (adapted from Suhler et al.[8]). IOI was diagnosed by assessing clinical indicators, MRI imaging and an extensive laboratory panel and whenever possible a biopsy.[9] A biopsy for diagnostic confirmation was possible for all IOI except for

one IOI located within the orbital apex (case 1). One patient was diagnosed with IgG4-related orbital disease (IgG4+ ROD). The research team investigated clinical data, laboratory workup, and histopathology.

Table 1. Representation of the cases for diagnosis and PET/CT intensity values

Case	Final diagnosis	Location	Biopsy	Pain	RAPD	Proptosis (Hertel in mm)	BCVA (decimal)	PET SUVmax lesion	PET SUVmax bone marrow	PET SUV max LN level 2
1	IOI	Apex with posterior extension	–	Moderate	No	Yes (24–20)	0.6	1.04 (moderate)	2.07	11.36
2	IOI	Myositis	+	Severe	No	Yes[a]	1.0	0.68 (low)	2.01	7.97
3	IOI	Lacrimal gland	+	Moderate	No	No	1.2	3.88 (high)	5.32	11.32
4	TED	Pan-myositis	–	None	No	Yes (23–23)	1.0	0.33 (low)	2.91	5.45
5	IgG4+	Myositis	+	Mild	No	Yes (16–24)	1.2	1.58 (moderate)	4.43	8.90
6	IOI	Diffuse mass	+	Moderate	No	Yes[a]	0.9	3.11 (high)	3.73	15.87
7	IOI	Diffuse mass	+	Moderate	No	Yes[a]	1.0	2.12 (high)	3.27	14.45
8	Meningioma	Apex	–	None	Yes	No	0.6	0.79 (low)	2.49	5.81
9	IOI	Diffuse mass	+	Severe	Yes	No	0.5	3.82 (high)	3.64	12.12
10	TED	Pan-myositis	–	Mild	No	Yes (29–29)	0.7	3.47 (high)	4.07	12.10
11	IOI	Myositis	+	Severe	No	No	0.9	4.24 (high)	3.52	13.71
12	IOI	Myositis	+	Severe	No	No	1.0	0.68 (low)	4.83	19.15

a = Clinical and radiological proptosis, not quantified with Hertel. **Abbreviations:** IOI = idiopathic orbital inflammation; TED = thyroid eye disease; RAPD = relative afferent pupillary defect; BCVA = best-corrected visual acuity

Patients

From the 12 patients (detailed description in **Table 1**), 8 were diagnosed with IOI, 2 patients with TED, 1 patient with IgG4+ ROD, and 1 patient ultimately with an

optic nerve meningioma. The patients were refractory to standard treatment in the following way: two patients (cases 5 and 6) received oral prednisolone treatment for more than 12 months with inability for tapering. The other 10 patients did not respond to treatment with oral prednisolone and 1 or multiple intravenous (IV) methylprednisolone treatments (range 1–6 IV methylprednisolone regimens). Four patients (cases 2, 3, 11 and 12) were given additional immunosuppressive treatment (either azathioprine 100–150 mg, tocilizumab 800 mg or methotrexate 20 mg/week). Both patients with TED did not respond to multiple IV methylprednisolone regimens and retained a clinical activity score (CAS) with a score of four (case 4) and five (case 10). Due to the nature of refractory orbital inflammation, all patients were either under oral prednisolone treatment at the time of the scan or were recently given oral or IV steroids.

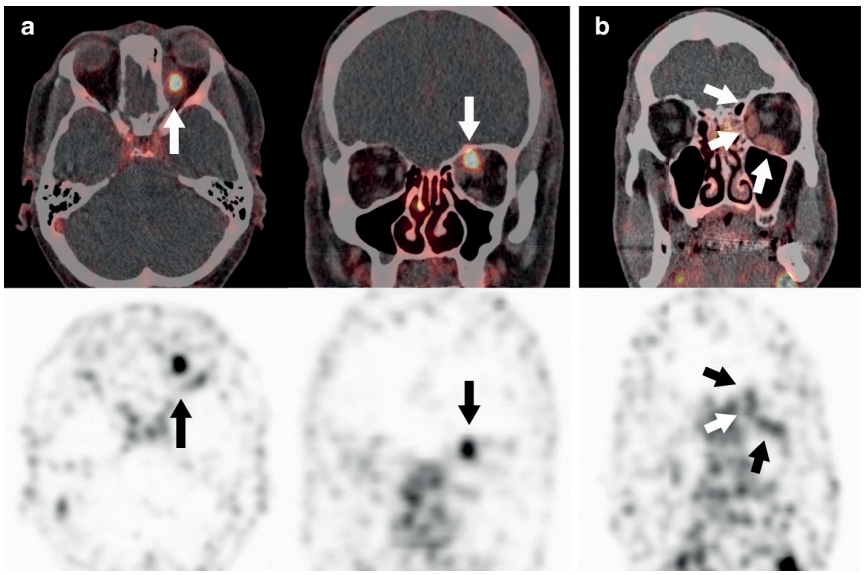

Figure 1. Examples of ^{89}Zr-rituximab PET/CT uptake. a, Strong uptake in fusion image and PET-only image for the axial and coronal planes (arrows point at the lesion, SUVmax > 2.0; case 6). b, Moderate uptake in fusion image and PET-only image (arrows point at affected muscles, SUVmax 1.0–2.0, case 5)

^{89}Zr-rituximab PET/CT procedure

Seventy-four megabecquerel ^{89}Zirconium (with a half-life of 78.4 h) was produced and labelled to 10 mg rituximab according to the procedures described previously.[10] No adverse effect occurred on administration of ^{89}Zr-rituximab. Three days after intravenous administration, we performed a PET/CT of the head on a TruePoint Biograph mCT40 scanner (Siemens, Erlangen, Germany). We performed a low dose CT scan using Care Dose 4D and Care kV, reference parameters: 40 mAs, 120 kV. Subsequently, the PET was acquired according to the European

Association of Nuclear Medicine (EANM) recommendations with a single bed position of 10 min with the following parameters: PET with time-of-flight and point spread function (TrueX) reconstruction, 4 iterations, 21 subsets, with a filter of 7.5 mm full width at half maximum.[11] We used tonsillar, submandibular, submental, pre- and post-auricular, and occipital lymph nodes as a positive control of CD20+ (B cell) targeting. For standardized uptake value (SUV) measurements, we used the lean body mass-corrected formula. We regarded a quantification of the PET-positivity (maximal SUV) above 2.0 to be a strong positivity, consistent with the PET-positivity of lymph nodes and bone marrow in the head and neck area, and a maximum SUV between 1.0 and 2.0 as moderate uptake.

Results

PET-CT analysis

In six patients, we found a high ^{89}Zr-rituximab PET uptake (standardized uptake value (SUV) >2.0) within the orbital masses (**Table 1**, example in **Figure 1a**). One patient with a strong PET uptake had an active TED with CAS 5. In two patients, a moderate ^{89}Zr-rituximab uptake was seen, of which one patient had an IOI in the orbital apex and one patient was diagnosed with IgG4+ ROD (**Figure 1b**). In four patients, there was no pathological ^{89}Zr-rituximab uptake. We diagnosed patients with a negative scan as myositis (two patients), active TED with CAS 4, and meningioma in the orbital apex (case 8) which became most likely after a positive Gallium-68-labelled DOTA-TATE PET/CT (**Figure 2b**), as meningiomas usually have a high somatostatin receptor expression.[12] In this last patient, a concurrent sinusitis of the right maxillary sinus coincidentally showed a strong ^{89}Zr-rituximab uptake (**Figure 2c**). Interestingly, IOI located in the lacrimal gland or diffuse within the orbit had strong uptake of ^{89}Zr-rituximab, whilst myositis and masses of the apex had moderate to no uptake. Strong ^{89}Zr-rituximab uptake was inhomogeneous with a focal intense uptake within the lesion.

Histopathology

Eight patients had an open incisional biopsy through a lid crease or swinging-eyelid surgical approach, dependent on the localization within the orbit.[3] For all but one (case 5), the histological images were not suggestive for IgG4-related disease. Histopathological examination in seven biopsies showed signs of a chronic inflammation with a lymphoplasmacytic infiltrate, characterized by both CD20+ B cells and CD3+ T cells. CD138+ plasma cells had a polytypic lambda and kappa distribution and either a predominant IgG or IgA differentiation for orbital and lacrimal gland tissue, respectively. In one biopsy, we only found fatty tissue without inflammation due to sampling error and a deep orbital localization.

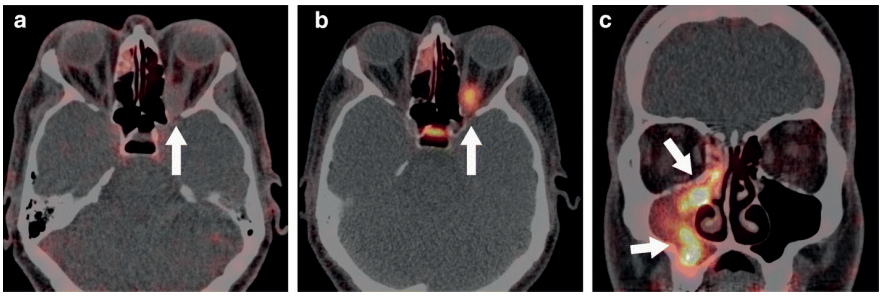

Figure 2. Patient with a meningioma in the left orbital apex and sinusitis of the right maxillary sinus (case 8). a Negative ^{89}Zr-rituximab PET/CT (white arrow, SUVmax < 1.0). b Positive 68Ga DOTA-TATE PET/CT, white arrow. c 89Zr-rituximab uptake in a co-existing sinusitis at the contralateral side, white arrows

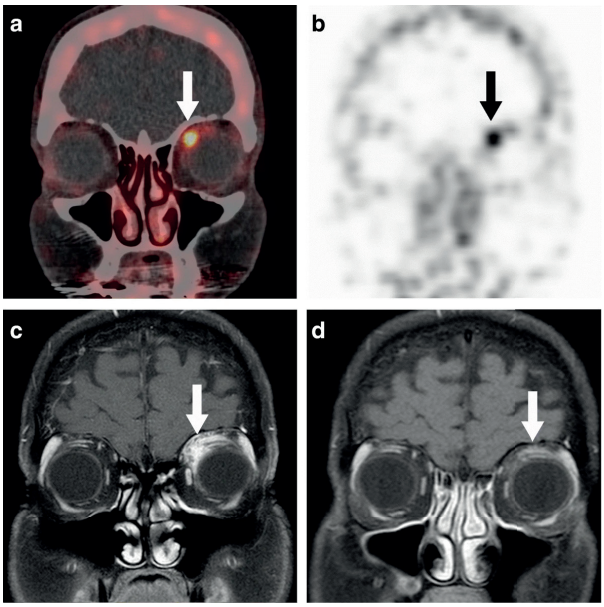

Figure 3. Rituximab treatment response (case 7). a, ^{89}Zr-rituximab PET/CT fusion image with focal uptake in the lesion, white arrow points at the lesion. b, PET only image, black arrow points at the lesion. Initial (c) and post-treatment MRI at 3 months after treatment (d), illustrating treatment response

Rituximab treatment

Four patients were treated with rituximab (2 × 1000 mg IV, MabThera, Roche) after a positive ^{89}Zr-rituximab PET/CT. All treated patients showed improvement of complaints within the first weeks after treatment. This effect was temporary in 3 out of 4 cases as some of the complaints returned to lesser extent. In one case, all complaints were initially gone (vision > 20/20, no pain and no diplopia), but some complaints returned 6 months later (case 7). A second rituximab treatment was given after 6 months and the patient responded well with remission of complaints. Three

other cases (case 9–11) had a significant reduction of complaints (improvement of visual acuity to 20/20, mild or no pain and improvement of eye motility). Of these, one received a second rituximab dose 4 months later (case 10), one had a relapse after 2 months and received additional treatment of oral prednisone (15 mg) and azathioprine (150 mg) (case 11), and one is currently monitored over 6 months whilst still improving (case 9). Two patients had an MRI scan after treatment with rituximab and both showed major radiological improvement with almost complete regression of the mass (case 7 and 9 Figure 3a–d).

Other treatments

Two patients with a positive scan did not receive rituximab treatment. One patient improved after treatment with oral prednisone and receiving infliximab for coexisting Crohn's disease (case 3) and the other patient improved on IV steroids (case 6). The latter patient was previously treated with oral prednisone for more than 12 months and had a biopsy after ^{89}Zr-rituximab PET/CT was performed. With a confirmed diagnosis of IOI, this patient was therefore first treated with IV steroids. Patients with a negative scan were not treated with rituximab and had stable disease, refractory to treatment. The patient with IgG4+ ROD (case 5) had a good response after additional IV steroids were given.

Discussion

We describe our experience of ^{89}Zr-rituximab PET/CT in 12 patients suspected of refractory orbital inflammation within the University Medical Center Utrecht. We have found a strong ^{89}Zr-rituximab uptake in orbital inflammatory diseases of the lacrimal gland and as a mass or diffuse within the orbit. Idiopathic myositis and involvement of the orbital apex showed ^{89}Zr-rituximab uptake to a lesser extent. A focal density was found in masses with a strong uptake. All four patients treated with rituximab after a positive ^{89}Zr-rituximab PET/CT had a good response during one or multiple treatments.

Five studies previously investigated the use of ^{89}Zr-rituximab PET/CT in humans with different disease entities. Two studies investigated B cell lymphoma in a total of 11 patients.[7,13] Lymphoma masses showed ^{89}Zr-rituximab PET uptake that was greater in the tumour mass without a preload of unlabelled rituximab.[7] The tumour uptake of labelled rituximab correlated with the in-tissue CD20 expression.[13] One study investigated the predictive value of ^{89}Zr-rituximab PET/CT for the effectiveness of rituximab treatment in rheumatoid arthritis patients.[5] A case report described the use of ^{89}Zr-rituximab PET/CT in the diagnostic process of neurolymphomatosis in the sciatic nerve.[6] Finally, one study investigated three patients with multiple

sclerosis, reporting no penetration of ^{89}Zr-rituximab in the brain.[14]

Besides Zirconium-89, intact CD20 labelling with rituximab has been performed with Iodine-124[15] for patients with rheumatoid arthritis and Technetium-99m[16] in several inflammatory conditions, showing feasibility for CD20 imaging. However, Zirconium-89 remains the most suitable for internalizing intact monoclonal antibodies.[17] ^{89}Zr-rituximab has a relatively long half-life and high effective dose of approximately 0.5 mSv/MBq.[18] The radiation dose should therefore be considered and balanced to the clinical benefits.

Surgical (open) biopsies are recommended for the diagnosis of orbital masses .[3] Unfortunately, biopsies deep in the orbit can be difficult, not-representative and potentially lead to severe complications to the optic nerve and extra-ocular muscles.[4,19] The ^{89}Zr-rituximab PET/CT can be of aid in distinguishing inflammatory and lymphoproliferative disorders from other orbital diseases, as we demonstrate in case 8 (**Figure 2**). This technique can, therefore, in combination with clinical and laboratory findings[9] and MRI imaging,[20] have additional value for a comprehensive diagnosis in difficult cases.

Our study shows that stronger focal ^{89}Zr-rituximab intensity can occur within the orbital mass (**Figure 3**). It was previously suggested that a higher tumour CD20+ expression correlated with a higher PET/CT intensity in lymphoma patients.[13] In our opinion, representable biopsies should yield the densest area of inflammatory cells within the tumour to provide the most information and exclude lymphoma. The yield of the inflammatory area within the biopsies was dependent on the morphology of the inflammation within the normal tissue as well as the depth of the mass within the orbit, reflecting the difficulty of an orbital biopsy. Because we show focal uptake in this study, we believe that the ^{89}Zr-rituximab PET/CT could be used as pre-biopsy orientation for targeting higher intensity areas during incisional biopsies for difficult cases.

The role of rituximab as a treatment in refractive orbital inflammatory disease is currently under investigation. Previous case reports and a phase I/II trial have indicated a strong potential for the effectiveness of rituximab treatment in refractory orbital inflammation.[8,21] However, not all patients benefit from this treatment, and the non-responders have an unnecessary exposure to potentially severe adverse effects. For IOI, the presence of a mixed B cell and T cell profile in the histopathological analysis of the masses reflects the involvement of both cells in the pathogenesis of the disease.[22] Although theoretically logical, there is no evidence of better rituximab effectivity in IOI patients with a more profound B cell

involvement. In TED, varying results have been published of the effectiveness of rituximab treatment.[23–27] Most early reports and a randomized controlled trial[24] describe clinical improvement with treatment in almost all patient, while another randomized controlled trial did not show an overall improvement compared to placebo. The search for factors that can predict the effectiveness of rituximab in TED and other orbital inflammatory diseases continues.[28]

The use of ^{89}Zr-rituximab PET/CT to predict rituximab treatment response has been demonstrated in a small cohort of rheumatoid arthritis patients by quantification of the uptake.[5] Although limited by the number of patients, we can now extrapolate this theory to orbital inflammatory diseases as we see a good response of rituximab in high-uptake patients in the current study. We would encourage future research investigating the predictive potential of rituximab therapy in inflammatory diseases, including TED, to use ^{89}Zr-rituximab PET/CT as an objective and measurable tool.

Several limitations of this study exist, inherent to the retrospective nature. We were not able to include patients diagnosed with a biopsy-proven orbital lymphoma. We would expect a high uptake in lymphoma patients[7,10] and a comparison with inflammatory orbital conditions is warranted for the potential for differentiation. Also, not all patients were treated with rituximab, including the patients with a negative scan. We could therefore not compare patients with a positive and negative scan for treatment effectivity.

Conclusion

This study describes our institutional experience with the ^{89}Zr-rituximab PET/CT in orbital inflammatory diseases. This technique has the potential to be a powerful tool for the detection of B cell-mediated disease within the orbit and ocular adnexa. By visualizing the CD20+ B cells, it can be a valuable addition to the diagnostic armamentarium for orbital inflammatory disease. Higher focal intensities within an orbital mass were found that can potentially pinpoint the location for more representative surgical biopsies. Patients with a strong ^{89}Zr-rituximab PET/CT uptake responded well to rituximab treatment. We encourage further research of this technique in the diagnostic process and to predict rituximab treatment response for orbital inflammatory diseases.

Abbreviations

^{89}Zr-rituximab PET/CT:	Zirconium-89-labelled rituximab positron emission tomography/computed tomography
CAS:	Clinical activity score
CD:	Cluster of differentiation
IgG4 + ROD:	IgG4+-related orbital disease
IOI:	Idiopathic orbital inflammation
TED:	Thyroid-associated eye disease

References

1. Shields JA, Shields CL, Scartozzi R. Survey of 1264 patients with orbital tumors and simulating lesions: the 2002 Montgomery lecture, part 1. Ophthalmology. 2004;111:997–1008.
2. Gordon LK. Orbital inflammatory disease: a diagnostic and therapeutic challenge. Eye. 2006;20:1196–206.
3. Mombaerts I, Rose GE, Garrity JA. Orbital inflammation: biopsy first. Surv Ophthalmol. 2016;61:664–9.
4. Dagi Glass LR, Freitag SK. Orbital inflammation: corticosteroids first. Surv Ophthalmol. 2016;61:670–3.
5. Bruijnen S, Tsang-A-Sjoe M, Raterman H, Ramwadhdoebe T, Vugts D, van Dongen G, et al. B-cell imaging with zirconium-89 labelled rituximab PET-CT at baseline is associated with therapeutic response 24 weeks after initiation of rituximab treatment in rheumatoid arthritis patients. Arthritis Res Ther. 2016;18:266.
6. de Jong A, Mous R, van Dongen GAMS, Hoekstra OS, Nievelstein RAJ, de Keizer B. (89) Zr-rituximab PET/CT to detect neurolymphomatosis. Am J Hematol. 2016;91:649–50.
7. Muylle K, Flamen P, Vugts DJ, Guiot T, Ghanem G, Meuleman N, et al. Tumour targeting and radiation dose of radioimmunotherapy with 90Y-rituximab in CD20+ B-cell lymphoma as predicted by 89Zr-rituximab immuno-PET: impact of preloading with unlabelled rituximab. Eur J Nucl Med Mol Imaging. 2015;42:1304–14.
8. Suhler EB, Lim LL, Beardsley RM, Giles TR, Pasadhika S, Lee ST, et al. Rituximab therapy for refractory orbital inflammation: results of a phase 1/2, dose-ranging, randomized clinical trial. JAMA Ophthalmol. 2014;132:572–8.
9. Mombaerts I, Bilyk JR, Rose GE, McNab AA, Fay A, Dolman PJ, et al. Consensus on diagnostic criteria of idiopathic orbital inflammation using a modified Delphi approach. JAMA Ophthalmol. 2017;135:769–76.
10. Verel I, Visser GWM, Boellaard R, Stigter-van Walsum M, Snow GB, van Dongen GAMS. 89Zr immuno-PET: comprehensive procedures for the production of 89Zr-labeled monoclonal antibodies. J Nucl Med. 2003;44:1271–81.
11. Boellaard R, Delgado-Bolton R, Oyen WJG, Giammarile F, Tatsch K, Eschner W, et al. FDG PET/CT: EANM procedure guidelines for tumour imaging: version 2.0. Eur J Nucl Med Mol Imaging. 2015;42:328–54.
12. Klingenstein A, Haug AR, Miller C, Hintschich C. Ga-68-DOTA-TATE PET/CT for discrimination of tumors of the optic pathway. Orbit. 2015;34:16–22.
13. Jauw YWS, Zijlstra JM, de Jong D, Vugts DJ, Zweegman S, Hoekstra OS, et al. Performance of 89Zr-labeled-rituximab-PET as an imaging biomarker to assess CD20 targeting: a pilot study in patients with relapsed/refractory diffuse large B cell lymphoma. PLoS One. 2017;12:e0169828 Glod JW, editor.
14. Hagens MH, Killestein J, Yaqub MM, van Dongen GA, Lammertsma AA, Barkhof F, et al. Cerebral rituximab uptake in multiple sclerosis: A 89 Zr-immunoPET pilot study. Mult Scler J. 2018;24:543–5.
15. Tran L, Huitema ADR, van Rijswijk MH, Dinant HJ, Baars JW, Beijnen JH, et al. CD20 antigen imaging with 124I-rituximab PET/CT in patients with rheumatoid arthritis. Hum Antibodies. 2011;20:29–35.
16. Malviya G, Anzola KL, Podestà E, Laganà B, Del Mastro C, Dierckx RA, et al. (99m)Tc-labeled rituximab for imaging B lymphocyte infiltration in inflammatory autoimmune disease patients. Mol Imaging Biol. 2012;14:637–46.
17. van Dongen GAMS, Poot AJ, Vugts DJ. PET imaging with radiolabeled antibodies and tyrosine kinase inhibitors: immuno-PET and TKI-PET. Tumour Biol. 2012;33:607–15 Springer.
18. Jauw YWS, Menke-van der Houven van Oordt CW, Hoekstra OS, Hendrikse NH, Vugts DJ, Zijlstra JM, et al. Immuno-positron emission tomography with Zirconium-89-labeled monoclonal antibodies in oncology: what can we learn from initial clinical trials? Front Pharmacol. 2016;7:131 Frontiers Media SA.
19. Chastain JB, Sindwani R. Anatomy of the orbit, lacrimal apparatus, and lateral nasal wall. Otolaryngol Clin N Am. 2006;39:855–64.
20. Hiwatashi A, Togao O, Yamashita K, Kikuchi K, Kamei R, Yoshikawa H, et al. Diffusivity of intraorbital lymphoma vs. inflammation: comparison of single shot turbo spin echo and multishot echo planar imaging techniques. Eur Radiol. 2018;28:325–30.
21. Abell RG, Patrick A, Rooney KG, McKelvie PA, McNab AA. Complete resolution of idiopathic

sclerosing orbital inflammation after treatment with rituximab. Ocul Immunol Inflamm. 2015;23:176–9.
22. Mombaerts I, Schlingemann RO, Goldschmeding R, Koornneef L. Idiopathic granulomatous orbital inflammation. Ophthalmology. 1996;103:2135–41.
23. Stan MN, Garrity JA, Carranza Leon BG, Prabin T, Bradley EA, Bahn RS. Randomized controlled trial of rituximab in patients with Graves' orbitopathy. J Clin Endocrinol Metab. 2015;100:432–41.
24. Salvi M, Vannucchi G, Currò N, Campi I, Covelli D, Dazzi D, et al. Efficacy of B-cell targeted therapy with rituximab in patients with active moderate to severe Graves' orbitopathy: a randomized controlled study. J Clin Endocrinol Metab. 2015;100:422–31.
25. Khanna D, Chong KKL, Afifiyan NF, Hwang CJ, Lee DK, Garneau HC, et al. Rituximab treatment of patients with severe, corticosteroid-resistant thyroid-associated ophthalmopathy. Ophthalmology. 2010;117:133–139.e2.
26. Silkiss RZ, Reier A, Coleman M, Lauer SA. Rituximab for thyroid eye disease. Ophthalmic Plast Reconstr Surg. 2010;26:310–4.
27. El Fassi D, Nielsen CH, Hasselbalch HC, Hegedüs L. Treatment-resistant severe, active graves' ophthalmopathy successfully treated with B lymphocyte depletion. Thyroid. 2006;16:709–10.
28. Stan MN, Salvi M. Management of endocrine disease: rituximab therapy for Graves' orbitopathy—lessons from randomized control trials. Eur J Endocrinol. 2017;176:R101–9.


Chapter 6.2

Zirconium-89-labelled rituximab PET-CT imaging of Graves' orbitopathy

Bart de Keizer,
Kamil G. Laban,
Rachel Kalmann

Eur J Nucl Med Mol Imaging. 2020 Mar;47(3):738-739.
doi: 10.1007/s00259-019-04599-8.

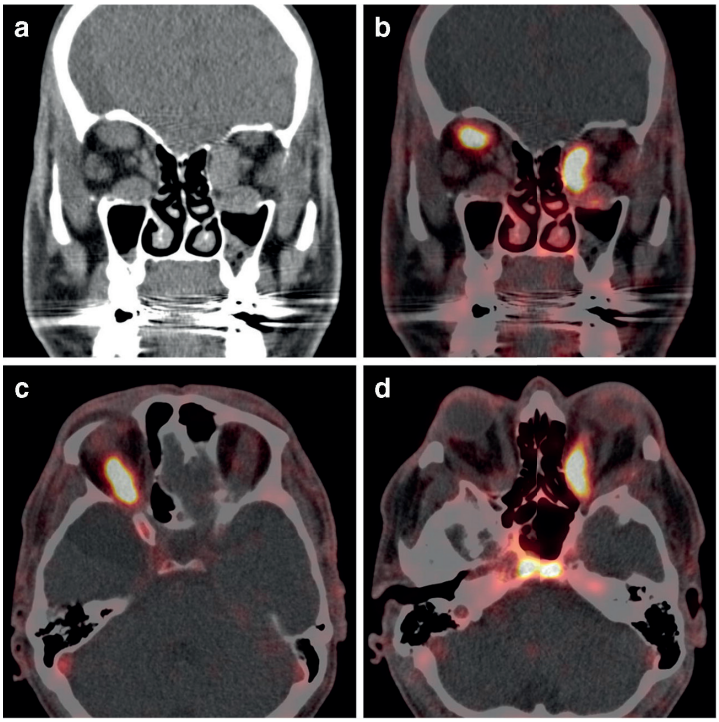

Figure 1

Graves' orbitopathy (GO) is the main extrathyroidal manifestation of Graves' disease. A proportion of patients have moderate to severe orbital inflammation, with corneal ulceration, intense pain or even compressive optic neuropathy.[1] High-dose glucocorticoids (GCs) are the first-line treatment in these patients. When high-dose GCs fail to reduce the inflammation, shared decision-making is recommended for selecting a second-line treatment. Options for treatment include a second course of intravenous GCs, oral GCs combined with orbital radiotherapy, rituximab or watchful waiting.[2] Rituximab treatment is not yet approved for clinical use in GO and roughly 50% do not have significant improvement 1 year after treatment.[3] In rheumatoid arthritis, zirconium-89-labelled rituximab (^{89}Zr-rituximab) PET-CT shows promising clinical value with higher rates of response to therapy in patients with higher ^{89}Zr-rituximab uptake in responders than in non-responders.[4] ^{89}Zr-rituximab PET scanning is approved by Dutch authorities to select patients for rituximab treatment and is used in our hospital to select patients with orbital inflammatory disease (including GO) that might benefit from rituximab treatment. In a recent retrospective study, we showed that of 4 patients with intense ^{89}Zr-rituximab uptake in orbital inflammatory disease, 3 patients responded well to rituximab treatment.[5] Here, we present a patient with GO refractory to intravenous GCs. PET-CT performed 3 days after 74 MBq ^{89}Zr-rituximab showed high uptake in orbital musculature. ^{89}Zr-rituximab binding more than in normal bone marrow and comparable to binding in normal lymph nodes was observed in thickened medial rectus muscle of the left eye (SUVmax 5.9) and the superior rectus muscle of the right eye (SUVmax 5.2) (**Figure 1 a** coronal CT reconstruction, **b** coronal PET-CT reconstruction, **c** axial PET-CT reconstruction of right superior rectus muscle and **d** axial PET-CT reconstruction of left medial rectus muscle). Because of high ^{89}Zr-rituximab uptake, rituximab treatment was initiated.

Compliance with Ethical Standards: The authors declare that they have no conflicts of interest. All procedures performed in studies involving human participants were in accordance with the ethical standards of the institutional and/or national research committee and with the 1964 Helsinki declaration and its later amendments or comparable ethical standards. Informed consent was obtained from the participant included in the study.

References

1. Bahn RS. Graves' ophthalmopathy. N Engl J Med. 2010;362:726–38
2. Bartalena L, Baldeschi L, Boboridis K, Eckstein A, Kahaly GJ, Marcocci C, et al. The 2016 European Thyroid Association/European Group on Graves' Orbitopathy Guidelines for the Management of Graves' Orbitopathy. Eur Thyroid J. 2016;5:9–26
3. Stan MN, Garrity JA, Leon BGC, Prabin T, Bradley EA, Bahn RS. Randomized controlled trial of rituximab in patients with Graves' orbitopathy. J Clin Endocrinol Metab. 2015;100:432–41.
4. Bruijnen S, Tsang-A-Sjoe M, Raterman H, Ramwadhdoebe T, Vugts D, van Dongen G, et al. B-cell imaging with zirconium-89 labelled rituximab PET-CT at baseline is associated with therapeutic response 24 weeks after initiation of rituximab treatment in rheumatoid arthritis patients. Arthritis Res Ther. 2016:18:266.
5. Laban KG, Kalmann R, Leguit RJ, de Keizer B. Zirconium-89-labelled rituximab PET-CT in orbital inflammatory disease. EJNMMI Res. 2019;9:69.


Chapter 7

A pan-inflammatory microRNA-cluster is associated with orbital non-Hodgkin lymphoma and idiopathic orbital inflammation

Kamil G. Laban
Rachel Kalmann
Cornelis P. J. Bekker
Sanne Hiddingh
Rob L. P. van der Veen
Christine A. E. Eenhorst
Stijn W. Genders
Maarten P. Mourits
Fleurieke H. Verhagen
Emmerik F. A. Leijten
Saskia Haitjema
Mark C. H. de Groot
Timothy R. D. J. Radstake
Joke H. de Boer
Jonas J. W. Kuiper

Eur J Immunol. 2020 Jan;50(1):86-96.
doi: 10.1002/eji.201948343.

Abstract

Non-Hodgkin orbital lymphoma (NHOL) and idiopathic orbital inflammation (IOI) are common orbital conditions with largely unknown pathophysiology that can be difficult to diagnose. In this study we aim to identify serum miRNAs associated with NHOL and IOI. We performed *OpenArray®* miRNA profiling in 33 patients and controls. Differentially expressed miRNAs were technically validated across technology platforms and replicated in an additional cohort of 32 patients and controls. We identified and independently validated a serum miRNA profile of NHOL that was remarkably similar to IOI and characterized by an increased expression of a cluster of eight miRNAs. Pathway enrichment analysis indicated that the miRNA-cluster is associated with immune-mediated pathways, which we supported by demonstrating the elevated expression of this cluster in serum of patients with other inflammatory conditions. The cluster contained *miR-148a*, a key driver of B-cell tolerance, and *miR-365* that correlated with serum IgG and IgM concentrations. In addition, *miR-29a* and *miR-223* were associated with blood lymphocyte and neutrophil populations, respectively. NHOL and IOI are characterized by an abnormal serum miRNA-cluster associated with immune pathway activation and linked to B cell and neutrophil dysfunction.

Introduction

Non-Hodgkin orbital lymphoma (NHOL) is the most common orbital malignancy in adults.[1] Early and accurate diagnosis is essential to reduce metastatic spread, and avoid disease-related morbidity and mortality. NHOL can be lethal without timely intervention, but prognosis varies across disease subtypes.[2] Generally, NHOL first presents as a non-specific mass within the orbit or ocular adnexa, which may be difficult to differentiate from *idiopathic orbital inflammation* (IOI), the most common non-thyroid associated orbital inflammatory condition.[3-7] Consequently, an incisional biopsy is required to accurately diagnose both diseases.[1,8] However, a surgical biopsy can be technically challenging in case of deep orbital localization of the mass, which increases the risk for complications and non-representative tissue biopsies. Therefore, less invasive tools to differentiate NHOL from inflammatory orbital disease are warranted. Although imaging-based disease differentiation is advancing,[9] studies that explore blood-based differentiation of NHOL and IOI are scarce. Additionally, the pathophysiology of NHOL and IOI remain largely unknown. MicroRNAs (miRNAs) are small non-coding regulatory RNAs that are present in almost all biological tissues and regulate gene expression by interfering with RNA translation.[10] Changes in the composition of miRNAs are associated with a plethora of human pathologies, including inflammation and cancer.[11-13] Consequently, miRNAs are candidate biomarkers that may aid in diagnosis and prognostic studies.[14,15] Direct comparison of the serum miRNA profile of NHOL and IOI is currently lacking, but may provide a framework for understanding the miRNA composition of these orbital conditions for future differentiation and elucidation of the underlying mechanisms involved. In this exploratory study, we identify and validate NHOL- and IOI-related miRNA profiles in serum of two Dutch cohorts of patients and controls. In addition, we reference six non-orbital inflammatory conditions as disease controls to better understand miRNA expression changes.

Results

Patients

Demographics of the discovery and replication cohorts of are described in **Table 1**. Note, in both cohorts the mean age of the NHOL group was higher compared to the IOI and control groups, which is inherent to the representative age distribution for each of these conditions. In contrast, the mean age of the discovery and replication cohorts was similar for each orbital condition.

MiRNA analysis

To detect differences between NHOL, IOI, and healthy controls (HC), we performed

a broad serum OpenArray® profiling of the discovery cohort (Figure 1A). We detected 399 miRNAs of which 120 miRNAs remained after quality control (Supporting Information Table S1). Principle component analysis of the serum miRNA identified two samples that were considered technical outliers (Figure 1B) that were excluded for further analysis because their expression levels strongly skewed group-level characteristics.

Table 1. Cohort demographics

Discovery cohort	Discovery			Replication		
	IOI	NHOL	HC	IOI	NHOL	HC
	n=14	*n=10*	*n=9*	*n=8*	*n=8*	*n=16*
Female[a]	2 (86%)	5 (50%)	6 (67%)	6 (75%)	5 (63%)	10 (63%)
Age (years)[b]	48.7 ± 17.6	60.6 ± 9.7	47.1 ± 14.4	48.5 ± 17.2	64.9 ± 17.3	47.9 ± 10.7
NHOL subtype[a]						
EMZL	–	7 (70%)	–	–	4 (50%)	–
DLBCL	–	1 (10%)	–	–	1 (13%)	–
Follicular	–	1 (10%)	–	–	2 (25%)	–
Other	–	1 (10%)	–	–	1 (13%)	–

a = number (%), b = mean (standard deviation). **Abbreviations**: IOI, idiopathic orbital inflammation; NHOL, non-Hodgkin orbital lymphoma; HC, healthy control; EMZL, extranodal marginal zone lymphoma; DLBCL, diffuse large B cell lymphoma. Other NHOL types were a small lymphocytic lymphoma in the discovery cohort and a mantle-cell lymphoma in the replication cohort.

In the remaining 31 samples, the overall miRNA expression was higher in the NHOL and IOI groups compared to the control group (Figure 1C, Supporting Information Table S1). Head-to-head comparison of miRNA profiles between the investigated groups revealed several differentially expressed miRNAs (Figure 2). The most differentially expressed miRNAs were found when comparing each of the orbital disease groups with controls. The mean levels of miRNAs were slightly higher in the IOI compared to NHOL group, but only U6 small nuclear RNA (*U6 snRNA*) exceeded the fold change (FC) >2.0 and $p < 0.05$ criterion (Figure 2A). A total of 12 miRNAs were selected for technical validation (Supporting Information Table S2). This selected panel consisted of the most differentially expressed miRNAs (miR-29a-3p, miR-193a-5p, miR-223-3p, miR-223-5p, miR-148a-3p, miR-365a-3p, miR-143-3p, and U6 snRNA, see Figure 2) and miR-140-5p, miR-215-5p, and miR-491-5p that are associated with inflammation and neoplasm,[16-18] and highly correlated with the differentially expressed miRNAs (with a Spearman's $\rho > 0.75$). We also included miR-221-3p as a control in the validation phase,

because this miRNA was not differentially expressed in the discovery cohort. The level of expression and variance of the selected miRNA panel considered for validation and replication was representative for the entire serum miRNA profile (i.e. not biased, Supporting Information Figure S1). Analysis corrected for age and sex revealed no other miRNAs of interest for the comparison between NHOL and IOI.

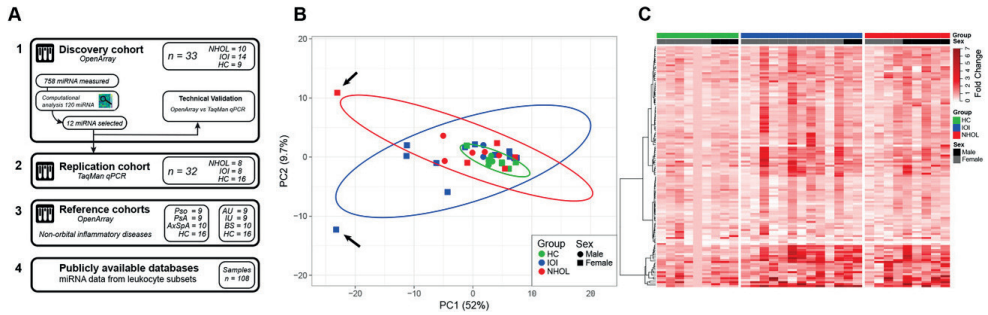

Figure 1. The serum miRNA profile of the discovery cohort. (A) Flowchart with the cohorts and technologies used in this study. (B) Principle component analysis with a projection of the first two components of all serum samples within the discovery cohort (n = 33). The ellipses represent the centre and the 95% confidence interval of the samples in each group. Two samples highlighted by black arrows were considered outliers and were excluded from further analysis. (C) Heatmap of the fold changes of spike-in normalized data compared to HC in expression of 120 serum miRNAs in the discovery cohort (n = 31). Relative miRNA expression is depicted in fold changes (FC, or Singular Value Decomposition imputed values, max 10%). Hierarchical clustering of the rows was performed using the Euclidian distance with Ward linkage method. Abbreviations: PC, principle component, IOI, idiopathic orbital inflammation; NHOL, non-Hodgkin orbital lymphoma; HC, healthy control.

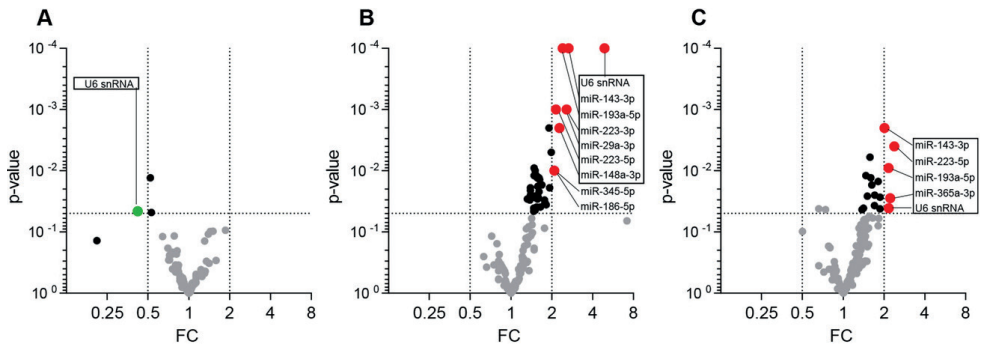

Figure 2. Volcano plot of head-to-head group comparisons for serum miRNAs in the discovery cohort. (A) The comparison between serum miRNA levels of the NHOL group (n = 13) and IOI group (n = 9). (B) The comparison between the IOI (n = 13) group with HC group (n = 9). (C) The comparison between the NHOL group (n = 9) and HC group (n = 9). Differentially expressed microRNAs are highlighted in green/red. The analysis was performed by independent samples t-test in the Thermo Fisher Cloud software. Differentially expressed miRNAs selected for replication are highlighted in boxes. Abbreviations: FC, fold change; IOI: idiopathic orbital inflammation; NHOL, non-Hodgkin orbital lymphoma; HC, healthy control.

A cluster of eight miRNAs is associated with NHOL and IOI

Having selected miRNAs of interest using the *OpenArray®* approach, we next aimed to validate the observations across technology platforms by measuring the levels of the twelve miRNAs using TaqMan single reverse transcription quantitative polymerase-chain reaction (RT-qPCR). We observed a strong correlation ($\rho > 0.75$; $p < 0.01$) between the expression levels obtained by *OpenArray®* and TaqMan RT-qPCR for 10/12 miRNAs, and considered these miRNAs technically validated (**Figure 3**, **Supporting Information Table S2**). Next, we aimed to replicate our findings in a second cohort of 32 patients and controls (**Table 1**). We measured the levels of the technically validated miRNA in serum of the second (replication) cohort by RT-qPCR and observed that 8/10 miRNAs were differentially expressed between the groups with consistent direction of effect compared to HC. These eight miRNAs were considered biologically replicated. (**Figure 3**, **Supporting Information Table S2**). Note that the expression levels of the biologically replicated miRNAs were significantly higher expressed in the disease groups compared to healthy controls (**Figure 3**). Comparison of the data of the eight miRNAs revealed strong correlation of the expression levels, indicating co-expression, which we will further refer to as a 'cluster' of miRNAs in serum of patients (**Figure 4B**).

Next, we combined the RT-qPCR data from the discovery and replication cohorts to investigate the discriminative power of the miRNAs between the NHOL, IOI, and HC group. We observed a statistically significant discriminative power (area under the receiver operator curve range 0.72–0.92) with several cut-off values with FC < 2 for all miRNAs in the cluster for the diseased groups compared to the control group (**Supporting Information Table S3**). We observed a low discriminative power between NHOL and IOI, owing to the larger variation in expression in patients. However, the mean expression levels for miRNAs of the cluster were all slightly higher in IOI patients compared to NHOL (**Figure 4C**). The expression levels of the eight miRNAs did not correlate with age and sex and consequently, correction for age and sex did not influence the outcome of the data.

Figure 3. (page to the right) Eight serum microRNAs are increased in patients with NHOL and IOI. (A) miRNA expression of the Discovery cohort using OpenArray (n = 31). The relative expression of microRNAs is represented in fold changes (FC) of the diseased groups compared to healthy controls. p-values are calculated with an independent t-test on ΔΔCrt data. (B) Technical validation of the samples used for the OpenArray platform in a TaqMan single RT-qPCR assay. Technical validation was assessed using a Spearman's ρ correlation between Crt data (OpenArray) and Ct data (TaqMan RT-qPCR). (C) Results of the biological replication in an independent cohort using the TaqMan single RT-qPCR assay (n = 32). Relative expression is the fold change differences between the diseased groups and healthy control. Independent t-test is used on ΔΔCt data. (D) Results of the TaqMan single RT-qPCR of both cohorts (n = 63). Relative expression is the fold change differences between the diseased groups and the mean of the combined healthy control groups. Kruskal–Wallis statistics with post-hoc Dunn's test is used on ΔΔCt data. *p < 0.05, **p < 0.01, ***p < 0.001. Abbreviations: IOI, idiopathic orbital inflammation; NHOL, non-Hodgkin orbital lymphoma; HC, healthy control. The median expression is indicated for each group by a black line and quartiles with dotted lines.

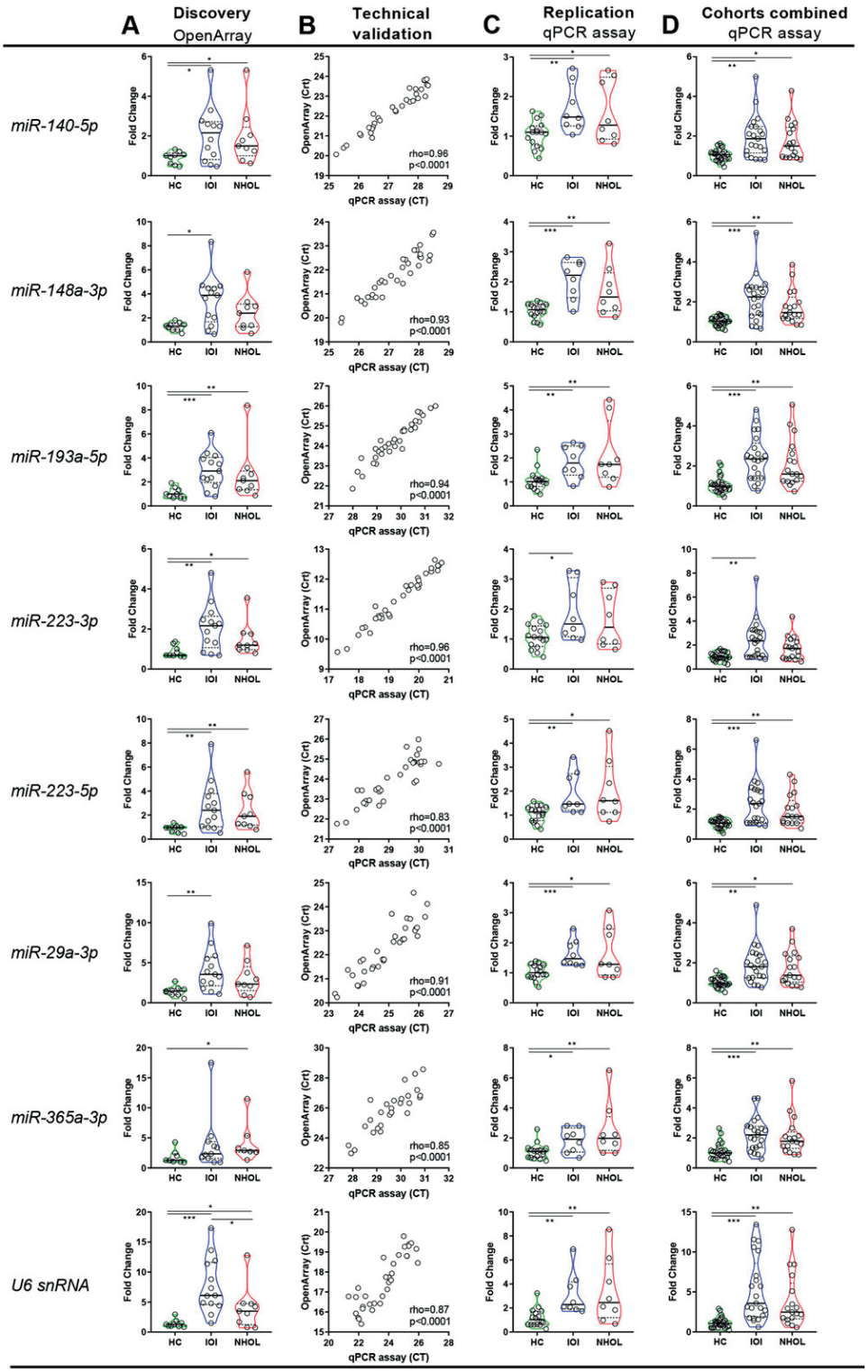
A Discovery OpenArray
B Technical validation
C Replication qPCR assay
D Cohorts combined qPCR assay
miR-140-5p
miR-148a-3p
miR-193a-5p
miR-223-3p
miR-223-5p
miR-29a-3p
miR-365a-3p
U6 snRNA
Fold Change
OpenArray (Crt)
qPCR assay (CT)
HC
IOI
NHOL
rho=0.96 p<0.0001
rho=0.93 p<0.0001
rho=0.94 p<0.0001
rho=0.96 p<0.0001
rho=0.83 p<0.0001
rho=0.91 p<0.0001
rho=0.85 p<0.0001
rho=0.87 p<0.0001

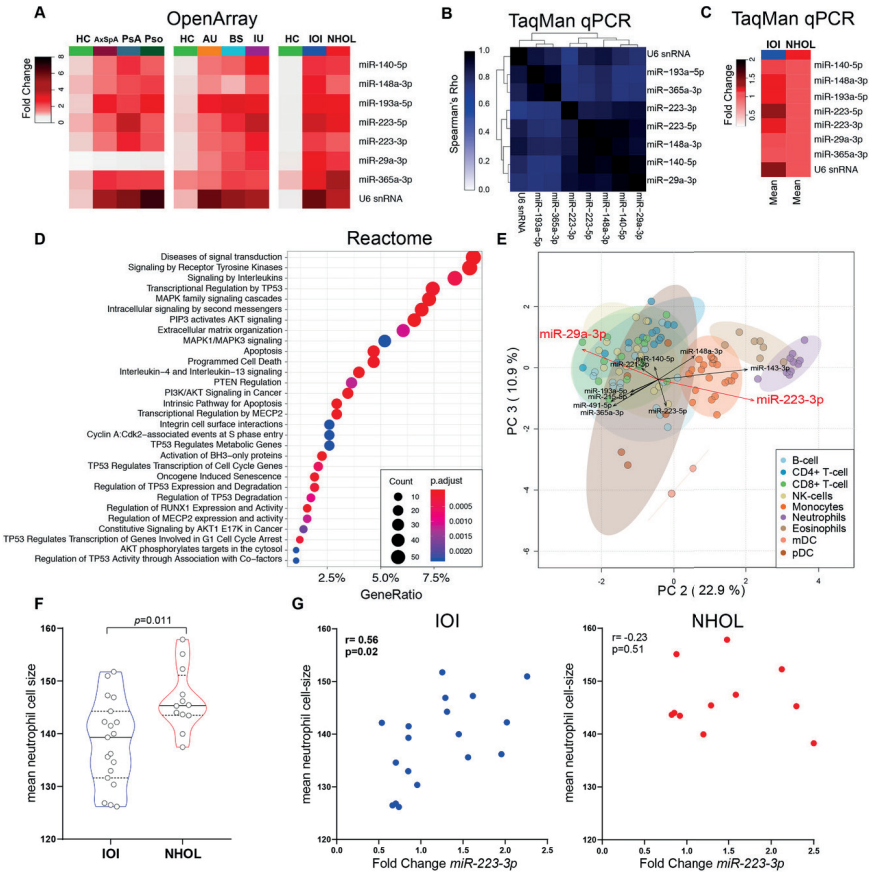

Figure 4. Investigation of the serum miRNA-cluster in inflammatory conditions and pathway enrichment analysis. (A) Heatmap of the validated miRNAs in independently analysed datasets of the investigated conditions and the referenced chronic inflammatory conditions (total samples n = 113). The relative miRNA expression per group is depicted as the mean fold changes compared to controls (HCs) and color-coded. (B) Correlation between the cluster of eight replicated miRNAs (all Spearman's ρ coefficients > 0.7, p < 0.001). Clustering of miRNA data was performed in Metaboanalyst of ΔΔCt data from TaqMan single RT-qPCR results of the discovery and replications cohorts of NHOL and IOI (n = 63). (C) Relative expression of the serum miRNA-cluster of TaqMan single RT-qPCR data from the discovery and replication cohorts (n = 63), depicted as mean fold change of IOI compared to NHOL. (D) Pathway enrichment analysis of 908 genes associated with the eight replicated miRNAs using the R package clusterProfiler with the Reactome database. The top 30 pathways are depicted (FDR adjusted p-value with a cut-off p < 0.05). (E) Principle component analysis (PCA) of miRNAs that were selected for replication in our study in 108 samples across nine blood leukocyte subsets. U6 snRNA was not available for this dataset. We excluded the first PCA dimension to reduce technical variation and batch effects. Individual loadings are projected over the individually plotted samples. Coloured ellipses represent the 95% confidence interval of the samples for each population. The miR-223-3p and miR-29a-3p showed the largest separation and are highlighted in red. (F) Violin plots of CELL-DYN Sapphire measured mean neutrophil size (0° Axial Light Loss) for the NHOL and IOI groups. The median bar (black line) and quartiles (dotted line) are shown within the violin plots. The Mann–Whitney U test was used for group comparison. (G) Pearson's correlation of relative expression of miR-223-3p and the mean neutrophil size within the NHOL and IOI groups are plotted separately. Abbreviations: IOI, idiopathic orbital inflammation; NHOL, non-Hodgkin orbital lymphoma; HC, healthy control; IU, idiopathic intermediate uveitis; AU, anterior uveitis; BS, Birdshot uveitis; AxSpA, axial spondyloarthritis; Pso, psoriasis; PsA, psoriatic arthritis; PC, principle component.

The serum miRNA-cluster is typically increased in inflammatory disease
Since overall the miRNA-cluster showed the highest expression in IOI cases, we hypothesized that the cluster may regulate immune pathways and would also be elevated in serum of cases with other chronic inflammatory conditions. To investigate this, we determined the expression of the cluster in serum of 57 patients with non-infectious uveitis,[16] psoriasis, psoriatic arthritis, axial spondyloarthritis, and compared this to 26 unaffected controls. The serum miRNA profile for these conditions is outlined in Supporting Information Figure S2. Interestingly, we observed that in general the miRNA-cluster was upregulated in these inflammatory conditions (Figure 4A).

To explore the association of the miRNA-cluster with immune pathways in more detail, we used *miRTargetLink*[19] to extract putative gene targets of miRNA in the cluster. In total, 908 genes were reported to have evidence for interaction with any of the eight miRNAs. Pathway enrichment analysis was performed on the entire set of genes (*n = 908*) associated with this miRNA-cluster, and revealed enrichment for pathways related to cancer and inflammation, including mitogen-activated protein kinase signalling, p53 signalling, and interleukin signalling (Figure 4D, and Supporting Information Figure S3). A detailed pathway-enrichment analysis for each individual miRNA is outlined in Supporting Information Figure S3.

The serum miRNA-cluster is associated with myeloid and lymphoid lineages
Having established the link between the miRNA-cluster and inflammation, we hypothesized that the expression levels of the miRNA-cluster in serum may inform on changes in the composition of blood leukocytes. To explore if the miRNA-cluster is associated with specific leukocyte populations in blood, we used miRNA profiling data of nine blood leukocyte populations (*n = 108* samples). Considering the 12 selected miRNAs from the discovery cohort for principal component analysis, we observed that myeloid and lymphoid lineages could be distinguished primarily by the magnitude of difference of the levels of expression for *miR-223-3p* and *miR-29a-3p* (Figure 4E). Indeed, *miR-223-3p* is predominantly expressed in monocyte, eosinophil, and neutrophil cells, while *miR-29a-3p* is more abundantly expressed in $CD4^+$ and $CD8^+$ T cells, B cells, and NK cells (Supporting Information Figure S4). The increased expression of *miR-223-3p* and *miR-29a-3p* in certain leukocyte populations suggests that changes in leukocytes composition in blood may underlie the increase in the miRNA cluster in blood of patients with IOI and NHOL.

To test for associations between the blood leukocyte composition and serum miRNA levels, we evaluated the absolute frequency of several leukocyte populations in whole blood of both cohorts (Supporting Information Figure S5A). Although the

frequency of all leukocyte populations in available whole blood of patients was within normal range (Supporting Information Figure S5A), NHOL patients showed a higher mean neutrophil cell size compared to IOI patients (Figure 4F). In addition, the neutrophil cell size and serum *miR-223-3p* levels showed moderate positive correlation (Spearman's ρ = 0.56) in patients with IOI, but not in NHOL patients (Figure 4G). These analyses suggest that the serum miRNA cluster is associated with neutrophil status in blood.

The levels of miR-365a-3p correlate with serum immunoglobulin

Inspired by the observations of miRNAs and the leukocyte composition, we compared the identified miRNA levels in serum with available clinical and demographic parameters relevant for orbital diseases. Correlation analysis revealed no association between the levels of each of the eight miRNAs and age or sex. We did observe a correlation between *miR-365a-3p* and serum Immunoglobulin-G and Immunoglobulin-M in NHOL and IOI patients at nominal significance (Supporting Information Table S4). No notable correlations were found between any of the eight miRNAs and C-reactive protein, erythrocyte sedimentation rate, rheumatoid factor, anti-nuclear antibodies, or soluble interleukin 2 levels.

Because B cells are implicated in both the aetiology of NHOL and orbital inflammation, we finally compared the expression of 19 miRNAs previously implicated in B cell autoimmunity and B cell lymphoma between IOI and NHOL.[20] This analysis revealed that the mean expression of B cell associated miRNAs in serum was similar between NHOL and IOI patients (Supporting Information Figure S5B).

Discussion

In this study we discovered a remarkably similar miRNA profile for NHOL and IOI, and eight miRNAs were upregulated as part of a miRNA cluster in both NHOL and IOI compared to control. The eight miRNAs were found to be upregulated in several inflammatory diseases and related to inflammatory and oncological pathways.

With our results we show that local orbital disease leaves a molecular footprint in peripheral blood. This is consistent with other studies that reported changes in miRNA composition in tissues distinct from the primary location of clinical disease.[16,21-23] Previous studies have investigated miRNA profiles in non-Hodgkin lymphoma, most often the diffuse large B cell lymphoma subtype (DLBCL).[11,14,24] DLBCL is a relative infrequent subtype of NHOL,[2] reflected by only two cases in

our study. In contrast, the most frequent NHOL subtype in our study was extranodal marginal zone lymphoma (EMZL), for which serum miRNAs studies are rare.[11,24] Nonetheless, studies of lymphoma biopsies have shown an increased expression of *miR-223* and *miR-193* in EMZL,[25] and a downregulation of *miR-29a*, *miR-223*, and *miR-140* in DLBCL.[26] This makes it tempting to speculate that the here-identified miRNA-cluster orchestrates pathological mechanisms associated with non-Hodgkin lymphoma, although the spatiotemporal miRNA expression may be dependent on the subtype of disease.

Additional analysis sheds light on the function of cluster of miRNAs: we demonstrate that the miRNAs associated with NHOL are shared with a wide variety of chronic (orbital) inflammatory conditions, strongly suggesting that these miRNAs function in immune-mediated pathways and may be considered "pan-inflammatory". Indeed, pathway enrichment analysis for miRNA-target genes supports the hypothesis that these miRNAs regulate inflammatory and interleukin signalling. This is further supported by gene-expression studies of orbital biopsies that show interleukin, interferon, and TGF-signalling involvement.[27,28] NHOL is driven by chromosomal translocations that drive B cell malignant growth,[29] accompanied by chronic immune activation.[30,31] The precise aetiology of IOI is unknown, yet B cell infiltration is also observed in IOI biopsies.[27,32] Although the serum concentration of B cell associated miRNAs was similar between NHOL and IOI patients (**Supporting Information Table S4**), we observed that the mean levels of miRNAs in the identified cluster were slightly increased in IOI patients compared to NHOL. This increase is of interest because *miR-148a* and *miR-365* of the cluster are linked to specific B cell mechanisms. The microRNA *miR-148a* is a key regulator of B-cell tolerance and causes lethal autoimmune disease when increased in lupus-prone mice.[33] For *miR-365*, we observed that the expression correlated with serum IgG and IgM. *MiR-365* has been shown to regulate IL-6 signalling, which is important for B-cell differentiation.[34] Noteworthy, the levels of *miR-148a* and *miR-365* were not linked to the general B cell population (**Supporting Information Figure S4**). Therefore, future studies on *miR-148a* and *miR-365* in specific B cell populations may aid in the differentiation of NHOL from IOI.

MiRNAs derived from leukocytes in blood are a major source of serum miRNAs and we observed that *miR-223-3p* and *miR-29a* were strongly associated with myeloid and lymphoid populations, respectively. A major source of *miR-223* in blood is neutrophils.[35] Although the neutrophil frequency in whole blood was not increased in patients with NHOL and IOI, we did observe that the neutrophil cell size in NHOL patients was higher compared to IOI. Note that the neutrophil cell size showed a wider ranger in IOI patients and exhibited a positive correlation

with the serum levels of *miR-223-3p* in serum of IOI patients. As we observe a 'pathological' increase of *miR-223-3p* in orbital disease, the increased neutrophil cell size could therefore be related to disease mechanisms. For example, blood neutrophil size increases after stimulation with various agonists.[36] Neutrophils are known to infiltrate lymphoma tissues where they can produce APRIL, a potent factor that can induce B cell neoplasia and is linked to tumour aggressiveness and disease outcome.[37] Alternatively, neutrophils have been shown to protect lymphoma B cells against chemotherapeutic agents by direct cell interaction.[38] These neutrophil functions support a role for neutrophils in NHOL, but follow-up studies on the relation between *miR-223* and neutrophils in NHOL are warranted. This relation may be of interest since the serum levels of *miR-223* have been linked with poor cancer prognosis.[39]

Considering these associations, more detailed investigation of circulatory cellular compartments and neutrophil populations could reveal changes in other leukocyte populations that may differentiate NHOL from IOI. The lack of association between miRNA levels and other clinical parameters may in part be caused by heterogeneity among patients. We noted that the expression of cluster miRNAs was highly variable amongst patients. Better understanding of this heterogeneity and the link to disease outcomes may provide opportunities to conduct personalized therapy adjustments or prognosis predictions.

Using discovery, technical validation and independent replication of serum miRNAs, we showed high concordance of the *OpenArray®* with targeted RT-qPCR. Although the *Area Under the Receiver Operating Characteristics* suggest that subtle changes in miRNA levels in serum (FC < 2) may be relevant to distinguish patients from controls (**Supporting Information Table S3**), we show that reproducible changes in miRNAs are the best in those with FC > 2. This suggests a limitation of the *OpenArray®* platform, as it may be less sensitive to accurately detect subtle differences in miRNA expression, and small RNA sequencing would be more appropriate to further investigate other candidates. We aimed to identify miRNAs that were distinct between NHOL and IOI, but identified strong disease signatures that were shared by these conditions.

NHOL covers several disease subtypes with varying disease course and underlying molecular circuitry.[1] Most NHOL were of the EMZL subtype in this study (**Table 1**) and we were therefore unable to compare NHOL subtypes. Previously, a comparison of miRNA profiles in NHOL tissue of EMZL and DLBCL have been found to differ,[40] although this was not compared in peripheral blood and did not include a control group. Three NHOL patients included in this study had a history of lymphoma in remission. Although they could be considered secondary NHOL, their

results were comparable to the NHOL group as a whole and were not considered outliers within the data. Idiopathic conditions such as IOI that are diagnosed based on exclusion may show relatively high variability of disease characteristics, which would require large sample size to dissect disease endotypes to better differentiate these from NHOL.

The variability within the IOI population is supported by previous gene expression studies that suggest overlap between an IOI subgroup and disease such as GPA.[28] However, IOI remains a clinical entity,[7] classically treated with oral immunosuppressant therapy.[4,6]

Our study suggests that serum miRNAs analysed by the *OpenArray®* platform provide no feasible clinical biomarkers to differentiate NHOL from IOI. However, the results of the current study should be considered a stepping-stone into deeper understanding the close relation between these orbital pathologies and guide future studies that use molecular phenotyping for differentiation. For future studies we would recommend the use of functional experiments for the miRNA cluster found in this study. Additionally, peripheral blood immune-phenotyping could reveal cell-types of interest for differentiation of NHOL and IOI.

In conclusion, we observed overlapping serum miRNA profiles between NHOL and IOI, and identified a pan-inflammatory miRNA-cluster upregulated in patients of both diseases compared to controls. The findings of this study bring new insights in the complex and possibly overlapping pathophysiology of NHOL and IOI.

Materials and methods

Ethical considerations

This cross-sectional case-control study was conducted in compliance with the Helsinki principles. Ethical approval was requested and obtained from the local Medical Ethical Research Committee in Utrecht and all patients signed written informed consent before participation.

Discovery and replication cohorts

In total, 40 NHOL (*n = 18*) and IOI (*n = 22*) patients and 25 unaffected controls (HC) were included in this study (**Figure 1A**). All patients were recruited at the department of Ophthalmology at the University Medical Center Utrecht, Utrecht, The Netherlands between February 2015 and May 2018. We performed serum miRNA experiments in a discovery cohort (NHOL: *n = 10*, IOI: *n = 14*, HC: *n = 9*) and one year later a replication cohort (NHOL: *n = 8*, IOI: *n = 8*; HC: *n = 16*). All patients were diagnosed by an ophthalmologist specialized in orbital diseases.

NHOL patients were diagnosed following WHO criteria with histopathological assessment of incisional biopsies.[41] Within the histopathologic examination, the pathologist assessed B and T cell specific markers (CD3, CD5, CD20, CD79α) and specific B cell subset markers (BCL2, BCL6, CD10, CD23, CD30, Cyclin D-1, MUM-1, and κ and λ light chains) for NHOL subtyping. Additional molecular analysis included PCR to assess monoclonality in all but two biopsies and translocations were assessed by fluorescence in situ hybridization in patients with DLBCL.

IOI were diagnosed based on exclusion of infection, specific orbital inflammatory disorder (e.g. thyroid eye disease, granulomatosis with polyangiitis (former Wegener's disease), sarcoidosis, primary Sjögren's syndrome, benign lymphoid hyperplasia, histiocytic disease or IgG4-related pathology), or malignant neoplasia based on consensus criteria.[7,8] Histopathological confirmation of incisional biopsies was obtained in all patients, except in patients with idiopathic myositis (*n = 6*). All IOI biopsies revealed a non-specific polymorphous plasmalymphocytic infiltrate, negative for IgG4, with or without the presence of neutrophils, eosinophils, histiocytes, and macrophages, and varying amounts of fibrosis in the connective tissue. Idiopathic myositis was diagnosed based on the presence of pain, diplopia, (paretic) motility reduction, and pain with eye-movement, negative laboratory findings (e.g. negative antibodies and normal serum IgG4 levels) and extra-ocular muscle swelling with contrast-enhancement on *magnetic resonance imaging*.[7]
All patients had blood withdrawal at the time of diagnosis in active disease and before treatment initiation. Additionally, none of the patients received systemic corticosteroids three months — or immunomodulatory treatment in the last six months — prior to blood withdrawal, except for one patient of the validation cohort (low dose of 2.5 mg oral prednisolone daily). Also, patients had not received radiation treatment or chemotherapy in the last year before sampling. A total of 25 anonymous blood-donors with no history of inflammatory disease or malignancies were included as an unaffected control group.

Reference cohorts

To assess specificity for orbital disease associated miRNAs, we included local and systemic inflammatory reference groups of which *OpenArray®* miRNA data was available in our center. *OpenArray®* data were obtained for 28 patients with anterior uveitis, idiopathic intermediate uveitis, and Birdshot uveitis, and 16 controls from a recent serum miRNA profiling study.[16] In addition, we collected serum from 29 patients with psoriasis, psoriatic arthritis, axial spondyloarthritis, and 10 controls, of which data has not been published previously and therefore described in more detail. Briefly, patients were recruited from the Department of Rheumatology & Clinical Immunology of the University Medical Center Utrecht, Utrecht, The Netherlands with active disease and were free from systemic immunomodulatory treatment at

the time of blood withdrawal. Psoriasis patients were diagnosed by dermatologists with a consultation by a rheumatologist. Psoriatic arthritis was classified by a rheumatologist following the CASPAR criteria,[42] and axial spondyloarthritis was classified by a rheumatologist in accordance with Assessment of SpondyloArthritis International Society classification criteria.[43]

OpenArray® profiling

Blood was drawn in serum tubes containing separating gel and clot activator (BD Vacutainer), rested for 30 min at room temperature and centrifuged for 10 min at 2000 × *g*. Serum was isolated and stored at −80°C until measurements were performed as previously described by *Verhagen et al. 2018*.[16] In brief, RNA was extracted from 200 µL serum using Exiqon's MiRCURY™ RNA Isolation Kit for biofluids (Exiqon, Denmark), according to manufacturer's instructions. We used non-human miRNA (*ath-miR-159a*) as spike-in control for normalization in data-analysis. Screening for miRNAs was performed using Taqman real-time PCR on the *OpenArray®* platform (Thermo Fisher Scientific, USA) according to manufacturer's instruction.

With this technique, a total of 758 miRNAs could be screened in two primer pools, pool A and pool B (Life Technologies). Reverse transcription (RT) was performed on 2.5 µL isolated RNA using multiplex RT primers (v2.1 for pool A and v3.0 for pool B) and the TaqMan miRNA RT kit (Thermo Fisher Scientific, USA). Megaplex™ PreAmp Primers and TaqMan PreAmp Master Mix (Thermo Fisher Scientific, USA) were used for preamplification of RT products with the following thermal cycler conditions: 10 min at 95°C, 2 min at 55°C, 2 min at 72°C, 16 cycles of 15 sec at 95°C, and 4 min at 60°C, followed by a single cycle of 10 min at 96°C (Biometra® Thermocycler). The pre-amplified products were diluted (1:40) in 0.1xTE buffer (pH 8) and (1:2) with the TaqMan *OpenArray®* Real-Time PCR Master Mix. MiRNA profiling was performed on the QuantStudio 12 K Flex Real-Time PCR system (Thermo Fisher Scientific, USA). The miRNA expression levels were analysed using the ThermoFisher Cloud software v1.0 (www.thermofisher.com). Samples with an amplification score <1.25 were excluded and the expression levels converted to the platforms relative cycle threshold (Crt) values. MiRNAs with a mean Crt > 27 were considered to be below the detection level and excluded from further analysis. For the included miRNAs (mean Crt < 27 in all samples), individual samples with Crt > 27 were set to Crt = 27. We excluded miRNAs for further analysis if these were detected in < 80% of all samples. The relative expression was defined as the ΔCrt value, which is calculated to normalize the data by subtraction the mean Crt-value of the spike-in control from the mean Crt for each miRNA ($\Delta Crt = Crt_{mean\ target} - Crt_{mean\ spike\text{-}in}$). Differences in miRNA expression levels were assessed comparing the comparative threshold

cycle method.[44] Relative miRNA expression levels are presented as Fold Change (FC = $2^{-\Delta\Delta Crt}$, where $\Delta\Delta Crt = \Delta Crt_{sample} - \Delta Crt_{reference}$) with a mean ΔCrt of the control group as reference (set at mean FC = 1). We considered differentially expressed miRNAs with a threshold values of FC > 2.0 and $p < 0.05$. We selected miRNAs for validation based on a combination of the highest FC difference and lowest *p*-values between the study groups, and strong correlations. A non-differentially expressed miRNA was taken along as control.

Single RT-qPCR assay for validation

Single TaqMan RT-qPCR was performed for 12 miRNAs selected for validation (**Supporting Information Table S2**). The cDNA was synthesized from 2.5μL RNA using individual miRNA-specific stem-loop primers according to manufacturer's instructions in the presence of 3.3 U/μL MultiScribe RT enzyme (Thermo Fisher). After addition of the TaqMan Fast Advance Master Mix and specific primers, miRNA expression was quantified in duplicate using the QuantStudio 12 K Flex Real-Time PCR system. *Anth-miR-159a* was used as the spike-in control. Technical validation was defined as strong correlation (Spearman's ρ correlation > 0.75 and $p < 0.05$) between Crt values from the OpenArray and cycle threshold (Ct) values from the RT-qPCR assay for each individual miRNA target. Next, technically validated miRNAs were independently assessed using a second cohort ($n = 32$) for biological replication. Analysis of relative miRNA expression for the RT-qPCR assay was similar to the analysis of the *OpenArray®* profiling, using the median ΔCt value for the control group as a reference (set at 1).

Statistical analysis

The discovery cohort analysis of the *OpenArray®* profiling was performed within the Thermo Fisher Cloud software and the replication cohort using IBM SPSS Statistics for Windows, Version 25.0, released in 2017 (Armonk, NY: IBM Corp). The Thermo Fisher Cloud software exploits an independent samples *t*-test to compare ΔΔCrt data to one randomly selected representative reference control sample using a two-tailed *p*-value threshold of 0.05. For technical validation of the discovery cohort for *OpenArray®* and RT-qPCR array data we used the Spearman rank correlation test. For comparison with the discovery cohort we used an independent samples *t*-test for the replication cohort. For the analysis of the combined discovery and replication cohorts we used the Kruskal–Wallis test with post-hoc Dunn's correction to adjust *p*-values. Additionally, a Benjamini–Hochberg correction was deployed on the combined cohort results to correct for multiple testing.[45] We associated miRNA expression with clinical characteristics (**Supporting Information Table S4**) using the ΔΔCt of the combined analysis (both cohorts). Principal component analysis and hierarchical cluster analysis of the

OpenArray® data were conducted using the MetaboAnalyst servers v4.0 or the heatmap.2 function in the R *gplot* package.[46] GraphPad Prism (GraphPad, La Jolla, CA, USA) was used for violin- and volcanoplots.

MiRNA gene target analysis

Target genes of the validated miRNAs were mapped using *miRTargetLink*.[19] The R package *clusterProfiler* was used for pathway enrichment analyses,[47] exploiting the *Kyoto Encyclopaedia of Genes and Genomes* (KEGG) pathways[48] and *Reactome Pathway Knowledgebase*[49] databases.

MiRNA profiling in circulatory leukocyte cell subsets

Global MicroRNA expression data of nine primary purified leukocyte populations were derived from four non-coding RNA microarray data sets available via the Gene Expression Omnibus public repository of the NCBI (accession no. GSE19183, GSE28487, GSE28489, GSE98830). The FACS-sorted populations were obtained from 12 unaffected controls and include multiple populations from the same individuals. Raw data scans (.CEL files) were read into R (R version 3.3.2). Samples were pre-processed with Affy package version 3.3.1 for Affymetrix Multispecies miRNA-1 Array and Limma package version 3.3.3 for Agilent-021827 Human miRNA Microarray. A total of 825 overlapping human micro-RNAs for 108 samples were pooled and quantile-normalized. A principle component analysis was performed to interrogate miRNA expression profiles for the selected miRNAs of the validation phase (except for U6 snRNA that was not available within the dataset) using MetaboAnalyst 3.05 with the exception of the first component to reduce technical variation and batch effect.[50]

Whole blood leukocyte counts

Leukocyte counts, leukocyte subset counts, as well as leukocyte cell size and leukocyte complexity in blood were obtained for most patients from routine analysis of whole blood samples by the CELL-DYN Sapphire (Abbott Diagnostics, Santa Clara, CA, USA), an automated routine haematology analyser that uses spectrophotometry, electrical impedance, and laser light scattering.[51] The neutrophil cell size and complexity were determined by optical scatter using 0° Axial Light Loss for cell size and 7° Intermediate Angle Scatter for complexity. CELL-DYN data from the Utrecht Patient Oriented Database (UPOD) were used. UPOD is an infrastructure of relational databases comprising data on patient characteristics, hospital discharge diagnoses, medical procedures, medication orders, and laboratory tests for all patients treated at the University Medical Center Utrecht, Utrecht, The Netherlands since 2004. UPOD data acquisition and management is in accordance with current regulations concerning privacy and ethics. The

structure and content of UPOD have been described in more detail elsewhere.[52]

Acknowledgments

This study was supported by unrestricted grants from the Dr. F.P Fischerstichting, Stichting Lijf & Leven, Rotterdamse Stichting Blindenbelangen and Stichting Ankie Hak. The funders had no role in study design, data collection and analysis, decision to publish, or preparation of the manuscript. K.G.L., R.K., T.R.D.J.R., J.H.dB., and J.J.W.K. devised the study. NHOL and IOI patients were recruited by R.K., R.L.P.V., C.A.E.E., S.W.G., M.M.P.M., and K.G.L. Serum was isolated by K.G.L. and S.H., while K.G.L. and C.B. performed the miRNA measurements. F.H.V. and E.J.L recruited patients, isolated serum and conducted miRNA profiling of patients with uveitis and rheumatic conditions. S.H and M.C.H.dG provided the CELL–DYN UPOD data. K.G.L. and J.J.W.K. performed data analysis and wrote the manuscript. All authors reviewed the manuscript.

Conflict of interest

The authors declare no financial or commercial conflict of interest.

References

1. Olsen TG and Heegaard S. Orbital lymphoma. Surv. Ophthalmol. 2019. 64: 45– 66.
2. Olsen TG, Holm F, Mikkelsen LH, Rasmussen PK, Coupland SE, Esmaeli B, Finger PT, et al. Orbital lymphoma—an international multicenter retrospective study. Am. J. Ophthalmol. 2019. 199: 44– 57.
3. Ben Simon GJ, Cheung N, McKelvie P, Fox R and McNab AA. Oral chlorambucil for extranodal, marginal zone, B-cell lymphoma of mucosa-associated lymphoid tissue of the orbit. Ophthalmology 2006. 113: 1209– 13.
4. Yuen SJA, and Rubin PAD. Idiopathic orbital inflammation: distribution, clinical features, and treatment outcome. Arch. Ophthalmol. (Chicago, Ill. 1960). 2003. 121: 491– 9.
5. Yan J, Wu Z and Li Y. The differentiation of idiopathic inflammatory pseudotumor from lymphoid tumors of orbit: analysis of 319 cases. Orbit 2004. 23: 245– 54.
6. Gordon LK. Orbital inflammatory disease: a diagnostic and therapeutic challenge. Eye 2006. 20: 1196– 1206.
7. Mombaerts I, Bilyk JR, Rose GE, McNab AA, Fay A, Dolman PJ, Allen RC, et al. Consensus on diagnostic criteria of idiopathic orbital inflammation using a modified delphi approach. JAMA Ophthalmol. 2017. 135: 769– 776.
8. Mombaerts I, Rose GE and Garrity JA. Orbital inflammation: biopsy first. Surv. Ophthalmol. 2016. 61: 664– 669.
9. Hiwatashi A, Togao O, Yamashita K, Kikuchi K, Kamei R, Yoshikawa H, Takemura A et al. Diffusivity of intraorbital lymphoma vs. inflammation: comparison of single shot turbo spin echo and multishot echo planar imaging techniques. Eur. Radiol. 2018. 28: 325– 330.
10. Baek D, Villén J, Shin C, Camargo FD, Gygi SP and Bartel DP. The impact of microRNAs on protein output. Nature 2008. 455: 64– 71.
11. Solé C, Arnaiz E and Lawrie CH. MicroRNAs as biomarkers of B-cell lymphoma. Biomark. Insights. 2018. 13: 117727191880684. https://doi.org/10.1177/1177271918806840.
12. Marques-Rocha JL, Samblas M, Milagro FI, Bressan J, Martínez JA and Marti A. Noncoding RNAs, cytokines, and inflammation-related diseases. FASEB J. 2015. 29: 3595– 611.
13. Mi S, Zhang J, Zhang W and Huang RS. Circulating microRNAs as biomarkers for inflammatory diseases. MicroRNA (Shariqah, United Arab Emirates). 2013. 2: 63– 71.
14. Larrabeiti-Etxebarria A, Lopez-Santillan M, Santos-Zorrozua B, Lopez-Lopez E and Garcia-Orad A. Systematic review of the potential of microRNAs in diffuse large B cell lymphoma. Cancers (Basel). 2019. 11: 144.
15. Tuo J, Shen D, Yang HH and Chan CC. Distinct microRNA-155 expression in the vitreous of patients with primary vitreoretinal lymphoma and uveitis. Am. J. Ophthalmol. 2014. 157: 728– 34.
16. Verhagen FH, Bekker CPJ, Rossato M, Hiddingh S, de Vries L, Devaprasad A, Pandit A et al. A disease-associated microRNA cluster links inflammatory pathways and an altered composition of leukocyte subsets to noninfectious uveitis. Invest. Ophthalmol. Vis. Sci. 2018. 59: 878– 888.
17. Singh A, Bhattacharyya N, Srivastava A, Pruett N, Ripley RT, Schrump DS and Hoang CD. MicroRNA-215-5p treatment suppresses mesothelioma progression via the MDM2-p53-signaling axis. Mol. Ther. 2019. 27: 1665– 1680.
18. Zhang Q, Weng Y, Jiang Y, Zhao S, Zhou D and Xu N. Overexpression of miR-140-5p inhibits lipopolysaccharide-induced human intervertebral disc inflammation and degeneration by downregulating toll-like receptor 4. Oncol. Rep. 2018. 40: 793– 802.
19. Hamberg M, Backes C, Fehlmann T, Hart M, Meder B, Meese E and Keller A. miRTargetLink—miRNAs, genes and interaction networks. Int. J. Mol. Sci. 2016. 17: 564.
20. Zheng B, Xi Z, Liu R, Yin W, Sui Z, Ren B, Miller H, et al. The function of microRNAs in B-cell development, lymphoma, and their potential in clinical practice. Front. Immunol. 2018. 9: 936.
21. Khoury S and Tran N. Circulating microRNAs: potential biomarkers for common malignancies. Biomark. Med. 2015. 9: 131– 151.
22. Correia CN, Nalpas NC, McLoughlin KE, Browne JA, Gordon SV, MacHugh DE and Shaughnessy RG. Circulating microRNAs as potential biomarkers of infectious disease. Front. Immunol. 2017. 8: 118.
23. Backes C, Meese E and Keller A. Specific miRNA disease biomarkers in blood, serum and plasma: challenges and prospects. Mol. Diagn. Ther. 2016. 20: 509– 518.
24. Fernandez-Mercado M, Manterola L and Lawrie C. MicroRNAs in lymphoma: regulatory role

and biomarker potential. Curr. Genomics 2015. 16: 349– 358.
25. Arribas AJ, Campos-Martín Y, Gómez-Abad C, Algara P, Sánchez-Beato M, Rodriguez-Pinilla MS, Montes-Moreno S, et al. Nodal marginal zone lymphoma: gene expression and miRNA profiling identify diagnostic markers and potential therapeutic targets. Blood 2012. 119: e9– e21.
26. Caramuta S, Lee L, Ozata DM, Akçakaya P, Georgii-Hemming P, Xie H, Amini RM, et al. Role of microRNAs and microRNA machinery in the pathogenesis of diffuse large B-cell lymphoma. Blood Cancer J. 2013. 3: e152.
27. Wladis EJ, Iglesias BV and Gosselin EJ. Characterization of the molecular biologic milieu of idiopathic orbital inflammation. Ophthalmic Plast. Reconstr. Surg. 2011. 27: 251– 254.
28. Rosenbaum JT, Choi D, Wilson DJ, Grossniklaus HE, Harrington CA, Sibley CH, Dailey RA, et al. Orbital pseudotumor can be a localized form of granulomatosis with polyangiitis as revealed by gene expression profiling. Exp. Mol. Pathol. 2015. 99: 271– 278.
29. Takahashi H, Usui Y, Ueda S, Yamakawa N, Sato-Otsubo A, Sato Y, Ogawa S, et al. Genome-wide analysis of ocular adnexal lymphoproliferative disorders using high-resolution single nucleotide polymorphism array. Invest. Ophthalmol. Vis. Sci. 2015. 56: 4156– 65.
30. Makgoeng SB, Bolanos RS, Jeon CY, Weiss RE, Arah OA., Breen EC, Martínez-Maza O, et al. Markers of immune activation and inflammation, and non-hodgkin lymphoma: a meta-analysis of prospective studies. JNCI cancer Spectr. 2018. 2: pky082.
31. Smedby KE and Ponzoni M. The aetiology of B-cell lymphoid malignancies with a focus on chronic inflammation and infections. J. Intern. Med. 2017. 282: 360– 370.
32. Ho VH, Chevez-Barrios P, Jorgensen JL, Silkiss RZ, Silkis RZ and Esmaeli B. Receptor expression in orbital inflammatory syndromes and implications for targeted therapy. Tissue Antigens 2007. 70: 105– 9.
33. Gonzalez-Martin A, Adams BD, Lai M, Shepherd J, Salvador-Bernaldez M, Salvador JM, Lu J, et al. The microRNA miR-148a functions as a critical regulator of B cell tolerance and autoimmunity. Nat. Immunol. 2016. 17: 433– 40.
34. Xu Z, Xiao SB, Xu P, Xie Q, Cao L, Wang D, Luo R, et al. miR-365, a novel negative regulator of interleukin-6 gene expression, is cooperatively regulated by Sp1 and NF-κB. J. Biol. Chem. 2011. 286: 21401– 21412.
35. Tsitsiou E and Lindsay MA. microRNAs and the immune response. Curr. Opin. Pharmacol. 2009. 9: 514– 20.
36. Bashant KR, Vassallo A, Herold C, Berner R, Menschner L, Subburayalu J, Kaplan MJ, et al. Real-time deformability cytometry reveals sequential contraction and expansion during neutrophil priming. J. Leukoc. Biol. 2019. https://doi.org/10.1002/JLB.MA0718-295RR.
37. Schwaller J, Schneider P, Mhawech-Fauceglia P, McKee T, Myit S, Matthes T, Tschopp J, et al. Neutrophil-derived APRIL concentrated in tumor lesions by proteoglycans correlates with human B-cell lymphoma aggressiveness. Blood 2007. 109: 331– 8.
38. Hirz T, Matera EL, Chettab K, Jordheim LP, Mathé D, Evesque A, Esmenjaud J, et al. Neutrophils protect lymphoma cells against cytotoxic and targeted therapies through CD11b/ICAM-1 binding. Oncotarget 2017. 8: 72818– 72834.
39. Li Z, Yang Y, Du L, Dong Z, Wang L, Zhang X, Zhou X, et al. Overexpression of miR-223 correlates with tumor metastasis and poor prognosis in patients with colorectal cancer. Med. Oncol. 2014. 31: 256.
40. Hother C, Rasmussen PK, Joshi T, Reker D, Ralfkiær U, Workman CT, Heegaard S, et al. MicroRNA profiling in ocular adnexal lymphoma: a role for MYC and NFKB1 mediated dysregulation of microRNA expression in aggressive disease. Invest. Ophthalmol. Vis. Sci. 2013. 54: 5169– 75.
41. Swerdlow SH, Campo E, Pileri SA, Harris NL, Stein H, Siebert R, Advani R, et al. The 2016 revision of the World Health Organization classification of lymphoid neoplasms. Blood 2016. 127: 2375– 2390.
42. Taylor W, Gladman D, Helliwell P, Marchesoni A, Mease P, Mielants H, CASPAR Study Group. Classification criteria for psoriatic arthritis: Development of new criteria from a large international study. Arthritis Rheum. 2006. 54: 2665– 2673.
43. Rudwaleit M, van der Heijde D, Landewé R, Listing J, Akkoc N, Brandt J, Braun J, et al. The development of Assessment of SpondyloArthritis international Society classification criteria for axial spondyloarthritis (part II): validation and final selection. Ann. Rheum. Dis. 2009. 68: 777– 83.
44. Livak KJ and Schmittgen TD. Analysis of relative gene expression data using real-time

quantitative PCR and the 2(-Delta Delta C(T)) method. Methods 2001. 25: 402– 8.
45. Benjamini Y and Hochberg Y. Controlling the false discovery rate: a practical and powerful approach to multiple testing. J. R. Stat. Soc. Ser. B. 1995. 57: 289– 300.
46. Li Y, Lip G, Chong V, Yuan J and Ding Z. Idiopathic orbital inflammation syndrome with retro-orbital involvement: a retrospective study of eight patients rosenbaum JT, ed. PLoS One 2013. 8: e57126.
47. Yu G, Wang LG, Han Y and He QY. clusterProfiler: an R package for comparing biological themes among gene clusters. OMICS 2012. 16: 284– 7.
48. Kanehisa M and Goto S. KEGG: kyoto encyclopedia of genes and genomes. Nucleic Acids Res. 2000. 28: 27– 30.
49. Fabregat A, Jupe S, Matthews L, Sidiropoulos K, Gillespie M, Garapati P, Haw R, et al. The reactome pathway knowledgebase. Nucleic Acids Res. 2018. 46: D649– D655.
50. Leek JT, Scharpf RB, Bravo HC, Simcha D, Langmead B, Johnson WE, Geman D, et al. Tackling the widespread and critical impact of batch effects in high-throughput data. Nat. Rev. Genet. 2010. 11: 733– 9.
51. Groeneveld KM, Heeres M, Leenen LPH, Huisman A and Koenderman L. Immunophenotyping of posttraumatic neutrophils on a routine haematology analyser. Mediators Inflamm. 2012. 2012: 509513.
52. ten Berg MJ, Huisman A, van den Bemt PMLA, Schobben AFAM, Egberts ACG and van Solinge WW. Linking laboratory and medication data: new opportunities for pharmacoepidemiological research. Clin. Chem. Lab. Med. 2007. 45.

Supporting Information Table S1. OpenArray® results of 120 microRNAs in the serum of patients and controls used for analysis.

Assay			HC		IOI		NHOL	
ID	miR-assay ID	miR-Base ID	Mean ΔCrt (SE)	FC (95% CI)	Mean ΔCrt (SE)	FC (95% CI)	Mean ΔCrt (SE)	FC (95% CI)
379	hsa-let-7c	hsa-let-7c-5p	14.65 (0.18)	1.00 (0.76-1.32)	14.22 (0.16)	1.35 (1.06-1.72)	14.53 (0.19)	1.09 (0.81-1.48)
387	hsa-miR-10a	hsa-miR-10a-5p	13.96 (0.2)	1.00 (0.73-1.37)	14.05 (0.17)	0.94 (0.72-1.23)	14.20 (0.27)	0.85 (0.55-1.31)
390	hsa-miR-15b	hsa-miR-15b-5p	8.10 (0.14)	1.00 (0.80-1.25)	7.86 (0.28)	1.18 (0.77-1.80)	7.93 (0.21)	1.12 (0.81-1.55)
391	hsa-miR-16	hsa-miR-16-5p	5.26 (0.11)	1.00 (0.84-1.19)	4.61 (0.25)	1.57 (1.08-2.28)	4.73 (0.25)	1.45 (0.98-2.14)
395	hsa-miR-19a	hsa-miR-19a-3p	9.77 (0.08)	1.00 (0.88-1.13)	9.10 (0.26)	1.59 (1.08-2.35)	9.25 (0.24)	1.43 (0.98-2.09)
396	hsa-miR-19b	hsa-miR-19b-3p	3.95 (0.05)	1.00 (0.92-1.08)	3.36 (0.23)	1.51 (1.06-2.14)	3.29 (0.17)	1.58 (1.20-2.10)
397	hsa-miR-21	hsa-miR-21-5p	6.57 (0.13)	1.00 (0.82-1.23)	6.10 (0.15)	1.39 (1.11-1.73)	6.01 (0.15)	1.47 (1.16-1.87)
399	hsa-miR-23a	hsa-miR-23a-3p	12.56 (0.12)	1.00 (0.81-1.23)	11.91 (0.19)	1.56 (1.16-2.11)	11.87 (0.20)	1.60 (1.16-2.22)
402	hsa-miR-24	hsa-miR-24-3p	4.78 (0.15)	1.00 (0.78-1.28)	4.28 (0.20)	1.42 (1.05-1.92)	4.36 (0.22)	1.34 (0.94-1.91)
403	hsa-miR-25	hsa-miR-25-3p	8.13 (0.12)	1.00 (0.82-1.22)	7.42 (0.23)	1.63 (1.16-2.29)	7.64 (0.30)	1.40 (0.87-2.26)
405	hsa-miR-26a	hsa-miR-26a-5p	7.54 (0.11)	1.00 (0.84-1.19)	7.84 (0.21)	0.82 (0.59-1.13)	7.75 (0.19)	0.87 (0.64-1.18)
407	hsa-miR-26b	hsa-miR-26b-5p	8.17 (0.10)	1.00 (0.86-1.17)	8.13 (0.23)	1.03 (0.73-1.46)	8.25 (0.22)	0.95 (0.67-1.34)
408	hsa-miR-27a	hsa-miR-27a-3p	8.93 (0.13)	1.00 (0.82-1.22)	8.51 (0.22)	1.34 (0.95-1.87)	8.50 (0.19)	1.35 (1.00-1.83)
409	hsa-miR-27b	hsa-miR-27b-3p	10.17 (0.13)	1.00 (0.82-1.23)	10.06 (0.18)	1.08 (0.82-1.41)	9.67 (0.18)	1.41 (1.06-1.88)
411	hsa-miR-28	hsa-miR-28-5p	10.24 (0.17)	1.00 (0.76-1.31)	10.47 (0.18)	0.85 (0.65-1.13)	10.61 (0.19)	0.78 (0.57-1.05)
413	hsa-miR-29b	hsa-miR-29b-3p	13.79 (0.33)	1.00 (0.59-1.69)	13.22 (0.26)	1.48 (1.00-2.20)	12.93 (0.31)	1.81 (1.10-2.98)
416	hsa-miR-30a-3p	hsa-miR-30a-3p	15.01 (0.16)	1.00 (0.77-1.30)	14.99 (0.14)	1.01 (0.83-1.25)	14.99 (0.20)	1.01 (0.74-1.40)
417	hsa-miR-30a-5p	hsa-miR-30a-5p	7.24 (0.08)	1.00 (0.89-1.13)	6.83 (0.15)	1.32 (1.05-1.65)	7.15 (0.38)	1.06 (0.58-1.94)
419	hsa-miR-30c	hsa-miR-30c-5p	6.07 (0.13)	1.00 (0.81-1.23)	6.29 (0.20)	0.86 (0.64-1.16)	6.29 (0.15)	0.86 (0.67-1.10)
420	hsa-miR-30d	hsa-miR-30d-5p	10.27 (0.12)	1.00 (0.82-1.22)	9.81 (0.16)	1.38 (1.09-1.75)	10.21 (0.44)	1.04 (0.52-2.10)
422	hsa-miR-30e-3p	hsa-miR-30e-3p	12.63 (0.15)	1.00 (0.79-1.26)	12.35 (0.30)	1.22 (0.78-1.92)	12.43 (0.24)	1.15 (0.79-1.69)
426	hsa-miR-34a	hsa-miR-34a-5p	11.8 (0.15)	1.00 (0.79-1.27)	11.33 (0.10)	1.39 (1.19-1.62)	11.39 (0.35)	1.33 (0.77-2.31)
431	hsa-miR-92a	hsa-miR-92a-3p	3.56 (0.08)	1.00 (0.88-1.14)	3.28 (0.22)	1.21 (0.87-1.68)	3.46 (0.2)	1.07 (0.77-1.47)
435	hsa-miR-99a	hsa-miR-99a-5p	13.64 (0.17)	1.00 (0.75-1.33)	13.12 (0.21)	1.43 (1.03-2.00)	13.44 (0.25)	1.15 (0.76-1.75)
436	hsa-miR-99b	hsa-miR-99b-5p	9.99 (0.15)	1.00 (0.79-1.27)	10.29 (0.23)	0.81 (0.57-1.16)	10.60 (0.22)	0.66 (0.46-0.94)
439	hsa-miR-103	hsa-miR-103a-3p	9.13 (0.13)	1.00 (0.81-1.23)	9.14 (0.27)	0.99 (0.65-1.52)	9.16 (0.26)	0.98 (0.62-1.55)
442	hsa-miR-106b	hsa-miR-106b-5p	6.94 (0.06)	1.00 (0.90-1.11)	6.54 (0.26)	1.32 (0.89-1.96)	6.84 (0.21)	1.07 (0.76-1.51)
449	hsa-miR-125b	hsa-miR-125b-5p	11.72 (0.15)	1.00 (0.79-1.27)	11.15 (0.12)	1.48 (1.23-1.78)	11.14 (0.24)	1.49 (1.02-2.19)
451	hsa-miR-126#	hsa-miR-126-5p	9.43 (0.12)	1.00 (0.83-1.21)	9.58 (0.16)	0.90 (0.71-1.14)	9.41 (0.22)	1.01 (0.72-1.43)
452	hsa-miR-127	hsa-miR-127-3p	11.56 (0.22)	1.00 (0.70-1.42)	11.91 (0.29)	0.78 (0.51-1.21)	11.74 (0.26)	0.88 (0.58-1.35)

454	hsa-miR-130a	hsa-miR-130a-3p	8.09 (0.16)	1.00 (0.77-1.29)	8.24 (0.27)	0.90 (0.60-1.35)	8.04 (0.17)	1.04 (0.79-1.36)
456	hsa-miR-130b	hsa-miR-130b-3p	10.57 (0.09)	1.00 (0.86-1.16)	10.28 (0.24)	1.22 (0.85-1.74)	10.11 (0.18)	1.38 (1.03-1.84)
457	hsa-miR-132	hsa-miR-132-3p	10.01 (0.13)	1.00 (0.82-1.22)	9.54 (0.14)	1.39 (1.12-1.71)	9.58 (0.21)	1.34 (0.96-1.88)
464	hsa-miR-142-3p	hsa-miR-142-3p	7.10 (0.12)	1.00 (0.83-1.21)	7.29 (0.19)	0.88 (0.65-1.17)	7.28 (0.20)	0.88 (0.65-1.21)
468	hsa-miR-146a	hsa-miR-146a-5p	6.70 (0.13)	1.00 (0.82-1.23)	6.96 (0.25)	0.84 (0.57-1.22)	6.37 (0.23)	1.26 (0.88-1.80)
470	hsa-miR-148a	hsa-miR-148a-3p	10.42 (0.14)	1.00 (0.80-1.25)	9.23 (0.30)	2.28 (1.46-3.57)	9.70 (0.31)	1.65 (1.00-2.72)
471	hsa-miR-148b	hsa-miR-148b-3p	12.65 (0.27)	1.00 (0.65-1.55)	12.62 (0.27)	1.02 (0.68-1.54)	12.62 (0.26)	1.02 (0.68-1.54)
473	hsa-miR-150	hsa-miR-150-5p	6.49 (0.23)	1.00 (0.69-1.44)	6.17 (0.20)	1.25 (0.93-1.68)	6.46 (0.25)	1.02 (0.69-1.52)
475	hsa-miR-152	hsa-miR-152-3p	11.39 (0.16)	1.00 (0.77-1.29)	11.20 (0.15)	1.14 (0.90-1.44)	11.19 (0.17)	1.14 (0.87-1.51)
480	hsa-miR-181a	hsa-miR-181a-5p	10.87 (0.11)	1.00 (0.84-1.19)	11.00 (0.15)	0.91 (0.72-1.15)	11.3 (0.16)	0.74 (0.57-0.96)
491	hsa-miR-192	hsa-miR-192-5p	8.57 (0.18)	1.00 (0.75-1.33)	8.01 (0.18)	1.47 (1.12-1.94)	8.12 (0.22)	1.36 (0.96-1.93)
493	hsa-miR-194	hsa-miR-194-5p	13.49 (0.23)	1.00 (0.69-1.45)	13.33 (0.25)	1.12 (0.76-1.63)	13.46 (0.15)	1.02 (0.80-1.30)
494	hsa-miR-195	hsa-miR-195-5p	9.36 (0.11)	1.00 (0.85-1.18)	8.61 (0.26)	1.69 (1.13-2.51)	8.87 (0.24)	1.40 (0.95-2.06)
507	hsa-miR-203	hsa-miR-203a-3p	14.04 (0.36)	1.00 (0.55-1.81)	13.94 (0.23)	1.07 (0.75-1.52)	13.51 (0.34)	1.45 (0.85-2.47)
508	hsa-miR-204	hsa-miR-204-5p	14.17 (0.25)	1.00 (0.67-1.50)	13.98 (0.27)	1.14 (0.76-1.72)	14.21 (0.21)	0.97 (0.70-1.37)
515	hsa-miR-212	hsa-miR-212-3p	13.55 (0.28)	1.00 (0.64-1.57)	13.16 (0.25)	1.32 (0.91-1.91)	13.43 (0.18)	1.09 (0.82-1.45)
518	hsa-miR-215	hsa-miR-215-5p	10.34 (0.06)	1.00 (0.91-1.10)	9.71 (0.20)	1.54 (1.13-2.11)	9.48 (0.27)	1.81 (1.17-2.80)
521	hsa-miR-218	hsa-miR-218-5p	13.78 (0.49)	1.00 (0.45-2.24)	13.33 (0.22)	1.36 (0.98-1.89)	14.25 (0.36)	0.72 (0.41-1.28)
524	hsa-miR-221	hsa-miR-221-3p	6.71 (0.14)	1.00 (0.79-1.26)	7.19 (0.25)	0.72 (0.50-1.05)	6.71 (0.13)	1.00 (0.82-1.23)
528	hsa-miR-301	hsa-miR-301a-3p	11.00 (0.23)	1.00 (0.69-1.44)	10.97 (0.28)	1.02 (0.67-1.56)	11.04 (0.22)	0.97 (0.68-1.38)
539	hsa-miR-324-5p	hsa-miR-324-5p	9.81 (0.13)	1.00 (0.81-1.24)	9.81 (0.21)	1.00 (0.73-1.37)	9.68 (0.21)	1.10 (0.79-1.53)
543	hsa-miR-328	hsa-miR-328-3p	7.88 (0.14)	1.00 (0.80-1.25)	8.13 (0.21)	0.84 (0.62-1.15)	8.20 (0.18)	0.80 (0.61-1.07)
546	hsa-miR-335	hsa-miR-335-5p	10.59 (0.11)	1.00 (0.84-1.19)	10.73 (0.24)	0.91 (0.63-1.31)	10.21 (0.18)	1.31 (0.99-1.73)
554	hsa-miR-361	hsa-miR-361-5p	12.00 (0.19)	1.00 (0.74-1.36)	11.01 (0.25)	1.98 (1.36-2.88)	11.38 (0.37)	1.54 (0.85-2.77)
563	hsa-miR-374	hsa-miR-374a-5p	9.20 (0.12)	1.00 (0.83-1.20)	9.11 (0.22)	1.06 (0.77-1.47)	9.15 (0.20)	1.04 (0.75-1.43)
564	hsa-miR-375	hsa-miR-375	11.08 (0.36)	1.00 (0.57-1.77)	11.25 (0.37)	0.89 (0.51-1.56)	11.22 (0.57)	0.91 (0.37-2.25)
565	hsa-miR-376a	hsa-miR-376a-3p	10.78 (0.42)	1.00 (0.51-1.96)	11.09 (0.38)	0.81 (0.46-1.43)	11.05 (0.27)	0.83 (0.54-1.28)
580	hsa-miR-20a	hsa-miR-20a-5p	3.94 (0.05)	1.00 (0.92-1.08)	3.53 (0.25)	1.32 (0.91-1.92)	3.64 (0.22)	1.23 (0.86-1.75)
587	hsa-miR-29c	hsa-miR-29c-3p	9.33 (0.09)	1.00 (0.87-1.15)	6.48 (1.40)	7.17 (0.86-59.5)	8.74 (0.30)	1.50 (0.93-2.41)
602	hsa-miR-30b	hsa-miR-30b-5p	5.69 (0.12)	1.00 (0.83-1.21)	6.04 (0.20)	0.79 (0.58-1.07)	5.86 (0.16)	0.89 (0.69-1.16)
1014	hsa-miR-20b	hsa-miR-20b-5p	11.62 (0.16)	1.00 (0.78-1.29)	11.06 (0.37)	1.48 (0.84-2.60)	11.19 (0.27)	1.35 (0.87-2.08)
1020	hsa-miR-365	hsa-miR-365a-3p	14.28 (0.27)	1.00 (0.64-1.57)	13.46 (0.36)	1.77 (1.01-3.11)	13.13 (0.37)	2.22 (1.20-4.12)
1090	hsa-miR-93	hsa-miR-93-5p	9.46 (0.16)	1.00 (0.77-1.29)	8.74 (0.28)	1.65 (1.08-2.52)	9.06 (0.28)	1.32 (0.85-2.04)

1097	hsa-miR-146b	hsa-miR-146b-5p	10.36 (0.10)	1.00 (0.85-1.18)	9.98 (0.18)	1.30 (0.99-1.71)	9.94 (0.22)	1.34 (0.94-1.90)
1141	hsa-miR-451	hsa-miR-451a	3.11 (0.06)	1.00 (0.90-1.11)	2.54 (0.25)	1.49 (1.03-2.17)	2.79 (0.21)	1.25 (0.90-1.74)
1187	hsa-miR-140	hsa-miR-140-5p	10.91 (0.19)	1.00 (0.74-1.34)	9.96 (0.32)	1.93 (1.19-3.14)	10.01 (0.31)	1.87 (1.14-3.08)
1271	hsa-miR-363	hsa-miR-363-3p	12.34 (0.20)	1.00 (0.70-1.44)	12.05 (0.15)	1.22 (0.96-1.54)	12.41 (0.15)	0.95 (0.74-1.22)
1274	hsa-miR-410	hsa-miR-410-3p	13.04 (0.29)	1.00 (0.62-1.61)	12.98 (0.32)	1.04 (0.64-1.70)	13.01 (0.35)	1.02 (0.58-1.81)
1319	hsa-miR-374-5p	hsa-miR-374b-5p	10.56 (0.12)	1.00 (0.83-1.20)	10.68 (0.24)	0.92 (0.64-1.32)	10.74 (0.20)	0.88 (0.64-1.21)
1338	rno-miR-7#	hsa-miR-7-1-3p	11.78 (0.14)	1.00 (0.80-1.25)	11.30 (0.26)	1.40 (0.95-2.05)	11.18 (0.20)	1.51 (1.11-2.07)
1515	hsa-miR-660	hsa-miR-660-5p	10.05 (0.09)	1.00 (0.86-1.16)	9.48 (0.18)	1.48 (1.13-1.95)	9.58 (0.26)	1.38 (0.91-2.10)
1518	hsa-miR-532	hsa-miR-532-5p	10.79 (0.12)	1.00 (0.83-1.21)	10.19 (0.17)	1.51 (1.17-1.96)	10.32 (0.24)	1.39 (0.95-2.03)
1597	hsa-miR-645	hsa-miR-645	15.70 (0.15)	1.00 (0.79-1.27)	15.33 (0.17)	1.29 (0.99-1.67)	15.23 (0.26)	1.38 (0.91-2.08)
1610	hsa-miR-411	hsa-miR-411-5p	14.16 (0.22)	1.00 (0.69-1.44)	13.96 (0.28)	1.15 (0.75-1.78)	13.99 (0.26)	1.13 (0.75-1.71)
1630	hsa-miR-491	hsa-miR-491-5p	13.97 (0.19)	1.00 (0.74-1.35)	13.15 (0.30)	1.77 (1.13-2.78)	14.08 (0.16)	0.93 (0.72-1.19)
1821	hsa-miR-484	hsa-miR-484	5.70 (0.15)	1.00 (0.79-1.27)	5.59 (0.20)	1.08 (0.80-1.46)	5.74 (0.17)	0.97 (0.73-1.28)
1973	U6 snRNA	U6 snRNA	7.92 (0.16)	1.00 (0.77-1.29)	4.52 (0.27)	4.90 (3.26-7.37)	5.70 (0.44)	2.17 (1.07-4.41)
1984	hsa-miR-590-5p	hsa-miR-590-5p	11.87 (0.14)	1.00 (0.80-1.25)	11.25 (0.22)	1.54 (1.11-2.13)	11.55 (0.25)	1.25 (0.84-1.87)
1986	hsa-miR-766	hsa-miR-766-3p	12.89 (0.23)	1.00 (0.69-1.45)	12.58 (0.23)	1.23 (0.86-1.78)	12.85 (0.24)	1.03 (0.70-1.51)
2098	hsa-miR-223#	hsa-miR-223-5p	14.21 (0.18)	1.00 (0.75-1.34)	12.86 (0.31)	2.55 (1.60-4.07)	12.96 (0.31)	2.38 (1.44-3.92)
2112	hsa-miR-29a	hsa-miR-29a-3p	11.00 (0.23)	1.00 (0.70-1.43)	9.64 (0.26)	2.57 (1.73-3.81)	10.13 (0.36)	1.83 (1.03-3.25)
2122	hsa-miR-376c	hsa-miR-376c-3p	12.97 (0.32)	1.00 (0.60-1.68)	13.04 (0.39)	0.96 (0.53-1.72)	12.64 (0.32)	1.26 (0.75-2.10)
2139	hsa-miR-93#	hsa-miR-93-3p	15.97 (0.11)	1.00 (0.85-1.18)	15.28 (0.22)	1.61 (1.15-2.25)	15.33 (0.28)	1.56 (1.00-2.41)
2148	hsa-miR-144#	hsa-miR-144-5p	13.95 (0.25)	1.00 (0.67-1.49)	14.37 (0.36)	0.75 (0.43-1.29)	14.54 (0.56)	0.66 (0.27-1.63)
2161	hsa-miR-324-3p	hsa-miR-324-3p	13.98 (0.18)	1.00 (0.76-1.33)	13.15 (0.31)	1.78 (1.11-2.85)	13.36 (0.29)	1.54 (0.98-2.42)
2169	hsa-miR-106a	hsa-miR-106a-5p	5.42 (0.10)	1.00 (0.85-1.18)	5.19 (0.22)	1.18 (0.84-1.65)	5.19 (0.21)	1.18 (0.85-1.64)
2186	hsa-miR-345	hsa-miR-345-5p	13.25 (0.29)	1.00 (0.63-1.58)	12.19 (0.23)	2.09 (1.47-2.97)	12.65 (0.31)	1.51 (0.93-2.46)
2187	hsa-miR-942	hsa-miR-942-5p	12.93 (0.09)	1.00 (0.87-1.15)	12.38 (0.24)	1.47 (1.03-2.09)	12.90 (0.29)	1.02 (0.64-1.63)
2216	hsa-miR-128a	hsa-miR-128-3p	13.20 (0.22)	1.00 (0.70-1.42)	12.68 (0.21)	1.44 (1.04-1.99)	12.80 (0.31)	1.32 (0.81-2.16)
2228	hsa-miR-126	hsa-miR-126-3p	7.12 (0.20)	1.00 (0.72-1.38)	7.17 (0.19)	0.96 (0.72-1.29)	6.98 (0.23)	1.11 (0.77-1.60)
2245	hsa-miR-122	hsa-miR-122-5p	8.25 (0.23)	1.00 (0.70-1.44)	8.16 (0.32)	1.07 (0.66-1.73)	7.78 (0.42)	1.39 (0.71-2.72)
2246	hsa-miR-133a	hsa-miR-133a-3p	12.21 (0.50)	1.00 (0.45-2.24)	12.8 (0.42)	0.66 (0.35-1.25)	13.2 (0.22)	0.50 (0.35-0.72)
2249	hsa-miR-143	hsa-miR-143-3p	11.92 (0.18)	1.00 (0.75-1.34)	10.65 (0.19)	2.41 (1.82-3.20)	10.90 (0.19)	2.02 (1.48-2.75)
2253	hsa-miR-101	hsa-miR-101-3p	13.48 (0.12)	1.00 (0.83-1.20)	12.79 (0.25)	1.61 (1.11-2.33)	12.93 (0.30)	1.46 (0.91-2.34)
2254	hsa-miR-151-3p	hsa-miR-151a-3p	14.51 (0.50)	1.00 (0.45-2.23)	15.18 (0.24)	0.63 (0.44-0.91)	14.29 (0.43)	1.17 (0.58-2.34)
2258	hsa-miR-340	hsa-miR-340-5p	14.61 (0.18)	1.00 (0.75-1.34)	13.97 (0.22)	1.55 (1.11-2.17)	14.10 (0.18)	1.42 (1.07-1.89)

2271	hsa-miR-185	hsa-miR-185-5p	11.99 (0.14)	1.00 (0.80-1.26)	11.39 (0.24)	1.51 (1.06-2.15)	11.56 (0.26)	1.35 (0.90-2.02)
2276	hsa-miR-222	hsa-miR-222-3p	10.79 (0.26)	1.00 (0.66-1.51)	9.93 (0.28)	1.82 (1.18-2.79)	10.02 (0.16)	1.71 (1.31-2.22)
2277	hsa-miR-320	hsa-miR-320a	7.05 (0.13)	1.00 (0.82-1.22)	6.74 (0.19)	1.23 (0.93-1.65)	6.82 (0.23)	1.17 (0.82-1.68)
2281	hsa-miR-193a-5p	hsa-miR-193a-5p	13.15 (0.19)	1.00 (0.74-1.36)	11.74 (0.23)	2.66 (1.88-3.77)	12.04 (0.31)	2.16 (1.31-3.55)
2283	hsa-let-7d	hsa-let-7d-5p	11.46 (0.26)	1.00 (0.66-1.53)	11.76 (0.27)	0.81 (0.54-1.21)	11.71 (0.13)	0.84 (0.68-1.04)
2285	hsa-miR-186	hsa-miR-186-5p	12.43 (0.24)	1.00 (0.68-1.46)	11.37 (0.29)	2.08 (1.35-3.20)	11.52 (0.33)	1.87 (1.11-3.17)
2289	hsa-miR-139-5p	hsa-miR-139-5p	10.68 (0.18)	1.00 (0.75-1.34)	10.87 (0.14)	0.88 (0.71-1.08)	10.81 (0.11)	0.92 (0.77-1.09)
2295	hsa-miR-223	hsa-miR-223-3p	-0.03 (0.15)	1.00 (0.79-1.26)	-1.13 (0.24)	2.15 (1.50-3.09)	-0.73 (0.22)	1.63 (1.15-2.31)
2296	hsa-miR-885-5p	hsa-miR-885-5p	10.82 (0.21)	1.00 (0.71-1.40)	10.9 (0.36)	0.94 (0.55-1.63)	10.23 (0.50)	1.50 (0.68-3.31)
2299	hsa-miR-191	hsa-miR-191-5p	6.43 (0.19)	1.00 (0.74-1.35)	6.32 (0.27)	1.08 (0.72-1.62)	6.30 (0.26)	1.09 (0.72-1.66)
2301	hsa-miR-22#	hsa-miR-22-5p	15.18 (0.20)	1.00 (0.72-1.39)	14.96 (0.24)	1.16 (0.81-1.67)	14.67 (0.26)	1.43 (0.95-2.15)
2308	hsa-miR-17	hsa-miR-17-5p	5.20 (0.09)	1.00 (0.87-1.15)	5.00 (0.22)	1.15 (0.82-1.61)	5.00 (0.21)	1.16 (0.82-1.62)
2324	hsa-miR-744	hsa-miR-744-5p	12.79 (0.25)	1.00 (0.67-1.48)	12.40 (0.29)	1.31 (0.85-2.03)	12.40 (0.30)	1.31 (0.80-2.14)
2332	hsa-miR-409-3p	hsa-miR-409-3p	12.16 (0.34)	1.00 (0.58-1.72)	12.46 (0.42)	0.81 (0.43-1.54)	11.97 (0.24)	1.14 (0.78-1.68)
2338	hsa-miR-483-5p	hsa-miR-483-5p	12.71 (0.18)	1.00 (0.75-1.34)	12.06 (0.17)	1.58 (1.21-2.05)	12.25 (0.43)	1.38 (0.69-2.76)
2340	hsa-miR-423-5p	hsa-miR-423-5p	11.86 (0.13)	1.00 (0.82-1.22)	10.93 (0.21)	1.91 (1.38-2.64)	11.33 (0.25)	1.44 (0.96-2.15)
2349	hsa-miR-574-3p	hsa-miR-574-3p	11.13 (0.13)	1.00 (0.81-1.23)	10.55 (0.21)	1.50 (1.10-2.05)	10.95 (0.24)	1.13 (0.78-1.66)
2355	hsa-miR-532-3p	hsa-miR-532-3p	14.17 (0.15)	1.00 (0.78-1.29)	14.10 (0.18)	1.06 (0.80-1.39)	14.25 (0.19)	0.95 (0.70-1.29)
2367	hsa-miR-193b	hsa-miR-193b-3p	11.20 (0.17)	1.00 (0.76-1.32)	10.77 (0.20)	1.35 (0.99-1.83)	10.81 (0.40)	1.31 (0.69-2.50)
2422	hsa-miR-18a	hsa-miR-18a-5p	12.15 (0.09)	1.00 (0.87-1.15)	12.06 (0.22)	1.06 (0.76-1.49)	12.09 (0.21)	1.05 (0.75-1.45)
2446	hsa-miR-28-3p	hsa-miR-28-3p	11.3 (0.14)	1.00 (0.80-1.25)	10.97 (0.19)	1.26 (0.95-1.68)	11.03 (0.22)	1.21 (0.84-1.74)
2844	hsa-miR-320B	hsa-miR-320b	15.92 (0.11)	1.00 (0.84-1.19)	15.30 (0.23)	1.54 (1.08-2.20)	15.15 (0.30)	1.70 (1.05-2.75)
2884	hsa-miR-1274B	NAa	7.40 (0.20)	1.00 (0.72-1.38)	7.09 (0.18)	1.24 (0.94-1.63)	7.74 (0.34)	0.79 (0.46-1.36)
2895	hsa-miR-720	NAa	10.18 (0.17)	1.00 (0.76-1.31)	10.04 (0.22)	1.10 (0.79-1.53)	10.37 (0.27)	0.88 (0.56-1.37)

Abbreviations: IOI: idiopathic orbital inflammation, NHOL: non-Hodgkin orbital lymphoma, HC: healthy control, miR or miRNA: microRNA, FC: fold change, SE: standard error, 95% CI: 95% confidence interval, hsa: homo sapiens. All microRNAs had an abundant expression (amplification score >1.24 , mean Crt <27) and were expressed in >80% of samples.

Supporting Information Table S2. Discovery and replication cohort of 14 serum miRNA selected for validation.

			Discovery (n=33)		Technical validation		Replication (n=34)		Cohorts combined (n=67)	
miR	versus		FC (95% CI)	P*	ρ	P**	FC (range)	P*	P***	adj.P***
miR-140-5p	NHOL	IOI	0.97 (0.59-1.60)	0.917			1.00 (0.62-1.37)	0.607		1.000
	IOI	HC	1.93 (1.19-3.14)	0.019	0.955	<0.001	1.70 (1.24-2.17)	0.004	0.001	0.005
	NHOL	HC	1.87 (1.14-3.08)	0.027			1.61 (1.00-2.21)	0.045		0.037
miR-143-3p	NHOL	IOI	0.84 (0.61-1.14)	0.349						
	IOI	HC	2.41 (1.82-3.20)	<0.001	0.421	0.018				
	NHOL	HC	2.02 (1.48-2.75)	0.002						
miR-148a-3p	NHOL	IOI	0.72 (0.44-1.19)	0.287			0.87 (0.54-1.19)	0.256		1.000
	IOI	HC	2.28 (1.46-3.57)	0.002	0.926	<0.001	2.08 (1.58-2.58)	<0.001	<0.001	0.001
	NHOL	HC	1.65 (1.00-2.72)	0.059			1.70 (1.06-2.33)	0.009		0.009
miR-193a-5p	NHOL	IOI	0.81 (0.49-1.34)	0.45			1.22 (0.63-1.80)	0.800		1.000
	IOI	HC	2.66 (1.88-3.77)	<0.001	0.942	<0.001	1.84 (1.32-2.35)	0.004	<0.001	0.001
	NHOL	HC	2.16 (1.31-3.55)	0.009			2.15 (1.11-3.19)	0.005		0.003
miR-215-5p	NHOL	IOI	1.17 (0.76-1.82)	0.501						
	IOI	HC	1.54 (1.13-2.11)	0.012	0.553	0.002				
	NHOL	HC	1.81 (1.17-2.80)	0.015						
miR-221-3p	NHOL	IOI	1.39 (1.13-1.71)	0.108			0.82 (0.46-1.18)	0.263		-
	IOI	HC	0.72 (0.50-1.05)	0.117	0.934	<0.001	1.16 (0.64-1.68)	0.850	0.309	-
	NHOL	HC	1.00 (0.82-1.23)	0.994			0.75 (0.42-1.07)	0.053		-
miR-223-3p	NHOL	IOI	0.76 (0.54-1.07)	0.228			0.97 (0.55-1.39)	0.520		0.877
	IOI	HC	2.15 (1.50-3.09)	0.001	0.964	<0.001	1.90 (1.16-2.64)	0.011	0.001	0.003
	NHOL	HC	1.63 (1.15-2.31)	0.017			1.66 (0.94-2.38)	0.169		0.130
miR-223-5p	NHOL	IOI	0.93 (0.57-1.53)	0.817			1.13 (0.59-1.68)	0.958		1.000
	IOI	HC	2.55 (1.60-4.07)	0.001	0.834	<0.001	1.92 (1.24-2.59)	0.003	<0.001	0.003
	NHOL	HC	2.38 (1.44-3.92)	0.004			2.04 (1.05-3.02)	0.011		0.019
miR-29a-3p	NHOL	IOI	0.71 (0.40-1.27)	0.288			1.04 (0.63-1.45)	0.714		1.000
	IOI	HC	2.57 (1.73-3.81)	0.001	0.905	<0.001	1.65 (1.31-1.99)	<0.001	<0.001	0.003
	NHOL	HC	1.83 (1.03-3.25)	0.060			1.66 (1.01-2.31)	0.017		0.019
miR-365a-3p	NHOL	IOI	1.25 (0.67-2.33)	0.537			1.46 (0.64-2.28)	0.422		1.000
	IOI	HC	1.77 (1.01-3.11)	0.087	0.848	<0.001	1.82 (1.20-2.45)	0.022	<0.001	0.003
	NHOL	HC	2.22 (1.20-4.12)	0.028			2.52 (1.11-3.93)	0.003		0.007
miR-491-5p	NHOL	IOI	0.52 (0.41-0.67)	0.013			0.92 (0.56-1.27)	0.312		0.969
	IOI	HC	1.77 (1.13-2.78)	0.030	0.781	<0.001	1.54 (1.02-2.06)	0.053	0.015	0.022
	NHOL	HC	0.93 (0.72-1.19)	0.662			1.26 (0.77-1.74)	0.609		0.615
U6 snRNA	NHOL	IOI	0.44 (0.22-0.90)	0.040			1.18 (0.45-1.91)	0.753		1.000
	IOI	HC	4.90 (3.26-7.37)	<0.001	0.869	<0.001	3.16 (1.79-4.53)	0.001	<0.001	0.001
	NHOL	HC	2.17 (1.07-4.41)	0.041			3.41 (1.31-5.52)	0.007		0.003

Abbreviation: IOI: Idiopathic orbital inflammation, NHOL: non-Hodgkin orbital lymphoma, HC: healthy control, FC: fold changeb miR = microRNA, P: p-value, adj.P: adjusted p-value. Combined cohorts are data from TaqMan single RT-qPCR assay. * Independent samples T-test on ΔΔC(r)t data. ** Spearman's ρ on C(r)t data. *** Kruskal-Wallis with post hoc Dunn's correction and Benjamini-Hochberg correction for multiple testing (n=8 variables) resulting in adj.p-val on ΔΔCt data.

Supporting Information Table S3. Discriminating ability of the eight differentially expressed serum microRNAs using a Receiver Operating Characteristic analysis.

	miRNA	AUC	95% CI	Cutoff (FC)	Sensitivity	Specificity
IOI vs NHOL	miR-140-5p	0.55	0.36-0.74	1.15	0.52	0.65
	miR-148a-3p	0.62	0.44-0.80	1.28	0.57	0.77
	miR-193a-5p	0.60	0.41-0.78	1.24	0.57	0.71
	miR-223-3p	0.64	0.46-0.82	1.53	0.52	0.77
	miR-223-5p	0.59	0.40-0.77	1.35	0.52	0.77
	miR-29a-3p	0.56	0.37-0.75	1.16	0.52	0.65
	miR-365-3p	0.57	0.38-0.75	1.18	0.52	0.77
	U6 snRNA	0.61	0.43-0.80	1.08	0.67	0.59
IOI vs HC	miR-140-5p	0.80	0.67-0.94	1.28	0.71	0.84
	miR-148a-3p	0.84	0.71-0.98	1.37	0.76	0.96
	miR-193a-5p	0.89	0.79-0.98	1.30	0.86	0.80
	miR-223-3p	0.81	0.68-0.94	1.55	0.62	0.96
	miR-223-5p	0.82	0.70-0.94	1.84	0.57	1.00
	miR-29a-3p	0.83	0.71-0.96	1.35	0.67	0.92
	miR-365-3p	0.83	0.70-0.95	1.26	0.81	0.76
	U6 snRNA	0.92	0.83-1.00	1.53	0.90	0.80
NHOL vs HC	miR-140-5p	0.74	0.58-0.90	1.63	0.47	1.00
	miR-148a-3p	0.83	0.70-0.97	1.30	0.71	0.88
	miR-193a-5p	0.85	0.72-0.97	1.21	0.82	0.80
	miR-223-3p	0.72	0.55-0.89	1.71	0.53	1.00
	miR-223-5p	0.79	0.64-0.94	1.47	0.59	0.96
	miR-29a-3p	0.77	0.61-0.92	1.38	0.53	0.96
	miR-365-3p	0.82	0.69-0.95	1.43	0.77	0.80
	U6 snRNA	0.85	0.72-0.97	1.51	0.82	0.80

Abbreviations: miR: microRNA, AUC: area under the curve, 95% CI: 95% confidence interval, FC: fold change. Cutoff values were based on the Youden index.

Supporting Information Table S4. Correlation between patient and laboratory data with the miRNA cluster.

Clinical variable	Unit	N	U6 snRNA		miR-140-5p		miR-148a-3p		miR-193a-5p		miR-223-3p		miR-223-5p		miR-29a-3p		miR-365a-3p	
			r	p-val	r	p-val	r	p-val	r	p-val	r	p-val	r	p-val	r	p-val	r	p-val
Age	Years	63	0.03	0.84	-0.13	0.32	-0.12	0.34	-0.01	0.92	-0.16	0.20	-0.12	0.36	-0.06	0.61	-0.09	0.51
Gender	Female	63	-0.06	0.66	0.03	0.82	0.02	0.87	-0.10	0.43	0.14	0.27	0.03	0.83	-0.01	0.92	-0.08	0.52
CRP	mg/L	11	0.13	0.70	0.05	0.89	0.28	0.40	0.23	0.50	0.07	0.85	-0.05	0.89	-0.15	0.67	0.05	0.88
ESR	mm/h	25	-0.18	0.40	-0.06	0.76	0.13	0.55	0.06	0.76	0.01	0.95	-0.11	0.61	-0.14	0.50	-0.03	0.89
RF	IU/ml	25	-0.26	0.20	-0.24	0.26	-0.13	0.54	-0.18	0.38	-0.24	0.25	-0.23	0.26	-0.24	0.26	-0.01	0.96
Sol-IL2	pg/ml	25	0.11	0.60	0.08	0.71	-0.07	0.74	0.06	0.76	0.06	0.77	0.12	0.57	0.15	0.46	0.05	0.81
IgM	g/L	25	0.03	0.88	0.22	0.29	0.23	0.28	0.48	0.02	0.17	0.41	0.27	0.16	0.18	0.39	0.64	<0.001
IgG	g/L	13	-0.23	0.44	-0.02	0.96	-0.03	0.93	-0.49	0.09	-0.08	0.79	-0.20	0.52	-0.13	0.68	-0.62	0.02

Abbreviations: miR: microRNA, CRP: C-reactive protein, ESR: erythrocyte sedimentation rate, RF: rheuma factor, Sol-IL2: soluble interleukin-2, LMR: lymphocyte-monocyte ratio, IgG: immunoglobuline type G, IgM: immunoglobuline M. N = number of IOI and NHOL patients combined of both cohorts, with the exception of age and gender including also the control group. The microRNA fold changes are correlated to patient data. Depicted are the Pearson's r correlation coefficient with the corresponding P-value.

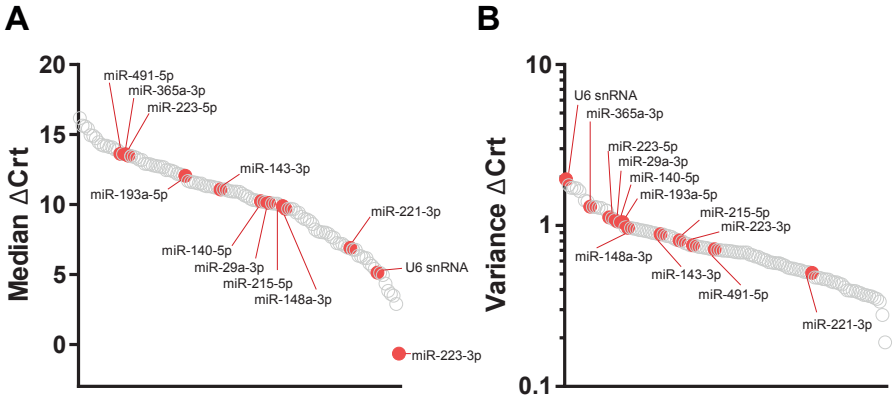

Supporting Information Figure S1. Quality control of OpenArray data for the selected miRNA for replication. The median (A) and the variance (B) of the ΔCrt values for all analysed miRNAs (n=120) within the entire discovery cohort are ordered on the median and variance value, respectively. The miRNAs selected for replication are highlighted and labelled.

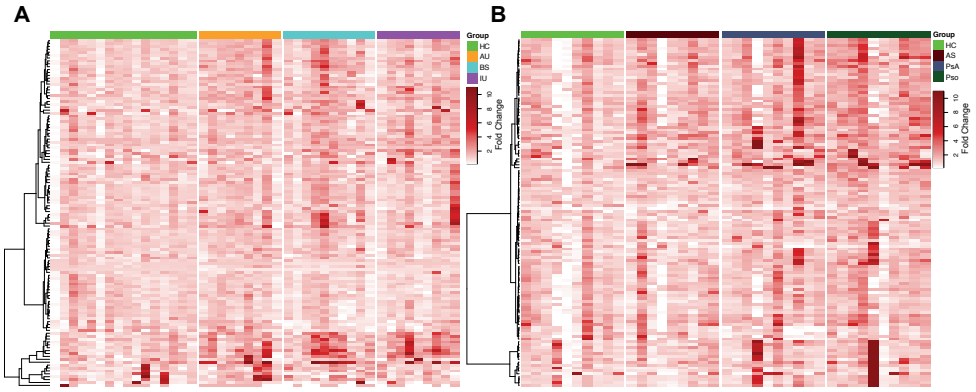

Supporting Information Figure S2. Heatmap of the fold change in expression of the same 120 miRNA detected in the orbital disease discovery cohort in patients with (A.) non-infectious uveitis and controls (n=44) and (B.) psoriatic arthritis, psoriasis, and ankylosing spondylitis and controls (n=39). Relative miRNA expression is depicted in fold changes (FC, or Singular Value Decomposition imputed values, max 10%). Clustering of the rows was performed using Euclidian distance with Ward linkage method. **Abbreviations**: HC: healthy control, IU: idiopathic intermediate uveitis, AU: anterior uveitis, BS: Birdshot uveitis, AxSpA: axial spondyloarthritis, Pso: psoriasis, PsA: psoriatic arthritis.

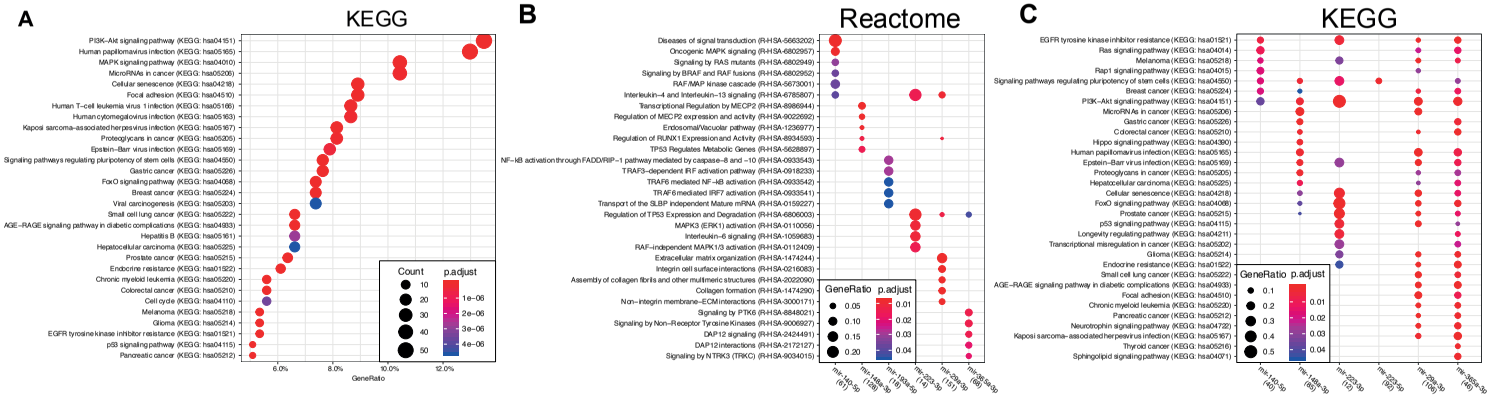

Supporting Information Figure S3. Pathway enrichment analysis using the R clusterProfiler package with representation for individual miRNAs. A. Pathway enrichment within the KEGG database of strong and weak gene association of the miRNAs combined. B & C. Reactome and KEGG database pathway enrichment performed with strong and weak gene association of each miRNA within the KEGG database. The top 5 pathway targets per miRNA are depicted that reached the FDR adjusted P-value cut-off P<0.05. Target pathways from associated genes of miR-193a-5p (in the Reactome database) and miR-223-5p (in the KEGG database) did not reach the cut-off significance and are not shown. miR-193a-5p and miR-223-5p had a low amount of strong associated genes, causing the low significance for individual miRNA pathway enrichment.

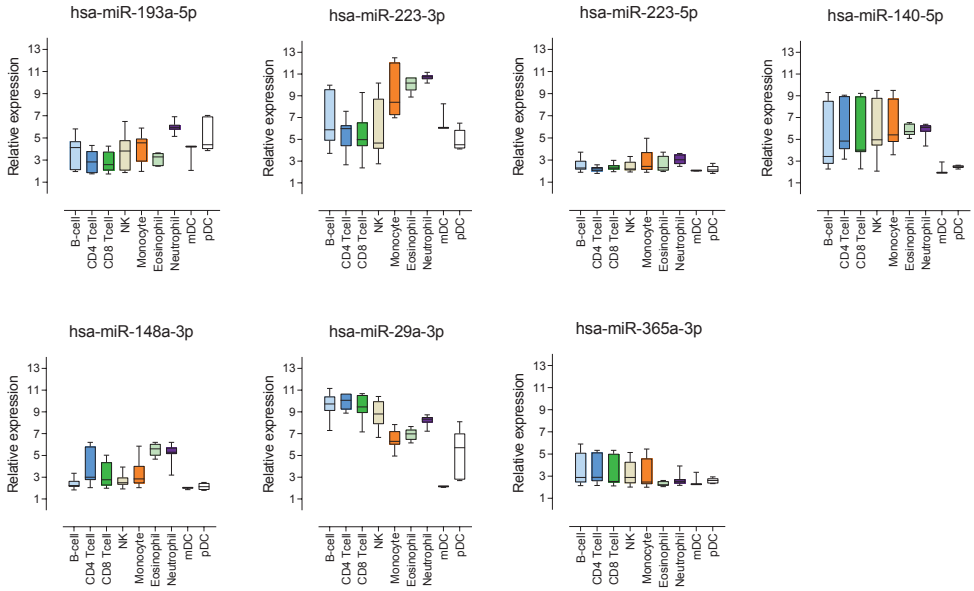

Supporting Information Figure S4. Normalized miRNA expression for each cell-subset (n=108). Depicted are mean with IQR and range.

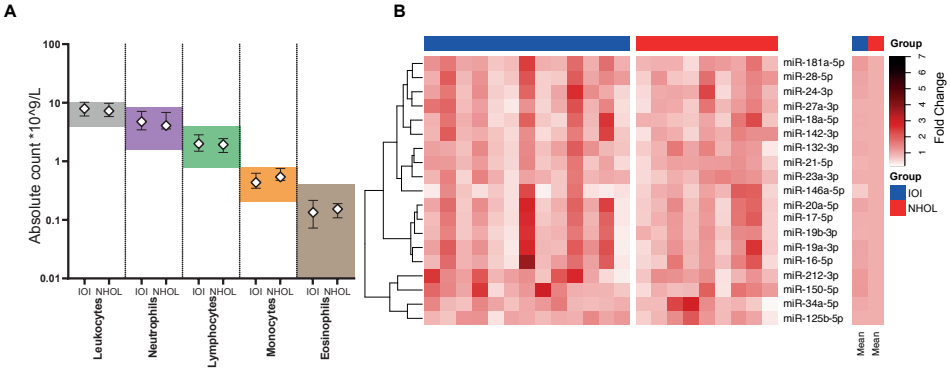

Supporting Information Figure S5. A. Absolute counts of leukocytes and major leukocyte subpopulations for IOI (n=18) and NHOL (n=11). Data is depicted for median with interquartile range for each group. The coloured areas represent the reference value of the normal population. B. Heatmap of the fold change in expression of miRNAs previously associated with B-cell auto-immunity and B-cell lymphoma. We compared the expression of 25 miRNAs previously associated with B-cell autoimmunity and lymphoma as reference in the OpenArray data of the discovery cohort. Of the 25 miRNAs, 21 (84%) passed our quality control and two miRNAs that were also present in the pan-inflammatory miRNA-cluster (miR-223 and miR-148a) were excluded resulting in 19 miRNAs. Relative miRNA expression is depicted in fold changes for IOI versus NHOL (FC, or Singular Value Decomposition imputed values, max 10%). Clustering of the rows was performed using Euclidian distance with Ward linkage method. A group mean is given for each miRNA. Abbreviations: IOI: idiopathic orbital inflammation, NHOL: non-Hodgkin orbital lymphoma.


Chapter 8

cDC2 and plasmacytoid dendritic cells diminish from tissues of patients with non-Hodgkin orbital lymphoma and idiopathic orbital inflammation

Kamil G. Laban
Rianne Rijken
Sanne Hiddingh
Jorre S. Mertens
Rob L. P. van der Veen
Christine A.E. Eenhorst
Aridaman Pandit
Timothy R.D.J. Radstake
Joke H. de Boer
Rachel Kalmann
Jonas J. W. Kuiper

Eur J Immunol. 2020 Apr;50(4):548-557.
doi: 10.1002/eji.201948370.

Abstract

Non-Hodgkin orbital lymphoma (NHOL) and idiopathic orbital inflammation (IOI) are common orbital conditions with largely unknown pathophysiology. To investigate the immune cell composition of these diseases, we performed standardized 29 parameter flow cytometry phenotyping in peripheral blood mononuclear cells of 18 NHOL patients, 21 IOI patients, and 41 unaffected controls. Automatic gating by FlowSOM revealed decreased abundance of meta-clusters containing dendritic cells in patients, which we confirmed by manual gating. A decreased percentage of (HLA-DR^{+}CD303^{+}CD123^{+}) plasmacytoid dendritic cells (pDC) in the circulation of IOI patients and decreased (HLA-DR^{+}CD11c^{+}CD1c^{+}) conventional dendritic cells (cDC) type-2 for IOI patients were replicated in an independent cohort of patients and controls. Meta-analysis of both cohorts demonstrated that pDCs are also decreased in blood of NHOL patients and highlighted that the decrease in blood cDC type-2 was specific for IOI patients compared to NHOL or controls. Deconvolution-based estimation of immune cells in transcriptomic data of 48 orbital biopsies revealed a decrease in the abundance of pDC and cDC populations within the orbital microenvironment of IOI patients. Collectively, these data suggest a previously underappreciated role for dendritic cells in orbital disorders.

Introduction

Non-Hodgkin orbital lymphoma (NHOL), the most common orbital malignancy in adults,[1] can be fatal due to metastatic spread. Prompt diagnosis is critical to disease management and prognosis. NHOL can present with similar symptoms as orbital inflammatory disease, such as idiopathic orbital inflammation (IOI), the most common non-thyroid associated orbital inflammatory disorder.[2-7] Differentiating between the two can be difficult, particularly when histopathology is inconclusive or when an incisional biopsy is difficult to obtain due to deep orbital localization.[8]

Although little is known about the pathophysiology of IOI, infiltration of B- and T-cells is considered a hallmark for this condition.[9] In contrast, NHOL is in almost all cases a B-cell malignancy caused by genetic translocations that affect the *NFKB1*, *BCL2*, *BCL6*, *MYC*, *EZH2*, or *MEF2B* genes, which result in B-cell hyper-proliferation.[1] Curiously, lymphoma occurs more frequently among patients with immune disorders characterized by B-cell hyperactivity, such as primary Sjögren's syndrome, a condition that may also affect the orbital cavity.[1] B cells repeatedly rearrange their genome by the variable (V), diversity (D), and joining (J) gene recombination, somatic hypermutation, and class switch recombination to be able to generate unique antigen receptors. However, these unique properties are not completely error-free and make B-cells vulnerable to transformation. The current view is that inflammatory conditions promote B-cell receptor activation and complex cellular signalling, which enhances the survival of potential malignant B cell clones and the development of lymphoma.[1,10-12] This suggests that IOI and NHOL may have overlapping molecular mechanisms. Interestingly, marginal zone lymphomas such as primary cutaneous marginal zone lymphoma, have, in addition to the B-cell proliferation, an increase in plasmacytoid DCs (pDCs) arranged in larger clusters with unknown function.[13] As the extranodal marginal zone lymphoma (EMZL) is the most common NHOL subtype,[14] pDCs could therefore also be involved in NHOL.

A recent study investigating flow cytometry of orbital biopsies demonstrate that the composition of B- and T-cells in orbital tissue is changed in NHOL and IOI patients.[15] However, it remains to be determined if PBMCs are also affected in these orbital conditions. Changes in immune cells as determined by flow cytometry of PBMCs may reveal new insights in the complex pathophysiology underlying orbital diseases that are currently largely unknown. To this end, we used flow cytometry to phenotype common and rare myeloid and lymphocyte populations in blood of two cohorts of NHOL and IOI patients and unaffected controls. Additionally, in an attempt to explain circulatory differences, we investigated local cellular composition by deconvoluting orbital transcriptomic data.

Table 1. Demographics of the discovery and replication cohorts

Cohort demographics	Discovery cohort			Validation cohort		
Discovery cohort	IOI (n = 13)	NHOL (n = 10)	HC (n = 25)	IOI (n = 8)	NHOL (n = 8)	HC (n = 16)
Female (%)	11 (85%)	5 (50%)	18 (72%)	6 (75%)	5 (63%)	10 (63%)
Age (years); mean ±SD	45.9 ± 14.8	60.6 ± 9.7	43.6 ± 14.1	48.5 ± 17.2	64.9 ± 17.3	47.9 ± 10.7
NHOL subtype, n (%)						
EMZL	–	7 (70%)	–	–	4 (50%)	–
DLBCL	–	1 (10%)	–	–	1 (13%)	–
Follicular	–	1 (10%)	–	–	2 (25%)	–
Other	–	1 (10%)	–	–	1 (13%)	–
Location			–			–
Lacrimal Gland	10 (77%)	3 (30%)	–	3 (38%)	–	–
Orbit	3 (23%)	5 (50%)	–	5 (63%)	7 (88%)	–
Conjunctiva	–	2 (20%)	–	–	1 (13%)	–

Abbreviations: IOI, idiopathic orbital inflammation; NHOL, non-Hodgkin orbital lymphoma; HC, healthy control; EMZL, extranodal marginal zone lymphoma; DLBCL, diffuse large B-cell lymphoma. Other NHOL types: discovery cohort, small lymphocytic lymphoma; replication cohort, mantle-cell lymphoma.

Results

Quality control

Detailed demographic information for the NHOL and IOI groups are presented in Table 1. In the discovery cohort, we performed standardized flow cytometry analysis of PBMCs in eight independent batches (Figure 1A). We assessed the data consistency within the batches by calibration beads and principle component analysis of manually gated data with internal control samples. Tracking by calibration beads revealed a stable performance in all channels across the batches (Figure 1B). Principal component analysis revealed clustering of the internal control samples, which suggests stable variance across all experiments (Figure 1C). Therefore, we removed the internal control samples and combined the eight batches for self-organizing-map-based gating by FlowSOM for comprehensive and unbiased mapping of all leukocyte populations.

NHOL and IOI are characterized by decreased circulating DC populations

FlowSOM considers all surface markers (in a cytometry panel) across all cells simultaneously, and uses unsupervised learning based on self-organizing maps (SOM) and hierarchical consensus meta-clustering to map all phenotypically similar cell clusters in a 2D spanning tree. Group differences and head-to-head

comparisons for all meta-clusters are shown in Supporting Information Table S1. For the mononuclear myeloid and dendritic cell panel, FlowSOM distinguished 17 meta-clusters (Figure 2A) of which four (A1–A3, A5) showed a different abundance between the groups at nominal significance ($p < 0.05$). Meta-clusters A2 ($CD14^+CD16^-CD11c^+$) represented classical monocytes and were increased in the NHOL group compared to the IOI group. Meta-clusters reminiscent of pDCs (A5, $HLA\text{-}DR^+CD303^+CD123^+$), were less abundant in IOI and NHOL compared to controls, while meta-clusters for conventional dendritic cells (cDC) type-2 (A3, $HLA\text{-}DR^+CD11c^+CD1c^+$) were specifically decreased in the IOI group, also compared to NHOL cases (Supporting Information Table S1).

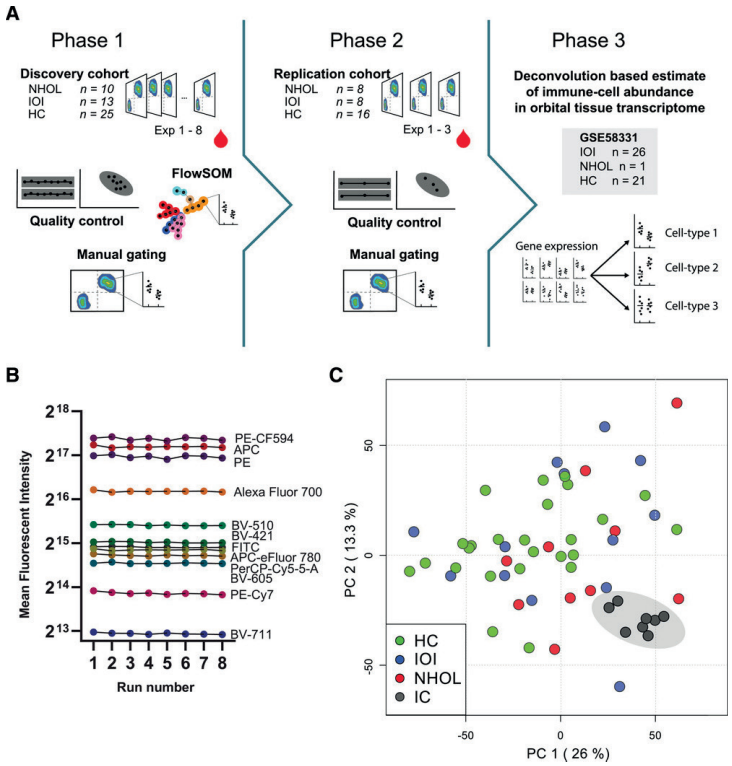

Figure 1. Study design and quality control. (A) Study design. High-dimensional immune profiling was performed in frozen PBMCs of patients with NHOL, IOI, and controls in two independent cohorts. Data from eight flow cytometry experiments (discovery cohort) were combined for automatic gating by FlowSOM. The populations identified by FlowSOM were confirmed by manual gating (Phase 1, n = 48). An independent cohort (Phase 2, n = 32) was used to replicate the observations from Phase 1. In Phase 3, we analysed orbital biopsies transcriptomic data for immune cell genes and used deconvolution algorithms to assess the relative immune cell abundance in the orbital microenvironment. (B) Mean fluorescent intensities for (rainbow) calibration beads across the eight experiment of Phase 1. (C) The first two principal components of the manually gated data of the discovery cohort (n = 48) and internal controls (n = 8). The grey ellipse highlights the cluster of the internal control samples. Abbreviations: Exp, experiment; HC, healthy control; IOI, idiopathic orbital inflammation; NHOL, non-Hodgkin orbital lymphoma; IC, internal control; PC, principle component.

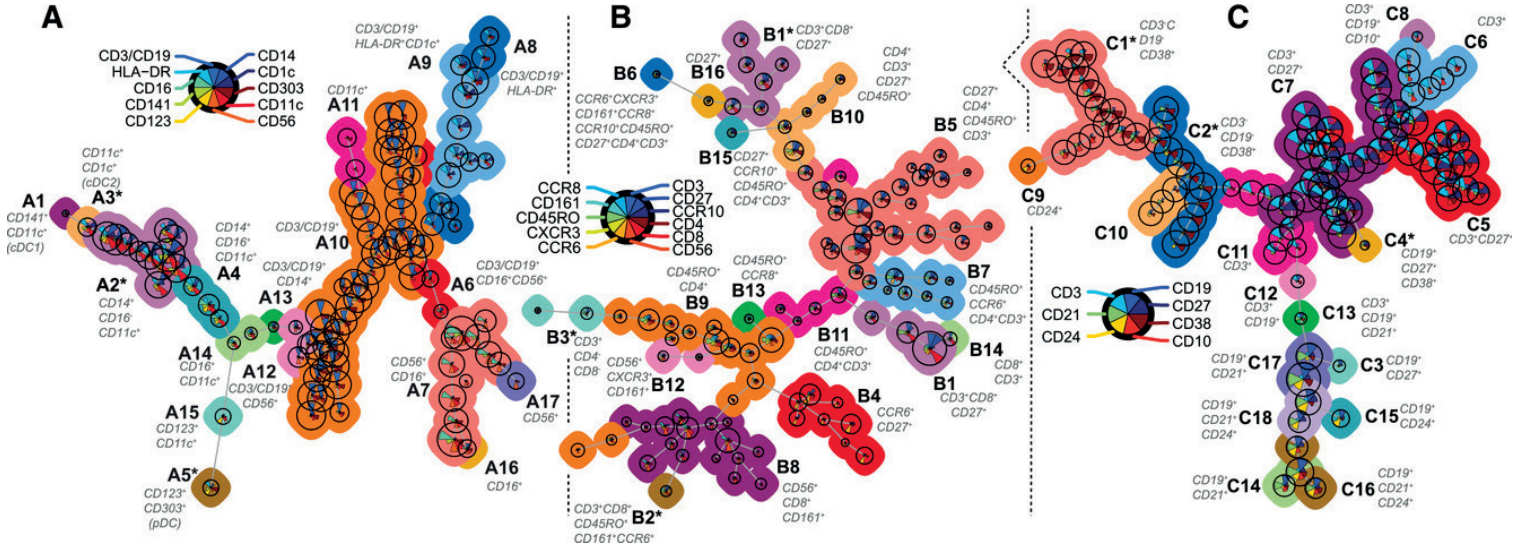

Figure 2. Automatic gating by FlowSOM for unbiased leukocyte composition mapping in orbital disease. FlowSOM tree for mononuclear myeloid and DC panel (A), the T-cell panel (B), and the B-cell panel (C) in 48 PBMC samples for the discovery cohort. Unsupervised clustering was used to identify meta-clusters (displayed by a unique colour) that represent related cell-lineages in the PBMC compartment (A1-C18). The size of the pie-chart is relative to the cluster size (i.e., percentage of the single cell gate). The star charts visualize the relative surface marker expression used to distinguish the clusters. Meta-cluster B3 contains double negative T-cells (CD4-CD8-) and NKT-cells. Group differences for each meta-cluster are indicated by "*" and details are shown in Supporting Information Table S1.

FlowSOM analysis of the T-cell panel (Figure 2B) revealed a different abundance for three of 16 meta-clusters. This was the result of a decrease in the abundance of $CD8^+CD27^+$ T-cells in patients (meta-cluster B1, which also contained populations with moderate CXCR3 expression), a decrease in a meta-cluster driven by $CD8^+CD45RO^+CD27^+CD161^+CCR6^+$ T-cells (B2), and lower abundance for a meta-cluster defined by a decrease in double negative ($CD4^-CD8^-$) T cells (B3) in NHOL patients.

In the B-cell panel (Figure 2C), we observed changes in four of 18 meta-clusters (C1–C4), of which two meta-clusters of B cells that express CD27 and CD38 (C3 and C4). Note that the increase in abundance of meta-clusters C1 and C2 most likely represents an increase in monocytes ($CD3^-CD19^-CD38^+$), because these clusters show strong correlation with the monocyte meta-clusters (e.g., meta-cluster A2 versus C2, Spearman's $\rho = 0.80$, $p < 0.001$).

Next, we were interested to validate these observations using manual gating. Manually gating data confirmed the increase in ($CD14^+CD16^-CD11c^+$) classical monocytes and decrease in $CD3^+CD8^+CD27^+$ and $CD3^+CD8^+CD45RO^+CD161^+CCR6^+$ T cells in NHOL patients. We also confirmed the decrease in pDCs in NHOL and IOI patients compared to controls and confirmed the decrease in cDC type-2 in IOI patients (Figure 3). None of the changes within the B cell population identified by FlowSOM were confirmed by manual gating (Supporting Information Table S2).

An independent cohort confirms a decrease in DC subsets for patients

Next, we conducted flow cytometry in an independent cohort of 16 patients and 16 controls to replicate the findings of the first cohort (Table 1). We replicated the decrease in pDCs in IOI compared to controls (Supporting Information Table S2; Figure 3), and the decrease in cDC type-2 in IOI patients with consistent direction of effect in the second cohort. In contrast to the other leukocyte populations investigated, DCs are rare within the single cell gate. Since this might affect power to detect group differences, we also evaluated the percentage of pDCs and cDC type-2 cells in the conventional lineage-negative ($CD3^-/CD19^-/CD56^-/CD14^-$) HLA-DR positive gate of the combined cohorts (Supporting Information Figure S1). This analysis confirmed the decreased expression of these DC populations in IOI (adjusted $p = 1.78 \times 10^{-3}$), and ascertains also the decrease in pDCs in NHOL compared to controls (adjusted $p = 1.48 \times 10^{-4}$). Analysis of the combined manual gated data of both cohorts also supports a specific decreased of cDC type-2 cells in IOI compared to NHOL (adjusted $p = 2.77 \times 10^{-2}$), which is in line with the initial observations by FlowSOM. Although age and sex differences are intrinsic to the diseases studied (Table 1), the effect of age or sex on the difference

in abundance of dendritic cells in blood was negligible (Supporting Information Table S3). In summary, we demonstrated a consistent decrease in circulating DCs, especially pDCs, in NHOL and IOI.

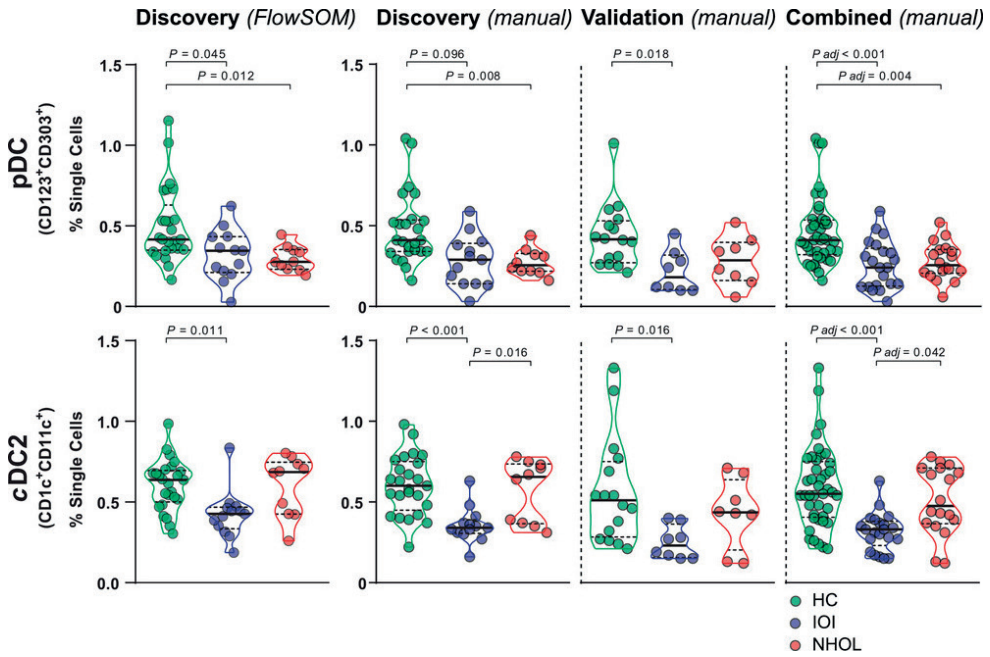

Figure 3. pDC and cDC2 populations in patients and controls. The percentage of pDC and cDC2 in the single cell gate for automatic gating with FlowSOM, and manual gating. Data for the discovery, validation, and combined cohorts are indicated. The Kruskal–Wallis tests with Dunn's post hoc test were used to assess differences between groups. The adjusted P-values are corrected using the Benjamini–Hochberg method. The median with interquartile ranges are indicated by black lines and dotted lines, respectively. Abbreviations: HC, healthy control; IOI, idiopathic orbital inflammation; NHOL, non-Hodgkin orbital lymphoma; pDC, plasmacytoid DCs; cDC2, conventional DCs type-2; p, nominal p-value; p adj, adjusted p-value.

DC alterations in biopsy material

Next, we were interested to explore the potential role of dendritic cells in the microenvironment of IOI. To this end, we investigated the transcriptome of orbital biopsies of 26 IOI patients and 21 controls. Available data from one NHOL patient was used for visualization only. Gene expression profiles revealed that various signature genes for cDCs (e.g., *CSF1R, NDRG2*) and pDCs (e.g., *NRP1*, *PTGDS*) are well expressed in biopsy tissues of patients and controls (Figure 4A). Differential expression analysis revealed that the expression of several of these DC signature genes (e.g., *NRP1, CSF1R, PTGDS*) are also changed in patients with IOI compared to controls (Figure 4B). Deconvolution approaches can be applied

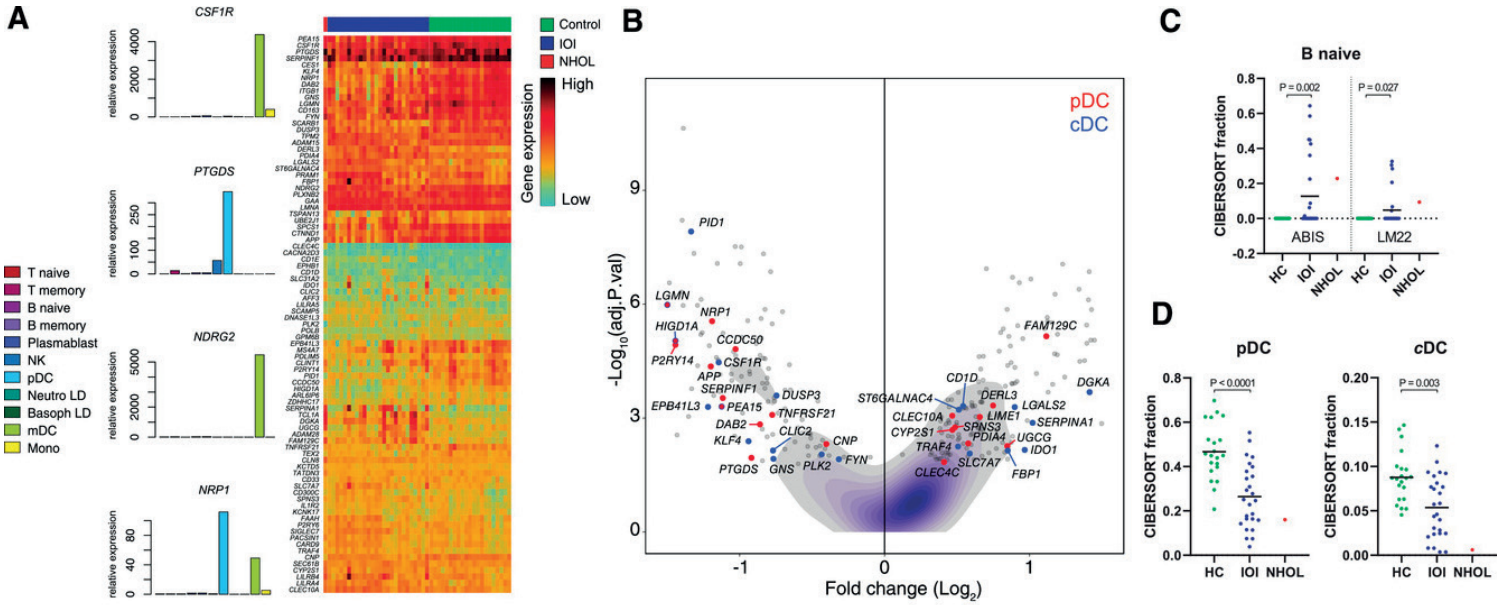

Figure 4. Dendritic cell gene signatures are present in orbital biopsies. (A) Gene expression profile of signature genes 16 of pDC and cDC in orbital biopsies of 26 IOI patients and 21 controls (GSE58331). The specificity of several hallmark genes for cDCs and pDCs are indicated by the barplots on the left. A larger version of the heatmap is available in the Supporting Information Fig. S2. (B) A volcano plot of the gene expression changes of 794 genes in orbital biopsies of 26 IOI patients versus 21 controls (data obtained from GSE58331). The density contour indicates the density estimation of the fold change in expression and p-values for the genes. Differentially expressed genes (-log10 of the FDR adjusted p-values from differential expression analysis in limma) are indicated by dots. Differentially expressed signature genes 16 for pDC and cDC subsets are highlighted in red and blue, respectively. Genes linked to both cDC and pDCs are indicated by both red and blue. (C) Deconvolution-based estimation by CIBERSORT of the fraction of naïve B cells (using ABIS or LM22 as signature sets to estimate the cell fraction) in biopsies of IOI and controls, and one NHOL sample. (D) Deconvolution-based CIBERSORT estimation of pDC and cDC fractions (ABIS signature set used) for the same samples as in (C). The Mann–Whitney U test was used to assess differences between groups. Group means are shown. Abbreviations: HC, healthy control; IOI, idiopathic orbital inflammation; NHOL, non-Hodgkin orbital lymphoma; NK, Natural Killer cells; neutron LD, low-density neutrophils; basoph LD, low-density basophils; mono, monocytes; pDC, plasmacytoid DC; cDC, conventional DC.

to bulk gene expression data to infer cellular composition of complex tissue mixtures.[16] We estimated the cellular fraction of cDCs and pDC from the gene expression data from IOI cases and controls using deconvolution-based estimation with CIBERSORT,[17] and estimated the fraction of B-cells as an internal control. B cells are well known to be increased in biopsies of IOI patients.[1,8] Because the leukocyte signature matrix often used for CIBERSORT (called LM22) does not contain reference data for pDC or cDCs, we used a signature data from a recently developed deconvolution algorithm "ABsolute Immune Signal" (ABIS) trained on pDC and cDC data. As expected, the relative fraction of B cells in biopsy material of IOI patients was increased (p = 0.002), because no B cells were estimated to be present in the control biopsies. Also, the relative proportion between cases and controls was very similarly estimated by CIBERSORT using either LM22 or ABIS signature sets (**Figure 4C**). Finally, the biopsies were estimated to contain heterogeneous fractions of pDCs and cDCs, indicating that DCs constitute the orbital microenvironment. Importantly, we observed a decrease in the estimated fraction of pDCs and cDCs (**Figure 4D**) in IOI cases compared to controls. In summary, the results suggest that orbital inflammation of IOI is associated with decreased DC populations in the ocular microenvironment.

Discussion

In this study, we observed decreased pDCs in peripheral blood of patients with IOI and NHOL, and a specific decrease in cDC type-2 cells in IOI patients, also compared to NHOL. Deconvolution-based estimation suggests that the drop in circulating dendritic cells in IOI patients can be accompanied by a lower abundance of these DC populations in the orbital microenvironment.

The contribution of dendritic cells to NHOL and IOI is currently unknown. Our analysis suggests that the abundance of these cells in blood and their gene expression in orbital tissues is altered, which warrants further functional analysis of these populations to better understand their contribution to orbital pathology. This could reveal new possibilities for future diagnostic and therapeutic strategies for NHOL and IOI management.

DCs are APCs that can initiate and drive immune responses in various human pathologies.[18] Although various subpopulations of DC populations are distinguished, much of their functional specialization during malignancy or inflammatory disease in humans remains to be elucidated.

The classical dogma considers discrete functions for DC subsets with pDC

effective in recognizing viral or endogenous nucleotides (e.g., DNA, RNA) upon which large amounts of INF are produced to induce inflammation.[18] The cDCs are considered important for the recognition of intracellular and extracellular pathogens and present exogenous Ags to T-cells.[18] In reality, however, the redundancy in function and magnitude of influence on immune responses is complex and context-dependent. Regardless, the significant role of dendritic cells in human disease has been unequivocally demonstrated; DCs play an important role in antitumor response toward malignant cells and are drivers of various severe inflammatory conditions.[19-21]

Similar to our results, a decrease in blood DCs is observed in inflammatory disorders, such as systemic lupus erythematosus[22] and the eye condition uveitis.[23] Also, a reduction in DC numbers in blood has been documented in patients with leukaemia,[24-27] multiple myeloma,[28] classical Hodgkin lymphoma,[29] and other types of cancer.[30] This phenomenon could be part of an immunosuppressive state caused by the tumour microenvironment, triggered by metabolic stress, hypoxia, or secretion of cytokines and alarmins that affect DCs.[30] Although in our analysis of the single cell gate did not show a consistent decrease of pDCs in NHOL patients, evaluation of this rare cell population in more conventional gates for manual gating (lineage-negative HLA-DR positive cell gate) showed a consistent decrease of pDCs in NHOL. The role of pDCs in cancer is supported by the observation of pDC restoration in peripheral blood in patients under anticancer treatment.[29] In contrast to pDC associated conditions such as primary Sjögren's syndrome and systemic sclerosis that show accumulation of pDCs at the side of inflammation,[22] we observed a moderate decrease in the estimated pDC numbers in biopsies. Here, it is important to consider that it was previously found that pDCs in mice can be segregated into multiple populations with functional differences. For example, pDCs with tolerogenic functions control T regulatory formation to maintain tolerance in mucosal sites.[31] Interestingly, pDCs are known to regulate B cell differentiation and Ig secretion through CD70 and IL-6.[32] The lower number of pDCs locally in concurrence with B cell infiltrate in IOI could therefore be driven by a negative feedback loop mediated by self-maintaining B-cell expansion, or pDC differentiation and activation affecting surface marker expression.[19] In blood, however, we observed no correlation between DC subtypes and the B-cell compartment.

In this study, we use a three-phase strategy to determine the changes in immune cells of NHOL and IOI. However, some limitations need to be addressed. Due to the rare and heterogeneous nature of orbital disease, clinical variation exists and may influence our observations. For example, analysis of NHOL subtypes would

be highly desirable, but considering the rare occurrence of disease, it is difficult to obtain sufficient number of samples to pursue such analysis. Three NHOL patients with a history of lymphoma in remission were comparable to other samples in the NHOL group. As with any idiopathic condition, the diagnosis IOI is established after exclusion of any known cause for orbital disease. Although future studies may proof distinct subtypes within the IOI group, there are currently no robust molecular subtypes of IOI that we could take along in our studies.[33]

Also, we demonstrated that transcriptomic signatures of orbital tissues show signature genes for DCs. For example, the expression of *NDRG2* and *CSF1R* suggests the presence of cDCs. N-myc downstream-regulated gene 2 (*NDRG2*) is a differentiation-related gene specifically linked to cDCs[34] and CSF1R expression is typically associated with cDC differentiation.[35] However, these genes are also implicated in monocyte to DC differentiation and we cannot conclusively state that the expression is limited to cDCs only in tissues. Also, as far as we are aware there is currently no transcriptomic data available that is trained to deconvolute cDC type-1 and cDC type-2 in (orbital) tissues. Future studies using single cell sequencing are warranted to dissect the subtle differences between monocyte derived inflammatory dendritic cells and cDCs in tissues.

Third, although the genes linked to pDCs such as *NRP1* and *PTGDS* are also expressed by non-hematopoietic cells, the changes in their gene expression in orbital tissue and circulating number of pDCs suggest that these observations may be causally linked in the aetiology of orbital disease. This is supported by the (multigene signature) deconvolution of the orbital transcriptome, which demonstrated a decrease in pDCs and cDCs in tissues of IOI patients, similar to the results from flow cytometry in blood. Also, using estimation of cell numbers, we confirm enrichment for B cells in orbital tissues—a phenomenon well documented in IOI and NHOL.[1,8] However, we emphasize that further research is needed to quantify the DC populations in orbital biopsies. Deconvolution methods based on gene expression profiles assume that the bulk gene expression profile constitutes the weighted sum of the cell type-specific transcriptomes. Although such algorithm-based strategies have revolutionized our understanding of the rich composition of biopsies, some cell types are very poorly deconvoluted in progressively complicated tissues. Also, patient-to-patient variability—as a result of difficulty in taking a representative orbital biopsy—will influence any deconvolution method, in particular for cell subsets that are difficult to distinguish due to data collinearity (i.e., having similar expression profiles). Future work in NHOL and IOI may benefit from benchmarking deconvolution methods by single cell sequencing data from orbital biopsies.

In conclusion, we discovered that DCs are reduced in peripheral blood of patients with NHOL and IOI and altered in the disease microenvironment. These results unveil a potentially novel role of DCs in orbital disease that warrants replication and functional understanding to determine its relevance for future diagnostic and treatment purposes.

Methods

Patients

In total, 39 patients and 41 controls (HC) were included in this study. Blood was collected from patients recruited at the University Medical Center Utrecht, Utrecht, The Netherlands between February 2015 and May 2018. Forty-one (self-reported) healthy control samples were obtained from a pool of employees of the University Medical Center Utrecht that provide voluntary unpaid blood donations for research purposes (Approved by the institutional review board). We immunophenotyped a discovery cohort (NHOL: n = 10, IOI: n = 13, HC: n = 25) and 1 year later an independent validation cohort (NHOL: n = 8, IOI: n = 8; HC: n = 16). This study was conducted in accordance with the Declaration of Helsinki and was performed with approval of the Institutional Review Board of the University Medical Centre Utrecht, The Netherlands (protocol #14-065). All patients included in this study gave written informed consent before participation.

All cases of NHOL were diagnosed and classified following WHO criteria with histopathological assessment of incisional biopsies[36] (see **Table 1** for details). Histopathologic examination of NHOL included assessment of B cell and T cell specific markers (CD3, CD5, CD20, CD79α) and specific B cell subset markers (BCL2, BCL6, CD10, CD23, CD30, Cyclin D-1, MUM-1, and κ and λ light chains) for NHOL subtyping. PCR-based clonality analysis was used and revealed monoclonality for NHOL, except two NHOL patients that showed a monotypic λ light chain expansion in histopathology. In addition, translocations were assessed by fluorescence in situ hybridization in patients with diffuse large B-cell lymphoma (DLBCL).

IOI, a diagnosis of exclusion, was considered in patients with an orbital mass without evidence of infection, lack of evidence for granulomatosis with polyangiitis, sarcoidosis, primary Sjögren's syndrome, benign lymphoid hyperplasia, IgG4-related pathology, histiocytic disease, or malignancy.[8-37] Note histopathological confirmation of incisional orbital biopsies was obtained for all patients, except for six patients with idiopathic myositis. In all IOI biopsies, a non-specific polymorphous

plasmalymphocytic infiltrate was seen, negative for IgG4, with or without the presence of neutrophils, eosinophils, histiocytes, and macrophages, and varying amounts of fibrosis in the connective tissue. Idiopathic myositis patients were diagnosed based on the presence of pain, diplopia, (paretic) motility reduction and pain with eye-movement, negative laboratory findings (e.g., no autoantibodies and normal serum IgG4 levels), and extra-ocular muscle swelling with contrast-enhancement on magnetic resonance imaging.[8,37]

All patients were diagnosed by an ophthalmologist specialized in orbital diseases. All patients had blood withdrawal at time of diagnosis and had active disease. Treatment was not yet initiated at the time of blood withdrawal. Additionally, none of the patients received systemic corticosteroids 3 months—or immunomodulatory treatment in the past 6 months—prior to blood withdrawal, except for one patient of the validation cohort (low dose of 2.5 mg oral prednisolone daily). Also, patients had not received radiation treatment or chemotherapy in the previous year before sampling.

Flow cytometry

The study design is depicted in **Figure 1A**. PBMCs were isolated by standard ficoll centrifugation of whole blood obtained by lithium heparin vacutainers (#367880, BD Vacutainer, BD Bioscience, USA) and stored overnight at -80°C using a freezing container (#BCS-405, CoolCell LX, Biocision, USA) and subsequently stored at liquid nitrogen. The two cohorts were measured separately 1 year apart. PBMC samples were measured by flow cytometry in batches of five to 12 samples per run, divided over 8 days for the first cohort and 3 days for the second cohort, 1 year apart. Per batch, 10 million PBMCs per sample were quickly thawed, washed with ice cold PBS and divided for staining with three antibody panels (see **Supporting Information Table S4**) with a specific amount of cells per panel; a mononuclear myeloid panel (1.9 million cells), a B cell panel (300 000 cells), and a memory T-cell panel (400 000 cells). PBMCs were incubated with 5% heat-inactivated mouse serum at room temperature for 15 min to reduce non-specific antibody binding. Cells were then plated in V-bottomed plates (#651101, Greiner Bio-one, Germany), washed with PBS supplemented with BSA (1%) and incubated for 20 min at 4°C in the dark with Brilliant Stain Buffer (#563794, BD Horizon, BD Bioscience, USA) and the fluorescently-conjugated antibodies. Next, the cells were washed and taken up in PBS supplemented with BSA (1%) and 0.1% sodium azide.

Flow cytometric analyses were performed on the BD LSR Fortessa™ Cell analyzer (BD Bioscience, USA), in adherence to previous reported guidelines.[38] Manual

gating of blinded data (i.e., coded samples) was done in FlowJo software (TreeStar Inc., USA). An example of the gating strategy basis is provided under Supporting Information Figure S3. Flow cytometer calibration was monitored before and after every run using eight peak Sphero™ Rainbow Calibration particles (#RCP-30-5A, Spherotech Inc., USA). The relative SD calculated with the coefficient of variation was <5% for all fluorescently conjugated antibodies across individual runs for the discovery and the validation cohorts, and <10% for both cohorts combined. Interassay variation was determined using aliquots of one control sample in each run in both cohorts. Across all runs the sample revealed relatively low interassay variation, showing a relative SD of <15% within all common leukocyte populations (population size >5% of single cells). Principle component analysis confirmed the high consistency of the individual runs (Figure 1B). After inspection of the manual gated data, we excluded CCR4 from the T-cell panel, because the overall fluorescent intensity for this chemokine receptor was indistinguishable from the Fluorescence Minus One control experiment. Note that we further expanded the B cell panel with antibodies directed to surface Igs in the second cohort (Supporting Information Table S4).

FlowSOM and Statistical analyses

Flow cytometry data were visualized with SOM clustering and Minimal Spanning Trees using the *FlowSOM,*[39] as described previously.[23] Briefly, single cell data (FSC-A versus FSC-H gates) were transformed using the *logicleTransform* function of the *flowCore* package.[40] The SOM was trained for a grid size of 100 (populations) with 2000 iterations. Consensus hierarchical clustering was used to annotate clusters, based on the *ConsensusClusterPlus* R package.[41] FlowSOM subsequently determined the appropriate number of (maximum 90 color-coded) meta-clusters using the Elbow criterion method. Meta-clusters represent lineages and closely related cell populations. Identified clusters that represented <0.1% of all single cells were ignored to prevent potential overfitting. Head-to-head comparison of the frequency of meta-clusters between the groups was performed using the Kruskal–Wallis test with subsequent Dunn's Bonferroni-corrected post hoc test in R 3.5 using the *FSA* package and *dunnTest* function. Group differences identified by *FlowSOM* at a nominal $p < 0.05$ were confirmed by manual gating (populations expressed as % of single cell gate) and considered validated if the group differences replicated at a nominal $p < 0.05$ and if these observations replicated at a nominal $p < 0.05$ and showed consistent direction of effect in an independent cohort of patients and controls. We combined manual gated data from cohort 1 and 2 for meta-analysis and corrected the *p*-values for multiple comparisons using the Benjamini–Hochberg method. For quality control, we conducted principal component analysis of manual gated data with MetaboAnalyst

v4.[42] Group data were reported as median with interquartile range. Violin plots were generated with Graphpad Prism version 8. 0 (GraphPad, La Jolla, CA, USA).

Orbital tissue transcriptome analysis and deconvolution

Gene expression data (Affymetrix U133Plus2 array) of 48 orbital cavity biopsies from IOI patients (n = 26) and a NHOL patient (n = 1, only used for visualization), and surgically residual orbital material from unaffected orbits (n = 21) were obtained from the NCBI Gene Expression Omnibus (accession number GSE58331).[33,43] The Affymetrix CEL files were simultaneous pre-processed and a differential expression analysis was conducted on all samples. Data were interrogated by GEO2R[44] from the GEO database, which builds on the *GEOquery* and *limma* R packages (i.e., differential expression analysis). The differential expression by the *limma* package uses a linear model on $\log_2$ transformed and quantile normalized data using lmFit function and adjusts p-values according to the Benjamini–Hochberg method. For deconvolution of the bulk patient profiles, expression profiles were analyzed by CIBERSORT[17] to estimate the cell fractions for pDC, cDC, and B cells in biopsy material. Because the CIBERSORT standard reference signature expression matrix for leukocytes (LM22) does not contain data for pDC and cDC subsets, we used microarray signature data from ABIS.[16] According to previous suggestion, output was processed by replacing negative numbers by zeros.[17] We used the estimated fraction of pDCs, cDC, and naïve B-cells for comparison between IOI and controls. We extracted the top 50 genes with the highest signal for pDCs and *c*DCs (87 unique genes) from the signature microarray reference of ABIS from the transcriptomic data to investigate the relative expression of DC genes in orbital biopsies.

Acknowledgements

We would like to thank Maarten Mourits and Stijn Genders for their assistance in the recruitment of patients. This study was supported by unrestricted grants from the Dr. F.P Fischerstichting, Stichting Lijf & Leven, Rotterdamse Stichting Blindenbelangen, and Stichting Ankie Hak. The funders had no role in study design, data collection and analysis, decision to publish, or preparation of the manuscript.

Conflict of interest

The authors declare no financial or commercial conflict of interest.

References

1. Olsen TG and Heegaard S. Orbital lymphoma. Surv. Ophthalmol. 2019. 64: 45– 66.
2. Gordon LK. Orbital inflammatory disease: a diagnostic and therapeutic challenge. Eye 2006. 20: 1196– 1206.
3. Yan J, Wu Z and Li Y. The differentiation of idiopathic inflammatory pseudotumor from lymphoid tumors of orbit: analysis of 319 cases. Orbit 2004. 23: 245– 254.
4. Yuen SJA and Rubin PAD. Idiopathic orbital inflammation. Arch. Ophthalmol. 2003. 121: 491.
5. Ben Simon GJ, Cheung N, McKelvie P, Fox R and McNab AA. Oral chlorambucil for extranodal, marginal zone, B-cell lymphoma of mucosa-associated lymphoid tissue of the orbit. Ophthalmology. 2006. 113: 1209– 1213.
6. Eenhorst CAE, Laban KG, Leguit RJ, Radstake TRDJ and Kalmann R. Orbital lymphomas missed by first biopsies of orbital masses. Acta Ophthalmol. 2017. 95: 858– 859.
7. Lam Choi VB, Yuen HKL, Biswas J and Yanoff M. Update in pathological diagnosis of orbital infections and inflammations. Middle East Afr. J. Ophthalmol. 2011. 18: 268– 276.
8. Mombaerts I, Bilyk JR, Rose GE, McNab AA, Fay A, Dolman PJ, Allen RC, et al. Consensus on diagnostic criteria of idiopathic orbital inflammation using a modified Delphi approach. JAMA Ophthalmol. 2017. 135: 769– 776.
9. Mombaerts I, Goldschmeding R, Schlingemann RO and Koornneef L. What is orbital pseudotumor? Surv. Ophthalmol. 41: 66– 78.
10. Sachen KL, Strohman MJ, Singletary J, Alizadeh AA, Kattah NH, Lossos C, Mellins ED, et al. Self-antigen recognition by follicular lymphoma B-cell receptors. Blood. 2012. 120: 4182– 4190.
11. Burger JA, Ghia P, Rosenwald A and Caligaris-Cappio F. The microenvironment in mature B-cell malignancies: a target for new treatment strategies. Blood. 2009. 114: 3367– 3375.
12. Gonzalez D, van der Burg M, Garcia-Sanz R, Fenton JA, Langerak AW, Gonzalez M, van Dongen JJM, et al. Immunoglobulin gene rearrangements and the pathogenesis of multiple myeloma. Blood. 2007. 110: 3112– 3121.
13. Kempf W, Kerl H and Kutzner H. CD123-positive plasmacytoid dendritic cells in primary cutaneous marginal zone B-cell lymphoma: a crucial role and a new lymphoma paradigm. Am. J. Dermatopathol. 2010. 32: 194– 196.
14. Olsen TG, Holm F, Mikkelsen LH, Rasmussen PK, Coupland SE, Esmaeli B, Finger PT, et al. Orbital lymphoma—an international multicenter retrospective study. Am. J. Ophthalmol. 2019. 199: 44– 57.
15. Kase S, Ishijima K, Uraki T, Suimon Y, Suzuki Y, Kase M and Ishida S. Usefulness of flow cytometry in diagnosis of IgG4-related ophthalmic disease and extranodal marginal zone B-cell lymphoma of the ocular adnexa. Anticancer Res. 2017. 37: 5001– 5004.
16. Monaco G, Lee B, Xu W, Mustafah S, Hwang YY, Carré C, Burdin N, et al. RNA-Seq signatures normalized by mRNA abundance allow absolute deconvolution of human immune cell types. Cell Rep. 2019. 26: 1627– 1640.e7.
17. Newman AM, Liu CL, Green MR, Gentles AJ, Feng W, Xu Y, Hoang CD, et al. Robust enumeration of cell subsets from tissue expression profiles. Nat. Methods 2015. 12: 453– 457.
18. Musumeci A, Lutz K, Winheim E and Krug AB. What Makes a pDC: Recent Advances in Understanding Plasmacytoid DC Development and Heterogeneity. Front. Immunol. 2019. 10. https://doi.org/10.3389/fimmu.2019.01222.
19. Galati D, Corazzelli G, De Filippi R and Pinto A. Dendritic cells in hematological malignancies. Crit. Rev. Oncol. Hematol. 2016. 108: 86– 96.
20. Hillen MR, Ververs FA, Kruize AA and Van Roon JA. Dendritic cells, T-cells and epithelial cells: a crucial interplay in immunopathology of primary Sjögren's syndrome. Expert Rev. Clin. Immunol. 2014. 10: 521– 531.
21. Affandi AJ, Carvalheiro T, Radstake TRDJ and Marut W. Dendritic cells in systemic sclerosis: Advances from human and mice studies. Immunol. Lett. 2018. 195: 18– 29.
22. Klarquist J, Zhou Z, Shen N and Janssen EM. Dendritic cells in systemic lupus erythematosus: from pathogenic players to therapeutic tools. Mediat. Inflamm. 2016. 2016: 1– 12.
23. Verhagen FH, Hiddingh S, Rijken R, Pandit A, Leijten E, Olde Nordkamp M, ten Dam-van Loon NH, et al. High-dimensional profiling reveals heterogeneity of the Th17 subset and its association with systemic immunomodulatory treatment in non-infectious uveitis. Front. Immunol. 2018. 9: 2519.

24. Mohty M, Isnardon D, Vey N, Brière F, Blaise D, Olive D and Gaugler B. Low blood dendritic cells in chronic myeloid leukaemia patients correlates with loss of CD34+/CD38– primitive haematopoietic progenitors. Br. J. Haematol. 2002. 119: 115– 118.
25. Dong R, Cwynarski K, Entwistle A, Marelli-Berg F, Dazzi F, Simpson E, Goldman JM, et al. Dendritic cells from CML patients have altered actin organization, reduced antigen processing, and impaired migration. Blood 2003. 101: 3560– 3567.
26. Orsini E, Guarini A, Chiaretti S, Mauro FR and Foa R. The circulating dendritic cell compartment in patients with chronic lymphocytic leukemia is severely defective and unable to stimulate an effective T-cell response. Cancer Res. 2003. 63: 4497– 506.
27. Saulep-Easton D, Vincent FB, Le Page M, Wei A, Ting SB, Croce CM, Tam C, et al. Cytokine-driven loss of plasmacytoid dendritic cell function in chronic lymphocytic leukemia. Leukemia. 2014. 28: 2005– 2015.
28. Brimnes MK, Svane IM and Johnsen HE. Impaired functionality and phenotypic profile of dendritic cells from patients with multiple myeloma. Clin. Exp. Immunol. 2006. 144: 76– 84.
29. Galati D, Zanotta S, Corazzelli G, Bruzzese D, Capobianco G, Morelli E, Arcamone M, et al. Circulating dendritic cells deficiencies as a new biomarker in classical Hodgkin lymphoma. Br. J. Haematol. 2019. 184: 594– 604.
30. Saxena M and Bhardwaj N. Re-emergence of dendritic cell vaccines for cancer treatment. Trends Cancer 2018. 4: 119– 137.
31. Lombardi V, Speak AO, Kerzerho J, Szely N and Akbari O. CD8α+β– and CD8α+β+ plasmacytoid dendritic cells induce Foxp3+ regulatory T cells and prevent the induction of airway hyper-reactivity. Mucosal Immunol. 2012. 5: 432– 443.
32. Shaw J, Wang YH, Ito T, Arima K and Liu YJ. Plasmacytoid dendritic cells regulate B-cell growth and differentiation via CD70. Blood 2010. 115: 3051– 3057.
33. Rosenbaum JT, Choi D, Wilson DJ, Grossniklaus HE, Sibley CH, Harrington CA, Planck SR, et al. Molecular diagnosis of orbital inflammatory disease. Exp. Mol. Pathol. 2015. 98: 225– 229.
34. Choi SC, Kim KD, Kim JT, Kim JW, Yoon DY, Choe YK, Chang YS, et al. Expression and regulation of NDRG2 (N-myc downstream regulated gene 2) during the differentiation of dendritic cells. FEBS Lett. 2003. 553: 413– 418.
35. Schraml BU, van Blijswijk J, Zelenay S, Whitney PG, Filby A, Acton SE, Rogers NC, et al. Genetic tracing via DNGR-1 expression history defines dendritic cells as a hematopoietic lineage. Cell 2013. 154: 843– 858.
36. Swerdlow SH, Campo E, Pileri SA, Harris NL, Stein H, Siebert R, Advani R, et al. The 2016 revision of the World Health Organization classification of lymphoid neoplasms. Blood 2016. 127: 2375– 2390.
37. Mombaerts I, Rose GE and Garrity JA. Orbital inflammation: biopsy first. Surv. Ophthalmol. 2016. 61: 664– 669.
38. Cossarizza A, Chang H, Radbruch A, Acs A, Adam D, Adam-Klages S, Agace WW, et al. Guidelines for the use of flow cytometry and cell sorting in immunological studies (second edition). Eur. J. Immunol. 2019. 49: 1457– 1973.
39. Van Gassen S, Callebaut B, Van Helden MJ, Lambrecht BN, Demeester P, Dhaene T and Saeys Y. FlowSOM: Using self-organizing maps for visualization and interpretation of cytometry data. Cytometry A 2015. 87: 636– 645.
40. Hahne F, LeMeur N, Brinkman RR, Ellis B, Haaland P, Sarkar D, Spidlen J, et al. flowCore: a Bioconductor package for high throughput flow cytometry. BMC Bioinformatics. 2009. 10: 106.
41. Wilkerson MD and Hayes DN. ConsensusClusterPlus: a class discovery tool with confidence assessments and item tracking. Bioinformatics. 2010. 26: 1572– 1573.
42. Chong J, Soufan O, Li C, Caraus I, Li S, Bourque G, Wishart DS, et al. MetaboAnalyst 4.0: towards more transparent and integrative metabolomics analysis. Nucleic Acids Res. 2018. 46: W486– W494.
43. Rosenbaum JT, Choi D, Harrington CA, Wilson DJ, Grossniklaus HE, Sibley CH, Salek SS, et al. Gene Expression Profiling and Heterogeneity of Nonspecific Orbital Inflammation Affecting the Lacrimal Gland. JAMA Ophthalmol. 2017. 135: 1156.
44. Barrett T, Wilhite S. E., Ledoux, P., Evangelista, C., Kim, I. F., Tomashevsky, M., Marshall, K. A. et al., NCBI GEO: archive for functional genomics data sets—update. Nucleic Acids Res. 2012. 41: D991– D995

Supporting Information Table S1. FlowSOM Metaclusters

MC					KW	Dunn's post-hoc		
		HC	IOI	NHOL	P-value	IOIvsHC	NHOLvsHC	IOIvsNHOL
A1	CD11c+CD141+ (cDC1)	0.08 [0.06, 0.08]	0.06 [0.05, 0.07]	0.06 [0.05, 0.08]	1,11E-01	1,08E-01	1,00E+00	8,14E-01
A2	CD14+CD16-CD11c+ (Classical monocyte)	12.88 [9.89, 15.50]	10.52 [8.82, 12.19]	17.97 [16.08, 21.14]	2,32E-02	6,21E-01	1,64E-01	1,88E-02
A3	CD11c+CD1c+ (cDC2)	0.64 [0.52, 0.69]	0.43 [0.35, 0.46]	0.69 [0.44, 0.73]	8,19E-03	1,11E-02	1,00E+00	4,01E-02
A4	CD14+CD16+CD11c+ (Intermediate monocyte)	1.39 [1.25, 2.10]	1.13 [0.64, 1.50]	1.70 [1.58, 2.41]	7,14E-02	4,11E-01	6,92E-01	6,86E-02
A5	CD303+CD123+ (pDC)	0.42 [0.35, 0.54]	0.35 [0.22, 0.43]	0.28 [0.24, 0.35]	4,28E-03	4,49E-02	1,18E-02	1,00E+00
A6	CD3+CD19+CD16+CD56+	1.45 [1.12, 2.08]	1.21 [0.91, 1.73]	1.08 [0.85, 1.77]	3,18E-01	1,00E+00	4,40E-01	1,00E+00
A7	CD56+CD16+	12.44 [6.99, 15.73]	10.14 [6.06, 14.15]	10.71 [7.48, 15.55]	9,33E-01	1,00E+00	1,00E+00	1,00E+00
A8	CD3+CD19+HLADR+	3.60 [2.12, 4.12]	3.46 [3.01, 4.23]	3.49 [2.96, 5.97]	3,52E-01	7,89E-01	6,70E-01	1,00E+00
A9	CD3+CD19+HLADR+CD1c+	4.80 [3.88, 8.03]	5.92 [4.88, 8.59]	5.69 [3.13, 8.35]	3,95E-01	5,52E-01	1,00E+00	9,99E-01
A10	CD3+CD19+	57.74 [53.15, 61.95]	58.74 [46.60, 65.10]	50.53 [43.41, 57.10]	1,98E-01	1,00E+00	3,29E-01	2,95E-01
A11	CD11c+	0.77 [0.56, 0.91]	0.84 [0.75, 1.17]	0.86 [0.58, 1.24]	3,42E-01	5,60E-01	9,29E-01	1,00E+00
A12	CD3+CD19+CD56+	1.15 [0.85, 1.77]	1.38 [0.94, 1.55]	1.33 [0.99, 1.56]	9,90E-01	1,00E+00	1,00E+00	1,00E+00
A13	CD3+CD19+CD14+	0.15 [0.12, 0.20]	0.13 [0.10, 0.14]	0.14 [0.12, 0.17]	1,67E-01	2,05E-01	1,00E+00	4,81E-01
A14	CD16+CD11c+	0.49 [0.35, 0.60]	0.33 [0.27, 0.45]	0.56 [0.40, 0.76]	1,21E-01	2,30E-01	1,00E+00	2,03E-01
A15	CD123+CD11c+	0.39 [0.23, 0.50]	0.34 [0.22, 0.49]	0.37 [0.27, 0.55]	8,37E-01	1,00E+00	1,00E+00	1,00E+00
A16	CD56+CD16+CD3+CD19+	0.47 [0.28, 0.74]	0.43 [0.33, 0.47]	0.65 [0.51, 0.72]	3,26E-01	1,00E+00	4,60E-01	6,27E-01
A17	CD56+	0.41 [0.30, 0.58]	0.27 [0.20, 0.44]	0.30 [0.20, 0.39]	1,62E-01	5,79E-01	2,49E-01	1,00E+00
B1	CD3+CD8+CD27+	15.72 [12.65, 18.50]	13.07 [9.97, 17.79]	7.84 [6.99, 14.87]	3,08E-02	1,00E+00	2,50E-02	3,08E-01
B2	CD3+CD8+CD45RO+CD161+CCR6+	0.56 [0.39, 0.83]	0.25 [0.14, 0.62]	0.15 [0.09, 0.40]	1,08E-02	5,84E-01	8,49E-03	3,28E-01
B3	CD3+CD4-CD8-	0.89 [0.61, 1.10]	0.77 [0.57, 0.92]	0.42 [0.29, 0.59]	7,44E-03	9,67E-01	5,23E-03	1,43E-01
B4	CCR6+(CD27+)	7.32 [4.90, 10.38]	8.58 [7.40, 10.95]	7.14 [4.88, 13.81]	4,88E-01	6,98E-01	1,00E+00	1,00E+00
B5	CD3+CD4+CD27+CD45RO+	31.22 [24.98, 34.75]	28.07 [20.58, 37.30]	29.77 [25.23, 34.87]	9,91E-01	1,00E+00	1,00E+00	1,00E+00
B6	CCR6+CXCR3+CD161+CCR8+CCR10+CD45RO+CD27+CD4+CD3+	0.23 [0.17, 0.31]	0.19 [0.15, 0.21]	0.19 [0.14, 0.24]	4,94E-01	9,71E-01	1,00E+00	1,00E+00
B7	CD45RO+CCR6+CD4+CD3+	4.78 [3.69, 6.02]	5.64 [3.90, 7.96]	4.20 [2.94, 5.66]	5,09E-01	1,00E+00	1,00E+00	7,56E-01
B8	CD56+CD8+CD161+	13.63 [9.63, 17.36]	13.42 [7.53, 17.26]	12.83 [10.13, 17.29]	9,49E-01	1,00E+00	1,00E+00	1,00E+00
B9	CD45RO+CD4+	17.09 [14.42, 19.97]	14.23 [13.10, 16.08]	24.41 [13.58, 27.48]	9,72E-02	3,43E-01	1,00E+00	1,10E-01
B10	CD45RO+CD27+CD4+CD3+	3.17 [2.60, 3.66]	3.13 [2.18, 5.06]	3.18 [2.59, 3.58]	8,37E-01	1,00E+00	1,00E+00	1,00E+00
B11	CD45RO+CD4+CD3+	2.32 [1.96, 2.71]	2.95 [1.85, 3.43]	2.87 [2.16, 3.78]	4,00E-01	8,12E-01	8,25E-01	1,00E+00
B12	CD56+CXCR3+CD161+	0.63 [0.46, 0.89]	0.44 [0.36, 0.65]	0.66 [0.47, 0.67]	2,80E-01	3,59E-01	1,00E+00	7,72E-01

B13	CD45RO+CCR8+	0.07 [0.04, 0.10]	0.08 [0.07, 0.20]	0.10 [0.06, 0.18]	4,35E-01	1,00E+00	6,92E-01	1,00E+00
B14	CD3+CD8+	0.50 [0.33, 1.34]	0.44 [0.29, 0.60]	0.47 [0.24, 1.23]	6,23E-01	1,00E+00	1,00E+00	1,00E+00
B15	CD3+CD4+CD27+CD45RO+CCR10+	0.27 [0.16, 0.41]	0.25 [0.18, 0.47]	0.23 [0.17, 0.46]	8,80E-01	1,00E+00	1,00E+00	1,00E+00
B16	CD27+	0.30 [0.23, 0.46]	0.25 [0.14, 0.32]	0.33 [0.21, 0.38]	4,09E-01	5,85E-01	1,00E+00	9,93E-01
C1	CD3-CD19-CD38+	15.32 [12.60, 18.49]	12.90 [10.57, 15.21]	18.76 [17.41, 22.04]	4,25E-02	5,12E-01	3,47E-01	3,59E-02
C2	CD3-CD19-CD38+	11.48 [9.57, 13.78]	9.93 [8.27, 11.98]	15.50 [14.67, 17.90]	4,22E-02	7,41E-01	2,35E-01	3,66E-02
C3	CD19+CD27+	0.14 [0.10, 0.22]	0.18 [0.11, 0.40]	0.27 [0.21, 0.32]	7,90E-02	6,00E-01	9,21E-02	1,00E+00
C4	CD19+CD27+CD38+	0.07 [0.04, 0.10]	0.18 [0.10, 0.26]	0.12 [0.07, 0.22]	7,40E-03	1,13E-02	1,24E-01	1,00E+00
C5	CD3+CD27+	21.36 [15.71, 22.61]	21.12 [13.89, 25.36]	19.09 [14.62, 21.99]	4,59E-01	1,00E+00	8,50E-01	7,21E-01
C6	CD3+	3.54 [2.01, 7.85]	2.95 [1.55, 3.51]	2.13 [1.77, 4.78]	4,20E-01	1,00E+00	7,33E-01	1,00E+00
C7	CD3+CD27+	29.48 [24.64, 32.17]	33.59 [22.10, 36.59]	27.33 [24.14, 32.49]	3,01E-01	6,34E-01	1,00E+00	4,49E-01
C8	CD3+CD19+CD10+	0.01 [0.01, 0.02]	0.01 [0.01, 0.02]	0.02 [0.01, 0.06]	7,42E-01	1,00E+00	1,00E+00	1,00E+00
C9	CD24+	0.10 [0.07, 0.19]	0.12 [0.09, 0.16]	0.26 [0.17, 0.37]	1,32E-01	1,00E+00	1,52E-01	3,23E-01
C10	-	2.42 [1.76, 2.98]	1.72 [1.63, 3.70]	1.69 [1.61, 3.14]	8,27E-01	1,00E+00	1,00E+00	1,00E+00
C11	CD3+	3.76 [2.33, 10.00]	3.61 [1.56, 4.72]	2.53 [2.00, 5.44]	4,39E-01	9,93E-01	8,15E-01	1,00E+00
C12	CD3+CD19+	0.06 [0.04, 0.21]	0.06 [0.05, 0.11]	0.07 [0.05, 0.40]	6,38E-01	1,00E+00	1,00E+00	1,00E+00
C13	CD3+CD19+CD21+	0.02 [0.01, 0.03]	0.01 [0.01, 0.02]	0.01 [0.01, 0.04]	9,67E-01	1,00E+00	1,00E+00	1,00E+00
C14	CD19+CD21+	1.85 [0.99, 2.14]	2.60 [1.69, 2.73]	2.38 [1.05, 3.41]	3,78E-01	6,73E-01	9,08E-01	1,00E+00
C15	CD19+CD24+	0.12 [0.07, 0.18]	0.11 [0.08, 0.41]	0.15 [0.10, 0.21]	8,47E-01	1,00E+00	1,00E+00	1,00E+00
C16	CD19+CD21+CD24+	1.17 [0.86, 1.88]	1.39 [1.00, 1.90]	1.17 [0.83, 1.77]	8,50E-01	1,00E+00	1,00E+00	1,00E+00
C17	CD19+CD21+	2.64 [1.51, 3.16]	4.11 [2.72, 4.23]	3.20 [1.50, 5.88]	2,66E-01	3,66E-01	1,00E+00	1,00E+00
C18	CD19+CD21+CD24+	1.93 [1.20, 2.27]	1.76 [1.14, 2.44]	0.78 [0.65, 1.96]	2,31E-01	1,00E+00	2,62E-01	7,51E-01

KW = Kruskal Wallis test, with subsequent Dunn's post-hoc correction; MC = meta-cluster; pDC = Plasmacytoid dendritic cells; cDC1 = conventional dendritic cells type-1; cDC2 = conventional dendritic cells type-2; HC = Healthy control; IOI = Idiopathic orbital inflammation; NHOL = non-Hodgkin orbital lymphoma.

Supporting Information Table 2. Manual gating of the FlowSOM selected populations.

				Discovery cohort		KW	Dunn's post-hoc		
M	Population	Percentage of	HC	IOI	NHOL	P-value	IOIvsHC	NHOLvsHC	IOIvsNHOL
A2	CD14+CD16-CD11c+ (Classical monocyte)	Single Cells	12.00 [9.21, 14.50]	9.85 [7.78, 11.40]	16.80 [15.43, 20.38]	1,58E-02	4,78E-01	1,54E-01	1,21E-02
A5	CD303+CD123+ (pDC)	Single Cells	0.41 [0.34, 0.53]	0.29 [0.14, 0.38]	0.26 [0.22, 0.32]	1,16E-03	9,61E-03	7,87E-03	1,00E+00
-	CD303+CD123+ (pDC)	Lieage-HLADR+	19.40 [15.70, 25.20]	15.20 [10.50, 17.60]	11.00 [8.76, 12.80]	1,38E-03	9,76E-02	1,66E-03	5,46E-01
A3	CD11c+CD1c+ (cDC2)	Single Cells	0.60 [0.48, 0.74]	0.34 [0.31, 0.37]	0.66 [0.38, 0.72]	3,10E-04	2,45E-04	1,00E+00	1,62E-02
-	CD11c+CD1c+ (cDC2)	Lineage-HLADR+	25.60 [21.40, 33.60]	18.20 [15.40, 23.60]	22.10 [13.75, 28.28]	3,28E-02	2,86E-02	7,68E-01	8,18E-01
B1	CD3+CD8+CD27+	Single Cells	7.15 [4.34, 9.66]	4.73 [2.23, 8.85]	3.42 [2.56, 3.85]	1,89E-02	4,73E-01	1,75E-02	5,77E-01
B1	CD3+CD8+CD27+ CD45RO+	Single Cells	4.78 [3.01, 6.60]	4.12 [3.30, 5.00]	3.21 [2.41, 5.57]	4,74E-01	1,00E+00	7,80E-01	8,37E-01
B2	CD3+CD8+CD45RO+ CD161+CCR6+	Single Cells	0.44 [0.24, 0.87]	0.27 [0.16, 0.53]	0.14 [0.06, 0.43]	4,01E-02	9,68E-01	3,44E-02	4,45E-01
B3	CD3+CD8-CD4-	Single Cells	3.29 [1.97, 5.01]	2.45 [2.15, 3.54]	2.02 [1.71, 2.70]	9,20E-02	1,00E+00	8,69E-02	5,38E-01
C4	CD19+CD27+CD38+	Single Cells	0.03 [0.02, 0.05]	0.07 [0.03, 0.15]	0.06 [0.02, 0.12]	5,87E-02	9,38E-02	3,04E-01	1,00E+00
			Replication cohort			KW	Dunn's post-hoc		
M	Population	Percentage of	HC	IOI	NHOL	P-value	IOIvsHC	NHOLvsHC	IOIvsNHOL
A2	CD14+CD16-CD11c+ (Classical monocyte)	Single Cells	11.55 [9.03, 16.93]	11.80 [10.22, 14.62]	15.85 [10.83, 19.97]	5,17E-01	1,00E+00	9,51E-01	8,96E-01
A5	CD303+CD123+ (pDC)	Single Cells	0.41 [0.29, 0.51]	0.18 [0.11, 0.29]	0.28 [0.18, 0.37]	1,42E-02	1,80E-02	1,98E-01	1,00E+00
-	CD303+CD123+ (pDC)	Lineage-HLADR+	20.95 [15.25, 28.23]	9.46 [8.15, 14.57]	13.25 [9.11, 14.75]	3,67E-03	1,17E-02	3,11E-02	1,00E+00
A3	CD11c+CD1c+ (cDC2)	Single Cells	0.51 [0.31, 0.71]	0.23 [0.16, 0.31]	0.43 [0.35, 0.55]	2,10E-02	1,64E-02	1,00E+00	3,03E-01
-	CD11c+CD1c+ (cDC2)	Lineage-HLADR+	25.95 [21.78, 31.45]	13.90 [10.85, 16.18]	18.70 [10.14, 27.02]	1,12E-02	1,09E-02	2,99E-01	8,23E-01
B1	CD3+CD8+CD27+	Single Cells	6.36 [3.60, 8.11]	5.06 [3.18, 7.48]	2.43 [1.38, 5.64]	1,73E-01	1,00E+00	1,88E-01	6,31E-01
B1	CD3+CD8+CD27+ CD45RO+	Single Cells	4.55 [3.69, 6.21]	4.36 [3.06, 6.36]	4.77 [3.79, 6.11]	8,54E-01	1,00E+00	1,00E+00	1,00E+00
B2	CD3+CD8+CD45RO+ CD161+CCR6+	Single Cells	0.45 [0.33, 0.81]	0.26 [0.09, 0.69]	0.32 [0.08, 0.47]	1,53E-01	4,57E-01	2,63E-01	1,00E+00
B3	CD3+CD8-CD4-	Single Cells	1.96 [1.75, 3.16]	2.33 [1.90, 2.66]	2.27 [1.41, 3.04]	9,65E-01	1,00E+00	1,00E+00	1,00E+00
C4	CD19+CD27+CD38+	Single Cells	0.02 [0.01, 0.06]	0.05 [0.03, 0.06]	0.03 [0.01, 0.05]	4,32E-01	8,24E-01	1,00E+00	6,91E-01
			Cohorts combined			KW*	Dunn's post-hoc*		

M	Population	Percentage of	HC	IOI	NHOL	P-adj	IOIvsHC	NHOLvsHC	IOIvsNHOL
A2	CD14+CD16-CD11c+ (Classical monocyte)	Single Cells							
A5	CD303+CD123+ (pDC)	Single Cells	0.41 [0.33, 0.53]	0.24 [0.13, 0.34]	0.26 [0.21, 0.35]	2,67E-05	2,96E-04	4,12E-03	1,00E+00
-	CD303+CD123+ (pDC)	Lin-eage-HLADR+	19.40 [15.60, 26.70]	14.60 [8.58, 17.60]	11.40 [9.00, 13.73]	2,67E-05	1,78E-03	1,48E-04	1,00E+00
A3	CD11c+CD1c+ (cDC2)	Single Cells	0.55 [0.41, 0.74]	0.33 [0.27, 0.37]	0.47 [0.38, 0.70]	2,67E-05	5,88E-05	1,00E+00	2,77E-02
-	CD11c+CD1c+ (cDC2)	Lin-eage-HLADR+	25.60 [21.40, 31.60]	15.90 [12.00, 22.60]	21.50 [12.05, 28.83]	3,50E-04	3,50E-04	2,08E-01	7,03E-01
B1	CD3+CD8+CD27+	Single Cells							
B1	CD3+CD8+CD27+ CD45RO+	Single Cells							
B2	CD3+CD8+CD45RO+ CD161+CCR6+	Single Cells							
B3	CD3+CD8-CD4-	Single Cells							
C4	CD19+CD27+CD38+	Single Cells							

KW = Kruskal Wallis test with subsequent Dunn's correction; * = Kruskal Wallis test and subsequent Dunn's correction adjusted for multiple testing with FDR method. pDC = Plasmacytoid dendritic cells; cDC2 = conventional dendritic cells type-2; HC = Healthy control; IOI = Idiopathic orbital inflammation; NHOL = non-Hodgkin orbital lymphoma; P-value = nominal P-value; P-adj = adjusted P- value; M = Meta-cluster

Supporting Information Table S3: ANOVA group comparisons and comparisons corrected for age and sex

Population	Percentage of	Metacluster	No correction		Corrected for age		Corrected for sex	
			P-value	P-adj*	P-value	P-adj*	P-value	P-adj*
CD14+CD16-CD11c+ (Classical monocyte)	Single Cells	A2	2,13E-02	3,04E-02	3,27E-01	3,87E-01	2,70E-02	3,38E-02
CD303+CD123+ (pDC)	Single Cells	A5	3,07E-05	1,54E-04	4,77E-04	2,39E-03	1,29E-05	6,47E-05
CD303+CD123+ (pDC)	Lineage-HLADR+	-	2,40E-07	2,40E-06	7,66E-06	7,66E-05	1,02E-07	1,02E-06
CD11c+CD1c+ (cDC2)	Single Cells	A3	3,65E-02	4,56E-02	2,61E-02	5,61E-02	2,05E-02	3,16E-02
CD11c+CD1c+ (cDC2)	Lineage-HLADR+	-	1,50E-02	3,00E-02	5,98E-03	1,99E-02	9,36E-03	2,04E-02
CD3+CD8+CD27+	Single Cells	B1	3,26E-03	1,09E-02	7,29E-01	7,29E-01	4,38E-03	1,46E-02
CD3+CD8+CD27+ CD45RO+	Single Cells	B1	5,31E-01	5,31E-01	3,11E-01	3,87E-01	5,15E-01	5,15E-01
CD3+CD8+CD45RO +CD161+CCR6+	Single Cells	B2	9,12E-03	2,28E-02	3,48E-01	3,87E-01	1,02E-02	2,04E-02
CD3+CD8-CD4-	Single Cells	B3	1,93E-02	3,04E-02	3,07E-01	3,87E-01	2,21E-02	3,16E-02
CD19+CD27+CD38+	Single Cells	C4	1,53E-01	1,70E-01	2,81E-02	5,61E-02	1,31E-01	1,46E-01

Analysis of variance (ANOVA) of the three groups with collumns corrected for age and sex. All statistics are given for nominal P-value and P-value adjusted for multiple comparisons with the FDR method. Abbreviations: pDC = Plasmacytoid dendritic cells; cDC2 = conventional dendritic cells type-2; HC = Healthy control; IOI = Idiopathic orbital inflammation; NHOL = non-Hodgkin orbital lymphoma; P-value = nominal P-value; P-adj = adjusted P-value.

Supplemental Table 4. Flow cytometry panels

	Discovery Cohort					Replication Cohort				
	Fluoro-chrome	Marker	Dilu-tion	Clone	Company	Fluoro-chrome	Marker	Dilu-tion	Clone	Company
mononuclear myeloid and dendritic cell panel	FITC	CD123	1:20	7G3	BD Pharmin-gen	FITC	CD123	1:20	7G3	BD Pharmin-gen
	APC	CD1c	1:10	L161	BioLegend	APC	CD1c	1:10	L161	BioLegend
	AF700	CD3	1:40	UCHT1	BioLegend	AF700	CD3	1:40	UCHT1	BioLegend
	AF700	CD19	1:50	HIB19	eBioscience	AF700	CD19	1:50	HIB19	eBioscience
	eFluor780	CD14	1:40	61D3	eBioscience	eFluor780	CD14	1:40	61D3	eBioscience
	BV421	HLA-DR	1:00	L243	BioLegend	BV421	HLA-DR	1:00	L243	BioLegend
	BV510	CD16	1:00	3G8	BD Horizon	BV510	CD16	1:00	3G8	BD Horizon
	BV711	CD141	1:50	1A4	BD Horizon	BV711	CD141	1:50	1A4	BD Horizon
	PE	CD56	1:10	CMSSB	eBioscience	PE	CD56	1:10	CMSSB	eBioscience
	PE-Cy7	CD303	1:40	201A	BioLegend	PE-Cy7	CD303	1:40	201A	BioLegend
	PE-CF594	CD11c	1:200	B-LY6	BD Horizon	PE-CF594	CD11c	1:200	B-LY6	BD Horizon
T-cell panel	FITC	CXCR3	1:40	G025H7	BioLegend	FITC	CXCR3	1:40	G025H7	BioLegend
	Per-CP-CY5.5	CD4	1:25	SK3	BD	Per-CP-CY5.5	CD4	1:25	SK3	BD
	APC	CCR10	1:10	314305	R&D Systems	APC	CCR10	1:10	314305	R&D Systems
	AF700	CD3	1:40	UCHT1	BioLegend	AF700	CD3	1:40	UCHT1	BioLegend
	eFluor780	CD27	1:20	0323	eBioscience	eFluor780	CD27	1:20	0323	eBioscience
	BV421	CCR8	1:10	433H	BD Horizon	BV421	CCR8	1:10	433H	BD Horizon
	BV510	CD161	1:20	DX12	BD Horizon	BV510	CD161	1:20	DX12	BD Horizon
	BV605	CCR4	1:40	1G1	BD Horizon	BV605	CCR4	1:40	1G1	BD Horizon
	BV711	CD45RO	1:100	UCHL1	BioLegend	BV711	CD45RO	1:100	UCHL1	BioLegend
	PE	CCR6	1:40	11A9	BD Pharmin-gen	PE	CCR6	1:40	11A9	BD Pharmin-gen
	PE-Cy7	CD8	1:200	SK1	BD	PE-Cy7	CD8	1:200	SK1	BD
	PE-CF594	CD56	1:20	B159	BD	PE-CF594	CD56	1:20	B159	BD
B-cell panel	Per-CP-CY5.5	CD38	1:100	HIT2	BD Pharmin-gen	FITC	IgG	1:200	NA	Southern Biotech
	APC	CD27	1:50	L128	BD	Per-CP-CY5.5	CD38	1:100	HIT2	BD Pharmin-gen
	AF700	CD3	1:40	UCHT1	BioLegend	APC	CD27	1:50	L128	BD
	eFluor780	CD19	1:20	HIB19	eBioscience	AF700	CD3	1:40	UCHT1	BioLegend
	BV510	Viability stain	1:100	NA	eBioscience	eFluor780	CD19	1:20	HIB19	eBioscience
	BV711	CD21	1:20	B-ly4	BD	BV421	Viability stain	1:100	NA	eBioscience
	PE-Cy7	CD10	1:100	HI10A	BD	BV510	IgD	1:50	IA6-2	Biolegend
	PE-CF594	CD24	1:200	ML5	BD Horizon	BV711	CD21	1:20	B-ly4	BD
						PE	IgA	1:400	NA	Southern Biotech
						PE-Cy7	CD10	1:100	HI10A	BD
						PE-CF594	CD24	1:200	ML5	BD Horizon

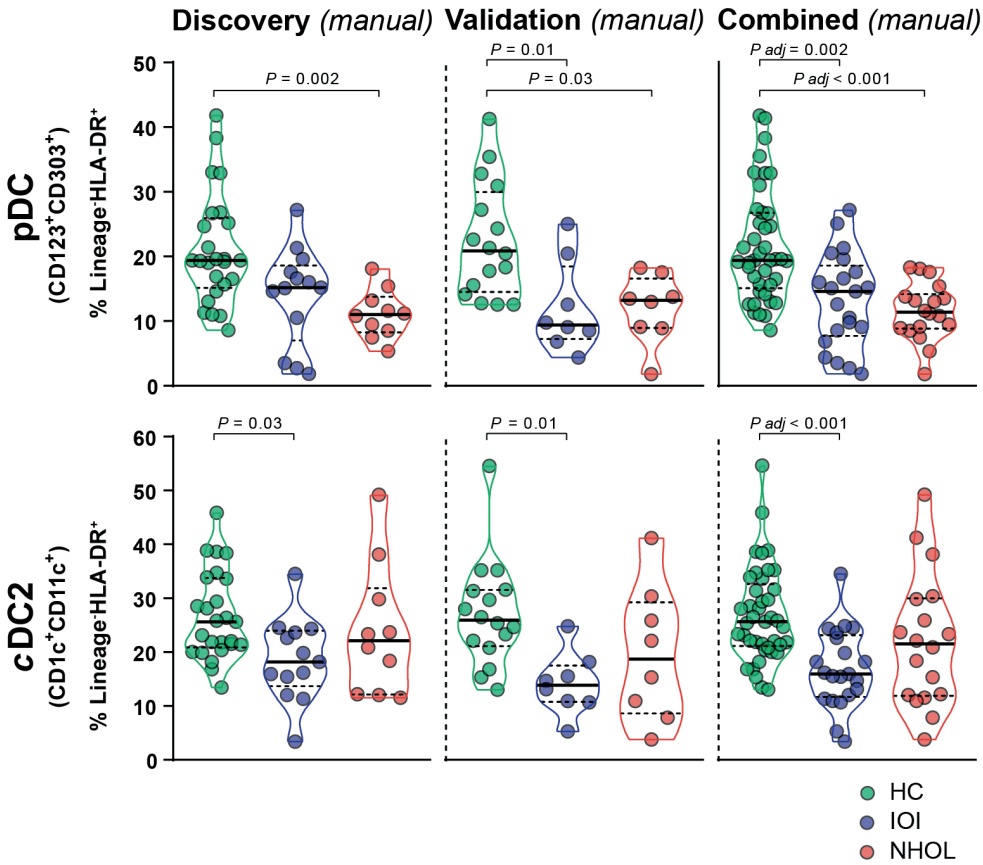

Supporting Information Figure S1. pDC and cDC2 populations in patients and controls. The percentage of pDC and cDC2 cells in the lineage-negative (CD3-/CD19-/CD56-/CD14-) HLA-DR-positive gate. Data for the discovery, validation and combined cohorts are indicated. The Kruskal-Wallis tests with Dunn's post-hoc test were used to assess differences between groups. The adjusted P-values are corrected using the Benjamini-Hochberg method. The median with interquartile ranges are indicated by black lines and dotted lines, respectively. Abbreviations: HC = healthy control, IOI = idiopathic orbital inflammation, NHOL = non-Hodgkin orbital lymphoma, pDC = plasmacytoid dendritic cells, cDC2 = conventional dendritic cells type-2, P = nominal P-value; P adj = adjusted P-value.

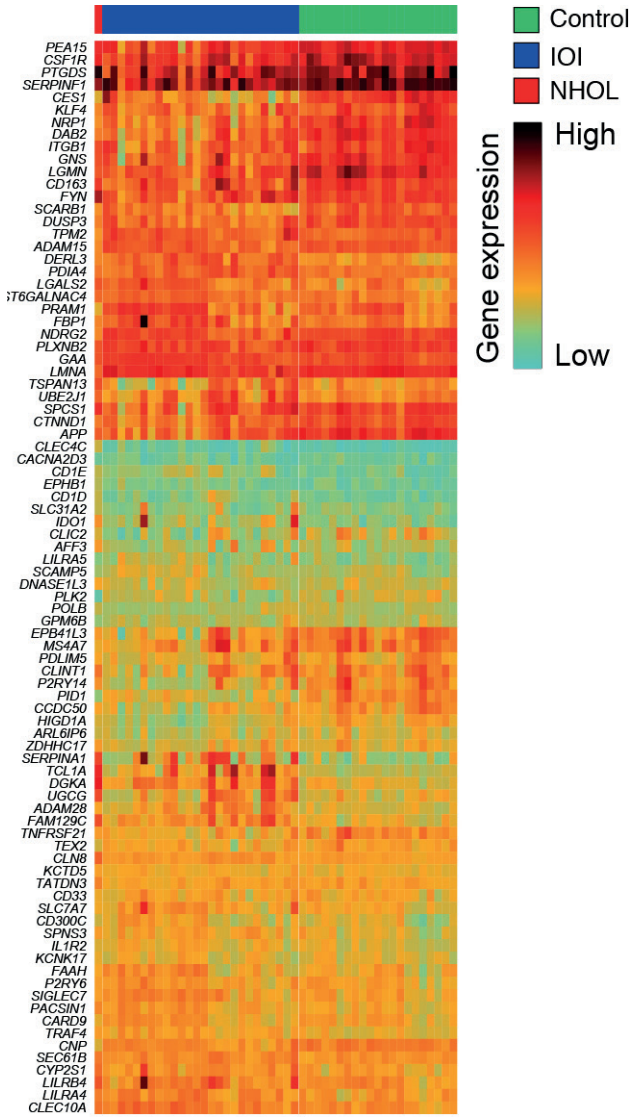

Supporting Information Figure S2. A larger representation of the heatmap displayed in Fig. 4. The gene expression profiles of signature genes of pDC and cDC in orbital biopsies of 26 IOI patients and 21 controls from GSE58331 are displayed.

Monocyte & Dendritic Cell panel

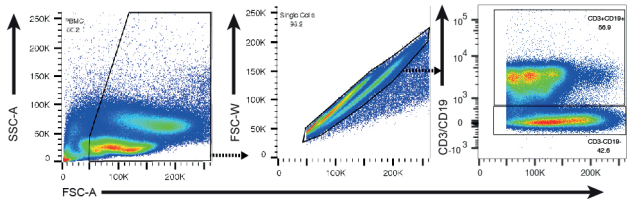

B-cell panel

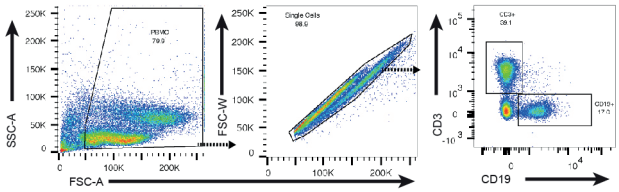

T-cell panel

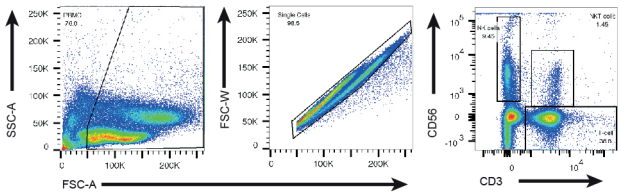

Supporting Information Figure S3. Examples of the gating strategy basis for the monocyte and dendritic-cell panel; T-cell panel; and B-cell panel.


Chapter 9

Mass-spectrometry imaging of orbital biopsies identifies disease-specific peptide profiles

Kamil G. Laban
Rachel Kalmann
Roos J. Leguit
Timothy R.D.J. Radstake
Jonas J.W. Kuiper
Joke H. de Boer
Ron M.A. Heeren
Tiffany Porta Siegel

Manuscript in preparation

Abstract

Background and purpose: Histopathological diagnosis of non-Hodgkin orbital lymphoma (NHOL) and idiopathic orbital inflammation (IOI) can be challenging and may benefit from deep molecular profiling technologies. For this purpose, we used mass-spectrometry imaging (MSI) to investigate the peptide fingerprint of open biopsy tissues of NHOL and IOI cases.

Methods: Formalin-fixed paraffin-embedded incisional biopsies from NHOL (n = 9) and IOI (n = 8) cases were cut into 10 µm sections and subjected to untargeted MSI. Imaging acquisition was performed in positive mode over the mass-to-charge ratio range of *m/z* 500-3200 with a matrix-assisted laser desorption/ionization (MALDI) time-of-flight (TOF) instrument at a spatial resolution of 50x50 μm^2. Tissue sections were subsequently stained with hematoxylin and eosin, annotated and co-registered to the MSI data set.

Results: A peak list of 223 *m/z* ions from all tissue spectra was used for data analysis. Principle component analysis based on the peak-list separated NHOL and IOI patients. Probabilistic latent semantic analysis determined peptide profiles linked predominantly to NHOL, IOI and surrounding tissue areas. Head-to-head comparisons showed that 24 *m/z* ions were differentially expressed between samples of NHOL and IOI.

Conclusion: Mass-spectrometry imaging of peptide profiles can characterize NHOL and IOI in biopsy tissues. Moreover, specific profiles can be distinguished for infiltrates and surrounding tissue areas. These results may lead to improvement of molecular tissue diagnosis and disease classification.

Introduction

Non-Hodgkin orbital lymphoma (NHOL) is the most common orbital malignancy in adults.[1] Early and adequate treatment is critical to reduce local and systemic spread, especially for the more aggressive diffuse large B-cell lymphoma (DLBCL) subtype. The five-year lymphoma-related mortality rate has been found to be 12% for extra-nodal marginal zone lymphoma (EMZL), the most common subtype, and 48% for DLBCL.[1] Unfortunately, many cases are complicated by a difficult diagnostic process due to overlapping clinical, radiological and laboratory findings with inflammatory orbital disorders, most often idiopathic orbital inflammation (IOI).[2] Histopathology of biopsy material is therefore required for definite diagnosis.[1,3] In some cases, however, the affected tissues are located deep within the orbit and can be difficult to reach by incisional biopsies. For proper histopathological examination, assessment of the architectural context of the tissue is essential, because of varying degrees of in-tissue heterogeneity.[4] Consequently, larger biopsies are necessary and smaller biopsies or less-invasive approaches can be non-representative or have insufficient tissue-yield for diagnosis.[4,5]

Fortunately, molecular techniques are transforming the diagnostic process of orbital conditions.[6] Adding deep molecular profiling techniques to biopsy diagnosis can improve accuracy and has the advantage of a molecular classification over clinical classification. The latter may overcome the current view of large heterogeneity within a single diagnosis. Mass spectrometry imaging (MSI) can be used to examine the molecular peptide profile of formalin-fixed paraffin-embedded (FFPE) biopsy tissues, by investigating the *m/z* ion spectrum that defines peptides in surface areas of tissue sections.[7,8] These peptide profiles may elucidate biopsy contents and aid the diagnostic process. Especially in complex diseases, such as NHOL and IOI, where architectural structure is important for histopathological assessment, this exciting technology may increase diagnostics accuracy. We therefore investigated the potential of MSI profiling for differentiation between NHOL and IOI in this study, and elaborate on future diagnostic uses for orbital diseases.

Methods

Chemicals and reagents

Acetonitrile, ethanol (dehydrated), methanol, n-hexane, trifluoroacetic acid, ultrapure water (ULC/MS – CC/SFC water), and xylene (analytical reagent grade) were purchased from Biosolve BV, Valkenswaard, The Netherlands. α-Cyano-4-hydroxycinnamic acid (CHCA), citric acid monohydrate, cytochrome C (equine heart), and trypsin (porcine pancreas #T6567) were purchased from Sigma –

Aldrich, St. Louis, Montana, USA. Red Phosphorus, hematoxylin and eosin were purchased from Merck KGaA, Darmstadt, Germany.

Samples

This study was performed on FFPE material from anonymous patients that was redundant after diagnostic confirmation of orbital disease. In total 17 samples were included in this study of NHOL (*n=9*) and IOI (*n=8*) biopsies. All samples were biopsied from patients between 2002 and 2018 in the University Medical Center Utrecht, Utrecht, The Netherlands. This study was conducted in conformity with the declaration of Helsinki and its further amendments and the General Data Protection Regulation. The patient material was collected in accordance with the code "appropriate use of redundant tissue for clinical research" guidelines constructed by the Dutch Federation of Medical Research Societies (www.federa.org). The study protocol has been approved by the Institutional Review Board for biobank material (TC-BIO, number 17-644).

All NHOL patients were diagnosed following WHO criteria with histopathological assessment of incisional biopsies.[9] Diagnostic ancillary assessments were performed on indication and included a polymerase chain reaction (PCR) based clonality assessment, translocation analysis with fluorescence in situ hybridization, and specific mutations (including MYD88 mutation). Patients with IOI were diagnosed based on exclusion of infection, benign or malignant neoplasia, systemic disease, histiocytic disease or thyroid eye disease, granulomatosis with polyangiitis, sarcoidosis, primary Sjögren's syndrome, benign lymphoid hyperplasia, or IgG4-related pathology.[3,10] All IOI specimen were from open (incisional) biopsies, showing a non-specific (plasma) lymphocytic infiltrate in multiple samples.[3,10] All IOI biopsies were stained for IgG4 to exclude IgG4 related orbital disease.[3]

Sample preparation of FFPE tissue amenable for MSI analysis

The FFPE samples were cut in 10 µm sections and mounted on Indium-Tin-Oxide (ITO) coated slides (Delta Technologies, Loveland, USA), previously cleaned with n-hexane (sonicated for 7 min) and absolute ethanol (sonicated for 7 min) and coated with poly-L-lysine. One NHOL section and one IOI section were mounted on one slide. Next, the samples were prepared for MSI, adapted from previously described protocols.[7] In brief, the slides were pre-heated on a heating plate for 60 minutes at 60˚Celcius. The paraffin was removed by submersion in xylene (5 minutes and 10 minutes in separate holders). The slides were then washed twice in absolute ethanol (2 minutes) and twice in ultrapure water (5 minutes). We then performed antigen retrieval with 10 mM citric acid monohydrate at pH 6 as buffer in the Antigen Retriever 2100 (Aptum Biologics, Southampton, UK) according to

the manufacturer's instructions. The slides were cooled to room temperature within the apparatus and subsequently washed twice with ultrapure water (1 minute). The slides were then dried in a desiccator (15 minutes). For quality control, cytochrome C was spotted on the slide prior to the digestion step. On-tissue digestion followed by spraying a solution of trypsin (0.02 µg/µL in ultrapure water) with a SunCollect spraying system (SunChrom, Friedrichsdorf, Germany). The spraying of trypsin followed an HH moving pattern with x = 0.5 mm; y = 1.0 mm; z = 25 mm and the x,y speed of 900 mm/min. A total of 15 layers were applied at 10 µL/min flowrate. The slides were then incubated for 17 hours at 37°Celcius in a saturated environment using an airtight box filled with 50 mL methanol and 50 mL ultrapure water.

Next, the slides were marked with fiducials and coated with 7 mg/ml CHCA matrix in a buffer of 50% acetonitrile and 0.2% trifluoroacetic acid in ultrapure water. Ten layers of matrix were applied at room temperature with the SunCollect with increasing flowrate as follow: the first four layers with 10, 20, 30 and 40 µL/min, respectively and with 40 µL/min for the remaining passes. For the matrix deposition we used an HH pattern with x = 0.5 mm; y = 1.0 mm; z = 25 mm and the x,y speed of 900 mm/min.

MALDI-TOF MS

MSI measurements with high-speed imaging were performed on the Bruker rapifleX MALDI Tissuetyper™ time-of-flight (TOF) instrument (Bruker Daltonik GmbH, Bremen, Germany). Before measurements, the mass spectrometer was calibrated using 1µl of red phosphorous dissolved in acetone spotted on the glass slide out of tissue area on top of the matrix coating. The peptide measurements were performed in positive mode over a *m/z* range of 500-3200 with suppression up to 400 *m/z* and a spatial resolution of 50x50µm^2. At the beginning of the experiment the laser intensity, reflector voltage and global attenuator offset were optimized and used for the rest of the experiment. The focus setting was adjusted for each sample. In each spot, 800 laser shots were accumulated at a frequency of 10 kHz. After the peptide measurements, the matrix was removed with 100% ethanol and stained for hematoxylin and eosin (H&E), following the supplier's instructions. Optical images were obtained by the Mirax Desk high-resolution scanner (ZEISS, Oberkochen, Germany).

Data pre-processing

The raw data from the MALDI-TOF instrument were automatically loaded in Fleximaging software v.4.1 (Bruker Daltonik GmbH, Bremen, Germany) and then exported as MISsion file (.mis). Next, the files were imported into SCiLS Lab software v.2019a (SCiLS, Bremen, Germany) and the MSI image was semi-

automatically overlaid with the H&E staining of the slides included the fiducial markers. The tissue boundaries were defined and the tissues annotated by K.G.L and R.J.L. The combined samples were normalized by total ion count (TIC) and the overall mean spectrum was extracted and exported to mMass v.5.5,[11] where it was subjected to autoscaling, baseline subtraction, and smoothing (Gaussian algorithm with window size of 0.5 *m/z* and 3 cycles). Next, we performed peak picking on the spectrum with the peak intensity threshold relative to base peak set to 2%. After data pre-processing, a peak list of 223 *m/z* ions was imported back to SCiLS with the window size per peak adjusted to 0.5 Da. The mean spectrum intensity for each peak was exported for each tissue section into a .CSV file for further statistical analysis.

Data analysis

The .CSV files were imported into SPSS for Windows, version 25.0 (IBM Corp, Armonk, N.Y., USA). To investigate data-based group separation, we performed a principle component analysis (PCA) using MetaboAnalyst server version 4.0,[12] and report on the first 5 components. We next performed, a multivariable analysis using SCiLS Lab software with a probabilistic latent semantic analysis (pLSA) to cluster tissue areas, based on their peptide profiles. To cluster this complex tissue, 15 components were calculated with a linear model. The pLSA analysis allows for identification of molecular species that represent specific areas within tissues in a scaled spectrum, acting as a fingerprint for each tissue type within the sections. The corresponding areas were next compared to the annotated areas. Note that technical components, representing matrix remnants were not considered for further analysis in the PCA and pLSA analyses. In order to find individual discriminating peptides (*m/z* ions) between NHOL and IOI, we next used the Mann-Whitney-U test for univariate statistical testing, followed by a Benjamini-Hochberg correction for multiple testing. The discriminatory power for individual peptides were analyzed with receiver operator curve statistics.

Results

Exploratory patient clustering using PCA analysis

We loaded the peak data for each sample in MetaboAnalyst 4.0 and investigated the relationships between the samples using a principal component analysis (PCA). For the PCA analysis the peak data was TIC and quantile normalized and was scaled for visualization of the PCA. The distance between the groups was largest using the first and third component (**Figure 1)**. Components loadings, which are the correlation coefficients between the items and the identified components, suggest the ions at *m/z* 785.58, 898.68, 1095.78 and 1303.81 drive the variance

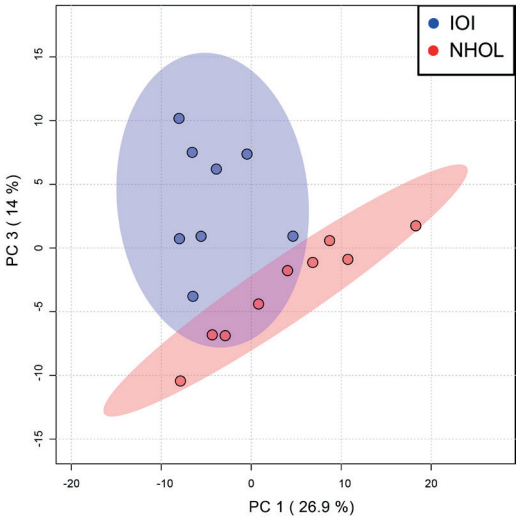

Figure 1. Unsupervised profiling of whole tissue analysis. Principle component analysis of the mean intensity of the 223 m/z ions for each sample, with projection of the first and third components. The dots represent each sample and the ellipses represent the 95% confidence intervals for each group. The analysis was performed in Metaboanalyst 4.0, with a quantile normalization and auto-scaling. **Abbreviations**: IOI = idiopathic orbital inflammation; NHOL = non-Hodgkin orbital lymphoma, PC = principle component.

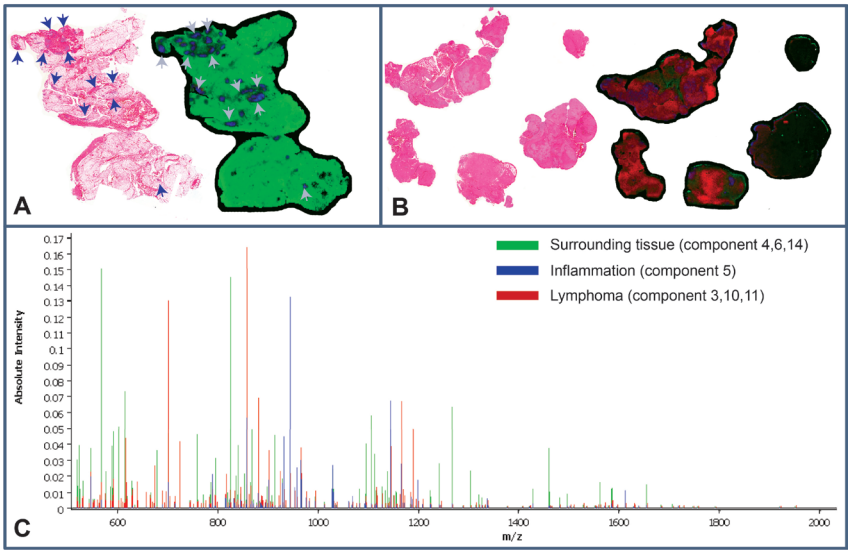

Figure 2. Multivariate analysis of a positive ion mode image acquired using probabilistic latent semantic analysis (pLSA) with 15 components. A. Hematoxylin and eosin (H&E) staining, and pLSA separated image of an IOI sample. The arrows point at IOI infiltrates. The pLSA separated image shows surrounding tissue in green (components 4,6,14) and the IOI infiltrates in blue (component 5). There are no red areas of lymphoma (component 3,10,11). B. H&E staining and pLSA separated image of a NHOL sample. Lymphoma tissue is depicted in red, surrounding tissue in green and inflammation tissue in blue. C. Corresponding absolute intensity of the pLSA spectrum, showing the contributions of specific m/z values to the grouped components for surrounding tissue, inflammation and lymphoma.

between NHOL and IOI. This finding reveals that peptide profiles could aid in the differentiation of both diseases.

Table 1. Differentially expressed m/z ions between NHOL and IOI

	Mean rank:		NHOL versus IOI		AUC outcome:	
m/z	NHOL	IOI	p-val	adj.p-val	NHOL	IOI
564.59	12,44	5,13	0,0029	0,045	0,931	0,069
586.54	5,56	12,88	0,0029	0,045	0,069	0,931
589.43	5,00	13,50	0,0005	0,045	0,000	1,000
602.53	5,44	13,00	0,0021	0,045	0,056	0,944
614.26	5,22	13,25	0,0011	0,045	0,028	0,972
723.67	12,44	5,13	0,0029	0,045	0,931	0,069
758.57	5,44	13,00	0,0021	0,045	0,056	0,944
760.18	5,78	12,63	0,0053	0,049	0,097	0,903
785.58	5,33	13,13	0,0015	0,045	0,042	0,958
795.61	5,44	13,00	0,0021	0,045	0,056	0,944
833.26	5,78	12,63	0,0053	0,049	0,097	0,903
836.62	5,78	12,63	0,0053	0,049	0,097	0,903
841.35	5,33	13,13	0,0015	0,045	0,042	0,958
852.61	5,67	12,75	0,0039	0,048	0,083	0,917
855.3	5,67	12,75	0,0039	0,048	0,083	0,917
868.69	5,78	12,63	0,0053	0,049	0,097	0,903
898.68	5,56	12,88	0,0029	0,045	0,069	0,931
1095.78	5,44	13,00	0,0021	0,045	0,056	0,944
1105.81	5,56	12,88	0,0029	0,045	0,069	0,931
1111.82	5,67	12,75	0,0039	0,048	0,083	0,917
1267.91	5,78	12,63	0,0053	0,049	0,097	0,903
1303.81	5,33	13,13	0,0015	0,045	0,042	0,958
1459.9	5,67	12,75	0,0039	0,048	0,083	0,917
2115.3	5,78	12,63	0,0053	0,049	0,097	0,903

Analysis was performed by the Mann–Whitney U test with an FDR correction for multiple testing. **Abbreviations**: NHOL = non-Hodgkin orbital lymphoma; IOI = idiopathic orbital inflammation; p-val = p-value; adj.p-val = adjusted p-value with FDR correction; AUC = area under the receiver operator curve

Individual peptides in head-to-head comparisons

We analyzed orbital biopsy samples of patients with NHOL and IOI to identify peptide differences between the two diseases. From whole tissue analysis, the comparison of mean spectra revealed 24 differentially expressed peptides (*m/z* ions) after correction for multiple testing (**Table 1**). ROC analysis revealed a high area under the curve for each of the 24 *m/z* ions, demonstrating a high accuracy for discrimination between NHOL and IOI. Interestingly, almost all *m/z* ions had a relative lower intensity in NHOL samples compared with IOI samples, except for the ions at *m/z* 564.59 and 723.67.

Clustering of area specific spectra using pLSA separation

The morphological architecture of NHOL samples often displayed a dense lymphocytic infiltrate that took up most of the biopsied tissue. IOI, on the other hand, had a more heterogeneous aspect and consisted of multiple small lymphocytic infiltrates in between normal tissue (**Figure 2A & B**). We therefore performed a pLSA of all sections, allowing for direct interpretation of loadings for the clustered areas. Although half of the components showed matrix remnants and peptides outside the tissue boundaries, spectra of seven components corresponded with the annotated areas (**Figure 2**). Component 5 reflected the IOI infiltrates, while component 4, 6 and 14 reflected tissue surrounding the diseased infiltrates. Component 3, 10 and 11 corresponded specifically to the NHOL infiltrates. Combined, these components revealed specific spectral profiles for NHOL and IOI infiltrates and surrounding tissue (**Figure 2C**). Individual peptides contributing to the pLSA area clustering, were not differentially expressed in head-to-head comparisons.

Discussion

In this study, we observed differences in peptide profile for the two diseases (PCA analysis), with 24 differentially expressed peptides that could differentiate NHOL from IOI by means of mass spectrometry imaging of tissue specimen. Interestingly, most peptides were present in relatively lower abundance in NHOL samples compared with IOI. We observed specific area profiles (pLSA analysis) that identified NHOL infiltrates, IOI infiltrates and surrounding tissues.

Although individual peptides were differentially expressed in a head-to-head comparison of the whole tissue, none of the peptides were differentially expressed when comparing area specific sites. This indicates that individual peptides do not fully grasp these complex diseases for area specific sites, and may be best investigated as part of a profile analysis to differentiate a lymphocytic infiltrate. It is possible that several mechanisms in the infiltrate and local response overlap between NHOL and IOI, and broad profiling is needed to identify subtle differences. This could be linked to a recent investigation showing overlap for inflammatory responses in circulation in both NHOL and IOI.[13]

The differential expression of peptides that we observed the whole tissue sections (**Table 1**), can be explained by the morphological differences between NHOL and IOI and molecular characteristics in the surrounding tissue. For example, *m/z* 898, 1105 and 1459 have been found to be associated with collagen alpha-1 chain precursors, and *m/z* 1111 with Annexin A2.[14] These peptides are more frequent in IOI biopsies and can be explained by the more fibrotic nature of the IOI samples.[15,16] Additionally, changes in surrounding tissue are observed

in several types of cancer,[17,18] and it is well known that the micro-environment of inflammation undergoes drastic molecular changes.[19]A further identification of the measured peptides is needed to elucidate involved pathophysiological pathways.

Interestingly, most differentially expressed peptides were less abundant in NHOL samples compared with IOI. It would be relevant for future studies to include healthy control specimen to be able to further explain a loss or gain of peptides in the local environment. This may be explained by different properties in the local environment that could lead to a more specific peptide profile. Additionally, crucial steps of the sample preparation (e.g. on-tissue digestion) could be more or less effective for certain tissue types. Nonetheless, these properties may be useful values for discrimination.

Several molecular profiling methods have been described for the assessment of orbital mass biopsies, especially to aid a malignant diagnosis.[4] The field of mass-spectrometry and mass-spectrometry imaging, however, has previously not been investigated for NHOL and IOI. The results of this study show that there is diagnostic potential in using a mass-spectrometry imaging approach for the molecular analysis of biopsy material of orbital diseases. The main advantage is having a molecular assessment that can be attributed to the architectural structure within a biopsy. This is an important feature as orbital mass lesions are often heterogeneous in histopathology.[4] Additionally, this technique can be used with formalin-fixed paraffin-embedded tissue, which is often the preferred fixative for pathological assessment of orbital biopsies.[4]

Molecular profiling can be included in less invasive technologies, for example the use of molecular techniques for FNAb in thyroid malignancies.[20] Currently, FNAb techniques are considered less successful in diagnosing orbital inflammatory or lymphoproliferative disease.[4] However, real-time mass-spectrometry techniques are developed to be used in vivo for diagnostic or surgical purposes.[21] Diagnostic work-up of orbital conditions through FNAb could potentially be improved by adding molecular techniques. Identification of usable profiles from morphological specimen is crucial for an accurate assessment and subtyping, and should be pursued in future research.
For the robustness and reproducibility of the data, this study will be complemented with data from a second, independent replication cohort and further identification of the found peptides through an MS/MS identification technique. Additionally, a classification model with an internal training, validation and test set will be performed to further evaluate the value of peptide profiling.

In conclusion, we demonstrate that peptide fingerprinting can discriminate NHOL from IOI using mass-spectrometry imaging in biopsies. Furthermore, we observed specific area profiles that identified NHOL infiltrates, IOI infiltrates and surrounding tissues. These results could lead to improvement of molecular tissue diagnosis and disease classification.

References

1. Olsen TG, Heegaard S. Orbital lymphoma. Surv Ophthalmol. 2019;64(1):45-66.
2. Sullivan TJ, Whitehead K, Williamson R, et al. Lymphoproliferative disease of the ocular adnexa: a clinical and pathologic study with statistical analysis of 69 patients. Ophthal Plast Reconstr Surg. 2005;21(3):177-188.
3. Mombaerts I, Bilyk JR, Rose GE, et al. Consensus on Diagnostic Criteria of Idiopathic Orbital Inflammation Using a Modified Delphi Approach. JAMA Ophthalmol. 2017;135(7):769-776.
4. Mombaerts I, Ramberg I, Coupland SE, Heegaard S. Diagnosis of orbital mass lesions: clinical, radiological, and pathological recommendations. Surv Ophthalmol. 2019;64:741-756.
5. Karcioglu ZA, Fleming JC, Haik BG. A prospective comparison of fine-needle aspiration cytopathology and histopathology in the diagnosis of orbital mass lesions. Br J Ophthalmol. 2010;94(1):128-130.
6. Manem VSK, Salgado R, Aftimos P, Sotiriou C, Haibe-Kains B. Network science in clinical trials: A patient-centered approach. Semin Cancer Biol. 2018;52(Pt 2):135-150.
7. Buck A, Heijs B, Beine B, et al. Round robin study of formalin-fixed paraffin-embedded tissues in mass spectrometry imaging. Anal Bioanal Chem. 2018;410(23):5969-5980.
8. Vaysse P-M, Heeren RMA, Porta T, Balluff B. Mass spectrometry imaging for clinical research – latest developments, applications, and current limitations. Analyst. 2017;142(15):2690-2712.
9. Swerdlow SH, Campo E, Pileri SA, et al. The 2016 revision of the World Health Organization classification of lymphoid neoplasms. Blood. 2016;127(20):2375-2390.
10. Mombaerts I, Rose GE, Garrity JA. Orbital inflammation: Biopsy first. Surv Ophthalmol. 2016;61(5):664-669.
11. Niedermeyer THJ, Strohalm M. mMass as a software tool for the annotation of cyclic peptide tandem mass spectra. Koomen JM, ed. PLoS One. 2012;7(9):e44913.
12. Chong J, Soufan O, Li C, et al. MetaboAnalyst 4.0: towards more transparent and integrative metabolomics analysis. Nucleic Acids Res. 2018;46(W1):W486-W494.
13. Laban KG, Kalmann R, Bekker CPJ, et al. A pan-inflammatory microRNA-cluster is associated with orbital non-Hodgkin lymphoma and idiopathic orbital inflammation. Eur J Immunol. 2020;50(1):86-96.
14. Groseclose MR, Massion PP, Chaurand P, Caprioli RM. High-throughput proteomic analysis of formalin-fixed paraffin-embedded tissue microarrays using MALDI imaging mass spectrometry. Proteomics. 2008;8(18):3715-3724.
15. Mombaerts I, Goldschmeding R, Schlingemann RO, Koornneef L. What is orbital pseudotumor? Surv Ophthalmol. 41(1):66-78.
16. Rosenbaum JT, Choi D, Wilson DJ, et al. Fibrosis, gene expression and orbital inflammatory disease. Br J Ophthalmol. 2015;99(10):1424-1429.
17. Castro NP, Osório CA, Torres C, et al. Evidence that molecular changes in cells occur before morphological alterations during the progression of breast ductal carcinoma. Breast Cancer Res. 2008;10(5):R87.
18. Northcott JM, Dean IS, Mouw JK, Weaver VM. Feeling Stress: The Mechanics of Cancer Progression and Aggression. Front cell Dev Biol. 2018;6:17.
19. Nourshargh S, Alon R. Leukocyte migration into inflamed tissues. Immunity. 2014;41(5):694-707.
20. Liu S, Gao A, Zhang B, et al. Assessment of molecular testing in fine-needle aspiration biopsy samples: An experience in a Chinese population. Exp Mol Pathol. 2014;97(2):292-297.
21. Pu F, Chiang S, Zhang W, Ouyang Z. Direct sampling mass spectrometry for clinical analysis. Analyst. 2019;144(4):1034-1051.


Chapter 10

Summary, general discussion and future perspectives

The orbit is an important anatomical region that protects the eye and holds adnexal structures necessary for eye-function. Two conditions that are common causes of orbital mass lesions are non-Hodgkin orbital lymphoma (NHOL) and idiopathic orbital inflammation (IOI).[1,2] Accurate and timely diagnosis is important for both disorders to prevent loss of eye function, morbidity and mortality if not treated timely.[2,3] NHOL can have local spread causing mass effects, while metastatic spread can cause systemic disease.[2] IOI can have mass effect, function loss and fibrosis leading to local complications.[3,4] Importantly, the two conditions can have overlapping clinical and radiological features that can make a diagnosis difficult.[2,3,5–7] Additionally, tissue diagnostics are crucial,[1,2] but can be complicated by not-representative biopsies in deep orbital localizations.[8] There is a need for additional less invasive strategies that can aid the clinician in the diagnostic process. In order to improve the current diagnostic process and explore new possibilities for minimally invasive diagnostic tools, we investigated the clinical presentation, a new imaging technique and molecular aspects of the underlying immunological profiles in blood and tissue of NHOL and IOI.

The importance of early and accurate diagnosis

Early and accurate diagnosis is essential in the treatment strategy of patients with NHOL, as systemic dissemination can lead to severe morbidity and mortality. [9] Systemic progression has been documented in primary NHOL in 20% of cases.[9] Systemic progression rate is more common in high-grade subtypes including diffuse large B-cell lymphoma (DLBCL), follicular lymphoma and mantle cell lymphoma (MCL).[10] Nonetheless, systemic disease is found in 14-16% of patients with extranodal marginal zone lymphoma (EMZL),[2,10] and disease related mortality rates up to 16% are seen in EMZL patients.[10]

Early and accurate diagnosis is important for IOI, as it can result in permanent symptoms and irreversible vision loss when effective treatment is delayed,[3] illustrated in **Chapter 4**. Patients with IOI who do not receive adequate treatment in the acute phase of the disease are more likely to have permanent damage and persistent complaints,[4] warranting early treatment and early diagnosis. In many cases, however, IOI is characterized by (severe) pain, prompting an expedited start of treatment. Note that starting therapy before completing the diagnostic work-up could lead to misdiagnosis.[11] Steroid treatment, as standard first line treatment, is frequently insufficient and secondary immunosuppressive treatment is commonly given.[3,12] In total, up to 37% of patients remain refractory to treatment.[3] Some complaints characterize refractory cases, including diplopia and vision loss,[13] both of which could persist due to irreversible damage or fibrosis prior to appropriate treatment strategies.[14]

In practice, diagnosis of NHOL and IOI can be difficult and lengthy.[5] In chapter 3, the time from start of symptoms to presentation is displayed, and is long for both diseases. In addition, diagnosis of orbital mass-lesions can have diagnostic delays and can be complicated by difficult biopsies. In chapter 2, four cases of NHOL with initial not-representative biopsies are reported, resulting in two patients with suspected systemic dissemination at final diagnosis. It is unclear if this could have been prevented by a correct diagnosis at presentation. Note that the localization of the mass-lesion within the orbit dictates the most adapt incisional biopsy approach.[11] Although all orbital biopsies should be performed by a skilled professional, deep orbital localizations can be especially difficult to access and retrieve optimal tissue specimen. Per-operatively, direct pathological examination with frozen sections can guide the biopsy operation and improve the chance of more representative biopsies.[15] Frozen sections, however, are limited in histopathological assessment, and confirmation is needed in qualitative good biopsies with the correct embedding for the intended diagnostic approach.[15] The location of inflammatory orbital mass lesions can also be indicative for the prognosis and residual complaints, as demonstrated in chapter 4 for patients with suspected IOI of the posterior orbit and orbital apex. These patients often have severe pain and a drastic vision loss at presentation, with a generally low visual outcome. The poor outcome can be attributed to a delay of effective treatment leading to permanent damage. In literature, cases with retro-orbital involvement tend to have more need of second line immunosuppressant's after incomplete response to corticosteroid therapies.[16] Improvement of the diagnostic process for these patients, and prediction of treatment response (see future perspectives) is therefore warranted.

New improvements in the diagnostic process for orbital mass-lesions

Clinical indicators at presentation

Signs and symptoms at presentation are regarded as clinical indicators that are largely non-specific in the diagnostic process of orbital mass-lesions.[1] In a large cohort of patients with NHOL and IOI (chapter 3), we found that characteristic inflammatory symptoms can be found in both diseases, but a combination of five clinical parameters can highly accurate differentiate NHOL from IOI. Compared to IOI, NHOL was characterized by age ≥60 years and proptosis, without pain, eyelid swelling or ptosis. This chapter includes an independent, multicenter replication cohort, in which the results were validated. However, there are several limitations that need to be considered, inherent to the retrospective design, including the difficulty for standardized assessment of clinical signs and symptoms. The localization of the orbital mass-lesions influences signs and symptoms, although

the 5-parameter model was highly accurate for both lacrimal gland and non-lacrimal gland localization. The results show a good clinical separation between NHOL and IOI, but should be confirmed in a prospective study to be used as clinical tool. This tool can result in an earlier diagnostic suspicion, before being confirmed by histopathology. The 5-parameter model can also be used to identify mismatches of signs and symptoms with histopathology in case of insufficient treatment response that would require a second biopsy, as described in chapter 2.

Imaging strategies

There is a strong potential for imaging strategies to improve the diagnostic process of orbital mass lesions, for example with DW-MRI.[17,18] In chapter 6, we describe the use of the zirconium-89-labelled rituximab positron-emitting-tomography/computed tomography (^{89}Zr-rituximab PET/CT) in patients with orbital inflammation. While fluorodeoxyglucose (FDG) PET/CT can have artefacts while visualizing the orbit due to eye-movement uptake and strong uptake of the brain,[19] the ^{89}Zr-rituximab PET/CT has a good visibility and specific CD20 uptake within the orbit. This specificity creates a potential in diagnostic use of the ^{89}Zr-rituximab PET/CT to visualise inflammatory and lymphoproliferative disorders of the orbit. Only a few recent studies have reported on ^{89}Zr-rituximab PET/CT in patients.[20–22] This includes an interesting paper describing the use of the tracer to predict outcome of rituximab treatment in patients with rheumatoid arthritis.[23] Moreover, in our study, four patients were treated with rituximab after a positive ^{89}Zr-rituximab PET/CT and had a good treatment response. Future studies on the predictive value of the ^{89}Zr-rituximab PET/CT for rituximab in orbital inflammatory disease are needed to fully assess this potential.

Blood-based differentiation

Laboratory findings have an important role to indicate other pathology underlying orbital mass-lesion, but are usually normal in NHOL and IOI.[1] We investigated serum microRNAs (miRNAs) and peripheral blood mononuclear cells (PBMCs) to understand the underlying immune-phenotype of NHOL and IOI in chapter 7 and chapter 8, respectively. Using an untargeted approach, we discovered striking similarities in the immune-phenotype of both diseases in serum miRNA profiles and PBMC profiles that differed with healthy control (HC) samples. The impact of these findings is discussed in the section *'New insights in the pathophysiological immune-alterations underlying orbital disease'* below. Regarding blood-based differentiation, we were not able to identify miRNAs that could distinguish NHOL from IOI (chapter 7). In the PBMC analysis using flow cytometry, however, we found a decrease of the conventional dendritic cell (cDC) type-2 population in the IOI group compared to NHOL (chapter 8). The decrease of cDC type 2 in

IOI suggest that, although we mostly find similarities, subtle differences in the underlying pathophysiology *can* be detected. As cDC type-2 has been implicated in other inflammatory disorders, such as uveitis,[24] a more detailed investigation into the role of cDC type-2 in NHOL and IOI is warranted.

Molecular tissue assessment

Despite the importance in histopathological examination,[15] novel techniques investigating molecular phenotypes in NHOL and IOI tissue are not able to take into account the morphological aspects characterizing these diseases.[25,26] In chapter 9, we discuss the use of spatially orientated peptide profiles with mass spectrometry imaging (MSI) in tissue samples of NHOL and IOI. Profile clustering analysis as well as individual peptides were able to distinguish NHOL from IOI, and identified NHOL and IOI infiltrates and surrounding tissue. Although identification of the peptides is needed to fully grasp the meaning of the differentially expressed peptides, this analysis can have impact on future studies to improve biopsy driven diagnosis. Once identified, the differentially expressed peptides from this untargeted technique could result in new targets for further research, as is being performed for several types of cancer.[27] Additionally, less invasive biopsy techniques (such as fine-needle aspiration) could benefit from area-specific peptide profiles discovered in chapter 9.

New insights in the pathophysiological immune-alterations underlying orbital disease

In this thesis, we investigated immune-phenotypes of NHOL and IOI to better understand underlying clinical and pathophysiological mechanisms. We therefore focussed on two techniques in peripheral blood, including serum miRNA profiles (chapter 7) and PBMC flow cytometry (chapter 8). Both modalities were studied in two independent cohorts to replicate the results. Additionally, we used two techniques in both studies to technically validate our result. This triple – analysis approach yielded a sensitive indication of orbital disease in blood of patients. Note that all patients had active disease when blood was drawn and were treatment naïve.

Serum miRNAs upregulated in NHOL and IOI

We investigated miRNA profiles in serum of patients with NHOL and IOI in chapter 7. We found that eight miRNAs were elevated in patients (both NHOL and IOI) compared to controls. The eight miRNAs strongly correlated with each other, reflecting a cluster that was upregulated in both diseases. The cluster included miRNAs that were previously found altered in EMZL and DLBCL specimen.[28,29] Additionally, the cluster was upregulated in other inflammatory disorders, which we demonstrated for uveitis, psoriasis, psoriatic arthritis and axial spondyloarthritis.[30]

This suggests that the miRNA cluster orchestrates several pathological mechanisms, over immune-mediated diseases. We therefore performed a pathway enrichment analysis yielding multiple inflammatory and interleukin signalling pathways. The involvement of these pathways is supported by previous gene-expression data of IOI biopsies that showed interleukin, interferon and TGF-signalling involvement.[25,31,32] Because miRNAs are mainly derived from leukocytes in blood, we investigated the role of immune-cell populations driving an upregulation of the miRNA cluster. Associations of miRNAs with B-cell mechanisms, important in both diseases, [32,33] have been described for *miR-148* and *miR-365*.[34,35] We supported this by observing a correlation between *miR-365* and serum immunoglobulin G and M. Furthermore, we found that *miR-223* was linked to myeloid populations in circulation, corroborating previous findings that neutrophils are a major source of *miR-223* in blood.[36] We further investigated neutrophil characteristic in the blood of patients, and report a larger neutrophil cell-size for NHOL compared to IOI (*P=0.011*). A larger neutrophil size could reflect neutrophil stimulation, suggesting a more prominent role of neutrophils in NHOL. Neutrophils are also associated with the production of APRIL, that induces B-cell malignancies and is linked to tumour aggressiveness,[37] and neutrophils are able to protect lymphoma-cells from chemotherapeutic agents.[38] Interestingly, *miR-223* has also been linked to poor cancer prognosis.[39]

In summary, we discovered an upregulation of a cluster of eight miRNAs in NHOL and IOI, associated with immune pathways activation and linked to B-cell and neutrophil dysfunction. As we now observe circulatory immune changes in peripheral blood serum of patients with NHOL and IOI, more in-depth techniques, including immune-cell phenotyping, could reveal targets for future diagnostic use. Functional investigation of circulatory B-cells and neutrophils could, additionally, lead to new disease management strategies targeting these pathophysiological sites. The heterogeneity within patients could also lead to molecular classifications and may provide opportunities to conduct personalized therapy adjustments or prognosis predictions.

Dendritic cell alterations in NHOL and IOI

Next to serum miRNA profiling, we investigated circulating immune-cells by isolating and phenotyping PBMCs in chapter 8, using flow cytometry. We found a decrease in circulatory plasmacytoid dendritic cells (pDC) for NHOL and IOI, and a decrease of type-2 cDCs for IOI compared to NHOL. Additionally, publicly available transcriptomic data from IOI biopsies showed a decrease in pDCs and type-2 cDCs within the local microenvironment.

In general, dendritic cells are antigen presenting cells that initiate and drive immune responses in various pathologies.[40] Dendritic cells play an important role in

anti-tumour response toward malignant cells and are drives of various inflammatory disorders.[41–43] Specialized subpopulations of dendritic cells are distinguished, in which pDCs produce interferon in response to viral or endogenous nucleotide recognition, while cDCs activate T-cells upon intra- or extracellular pathogen recognition.[40] Dendritic cells can be affected by an immunosuppressive state of the microenvironment triggered by metabolic stress, hypoxia or alarmins and cytokine secretion.[44] This is visible in a pDC decrease in certain inflammatory conditions[45,46] and malignancies.[44,47–52] In contrast to conditions such as primary Sjögren's syndrome,[45] we see a local decrease of dendritic cells in deconvoluted publicly available transcriptomic data of IOI biopsies.[25] A decrease in dendritic cells, especially pDCs could be driven by a negative feedback loop mediated by a concurrent self-maintaining expansive B-cell infiltrate, as pDCs are known to regulate B-cell differentiation and immunoglobulin secretion through CD70 and IL-6.[53] Alternatively, pDC differentiation and activation could affect surface marker expression,[41] leading to a perceived decrease guided by the markers used in chapter 8. The exact role of dendritic cells in the pathophysiology of orbital disorders remains to be elucidated. We encourage further research into dendritic cells, as we suggest a previously underappreciated role in the disease mechanisms for both NHOL and IOI.

Complex underlying pathophysiology

Although we describe new leads in the underlying pathophysiology of NHOL and IOI, the exact mechanisms remain largely unknown. In our understanding, there are multifactorial mechanisms involved including genetic, epigenetic and environmental factors. Intriguingly, we report the occurrence of IOI involving the exact same extraocular muscle in a similar fashion in twins (chapter 5), and previously (epi)genetic components are supported by the occurrence of IOI in families.[54] The role of specific infections preceding both NHOL and IOI have also been strongly debated in literature, but remain controversial.[2,55] Continuation of research with state-of-the-art technologies are needed to be able to further map the pathophysiology of these complex conditions.

Limitation of this thesis

Most limitations are addressed within the studies itself, but some general limitations need to be pointed out.

The studies in this thesis have focussed on two important orbital disorders, that are considered the most common causes of orbital mass-lesions. However, several disorders can display an orbital mass-lesion and are not covered in this thesis. In diseases other than NHOL and IOI, imaging and serology often guide the

differential diagnosis, as characteristic abnormalities are more likely to be present. It would be more desirable to have investigated and compared more causes of orbital mass-lesions, and this could be an opportunity for future research.

Although common causes of orbital mass-lesions, both NHOL and IOI are rare diseases in the general population. The low number of patients limits research abilities due to the heterogeneous nature in terms of clinical, histological, and molecular subtypes. It is difficult to obtain sufficient number of samples to pursue subset analysis, even in retrospective cohorts. For NHOL, histological subtypes have been well established,[56] with epidemiological and tissue-based molecular differences that define the histological subtypes.[2] However, there is a lack in blood based molecular profiling of NHOL subsets. For IOI, there are currently no robust molecular subtypes that can be identified in blood or tissue, and molecular overlap with other orbital conditions (e.g. specific inflammatory diseases) can be present.[25,57] The role of orbital localization in the molecular fingerprint of NHOL and IOI remains unknown.

Retrospective data have inherent limitations, such as non-standardized clinical assessments and missing data. Importantly, within recent years, new technical advances have become more broadly available and commonly used in the evaluation of orbital mass-lesions.[1,15] This leads to new standards within the diagnostic process.[1,15] Although the patients described in this thesis have been thoroughly screened following the most up-to-date diagnostic tests, not all recommended diagnostic tests were available for each patient. For instance, we re-evaluated IOI biopsies for the presence of IgG4 when this was not performed within the diagnostic process (generally prior to 2015), as IgG4 related orbital disease was previously regarded as idiopathic.[58]

Future perspectives and research opportunities

From a clinical and epidemiological standpoint, the importance of early and accurate diagnosis is evident, as the consequences of a delayed or inaccurate diagnosis can be devastating. The point of view from the patient in the diagnostic process, however, has not been in the forefront of study designs in orbital disease research. We would therefore advocate a quality of life assessment during the diagnostic process to assess the importance of swift and accurate diagnosis from the patient's point of view. Additionally, there is little knowledge of the quality of life of NHOL and IOI during the course of disease and final outcome. These assessments could be useful to better inform the patients during the diagnostic process and course of disease.

There are opportunities to improve a clinical differentiation, as we have described in chapter 3. To overcome the limitations posed in the retrospective study design, a prospective study with a standardized assessment is necessary to confirm the results. Additionally, machine learning algorithms can be more easily used with clinical assessments and facial imaging to improve the potential of the clinical presentation.[59] Machine learning opportunities for imaging could also be deployed, with a combination of modalities to help identify disease entities, including lymphoma.[60,61]

Opportunities with PET-CT imaging include radiolabelled tracers that can visualize specific receptors and proteins. Recently, the [68Ga]Ga-labelled Pentixafor PET-CT was proposed to sensitively quantify CXCR4, a mediator of leukocyte (including B-cell) migration, in extranodal marginal zone lymphomas including NHOL.[62] An upregulated CXCR4 expression has also been found in other lymphoma types, especially under hypoxic conditions.[63] It remains unknown what the expression of CXCR4 is in IOI and other orbital conditions, and this could be studied in the histology of orbital biopsies. If CXCR4 expression is different, a prospective clinical trial could be used to investigate uptake by PET-CT in patients with NHOL and IOI before treatment is started. Differences in uptake are quantifiable and thus comparable between the groups. Additionally, single-domain antibody fragments as nuclear PET tracers are being developed that can have a more specific penetration and good visualization of small (<1mm) mass-lesions.[64] Alternatively, the role of nuclear PET tracers as therapeutic options for high-grade NHOL is unclear. Recently however, malignant metastases in the orbit have been treated with sensitive therapeutic PET solutions.[65] PET-tracers as predictor of treatment effectivity, such as ^{89}Zr-rituximab PET/CT for rituximab treatment, could also be further explored.

We investigated several layers of the immune system in peripheral blood, and demonstrated evidence for systemic changes in the immune system related to localized orbital disease. Other circulatory '*omic*' layers could also reveal changes in the immune-phenotype and add clarity into the complex pathophysiology of NHOL and IOI. Cytokine analysis, for example, could be promising as specific local upregulated cytokines have been identified in IOI.[32] Alternatively, metabolite profiles have been extensively studied for cancer (including lymphoma) and inflammatory disorders.[66–68] Interestingly, circulatory platelets have been found to include cancerous or inflammatory RNA that can be identified and used as biomarkers.[69] In chapter 8, we identified dendritic cells populations to be altered in NHOL and IOI. We would therefore be highly interested to further investigate the transcriptomic composition of these cells, as this has been shown to differ in other

inflammatory conditions, including primary Sjögren's syndrome.[70] Because we found many similarities between IOI and NHOL in circulatory analysis of chapter 7 and chapter 8, the possibility of both diseases within a pathophysiological or molecular spectrum needs to be further explored.

Extended genetic studies, such as genome-wide association studies of NHOL and IOI are currently lacking, and are difficult to achieve because the rare incidence. However, collaborations, as reported in retrospective studies such as chapter 3 and recently shown in an international NHOL cohort,[10] are needed to pursue such achievements. Genetic variation between NHOL and IOI could have diagnostic potential, while shared polymorphisms could suggest shared pathophysiological mechanisms, as we find in serum miRNAs (chapter 7).

An alternative easily accessible, non-invasive diagnostic method could include molecular assessment of tear-fluid. Especially in case of lacrimal gland involvement, tear constitution could be altered, leading to changes in tear-film characteristics.[71] For inflammatory conditions deep within the orbit, such as thyroid eye disease (Graves' disease), several tear-fluid interleukins have also been associated with presence and activity of disease.[72–74] However, tear-fluid constitution can be strongly influenced by secretion rate and environmental factors.[75]

Although several hypothetical studies (described above) could benefit future patients with NHOL and IOI, an important question of this thesis could be explored by performing a prospective clinical trial incorporating several considerations mentioned. By combining clinical, imaging and laboratory finding, this trial could elucidate the potential of a multi-modular minimally-invasive diagnostic approach, that may eventually reduce the need for biopsies in IOI patients. Particularly in orbital mass lesions where a biopsy is not possible, the implications of such as trial would be highly visible. For this trial, the clinical presentation could be assessed by the 5-parameter clinical model, using standardized assessments with a photograph recorded presentation. These data could be combined with machine learning algorithms in imaging techniques and laboratory investigation of dendritic cells and neutrophils. When diagnosis is confirmed by histological and molecular assessments, analysis of the trial population could indicate if a reliable diagnosis before histology could be possible.

References

1. Mombaerts I, Bilyk JR, Rose GE, et al. Consensus on Diagnostic Criteria of Idiopathic Orbital Inflammation Using a Modified Delphi Approach. JAMA Ophthalmol. 2017;135(7):769–776.
2. Olsen TG, Heegaard S. Orbital lymphoma. Surv Ophthalmol. 2019;64(1):45–66.
3. Yuen SJA, Rubin PAD. Idiopathic orbital inflammation: distribution, clinical features, and treatment outcome. Arch Ophthalmol (Chicago, Ill 1960). 2003;121(4):491–499.
4. Bessant DA, Lee JP. Management of strabismus due to orbital myositis. Eye (Lond). 1995;9 (Pt 5)(5):558–563.
5. Gordon LK. Orbital inflammatory disease: a diagnostic and therapeutic challenge. Eye. 2006;20(10):1196–1206.
6. Yan J, Wu Z, Li Y. The differentiation of idiopathic inflammatory pseudotumor from lymphoid tumors of orbit: Analysis of 319 cases. Orbit. 2004;23(4):245–254.
7. Sullivan TJ, Whitehead K, Williamson R, et al. Lymphoproliferative disease of the ocular adnexa: a clinical and pathologic study with statistical analysis of 69 patients. Ophthal Plast Reconstr Surg. 2005;21(3):177–188.
8. Eenhorst CAE, Laban KG, Leguit RJ, Radstake TRDJ, Kalmann R. Orbital lymphomas missed by first biopsies of orbital masses. Acta Ophthalmol. 2017;95(8).
9. Martinet S, Ozsahin M, Belkacémi Y, et al. Outcome and prognostic factors in orbital lymphoma: a Rare Cancer Network study on 90 consecutive patients treated with radiotherapy. Int J Radiat Oncol Biol Phys. 2003;55(4):892–898.
10. Olsen TG, Holm F, Mikkelsen LH, et al. Orbital Lymphoma—An International Multicenter Retrospective Study. Am J Ophthalmol. 2019;199:44–57.
11. Mombaerts I, Rose GE, Garrity JA. Orbital inflammation: Biopsy first. Surv Ophthalmol. 2016;61(5):664–669.
12. Swamy BN, McCluskey P, Nemet A, et al. Idiopathic orbital inflammatory syndrome: Clinical features and treatment outcomes. Br J Ophthalmol. 2007;91(12):1667–1670.
13. Suhler EB, Lim LL, Beardsley RM, et al. Rituximab therapy for refractory orbital inflammation: results of a phase 1/2, dose-ranging, randomized clinical trial. JAMA Ophthalmol. 2014;132(5):572–578.
14. Rosenbaum JT, Choi D, Wilson DJ, et al. Fibrosis, gene expression and orbital inflammatory disease. Br J Ophthalmol. 2015;99(10):1424–1429.
15. Mombaerts I, Ramberg I, Coupland SE, Heegaard S. Diagnosis of orbital mass lesions: clinical, radiological, and pathological recommendations. Surv Ophthalmol. 2019;64:741–756.
16. Li Y, Lip G, Chong V, Yuan J, Ding Z. Idiopathic Orbital Inflammation Syndrome with Retro-Orbital Involvement: A Retrospective Study of Eight Patients. Rosenbaum JT, ed. PLoS One. 2013;8(2):e57126.
17. Sepahdari AR, Politi LS, Aakalu VK, Kim HJ, Razek AAKA. Diffusion-Weighted Imaging of Orbital Masses: Multi-Institutional Data Support a 2-ADC Threshold Model to Categorize Lesions as Benign, Malignant, or Indeterminate. Am J Neuroradiol. 2014;35(1):170–175.
18. Purohit BS, Vargas MI, Ailianou A, et al. Orbital tumours and tumour-like lesions: exploring the armamentarium of multiparametric imaging. Insights Imaging. 2016;7(1):43–68.
19. Purohit BS, Ailianou A, Dulguerov N, Becker CD, Ratib O, Becker M. FDG-PET/CT pitfalls in oncological head and neck imaging. Insights Imaging. 2014;5(5):585–602.
20. Jauw YWS, Zijlstra JM, de Jong D, et al. Performance of 89Zr-Labeled-Rituximab-PET as an Imaging Biomarker to Assess CD20 Targeting: A Pilot Study in Patients with Relapsed/Refractory Diffuse Large B Cell Lymphoma. Glod JW, ed. PLoS One. 2017;12(1):e0169828.
21. de Jong A, Mous R, van Dongen GAMS, Hoekstra OS, Nievelstein RAJ, de Keizer B. (89)Zr-rituximab PET/CT to detect neurolymphomatosis. Am J Hematol. 2016;91(6):649–650.
22. Muylle K, Flamen P, Vugts DJ, et al. Tumour targeting and radiation dose of radioimmunotherapy with (90)Y-rituximab in CD20+ B-cell lymphoma as predicted by (89)Zr-rituximab immuno-PET: impact of preloading with unlabelled rituximab. Eur J Nucl Med Mol Imaging. 2015;42(8):1304–1314.
23. Bruijnen S, Tsang-A-Sjoe M, Raterman H, et al. B-cell imaging with zirconium-89 labelled rituximab PET-CT at baseline is associated with therapeutic response 24 weeks after initiation of rituximab treatment in rheumatoid arthritis patients. Arthritis Res Ther. 2016;18(1):266.
24. Chen P, Denniston A, Hannes S, et al. Increased CD1c+ mDC1 with mature phenotype regulated by TNFα–p38 MAPK in autoimmune ocular inflammatory disease. Clin Immunol. 2015;158(1):35–46.

25. Rosenbaum JT, Choi D, Wilson DJ, et al. Molecular diagnosis of orbital inflammatory disease. Exp Mol Pathol. 2015;98(2):225–229.
26. Hother C, Rasmussen PK, Joshi T, et al. MicroRNA profiling in ocular adnexal lymphoma: a role for MYC and NFKB1 mediated dysregulation of microRNA expression in aggressive disease. Invest Ophthalmol Vis Sci. 2013;54(8):5169–5175.
27. Zhang B, Whiteaker JR, Hoofnagle AN, Baird GS, Rodland KD, Paulovich AG. Clinical potential of mass spectrometry–based proteogenomics. Nat Rev Clin Oncol. 2019;16(4):256–268.
28. Arribas AJ, Campos-Martín Y, Gómez-Abad C, et al. Nodal marginal zone lymphoma: gene expression and miRNA profiling identify diagnostic markers and potential therapeutic targets. Blood. 2012;119(3):e9–e21.
29. Caramuta S, Lee L, Ozata DM, et al. Role of microRNAs and microRNA machinery in the pathogenesis of diffuse large B-cell lymphoma. Blood Cancer J. 2013;3(10):e152.
30. Verhagen FH, Bekker CPJ, Rossato M, et al. A Disease-Associated MicroRNA Cluster Links Inflammatory Pathways and an Altered Composition of Leukocyte Subsets to Noninfectious Uveitis. Invest Ophthalmol Vis Sci. 2018;59(2):878–888.
31. Wladis EJ, Iglesias B V, Adam AP, Nazeer T, Gosselin EJ. Toll-like receptors in idiopathic orbital inflammation. Ophthal Plast Reconstr Surg. 2012;28(4):273–276.
32. Wladis EJ, Iglesias B V., Gosselin EJ. Characterization of the Molecular Biologic Milieu of Idiopathic Orbital Inflammation. Ophthalmic Plast Reconstr Surg. 2011;27(4):251–254.
33. Sharara N, Holden JT, Wojno TH, Feinberg AS, Grossniklaus HE. Ocular adnexal lymphoid proliferations. Ophthalmology. 2003;110(6):1245–1254.
34. Gonzalez-Martin A, Adams BD, Lai M, et al. The microRNA miR-148a functions as a critical regulator of B cell tolerance and autoimmunity. Nat Immunol. 2016;17(4):433–440.
35. Xu Z, Xiao S-B, Xu P, et al. miR-365, a Novel Negative Regulator of Interleukin-6 Gene Expression, Is Cooperatively Regulated by Sp1 and NF-κB. J Biol Chem. 2011;286(24):21401–21412.
36. Tsitsiou E, Lindsay MA. microRNAs and the immune response. Curr Opin Pharmacol. 2009;9(4):514–520.
37. Schwaller J, Schneider P, Mhawech-Fauceglia P, et al. Neutrophil-derived APRIL concentrated in tumor lesions by proteoglycans correlates with human B-cell lymphoma aggressiveness. Blood. 2007;109(1):331–338.
38. Hirz T, Matera E-L, Chettab K, et al. Neutrophils protect lymphoma cells against cytotoxic and targeted therapies through CD11b/ICAM-1 binding. Oncotarget. 2017;8(42):72818–72834.
39. Li Z, Yang Y, Du L, et al. Overexpression of miR-223 correlates with tumor metastasis and poor prognosis in patients with colorectal cancer. Med Oncol. 2014;31(11):256.
40. Musumeci A, Lutz K, Winheim E, Krug AB. What Makes a pDC: Recent Advances in Understanding Plasmacytoid DC Development and Heterogeneity. Front Immunol. 2019;10.
41. Galati D, Corazzelli G, De Filippi R, Pinto A. Dendritic cells in hematological malignancies. Crit Rev Oncol Hematol. 2016;108:86–96.
42. Hillen MR, Ververs FA, Kruize AA, Van Roon JA. Dendritic cells, T-cells and epithelial cells: a crucial interplay in immunopathology of primary Sjögren's syndrome. Expert Rev Clin Immunol. 2014;10(4):521–531.
43. Affandi AJ, Carvalheiro T, Radstake TRDJ, Marut W. Dendritic cells in systemic sclerosis: Advances from human and mice studies. Immunol Lett. 2018;195:18–29.
44. Saxena M, Bhardwaj N. Re-Emergence of Dendritic Cell Vaccines for Cancer Treatment. Trends in cancer. 2018;4(2):119–137.
45. Klarquist J, Zhou Z, Shen N, Janssen EM. Dendritic Cells in Systemic Lupus Erythematosus: From Pathogenic Players to Therapeutic Tools. Mediators Inflamm. 2016;2016:1–12. 8
46. Verhagen FH, Hiddingh S, Rijken R, et al. High-Dimensional Profiling Reveals Heterogeneity of the Th17 Subset and Its Association With Systemic Immunomodulatory Treatment in Non-infectious Uveitis. Front Immunol. 2018;9:2519.
47. Mohty M, Isnardon D, Vey N, et al. Low blood dendritic cells in chronic myeloid leukaemia patients correlates with loss of CD34+/CD38- primitive haematopoietic progenitors. Br J Haematol. 2002;119(1):115–118.
48. Dong R, Cwynarski K, Entwistle A, et al. Dendritic cells from CML patients have altered actin organization, reduced antigen processing, and impaired migration. Blood. 2003;101(9):3560–3567.
49. Orsini E, Guarini A, Chiaretti S, Mauro FR, Foa R. The circulating dendritic cell compartment in patients with chronic lymphocytic leukemia is severely defective and unable to stimulate

an effective T-cell response. Cancer Res. 2003;63(15):4497-4506.
50. Saulep-Easton D, Vincent FB, Le Page M, et al. Cytokine-driven loss of plasmacytoid dendritic cell function in chronic lymphocytic leukemia. Leukemia. 2014;28(10):2005-2015.
51. Brimnes MK, Svane IM, Johnsen HE. Impaired functionality and phenotypic profile of dendritic cells from patients with multiple myeloma. Clin Exp Immunol. 2006;144(1):76-84.
52. Galati D, Zanotta S, Corazzelli G, et al. Circulating dendritic cells deficiencies as a new biomarker in classical Hodgkin lymphoma. Br J Haematol. 2019;184(4):594-604.
53. Shaw J, Wang Y-H, Ito T, Arima K, Liu Y-J. Plasmacytoid dendritic cells regulate B-cell growth and differentiation via CD70. Blood. 2010;115(15):3051-3057.
54. Jacob M, Ollagnon Roman E, Vighetto A. Familial orbital myositis. J Neurol. 2007; 254(5):666-667.
55. Bijlsma WR, Kalmann R, Dekkers J, et al. Identification of infectious entities in idiopathic orbital inflammation biopsies. Br J Ophthalmol. 2013;97(5):664-665.
56. Swerdlow SH, Campo E, Pileri SA, et al. The 2016 revision of the World Health Organization classification of lymphoid neoplasms. Blood. 2016;127(20):2375-2390.
57. Rosenbaum JT, Choi D, Wilson DJ, et al. Orbital pseudotumor can be a localized form of granulomatosis with polyangiitis as revealed by gene expression profiling. Exp Mol Pathol. 2015;99(2):271-278.
58. Andrew NH, Sladden N, Kearney DJ, Selva D. An analysis of IgG4-related disease (IgG4-RD) among idiopathic orbital inflammations and benign lymphoid hyperplasias using two consensus-based diagnostic criteria for IgG4-RD. Br J Ophthalmol. 2015;99(3):376-381.
59. Delorme A, Pierce A, Michel L, Radin D. Intuitive Assessment of Mortality Based on Facial Characteristics: Behavioral, Electrocortical, and Machine Learning Analyses. EXPLORE. 2018;14(4):262-267.
60. Yu Y, Decazes P, Lapuyade-Lahorgue J, Gardin I, Vera P, Ruan S. Semi-automatic lymphoma detection and segmentation using fully conditional random fields. Comput Med Imaging Graph. 2018;70:1-7.
61. Nakagawa M, Nakaura T, Namimoto T, et al. Machine learning based on multi-parametric magnetic resonance imaging to differentiate glioblastoma multiforme from primary cerebral nervous system lymphoma. Eur J Radiol. 2018;108:147-154.
62. Haug AR, Leisser A, Wadsak W, et al. Prospective non-invasive evaluation of CXCR4 expression for the diagnosis of MALT lymphoma using [68Ga]Ga-Pentixafor-PET/MRI. Theranostics. 2019;9(12):3653-3658.
63. Oh YS, Kim HY, Song I-C, et al. Hypoxia induces CXCR4 expression and biological activity in gastric cancer cells through activation of hypoxia-inducible factor-1α. Oncol Rep. 2012;28(6):2239-2246.
64. Rashidian M, LaFleur MW, Verschoor VL, et al. Immuno-PET identifies the myeloid compartment as a key contributor to the outcome of the antitumor response under PD-1 blockade. Proc Natl Acad Sci. 2019;116(34):16971-16980.
65. Parghane R V., Basu S. Bilateral Orbital Soft-Tissue Metastases from Renal Neuroendocrine Tumor: Successful Theranostic Application of ^{68}Ga/^{177}Lu-DOTATATE with Improvement of Vision. J Nucl Med Technol. 2019;47(2):171-172.
66. Barberini L, Noto A, Fattuoni C, et al. The Metabolomic Profile of Lymphoma Subtypes: A Pilot Study. Molecules. 2019;24(13):2367.
67. Gupta L, Ahmed S, Jain A, Misra R. Emerging role of metabolomics in rheumatology. Int J Rheum Dis. 2018;21(8):1468-1477.
68. Verhagen FH, Stigter ECA, Pras-Raves ML, et al. Aqueous Humor Analysis Identifies Higher Branched Chain Amino Acid Metabolism as a Marker for Human Leukocyte Antigen-B27 Acute Anterior Uveitis and Disease Activity. Am J Ophthalmol. 2019;198:97-110.
69. Best MG, Wesseling P, Wurdinger T. Tumor-Educated Platelets as a Noninvasive Biomarker Source for Cancer Detection and Progression Monitoring. Cancer Res. 2018;78(13):3407-3412.
70. Hillen MR, Pandit A, Blokland SLM, et al. Plasmacytoid DCs From Patients With Sjögren's Syndrome Are Transcriptionally Primed for Enhanced Pro-inflammatory Cytokine Production. Front Immunol. 2019;10:2096.
71. Xue K, Ren H, Liu A, Qian J. Changes in Tear Film Characteristics in Patients With Idiopathic Dacryoadenitis. Ophthal Plast Reconstr Surg. 2017;33(1):31-34.
72. Chen Q. The expression of interleukin-15 and interleukin-17 in tears and orbital tissues of Graves ophthalmopathy patients. J Cell Biochem. 2019;120(4):6299-6303.
73. Song R, Wang B, Yao Q, Li Q, Jia X, Zhang J. Proteomics screening of differentially expressed

cytokines in tears of patients with Graves' ophthalmopathy. Endocrine, Metab Immune Disord – Drug Targets. 2019;19.
74. Kishazi E, Dor M, Eperon S, Oberic A, Hamedani M, Turck N. Thyroid-associated orbitopathy and tears: A proteomics study. J Proteomics. 2018;170:110–116.
75. Dammeier S, Martus P, Klose F, et al. Combined Targeted Analysis of Metabolites and Proteins in Tear Fluid With Regard to Clinical Applications. Transl Vis Sci Technol. 2018;7(6):22.

Appendices

Appendix I - Nederlandse samenvatting (summary in Dutch)

Een uitgebreid spectrum van aandoeningen kan zich uiten als een massa in de oogkas. Non-Hodgkin oogkas lymfoom (NHOL) is de meest voorkomende kanker rond het oog bij volwassenen en kan resulteren in ernstige ziekte en overlijden als een behandeling niet tijdig wordt gestart. Idiopathische oogkas inflammatie (IOI) is, na de oogziekte van Graves', de meest voorkomende ontsteking van de oogkas en kan resulteren in permanente schade aan het functioneren van het oog als deze niet goed behandeld wordt. Een snelle en goede diagnose zijn daarom essentieel, zeker ook omdat de behandelingen van deze twee aandoeningen heel anders zijn. Het diagnostische proces bij NHOL en IOI kan echter moeizaam zijn, omdat er overlap bestaat in de klinische presentatie en beeldvorming, en bloedonderzoek met name andere aandoeningen uitsluit. De diagnose moet daarom worden gesteld door het nemen van biopten tijdens een operatie, wat bij een deel van de patiënten niet kan of complicaties geeft doordat de aandoening diep in de oogkas zit. Het doel van dit proefschrift was daarom om verschillende aspecten van het diagnostische proces van NHOL en IOI te verbeteren en potentie van nieuwe mogelijkheden voor minimaal-invasieve diagnostische methoden te onderzoeken. Daarnaast exploreren we mechanismen die ten grondslag liggen aan NHOL en IOI, om zo meer inzicht te krijgen hoe de ziekte ontstaat. De achtergrond van de ziektebeelden en een beschrijving van de technieken gebruikt in dit onderzoek zijn beschreven in **hoofdstuk 1**.

In **hoofdstuk 2** wordt het belang van een goed biopt benadrukt, dat ook moet passen bij een klinische verdenking en anders herhaald moet worden. Vier patiënten worden beschreven, waarbij een tweede biopt nodig was om een diagnose van NHOL vast te stellen. Een vertraging kan ernstige consequenties hebben: twee van de vier patiënten werden verdacht van uitgezaaide ziekte toen de definitieve diagnose uiteindelijk gesteld werd.

Voor het inschatten van de klinische verdenking voor een van beide aandoeningen beschrijft **hoofdstuk 3** een klinisch model van vijf parameters die gezamenlijk zeer accuraat kunnen voorspellen of het om een NHOL of IOI gaat. Hoewel de parameters afzonderlijk gezien werden bij beide ziektebeelden, gaf een combinatie van de vijf parameters wel een duidelijk verschillende voorspelling. Hierbij werd gevonden dat een leeftijd boven de 60 jaar met het uitpuilen of naar voren komen van het oog, zonder pijn, zwelling of een hangend ooglid sterk paste bij NHOL. Het omgekeerde (leeftijd onder de 60, met een gezwollen en hangend ooglid met veel pijn, maar geen uitpuilend oog) paste juist bij IOI. Met dit model kon een kans op de juiste diagnose worden berekend, wat tot een score-model heeft

geleid. Deze resultaten vonden we in een grote groep patiënten met NHOL en IOI in het UMC Utrecht, maar vonden we ook terug (gevalideerd) in patiënten van de universitaire ziekenhuizen van Amsterdam, Leiden en Leuven, en het oogziekenhuis in Rotterdam. Het model was ook onafhankelijk van lokalisatie en NHOL-subtype, zeer accuraat voor het onderscheid tussen NHOL en IOI. Dit klinische model kan daarom gebruikt worden om vroeg in het diagnostische proces de juiste richting op te gaan en vertraging te voorkomen voordat een biopt genomen wordt. Omdat we in deze studie naar patiënten in het verleden hebben gekeken (retrospectief), adviseren we om dit model in een onderzoek-setting bij toekomstige patiënten (prospectief) te bevestigen.

Dat de locatie van de massa in de oogkas belangrijk is, wordt geïllustreerd in **hoofdstuk 4**. Hierin worden patiënten beschreven met een IOI in het diepste deel van de oogkas. Hoewel een IOI op deze locatie uiterst zelden voorkomt, is het een belangrijke aandoening omdat de prognose bij veel patiënten slecht is. In meer dan de helft van de gevallen vonden we dat de patiënten blind werden aan de aangedane zijde, en zijn er zelfs patiënten aan overleden. We zagen dat mensen met een slechte uitkomst vaker oudere, mannelijke patiënten met diabetes waren die zich presenteerden toen de klachten zeer hevig waren.

De complexiteit van het IOI-beeld wordt geïllustreerd in **hoofdstuk 5**, waarbij een eeneiige tweeling is beschreven, met allebei een IOI en een onbegrepen hersendruk verhoging. Het valt hierbij op dat de IOI precies op dezelfde plek ontstaat. Familiair voorkomende IOI is beschreven, maar er blijft veel onduidelijk hoe en waardoor het ontstaat.

In **hoofdstuk 6.1 en 6.2** wordt de potentie van een nieuw ontwikkelde scan, de ^{89}Zr-rituximab PET/CT, onderzocht en beschreven. Deze scan laat door middel van een radioactieve tracer specifieke cellen in het lichaam zien. In dit geval worden zogenaamde B-cellen uitgelicht, die betrokken zijn bij aandoeningen zoals NHOL en IOI. In patiënten met een IOI of de ziekte van Graves' zagen wij dat de scan heel goed kan laat zien waar afwijkingen zijn. Dit kan helpen bij het beter stellen van de diagnose en bij het nemen van biopten. Daarnaast heeft de scan mogelijk ook potentie voor het voorspellen van de effectiviteit van een specifieke behandeling met het middel rituximab, dat maar bij een deel van de patiënten effectief is.

Bloedonderzoek om verschillen en overeenkomsten die betrekking hebben op het ontstaan van de ziektebeelden uitgebreid te bestuderen, wordt beschreven in **hoofdstuk 7** en **hoofdstuk 8**. Beide hoofdstukken gaan over twee groepen

patiënten, die onafhankelijk van elkaar gemeten zijn, om de resultaten te versterken. Een nieuwe manier om naar het bloed te kijken, is door zogenaamde 'microRNAs' te meten (**hoofdstuk 7**). Deze kleine deeltjes kunnen verschillende cellen en cel-processen beïnvloeden en zijn overal in het lichaam te vinden. Bij meerdere soorten kanker en ontsteking zijn microRNAs in het bloed veranderd en dit bleek in ons onderzoek ook het geval bij NHOL en IOI. Voor het eerst zien we dat deze lokale ziekten van de oogkas in het bloed afwijkingen laten zien. In dit onderzoek vonden wij opvallend veel overeenkomsten tussen de twee ziektebeelden, die wel verschillend waren ten opzichte van gezonde controles. We zagen een sterk verhoogd cluster van 8 microRNAs die gekoppeld zijn aan specifieke witte bloedcellen. Een vervolgstap is daarom om immuun-cellen in het bloed te onderzoeken.

Om immuun-cellen in het bloed goed te bestuderen, maakten we gebruik van de flow cytometrie techniek, waarbij cellen in het bloed getypeerd en geteld werden (**hoofdstuk 8**). Hiermee bleek dat er opvallend weinig dendritische cellen in het bloed waren bij NHOL en IOI ten opzichte van gezonde controles. Bij speciale subtypen dendritische cellen was er ook een verschil tussen de ziektebeelden te zien. Daarbij konden we via publiek-beschikbare data achterhalen dat dendritische cellen ook in oogkas-weefsel minder aanwezig waren. Hieruit blijkt dat dendritische cellen een voorheen onbekende rol spelen bij het ontstaan van NHOL en IOI. Vervolgonderzoeken moeten nog uitwijzen wat de specifieke functie van dendritische cellen in de ziekteprocessen is.

In **hoofdstuk 9** wordt het gebruik van een nieuwe techniek beschreven om eiwit-profielen van bioptmateriaal te onderzoeken. Door middel van zogenaamde 'massaspectrometrie beeldvorming' konden we eiwitten in een weefseldoorsnede meten, en koppelen aan structuren in het weefsel. Met deze techniek zagen we duidelijke verschillen in de eiwit-vingerafdruk van NHOL en IOI, en 24 specifieke eiwitten die sterk verschillend waren. Met deze resultaten zou in de toekomst moleculaire diagnose makkelijker kunnen worden en wordt wellicht een nieuwe classificatie mogelijk. Omdat we de metingen nu in één groep gemeten hebben, willen we de resultaten van dit onderzoek herhalen in een onafhankelijke meting bij een tweede groep herhalen.

Concluderend heeft dit onderzoek op verschillende vlakken tot nieuwe inzichten in het diagnostische proces en de onderliggende oorzaken van NHOL en IOI geleid.

Appendix II - Dankwoord (acknowledgements)

Het promotieteam: Rachel, Jonas, Joke en Tim.
Ik had me geen betere begeleiding kunnen wensen. De afgelopen vier jaar heb ik me altijd gehoord, gesteund en gewaardeerd gevoeld, waarvoor ik jullie hartelijk wil danken. Door de sterke expertise van de groep, goede begeleiding en ruimte voor het starten en uitwerken van ideeën is dit een mooie en leerzame promotie geworden.

Beste Dr. Kalmann, Beste Rachel,
Nu ik met de opleiding begonnen ben mis ik ons dagelijkse meetings en contact, altijd met Noom die gezellig inbelde. Ik vond het geweldig om samen interessante casussen te bespreken, radiologiebeelden te doorlopen en oplossingen te zoeken voor de ontelbare uitdagingen die in dit project naar voren kwamen. Je passie voor de orbita is aanstekelijk, en je perfecte geheugen voor patiënten en feilloze klinische blik een enorme inspiratie. Bedankt voor je onvoorwaardelijke steun en de mooie momenten die we de afgelopen jaren beleefd hebben. Ik kijk uit naar meer samenwerking in de kliniek, waarin ik nog veel van je hoop te leren!

Beste Dr. Kuiper, Beste Jonas,
Ik bewonder je enorme toewijding voor alles waar je je voor inzet. Ik heb heel veel respect voor je heldere interpretatie en uitleg van de meest complexe technieken en resultaten, die je niet alleen een goede begeleider maar ook een hele goede docent maken. Als ik door de bomen het bos niet meer zag, wist jij er weer duidelijkheid te scheppen. Dank voor je eindeloze ideeën, suggesties en prettige samenwerking.

Beste Prof. dr. de Boer; Beste Joke,
Ik wil je bedanken dat je altijd een oog in het zeil hield en op de juiste momenten suggesties kon doen, met een altijd open en kritische blik. Dank voor de fijne samenwerking en de deur die altijd open staat voor vragen. Je onderzoekservaring en kennis in klinische toepasbaarheid van ofthalmo-immunologie waren onmisbaar voor dit project. Ik bewonder je grenzeloze inzet voor patiënten en onderzoek, en hoop veel van je te kunnen leren in de kliniek.

Beste Prof. dr. Radstake, Beste Tim,
Hartelijk dank voor de kans en vertrouwen om dit onderzoek te starten en de steun tijdens de uitvoering. Door je inzet heb je in het UMC een geweldig team bij elkaar gekregen, waar heel veel mooie dingen uit voortgekomen zijn. Ik heb heel veel respect voor hoe je alles wat je doet kan combineren, en dan nog steeds weet je als een van de eerste op mijn mails te reageren, waar ter wereld je ook bent. Ik wens je al het beste toe in de States!

Beste (oud) collega-onderzoekers,
Hoewel iedereen een eigen project heeft heb ik toch zeker het gevoel dat ik dit project samen met jullie gedaan heb. Ik wil jullie danken voor de goede sfeer, alle hulp en gezelligheid. Yvonne, Laura, Daniël, dank voor jullie tips als ervaren onderzoekers toen ik begon en nu ook weer als ervaren assistenten aan het begin van mijn opleiding. Laura, het lijkt alweer zo lang geleden dat je me begeleide voor 4 weken wetenschapsstage, maar ik ben het zeker niet vergeten. Nienke, heel lang was je de stabiele factor en de moeder van de onderzoeksgroep. Dankjewel en succes bij Heuvelrug! Fleurieke en Anne-Mieke, wat een geluk dat jullie harde werk de weg al had gebaand in de samenwerking van de oogheelkunde met de immunologie. Ik heb jullie hier heel veel voor te danken. Het was ook heel fijn dat jullie altijd open stonden voor vragen en dit nu ook doorzetten tijdens de opleiding. Een mooie herinnering is de prachtige reis naar Hawaii voor het ARVO-congres samen. Fleurieke, ik wil je in het bijzonder bedanken voor al je werk aan de METC-goedkeuring, je uitleg, aandacht, betrokkenheid en geduld. Dank dat je altijd wilde meedenken. Je bent een enorm waardevolle collega. Anna en Sara, samen staan we sterk en dat hebben we heel goed opgepakt. Het was heel fijn in ons hok, waar we verhalen en ergernissen deelden en elkaar hielpen. Nog even en we kunnen weer samen werken in de kliniek. Bas, Roos, Myrthe en Wouter, dank voor jullie hulp, de fijne werksfeer, gezelligheid en mooie momenten samen. Geniet van jullie promotietijd, dit gaat veel te snel voorbij. Brandan, Evianne, Carlyn en Els, heel veel succes met jullie projecten en dank voor jullie gezelligheid en interesse. Lude en Deniz, jullie gaan door met het grote METC-project, ik heb het volste vertrouwen in jullie! Deniz, jij gaat nu door met onderzoek naar orbita-ziekten bij Rachel. Ik wil jou in het bijzonder heel veel succes wensen en veel plezier met de ongelofelijk goede groep onderzoekers, artsen en medewerkers die het protmotiezonderzoek zo mooi maken.

Beste orbita/kind zorglijn Utrecht,
Ik wil het hele team bedanken voor de hulp bij het verzamelen van patiënten voor dit onderzoek, bij de logistieke uitdagingen en voor het bijdragen van belangrijke kennis. Specifiek wil ik Christine en Rob bedanken: ik heb veel van jullie kunnen leren en met veel plezier samen met jullie artikelen voor dit proefschrift geschreven. De dames van de orthoptie wil ik bedanken voor de interesse, kennis en gezelligheid. Jullie zijn een hele sterke en fijne groep! In het bijzonder wil ik Pascale Cooijmans bedanken: je hebt mij enorm geholpen bij het uitzoeken van patiënten voor de orbita database en je had een cruciale rol bij het verkrijgen van de de benodigde sponsoring voor dit onderzoek. Joyce, Jaenette en Petra wil ik bedankenvoor hun rol bij de zorg van orbita patienten en ondersteuning bij het I&I-cohort. Ik dank de dames van balie Geel voor de logistieke hulp, het geduld en het beantwoorden

van de eindeloze hoeveelheid vragen die ik had. Ook **Ralph** wil ik bedanken voor de logistieke ondersteuning. **Özlem** en **Willemien**. ik wil jullie heel veel succes en plezier wensen binnen de zorglijn!

Beste Dutch Orbital Society (DOS),
Voor het doen van onderzoek is samenwerking cruciaal. Daarom wil ik de DOS ook hartelijk danken voor de hulp bij het tot stand komen van dit proefschrift. In het bijzonder dank ik **Stijn Genders** en **Maarten Maurits** voor het meedenken en doorverwijzen van patiënten, en dank ik **Peerooz Saeed, Stijn Genders, Dyonne Hartong, Özlem Köse** en **Dion Paridaens** voor de fantastische samenwerking voor hoofdstuk 3 van dit proefschrift.

Beste prof. dr. Mombaerts, Beste Ilse,
Dankzij u is de samenwerking voor hoofdstuk 3 ook internationaal geweest. Dankuwel voor de kritische blik en vele suggesties. Ook wil ik u danken dat u wilde plaatsnemen in de beoordelingscommissie van dit proefschrift.

Beste collega's van het LTI/CTI – Dear collegues of the LTI/CTI,
Allereerst wil ik **Sanne** danken voor al haar hulp tijdens dit project. Je hebt me leren pipetteren en ervoor gezorgd dat ik vertrouwen kreeg in het lab te werken. Daarbij wil ik ook zeker alle **analisten van de Radstake groep** bedanken voor hun hulp en adviezen. In het bijzonder ook **Cornelis**, dank voor je hulp bij de RNA-isolaties en de metingen van het microRNA project. **Jeroen** en **Pien**, dank voor alle tips en adviezen bij de FACS-metingen.

I would like to thank all the members of the **Radstake group** for all the advice, practical help and the good times and memories you brought me, including the retreats, dinners and lasergame competitions. It was a great privilege to work with you and to be part of the group. A special thanks to **Joel** and **Jorre** and the secretaries **Anja** and **Diana** whom I frequently contacted. I also want to thank the **computational group** in particular, with **Aridaman and Rianne** for their help in the analysis of the flow cytometry data, their suggestions and feedback. **Ahbinandan** and **Weiyang** thanks for sharing your knowledge of complex statistics.

A special thanks to **Julia** for her statistical help and for always being there to answer my questions (basic or complex).

Importantly, I want to thank my roommates at the WKZ throughout these years, **Pawel, Matevz, Sara, Noortje, Alsya, Emmerik, Anna, Gerdien, Julliette, Anneline** and **Akashdip**. You are all great people, dear collegues and good company! Emmerik, jou wil ik in het bijzonder nog bedanken voor je microRNA data en je (wetenschappelijke) wijsheden. Met alles wat je doet verbaast het me niets als je straks al professor bent voordat je PhD binnen is.

Studying immunology together is better than alone, thanks you **Janeway-group**.

Prof. dr. Ron Heeren, dr. Tiffany Porta Siegel and the M4I in Maastricht,
Thank you, **Ron**, for the opportunity and supporting our great collaboration. I'm glad I stood in line to talk to you, after your talk at the DOPS conference all those years ago. Thank you for your hospitality, trust and the warm welcome. You are an inspirator with a wonderful group. A special thanks to **Tiffany**, we were able to get great data and ideas in this project. Thank you for your kindness, patience and practical help. The workshop you and Ron organized was perfect and I could not have done without it. I'm looking forward to finishing our article soon! **Britt, Naomi** and **Ronny** thank you for your valuable work during this project.

Daarnaast nog bijzondere dank aan **Albert Liem** voor je gastvrijheid en het altijd openstellen van je huis in Maastricht als ik metingen ging doen in het M4I lab. Je bent een van de vriendelijkste mensen die ik ken!

Beste drs. Leguit, Beste Roos,
Hartelijk dank voor de samenwerking met de pathologie en dat ik voor voor meerdere hoofdstukken in dit proefschrift gebruik heb mogen maken van je expertise. Ook dank voor de logistieke hulp bij het verzamelen van materiaal voor hoofdstuk 9. Hiervoor ook veel dank aan **Domenico** en **Petra**.

Beste dr. de Keizer, Beste Bart
Elke keer was het weer prachtig om de beelden te zien van de ^{89}Zr-rituximab PET/CT. Dank voor je vertrouwen, suggesties en ideeën, die we hopelijk in de toekomst nog verder kunnen uitwerken.

Beste UPOD,
Beste **Saskia**, leuk om je ook in een wetenschappelijke samenwerking tegen te komen, nadat ik je heb leren kennen in de PhD-council. Dank aan jou en **Mark** voor de UPOD data en de kritische blik in het microRNA project.

Beste onderzoeksbureau en ICT-ondersteuning DHS,
Beste **Tamara** en **Marianne**, dank voor alle tips en adviezen bij de regelgeving rond juridische- en METC-zaken. Beste **Ferry** en **Ruud**, jullie hielpen me altijd precies goed als het nodig was, zelfs als het extra veel inzet koste! Dank!

Beste Stafsecretariaat Oogheelkunde,
Beste **Suzan** en **Petra**, hartelijk dank voor alle organisatorische hulp, zoektochten in SAS, onderwijs support, antwoord op vele vragen en gezellige praatjes!

Beste AIOS Oogheelkunde,
Wat een topgroep zijn jullie! Het is een eer om me bij jullie te kunnen voegen. Dank voor de interesse en hulp tijdens het onderzoek en daarbuiten de AIOS weekenden, borrels en de wintersport die ik al mee heb mogen maken. De komende jaren worden heel mooi!

Beste graduate school of life sciences,
Dank aan de leden van de PhD-council voor de fijne en leerzame tijd! Onder andere onze PhD dag 2017 was een enorm succes! In het bijzonder dank aan Saskia Ebeling voor de zeer goede begeleiding en ondersteuning van de council. Ook dank ik de MD-PhD sensorgroep voor de nuttige discussies. Ik wil de infection & immunity bedanken en speciaal waardering uitspreken voor het werk van Jolanda en Erna. Ik heb genoten van de retraites, symposia en de leerzame bijeenkomsten.

Beste wetenschapsstudenten,
Beste Sanne, Stefan, Colette, Nicole, Richard, Peter, Khaled en Simone, dank voor jullie enorme inzet en enthousiasme. Het was een grote eer jullie te begeleiden , wat voor mij ook erg leerzaam was. Ik vond het super een aantal van jullie zelfs een tweede keer te mogen begeleiden, telkens weer zag ik enorme vooruitgang. Heel veel succes met jullie carrières!

Lieve vrienden, familie en schoonfamilie,
Dank voor jullie vriendschap en steun de afgelopen jaren. Zonder jullie hulp, ervaringsdeskundigheid en afleiding hadden deze jaren veel langer geduurd. In het bijzonder dank aan Ivo, mijn bro en paranimf, dank voor je hulp, onze talloze discussies en de praktische tips. Ik vond het prachtig betrokken te zijn geweest bij jouw verdediging en deze keer gaan we er dan ook weer een feestje van maken. Dank voor de avonturen die we de afgelopen jaren samen beleefd hebben en ik kijk uit naar onze volgende bestemming. Je bent een geweldige vent.

Lieve mama en papa,
Dank voor jullie eeuwige interesse en onvoorwaardelijke steun. Jullie blijven voor mij altijd een bron van inspiratie en motivatie om door te blijven gaan.

Lieve Vincent,
Grote broer, jij bent nu ook mijn parnimf en ik dank je voor je enorme steun, interesse en fijne discussies. Ik vind het heel mooi dat jij ineens vol de onderzoekswereld in duikt, nu ik me voorlopig meer ga focussen op de kliniek. Je hebt geweldige ideeen, ga zo door!

Lieve Tessa,

Jij hebt de toppen en dalen tijdens de afgelopen jaren van dichtbij meegemaakt. Je snapt ze het beste, zoals je mij ook zo goed snapt. Dank voor je hulp, lieve steun, dat je er bent en ook wie je bent. Dank voor alle mooie momenten die we samen hebben gehad en ik kijk uit naar al het moois dat we nog gaan beleven. Je bent de allerliefste en je maakt me zielsgelukkig!

Appendix III - List of publications

This thesis

Laban KG, Rijken R, Hiddingh S, Mertens JS, van der Veen RLP, Eenhorst CAE, Pandit A, Radstake TRDJ, de Boer JH, Kalmann R, Kuiper JJW. cDC2 and plasmacytoid dendritic cells diminish from tissues of patients with non-Hodgkin orbital lymphoma and idiopathic orbital inflammation. Eur J Immunol. 2020 Apr;50(4):548-557. doi: 10.1002/eji.201948370

de Keizer B, **Laban KG**, Kalmann R. Zirconium-89 labelled rituximab PET-CT imaging of Graves' orbitopathy. Eur J Nucl Med Mol Imaging. 2020 Mar;47(3):738-739. doi: 10.1007/s00259-019-04599-8

Laban KG, Kalmann R, Bekker CPJ, Hiddingh S, van der Veen RLP, Eenhorst CAE, Genders SW, Mourits MP, Verhagen FH, Leijten EFA, Haitjema S, de Groot MCH, Radstake TRDJ, de Boer JH, Kuiper JJW. A pan-inflammatory microRNA-cluster is associated with orbital non-Hodgkin lymphoma and idiopathic orbital inflammation. Eur J Immunol. 2020 Jan;50(1):86-96. doi: 10.1002/eji.201948343

Laban KG, Kalmann R, Leguit RJ, de Keizer B. Zirconium-89-labelled rituximab PET-CT in orbital inflammatory disease. EJNMMI Res. 2019 Jul 30;9(1):69. doi: 10.1186/s13550-019-0530-9

Eenhorst CAE, **Laban KG**, Leguit RJ, Radstake TRDJ, Kalmann R. Orbital lymphomas missed by first biopsies of orbital masses. Acta Ophthalmol. 2017 Dec;95(8):858-859. doi: 10.1111/aos.13350

Laban KG, Kuiper JJW, Kalmann R, de Boer JH, Radstake TRDJ. Reflections in the mirror - Idiopathic intracranial hypertension and non-specific orbital inflammation in identical twins. Acta Ophthalmol. 2017 Jun;95(4):e339-e340. doi: 10.1111/aos.13286

Other publications

Mensing LA, Vergouwen MDI, **Laban KG**, Ruigrok YM, Velthuis BK, Algra A, Rinkel GJE. Perimesencephalic Hemorrhage: A Review of Epidemiology, Risk Factors, Presumed Cause, Clinical Course, and Outcome. Stroke. 2018 Jun;49(6):1363-1370. doi: 10.1161/STROKEAHA.117.019843

Laban KG, Tobon-Morales RE, Hodge JA, Schreuder HW. Single benign metastasising leiomyoma of an inguinal lymph node. BMJ Case Rep. 2016 Aug 10;2016. pii: bcr2016216546. doi: 10.1136/bcr-2016-216546.

Backes D, Rinkel GJ, **Laban KG**, Algra A, Vergouwen MD. Patient- and Aneurysm-Specific Risk Factors for Intracranial Aneurysm Growth: A Systematic Review and Meta-Analysis. Stroke. 2016 Apr;47(4):951-7. doi: 10.1161/STROKEAHA.115.012162

Laban KG, Rinkel GJ, Vergouwen MD. Nosocomial infections after aneurysmal subarachnoid hemorrhage: time course and causative pathogens. Int J Stroke. 2015 Jul;10(5):763-6. doi: 10.1111/ijs.12494

Laban KG, Vergouwen MD, Dijkhuizen RM, Sena ES, Macleod MR, Rinkel GJ, van der Worp HB. Effect of endothelin receptor antagonists on clinically relevant outcomes after experimental subarachnoid hemorrhage: a systematic review and meta-analysis. J Cereb Blood Flow Metab. 2015 Jul;35(7):1085-9. doi: 10.1038/jcbfm.2015.89

Laban KG, Scheerlinck LM, van Leeuwen R. Prognostic Factors Associated with Visual Outcome after Pars Plana Vitrectomy with Internal Limiting Membrane Peeling for Idiopathic Epiretinal Membrane. Ophthalmologica. 2015;234(3):119-26. doi: 10.1159/000438677

Luykx JJ, **Laban KG**, van den Heuvel MP, Boks MP, Mandl RC, Kahn RS, Bakker SC. Region and state specific glutamate downregulation in major depressive disorder: a meta-analysis of (1)H-MRS findings. Neurosci Biobehav Rev. 2012 Jan;36(1):198-205. doi: 10.1016/j.neubiorev.2011.05.014

Appendix IV - PhD Curriculum Vitae

Courses Infection & Immunology (I&I) program
- Course Advances Immunology
- Admiraal van Kinsbergen Course
- I&I PhD retreat 2016
- I&I PhD retreat 2017
- Attendance Eijkman Lectures 2015-2019
- Attendance I&I symposium 2018 and 2019)

Courses Graduate School of Life Sciences (GSLS)
- Introductory Biostatistics for Researchers
- Achieving your Goals and Performance more successful in your PhD
- Analytic storytelling
- Presenting - Breaking Science
- GSLS PhD Day 2016 – 2018

Other courses
- Basiscursus Regelgeving en Organisatie voor Klinisch Onderzoekers (BROK) course
- M4I workshop
- Self-organised Janeway studygroup
- National PhD Day 2016

Committees/organization
- GSLS PhD Council 2016 - 2017
- GSLS PhD Day 2017
- GSLS Supervisor of the year 2017
- MD-PhD sensor committee 2017
- Education committee I&I 2016 - 2017
- Division of Surgical Specialties Science day 2019

Personal grants
- Bayer Ophthalmology Research Award (17.5K)

Grants as co-applicant/co-author
- Dr. F.P. Fischerstichting (25K + 50K)
- Stichting Lijf en Leven (110K)
- Rotterdamse Stichting Blindenbelangen (25K)
- Stichting Ankie Hak (60K)

Oral presentations
- AUMC nuclear medicine regional meeting January 2018
- European society of oculoplastic and reconstructive surgery conference 2017 & 2018
- Nederlands Oogheelkunde Genootschap (NOG) conference 2016 - 2019
- Dutch ophthalmology PhD students (DOPS) conference 2017

Poster presentations
- Association of research in vision and ophthalmology (ARVO) conference 2018
- Dutch ophthalmology PhD students (DOPS) conference 2016

Teaching activities
- Supervision of medical student research internship (4-6 weeks) 4 master students
- Supervision of medical student research internship (12 weeks) 7 master students

Appendix V - About the author

Kamil Laban was born on the 18th of January, 1989, in Utrecht, the Netherlands. He grew up in the centre of Utrecht, while attending primary and high-school at the Werkplaats Kindergemeenschap (Kees Boeke school) in Bilthoven. During the final years of high-school he also participated in the Junior College Utrecht program at the University of Utrecht. After graduating high-school, he started studying medicine at the University of Utrecht. During his studies he continued to develop his interests in science and participated in the bachelor and master honours programs at the same institute. He interrupted his studies to roam the world with his dear friend Ivo Soliman. In the final year of medicine, he completed his clinical internships for neurology and ophthalmology at the University Medical Center in Utrecht. He performed his research internship (master thesis) at the Toronto Western hospital in the field of neuro-intervention radiology. In 2015, he obtained his medical degree and started as PhD student for orbital diseases in a collaboration between the department of ophthalmology and the laboratory of translational immunology at the University Medical Center Utrecht. He was able to present the results of his research at several (inter)national conferences, and received the Bayer Ophthalmology Research Award in 2018. In December 2019, he started his residency to become an ophthalmologist at the University Medical Center in Utrecht. Together with Tessa, Kamil lives in Woerden.